Evolutionary recruitment and assembly of embryonic alternative splicing programs: insights form the Deuterostomia lineage

Demian Burguera Hernández

EVOLUTIONARY RECRUITMENT AND ASSEMBLY OF EMBRYONIC ALTERNATIVE SPLICING PROGRAMS

Insights from the Deuterostomia lineage

UNIVERSITAT DE BARCELONA

Memòria presentada per en
Demian Burguera Hernández

per optar al títol de **Doctor**

Tesi realitzada sota la direcció del Dr. Jordi Garcia Fernàndez i el Dr. Manuel Irimia al Departament de Genètica, Microbiologia i Estadística de la Universitat de Barcelona

Dr. Jordi Garcia Fernàndez	Dr. Manuel Irimia	Demian Burguera
Director de la tesi	director de la tesi	autor

Maig 2017

Per als qui promouen el pensament crític
i l'organització horitzontal col·lectiva
com a eines fonamentals vers l'emancipació popular.

“Las falacias y las flaquezas del pensamiento humano generan problemas sistemáticos y predecibles cuando intentamos comprender las complejidades de la realidad externa. Entre estos puntos débiles, nuestros intentos persistentes de construir sistemas que son hermosos en abstracto, lógicamente impecables y globalmente simplificados, siempre nos hacen salir del camino.”

Stephen Jay Gould, *Lying stones from Marrakech*.

ÍNDICE

INTRODUCCIÓN

Macroevolución y las causas orgánicas de la complejidad biológica.

Desde la aparición de los primeros organismos en el registro fósil, hemos observado la huella de formas de vida poblando el planeta a lo largo de su cronología. Con la suficiente perspectiva geológica, cada época temporal presenta organismos morfológicamente diferentes en mayor o menor grado. Hoy en día sabemos que estos organismos están relacionados con las formas predecesoras y, en ocasiones, también con las posteriores. La transformación de los seres vivos, que conecta filogenéticamente a todas las especies, es el proceso responsable de la generación de la biodiversidad acumulada en el historial evolutivo terrestre.

Esta diversidad se compone de organismos con diferentes patrones estructurales a múltiples niveles. Tradicionalmente, la división más profunda reconocida entre seres vivos es la que separa a procariotas y eucariotas, actualmente matizada en bacterias, arqueas y eucariotas. Otro gran eje de clasificación estructural podría establecerse entre linajes unicelulares y multicelulares. Siendo los primeros organismos del planeta seres unicelulares, el nivel de organización multicelular surgió independientemente en diversos clados como los hongos, las plantas o los animales (también llamados metazoos). Esta transición a la multicelularidad abrió las puertas a la aparición de múltiples planes corporales en el linaje de los metazoos, así como de una infinidad de innovaciones a nivel de tipos celulares y órganos.

La acumulación de estos nuevos caracteres a lo largo de trayectorias macroevolutivas dispares ha generado, en ciertos grupos animales, seres de complejidad estructural y funcional creciente. Sin embargo, este fenómeno no debe interpretarse como la pauta general del cambio organísmico, pues la evolución no genera inevitablemente formas más complejas que las anteriores dentro de un conjunto filético. Análisis cladísticos a diversas escalas revelan que el cambio macroevolutivo procede en todas las direcciones respecto al nivel de complejidad, siendo comunes tanto las simplificaciones o pérdidas de caracteres como las modificaciones o ganancias de los mismos (Finlay and Esteban, 2009). Por otro lado, una gradación intuitiva de la complejidad estructural puede resultar fácil de aplicar para organismos muy extremos, pero resulta mucho más complicada de

medir a la hora de comparar organismos menos dispares. Se han intentado aplicar diferentes parámetros para objetivizar estas cuantificaciones, como el número de tipos celulares, aunque esta clase de aproximaciones pueden resultar deficientes para medir la complejidad al nivel funcional y estructural entre organismos (Bell and Mooers, 1997).

Uno de los objetivos principales de la biología evolutiva desde sus inicios ha sido comprender el origen de esta complejidad variable. El descubrimiento del ADN como responsable de transferir la información genética de una generación a otra puso el foco sobre éstas moléculas para dilucidar las causas orgánicas de las diferencias en la complejidad de los organismos. Se estudió el tamaño de los genomas de especies eucariotas dispares para intentar trazar una correlación entre la cantidad de ADN y la complejidad organísmica (Mirsky and Ris, 1951). Sin embargo, los datos obtenidos rechazaron cualquier relación lineal, un resultado que fue etiquetado como el enigma del valor-C (Gregory, 2004). Más tarde, se descubrió que los genomas estaban repletos de regiones no codificantes que parecían no tener función. Esto condujo a ciertos autores a proponer que en realidad lo importante era el número de genes codificantes, no la cantidad total de ADN (Moore, 1984). No obstante, la secuenciación entera de genomas ha revelado una situación similar a la anterior, conocida como la paradoja del valor-G: no existe una correlación directa entre la complejidad percibida y el número de genes o familias génicas de una especie (Hahn and Wray, 2002).

Estas paradojas aparentes han recibido diversas explicaciones. Algunos autores, en la línea de sus predecesores, siguen sugiriendo que tiene que existir mayor *cantidad* de algún tipo de elemento derivado del genoma en los grupos de organismos con estructuras más elaboradas o complejas. La mayoría de estos investigadores apunta al transcriptoma, es decir, al conjunto de tránscritos expresados por el genoma. Sus planteamientos podrían dividirse principalmente en dos frentes no excluyentes, el que aboga por la importancia de los tránscritos no codificantes (Djebali et al., 2012), y el que destaca la cantidad de genes codificantes que presentan diversidad transcripcional mediante la producción de isoformas proteicas (Kanapin et al., 2010). Es necesario aclarar que ambas afirmaciones reposan mayormente sobre un trasfondo ideológico pan-adaptacionista, en el que se asume que la mayoría de elementos detectados a nivel de transcriptoma posee una función

a nivel organísmico. Si bien es cierto que se han descrito roles moleculares relevantes para ambos tipos de eventos transcripcionales en casos particulares, la relevancia funcional para la mayor parte de estos elementos constituye una incógnita (Niu and Jiang, 2013). De hecho, otros autores han argumentado que muchos de estos elementos no tienen por qué presentar una función seleccionada adaptativamente, si no que probablemente sean consecuencia de una transcripción *espuria* o *ruidosa* que no interfiere de manera deletérea con los roles esenciales del organismo (Doolittle et al., 2014).

En los últimos años se han publicado estudios aislados comparando datos transcriptómicos entre conjuntos todavía muy limitados de organismos, donde aseguran detectar una correlación entre los niveles de *splicing* alternativo (AS) y la complejidad organísmica (Chen et al., 2014). El splicing alternativo puede describirse brevemente como un proceso de regulación génica capaz de producir más de un tipo de tránscrito a partir de un solo locus génico. Sin embargo, toda precaución es poca a la hora de establecer una relación causal subyacente a estas correlaciones observadas, especialmente cuando la complejidad es cuantificada en base al número de tipos celulares. Además, diversos estudios sugieren que la maquinaria molecular encargada del *splicing* podría producir niveles elevados de isoformas sin ninguna función, que serían consecuencia de fallos del proceso en determinados contextos celulares (Pickrell et al., 2010). De hecho, han empezado a detectarse casos particulares que rompen claramente la asociación entre complejidad organísmica y AS. El ejemplo más llamativo es el del alga unicelular *Bigellowiella natans,* que presenta una de las tasas de AS más elevadas detectadas hasta el momento, sólo comparables al cerebro humano (Curtis et al., 2012). Interesantemente, el análisis del tipo de AS detectado en *B. natans* revela que una gran parte de los eventos observados son probablemente atribuibles a una producción descontrolada de isoformas sin función específica.

De todos modos, sí que parece plausible que determinados tipos celulares controlen parte de su actividad fisiológica mediante la regulación coordinada de un número elevado de eventos funcionales de AS. Uno de los casos más evidente detectados hasta el momento en animales es el sistema nervioso de organismos vertebrados que, aparte de exhibir una de las frecuencias más elevadas de AS junto a los testículos, presenta los mayores niveles

de conservación reguladora (Barbosa-Morais et al., 2012; Raj and Blencowe, 2015). Además, la proporción de exones alternativos con regulación específica de tejido que respetan la pauta de lectura es más elevada en muestras neuronales respecto al conjunto del resto de órganos (Irimia et al., 2014). Estos datos apuntan a un uso frecuente de este mecanismo regulador para la producción de isoformas proteicas específicas de neuronas, que posiblemente presenten propiedades moleculares distintas y necesarias en estas células. Paralelamente, un análisis transcriptómico en la mosca *Drosophila melanogaster* detectó niveles más elevados de producción de isoformas en los ganglios nerviosos respecto al resto de órganos, aunque aproximadamente la mitad se debían al uso de promotores alternativos (James B Brown et al., 2014). Por tanto, es probable que estos altos niveles de regulación génica por AS en el sistema nervioso de vertebrados e insectos refleje una herramienta funcional recurrente de los tipos celulares neurales.

Por otro lado, la clase de perspectivas que buscan las raíces de la complejidad organísmica en base a una supuesta complejidad transcriptómica podrían resultar excesivamente reduccionistas. En este sentido, son necesarios planteamientos alternativos que otorguen menos relevancia a la *cantidad* de elementos singulares del genoma y sus transcriptomas asociados, y más importancia a cómo éstos *interaccionan* entre sí. Sin negar la aportación individual necesaria de elementos moleculares diversos, el interés se centra en las conexiones establecidas entre ellos para generar complejidad funcional. Este enfoque prioriza la comprensión de las intrincadas relaciones entre el genoma y el organismo, investigando los procesos reguladores que producen la diversidad estructural y funcional interpretando la información genómica. En el estudio macroevolutivo, dicha perspectiva pretende dar una explicación materialista a aquellos cambios orgánicos que transcienden el nivel poblacional y quedan establecidos a un nivel jerárquico superior, desde las especies hasta clados mucho más amplios.

Del genoma al organismo: la importancia de establecer conexiones.

Los organismos multicelulares, especialmente los animales, adquieren sus principales órganos y estructuras mayoritariamente durante el desarrollo embrionario. Partiendo de una sola célula en la reproducción sexual, se generan múltiples tipos celulares en

localizaciones embrionarias determinadas que son las encargadas de construir los diferentes órganos dentro de un plan estructural armónico. A pesar de compartir mayoritariamente la misma secuencia genómica, los diferentes tipos celulares expresan tránscritos distintos de manera dinámica para controlar su identidad y fisiología, además de determinar la capacidad de interacción con otras células. El desarrollo es un proceso altamente intrincado en el que los tejidos embrionarios proliferan y se diferencian de manera coordinada para construir un organismo funcional respecto a un rol ecológico concreto. La alteración de estos procesos de desarrollo mediante modificaciones de la secuencia genómica es una de las herramientas básicas de la evolución para producir cambio orgánico duradero.

Puesto que la relación entre un genoma y su organismo resultante es muy compleja y difícil de predecir, es necesario analizar los niveles de organización biológica intermedios para conseguir conectar ambos extremos. Al nivel molecular, diversos procesos se coordinan física y temporalmente para obtener determinados RNAs en cada tipo celular. Estos fenómenos forman parte de lo que se conoce como regulación de la expresión génica, y son responsables de la producción de distintos tránscritos en contextos diferentes, cuyo conjunto se denomina transcriptoma. Un porcentaje de dichas moléculas de RNA contiene información codificante, que será traducida por la maquinaria ribosomal en cadenas de péptidos, la suma de los cuales constituye el proteoma.

Conjuntamente, estos elementos moleculares son los encargados de establecer a nivel celular una identidad, características fisiológicas concretas y capacidad de respuesta a estímulos externos. Las propiedades comunicativas entre células de un mismo y diferentes tejidos mediarán la coordinación necesaria para la formación de las estructuras del organismo a nivel macroscópico. Para comprender tanto la función de esta variabilidad molecular como para establecer la mecánica del cambio organísmico, son necesarias aproximaciones desde los distintos niveles de organización biológica. Por un lado, el estudio de los elementos genómicos, transcriptómicos y proteómicos es imprescindible para establecer diferencias moleculares entre especies y plantear las posibles bases materiales de la evolución estructural y funcional. Paralelamente, se requieren herramientas y conceptos de campos como la biología del desarrollo, para

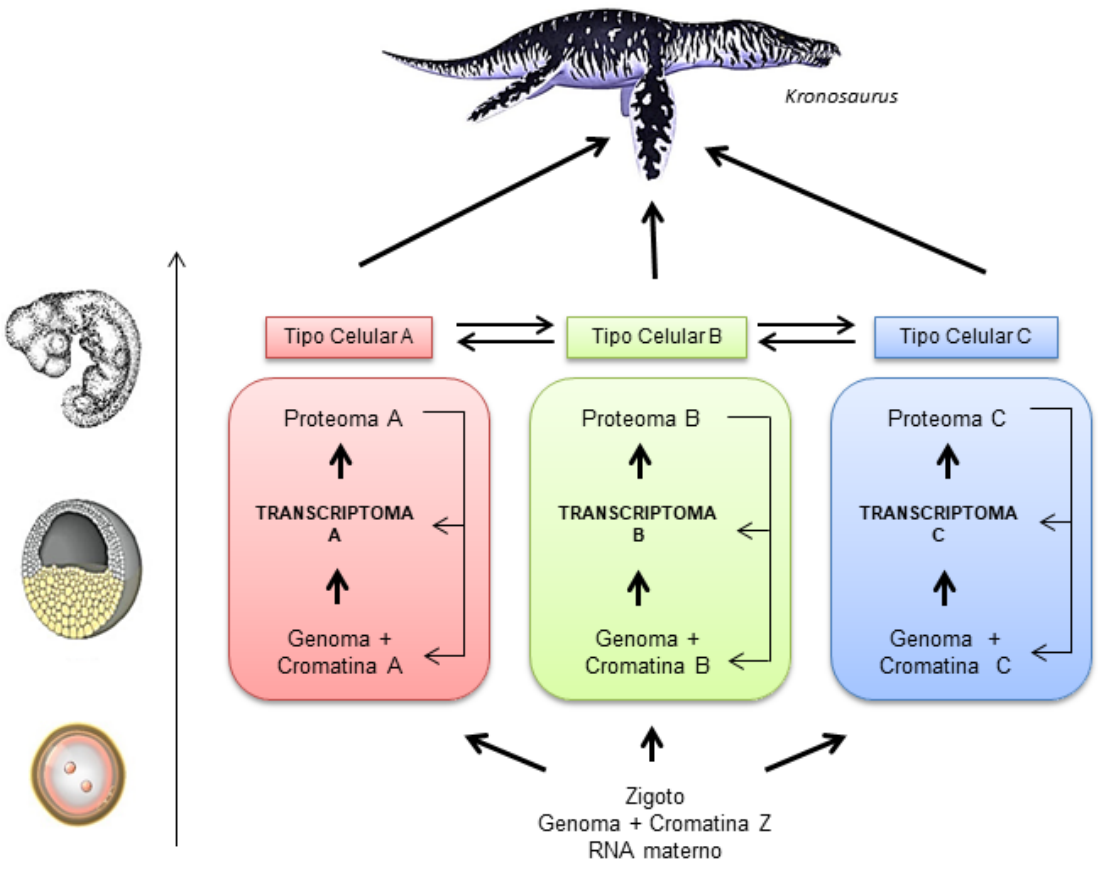

Figura I1 | Esquema de las interacciones entre los elementos moleculares en organismos multicelulares sexuales para construir las diferentes estructuras de un organismo ecológicamente viable.

determinar el impacto de los cambios moleculares.

Distintos elementos del genoma, el transcriptoma y el proteoma coordinan juntos la regulación génica.

Si bien la regulación a nivel de proteínas puede resultar esencial para la actividad celular, se asume que el transcriptoma refleja razonablemente bien las herramientas moleculares de que disponen las células. Inicialmente catalogado como un conjunto de RNAs mensajeros, de transferencia y ribosómicos en su mayoría, hoy sabemos que existen muchos más tipos de tránscritos con roles relevantes. La generación de este inventario

molecular, si bien codificado en última instancia por el genoma, está lejos de ser un proceso unidireccional y estático pues requiere de la interacción física continuada de elementos del genoma, el transcriptoma y el proteoma. Estos elementos se coordinan modulando la producción de un conjunto específico de tránscritos mediante procesos complejos como la transcripción, el *splicing* alternativo, el *editing*, o la poliadenilación. Para comprender la función de estas capas de regulación génica es necesario identificar los factores que intervienen en esos procesos, la lógica reguladora que los conecta, y las consecuencias fenotípicas que provoca su ausencia.

Tradicionalmente, la mayoría de estudios sobre expresión diferencial ha focalizado en el proceso de transcripción génica. La atención recibida es entendible puesto que constituye el primer paso, y probablemente el más central, en la generación de tránscritos. Aunque se trata de un fenómeno complejo que consta de múltiples etapas, la transcripción génica se concibe como la producción de moléculas de RNA mediante la lectura de un molde de DNA. Además del tránscrito y la cadena molde, durante la regulación de este proceso intervienen múltiples elementos procedentes mayoritariamente del genoma y el proteoma. El genoma aporta promotores basales, *enhancers*, *silencers* y aisladores. Estos elementos influyen en la activación o la represión de la transcripción mediante su interacción con una multitud de componentes del proteoma, como los factores de transcripción o las proteínas modificadoras de la cromatina (Calo and Wysocka, 2013). Por otro lado, cada vez son más los casos encontrados de tránscritos no codificantes que intervienen en la modulación de eventos de transcripción, involucrando también al transcriptoma (Geisler and Coller, 2013). De esta manera, la búsqueda de las causas concretas de los cambios en la expresión génica entre tejidos celulares o especies suele proceder mediante el estudio de la interacción de estos elementos.

No obstante, la importancia de otros mecanismos de regulación génica que operan a nivel post-transcripcional es cada día más clara. Por ejemplo, existen moléculas muy pequeñas de RNA, llamadas microRNAs, cuya función está relacionada con la degradación de uno o múltiples tránscritos diana, controlando así los niveles de expresión génica (Jonas and Izaurralde, 2015). Por otro lado, también se dan mecanismos reguladores que pueden producir secuencias distintas de RNA a partir de un solo locus génico, conocidas como

isoformas. Esta capacidad reside parcialmente en la maquinaria transcripcional mediante el uso de promotores alternativos que generan tránscritos diferenciados en la región 5'. Sin embargo, la regulación post-transcripcional permite ampliar la diversidad de secuencias de las isoformas en las regiones internas y finales de los RNAs. Entre estos procesos reguladores destaca el *splicing* alternativo (AS), un mecanismo que sucede durante la maduración de los tránscritos. La maquinaria spliceosomal interacciona con secuencias específicas del tránscrito saliente, a menudo a través de proteínas auxiliares específicas de tejido (proteoma) y en ocasiones también con el DNA molde (genoma) o estructuras secundarias y ediciones del RNA (transcriptoma), para generar unas isoformas determinadas (Gonzalez et al., 2015; Lev Maor et al., 2015; Zhou et al., 2014).

Splicing alternativo y su conexión con la estructura génica.

La regulación mediante splicing alternativo está indefectiblemente ligada a la estructura génica. La inmensa mayoría de genomas eucariotas contiene una proporción muy variable de unos elementos llamados intrones spliceosomales (a los que se va a hacer referencia como "intrones" en el texto subsiguiente para simplificar). Estos elementos forman parte de la secuencia interna de algunos genes, pero son eliminados de los tránscritos maduros durante o después de la transcripción. Desde su descubrimiento, las secuencias génicas han quedado divididas entre aquellas que serán incluídas en el tránscrito final, los exones, y las que no, los intrones. Los exones pueden contener tanto información codificante para proteínas (CDS) como secuencia no codificante (UTRs). Por su parte, los intrones son generalmente considerados como elementos no codificantes, aunque se han llegado a describir algunos casos que sí lo son (Irimia et al., 2008; Marquez et al., 2015).

A nivel macroevolutivo, esta disposición de la estructura génica no es una característica estática de cada locus. Genes ortólogos de linajes separados pueden exhibir estructuras muy diferentes respecto al número de exones que los forman. Este proceso se puede deber tanto a la ganancia y pérdida de intrones como a la aparición de nuevos exones (Merkin et al., 2015; Schmitz and Brosius, 2011). Entre los mecanismos moleculares más comunes de generación de nuevos exones se encuentra la duplicación de secuencias de ADN. Ésta puede darse frecuentemente a partir de una región interna del mismo gen, aunque también

se han descrito casos de duplicación de exones procedentes de otros loci (*exon shuffling*). Otro proceso capaz originar nuevos exones es la inserción de elementos móviles transponibles dentro de secuencias intrónicas, donde algunos fragmentos de la nueva secuencia pueden pasar a incluirse en los transcritos maduros tras unas pocas mutaciones. Finalmente, otra vía que pueden contribuir al exoma es la "exonización" de regiones intrónicas, fenómeno conocido como evolución exónica de *novo.*

El hallazgo de intrones en prácticamente todas las especies eucariotas estudiadas, ha conducido a la afirmación de que éstos aparecieron antes de la separación del último ancestro eucariota (Irimia and Roy, 2014). El número de intrones puede ser muy variable en distintos genomas: mientras que los humanos poseemos una media de unos 8,5 intrones por gen, la levadura *Saccharomyces cerevisiae* contiene solo 0,05. Estas densidades intrónicas elevadas o inferiores se hallan distribuidas de manera compleja en la filogenia eucariota, puesto que los organismos con muchos y pocos intrones no presentan ninguna separación cladística coherente (Collén et al., 2013). Esta situación es debida a escenarios históricos particulares de cada linaje. Por un lado, se han documentado casos de conservación intrónica profunda entre especies o grupos muy distantes, mientras que también se han documentado episodios de ganancia o pérdida masiva de intrones durante la evolución de múltiples linajes eucariotas (Csuros et al., 2011).

El proceso molecular de exclusión de los intrones está catalizado por la maquinaria spliceosomal, que consta de cinco RNAs pequeños (snRNAs) y más de doscientas proteínas (Wahl et al., 2009). La estructura de la mayoría de intrones está compuesta por elementos cuya secuencia es reconocida por dicha maquinaria para la realización de la reacción de *splicing*. Sus elementos básicos son los sitios de splicing a 5' y 3' en los extremos del intrón, la adenosina catalítica del punto de ramificación (*branch point*), y el tracto de polipirimidinas (*polypirimidine tract*) (Irimia and Blencowe, 2012). El resto de la secuencia intrónica es muy variable tanto en contenido como en tamaño (Irimia and Roy, 2008), habiéndose encontrado casos extremos en un mismo genoma que divergen en longitud por más de un millón de pares de bases. En algunos casos, la longitud de ciertos intrones podría estar relacionada con la presencia de elementos reguladores en la secuencia genómica (Irimia et al., 2011b) (artículo anexo 1).

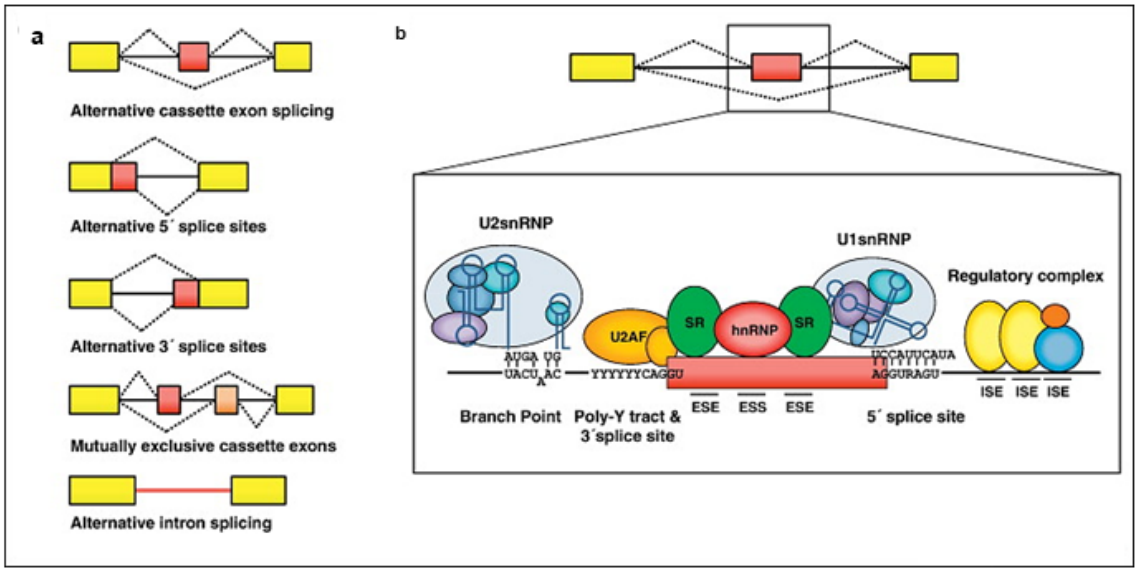

Figura I2 | En inglés; adaptada de Irimia M. et al. 2012. **(a)** Representación de los diferentes tipos principales de eventos de *splicing* alternativo. **(b)** Esquema de los diferentes elementos del genoma, el transcriptoma y el proteoma involucrados en la regulación del proceso de *splicing*.

A pesar de que la reacción de splicing suele ser muy precisa, el spliceosoma es capaz de generar frecuentemente más de una isoforma a partir de un solo locus génico mediante la inclusión diferencial de su secuencia en el tránscrito maduro (Wang et al., 2008). Este fenómeno, que se conoce como splicing alternativo (AS), se ha dividido tradicionalmente en diferentes clases dependiendo del tipo de secuencias implicadas en el proceso, a pesar de que esta clasificación no refleja a menudo la complejidad de algunos eventos. Las principales variantes son la inclusión diferencial de exones enteros (*cassettes exónicos*), el uso de sitios de splicing alternativos a 5' o a 3', eventos de exclusión mutua entre exones e incluso la retención de intrones (Fig I2a). De hecho, esta última clase constituye el tipo de AS más frecuente en la mayoría de clados eucariotas estudiados (Ner-Gaon et al., 2004; Sebé-Pedrós et al., 2013). Así, gran parte de linajes parece emplear este mecanismo para la regulación de los niveles de expresión génica, puesto que la retención intrónica implica frecuentemente la degradación del tránscrito (Braunschweig et al., 2014; Ge and Porse, 2014). Por otro lado, este proceso puede generar en ocasiones tránscritos mensajeros alternativos, especialmente cuando sucede en UTRs o hacia el final de la región codificante. También se han descrito casos de uno o más intrones retenidos que provocan el secuestro del RNA en el núcleo celular (Buckley et al., 2014). Dichos

intrones son eliminados del tránscrito dependiendo de una señal molecular determinada, pasando al citoplasma para ser traducidos en el momento apropiado. Otros casos de retención intrónica han sido relacionados también con el transporte citoplasmático del tránscrito afectado (Buckley et al., 2011) .

Unos pocos grupos filogenéticos presentan también proporciones elevadas de otros tipos de AS, especialmente respecto a la inclusión diferencial de exones *cassette,* como los eumetazoos. Este tipo de regulación también puede afectar a la expresión génica, por ejemplo, mediante la inclusión de codones stop prematuros que provocan la degradación del tránscrito por la vía NMD (*non-sense mediated decay*). Sin embargo, el potencial de este tipo de eventos abarca muchas otras posibilidades. Este proceso genera frecuentemente proteínas con secuencias de aminoácidos parcialmente diferentes, alterando en ocasiones distintos aspectos de su función molecular. Se han descrito isoformas proteicas que difieren en estabilidad, localización celular, actividad enzimática, etc (Kelemen et al., 2013). Recientemente, un análisis global sobre los dominios peptídicos de humano afectados por AS apunta a un impacto frecuente de este proceso en regiones desorganizadas que determinan la afinidad de las interacciones proteicas (Ellis et al., 2012). En resumen, este mecanismo ofrece la posibilidad de ajustar, innovar o incluso antagonizar las funciones moleculares del gen implicado dependiendo del contexto celular.

Impacto funcional de los eventos de *splicing* alternativo.

Resulta muy complicado predecir las consecuencias funcionales de eventos particulares incluso a nivel molecular, siendo necesaria una aproximación experimental para desentrañar su utilidad en el organismo. Hasta la fecha, se han descrito numerosos eventos de *splicing* alternativo con un impacto constatado a nivel celular u organísmico, especialmente en aquellos que se encuentran conservados en más de una especie.

Uno de los casos más estudiados de evento funcional y conservado determina la identidad sexual en varias especies de insectos (Gempe et al., 2009). En embriones de *Drosophila* dotados de cromosomas sexuales homólogos, se produce la inclusión del cuarto exón en

los tránscritos del factor de transcripción *doublesex*. Las dos isoformas se unen a las mismas regiones de ADN, pero presentan funciones bioquímicas generalmente opuestas respecto a la activación o represión de sus genes diana (Coschigano and Wensink, 1993). La presencia de la isoforma que incluye el cuarto exón en las hembras reprime la transcripción del programa de diferenciación sexual masculino. A pesar de que no todos los hexápodos presentan el mismo mecanismo, la aparición de esta regulación ha sido trazado hasta la base del clado, apoyando el AS de *doublesex* como el sistema molecular de determinación sexual ancestral en insectos (Price et al., 2015). Interesantemente, tanto las cascadas activadoras de esta regulación como los elementos activables por dicho factor de transcripción se encuentran mucho menos conservados entre distintos grupos de insectos (Shukla and Nagaraju, 2010).

Otro evento de *splicing* funcional de origen incierto es el descrito en algunas especies de vertebrados en diversos miembros de la familia *Fgfr* (Fgfr1, Fgfr2 y Fgfr3) que codifican para receptores de los ligandos *Fgf*. Estos genes presentan dos exones alternativos mutuamente excluyentes, llamados IIIb y IIIc, que codifican parte del tercer dominio inmunoglobulina de la proteína (Turner and Grose, 2010) (Fig. I3a). Ambas isoformas difieren en su capacidad de interacción respecto a los diferentes ligandos Fgf (Miki et al., 1992). Las isoformas que incluyen el exón IIIb, expresadas en células epiteliales, muestran una mayor afinidad por los ligandos secretados por células mesenquimales (Fgf3, Fgf7, Fgf10, etc) (Fig. I3b). La situación es la inversa para las células mesenquimales, cuyos receptores contienen el exón IIIc, proporcionándoles más afinidad por ligandos provenientes de células epiteliales (Fgf2, Fgf4, Fgf8, etc). Este sistema contribuye a generar una señalización cruzada entre tejidos epiteliales y mesenquimales de diversos órganos en desarrollo (Figura I3). En consecuencia, la morfogénesis de estructuras como las extremidades, los pulmones o el oído interno se ve severamente afectada tras la eliminación selectiva del exón IIIb en tejidos epiteliales de ratón (De Moerlooze et al., 2000; Pirvola et al., 2000) (Fig I3c).

Por otro lado, también se han descrito eventos de AS específicos de especie o de grupos muy reducidos con roles claramente funcionales. Uno de los más interesantes por su papel adaptativo se encuentra en el gen TRVP1, un sensor térmico involucrado en la detección

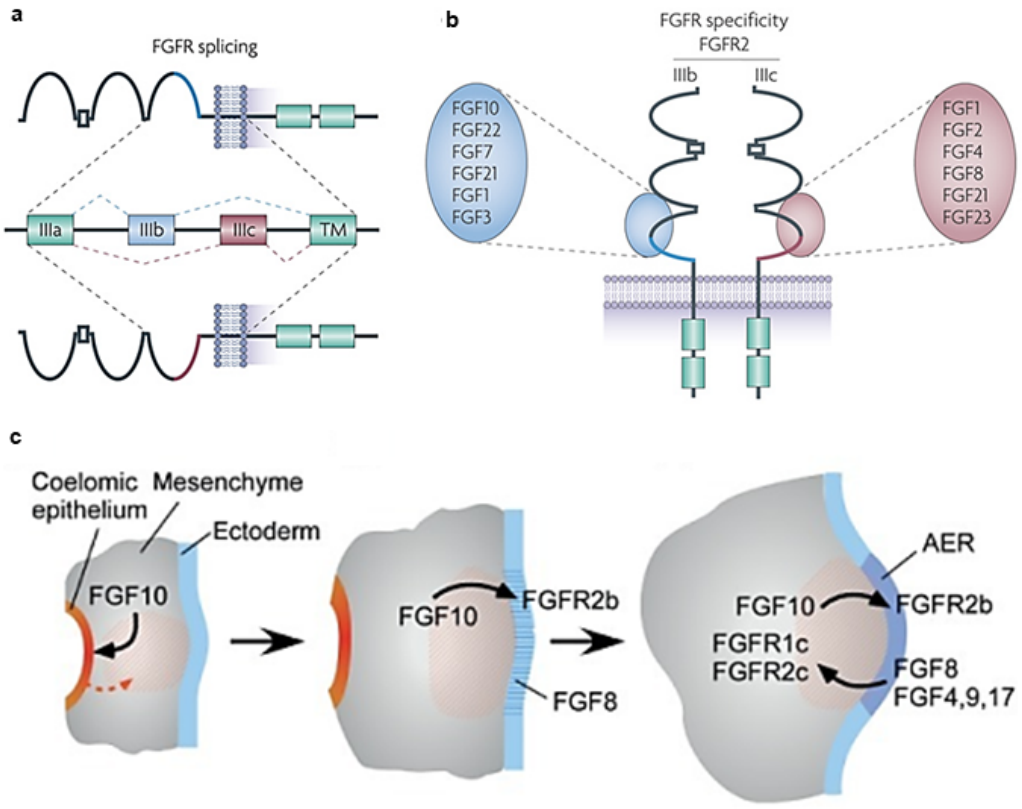

Figura I3 | En inglés. **(a,b)** Adaptada de Turner et al. 2010. **(a)** Esquema del evento de splicing mutuamente excluyente de los genes Fgfr1, Fgfr2 y Fgfr3 de mamíferos, que produce la inclusion del exón IIIb en epitelios y el exon IIIc en mesénquima. **(b)** Representación de aquellos ligandos con mayor afinidad para las dos isoformas producidas mediante la regulación post-transcripcional de dicho evento en el gen *Fgfr2*. **(c)** Adaptada de Ornitz et al. 2015. Esquema de las interacciones señalizadoras mediante la via FGF durante el desarrollo del primordio de la extremidad en ratón.

de temperaturas nocivas para el organismo (~40ºC) (Gracheva et al., 2011). Este gen contiene un exón alternativo compartido por diversos quirópteros cuya inclusión genera una proteína más corta en la región C- terminal. Esta isoforma, que reduce el umbral de detección térmico hasta los 31ºC, se expresa a unos niveles prácticamente residuales en los órganos sensoriales de murciélagos que se alimentan de frutas o insectos. Sin embargo, la inclusión de este exón particular está potenciada específicamente en el ganglio trigémino del vampiro *Desmodus rotundus.* Dicha estructura contiene las fibras sensoriales responsables de la detección de radiación infrarroja (>29ºC) emitida por la sangre caliente de sus presas. Por tanto, la regulación precisa de este evento de *splicing* está probablemente asociada a una adaptación evolutiva reciente de esta especie hematófaga.

Dinámicas evolutivas globales de la regulación génica mediante *splicing* alternativo.

A pesar de los casos descritos de eventos particulares de *splicing* con regulación similar en clados relativamente grandes, estudios transcriptómicos amplios apuntan hacia escenarios de baja conservación global. Por ejemplo, la comparación de los niveles de inclusión de exones cassette en distintos órganos de mamíferos y otros vertebrados reveló mayor similitud de los patrones de *splicing* entre los tejidos de una misma especie que entre órganos homólogos en general (Barbosa-Morais et al., 2012; Merkin et al., 2012). Este resultado es opuesto al obtenido mediante el cotejo interespecífico de los patrones de expresión génica, lo que sugiere tasas evolutivas comparativamente más elevadas en la regulación por AS. De hecho, un análisis reciente utilizando cinco especies de *Drosophila* ha descrito un resultado muy similar (Gibilisco et al., 2016). La repetición de este escenario en otros linajes podría apuntar a un fenómeno general respecto a las velocidades evolutivas relativas de la regulación génica por transcripción y por *splicing*.

No obstante, resulta adecuado recalcar que también se han descrito conjuntos conservados de exones alternativos cuya inclusión es regulada coordinadamente durante algún proceso biológico o en un tipo celular concreto. Por ejemplo, el corazón de mamíferos y aves sufre cambios dramáticos en los niveles de inclusión de una amplia batería de exones después del nacimiento (Kalsotra et al., 2008). Por otro lado, el sistema nervioso central constituye el órgano de vertebrados con las tasas más elevadas de similitud entre especies respecto a sus patrones de *splicing* alternativo. Especialmente conservada se encuentra la regulación de un programa de exones alternativos de entre 3 y 27 nucleótidos, cuya inclusión está mayormente potenciada en neuronas (Irimia et al., 2014). Estos microexones, a pesar de constituir alrededor del 1% de eventos de AS totales, representan un tercio de los exones neurales conservados entre humano y ratón que generan isoformas proteicas.

Mecanismos moleculares de regulación del splicing alternativo.

Como se ha mencionado anteriomente, la función celular u organísmica de las variantes de *splicing* está íntimamente ligada a una regulación adecuada en determinados contextos celulares. Esta regulación precisa de diversos factores para controlar los niveles de inclusión exónica. Se han descrito múltiples tipos de elementos moleculares que modulan el reconocimiento de la estructura génica por el spliceosoma y permiten regular la proporción de las distintas isoformas producidas por un gen (Wang et al., 2015). Entre estos componentes, destacan por un lado determinadas secuencias de bases situadas normalmente en los exones y/o intrones que forman parte del evento regulado (elementos en *cis*). Estas secuencias, una vez transcritas a RNA, constituyen sitios de unión para determinadas proteínas (elementos en *trans*) capaces de interaccionar con el spliceosoma directa o indirectamente modificando su actividad. Dichas proteínas auxiliares, conocidas como factores de *splicing*, pueden provocar tanto un incremento como una disminución en los niveles de inclusión exónica dependiendo del evento y el contexto celular (Fu and Ares, 2014). El nivel de expresión variable de este conjunto de factores de *splicing* influye decisivamente en el balance global de isoformas en los distintos tipos celulares (Fig. I4a).

Estos factores proteicos que intervienen en la regulación de eventos de AS acostumbran a presentar niveles de expresión muy variables en distintos órganos o tipos celulares (Grosso et al., 2008). Mientras que algunos de ellos se encuentran en niveles suficientemente elevados para ejercer su actividad en un conjunto relativamente amplio de tejidos, otros factores presentan patrones de expresión muy restringidos. En este sentido, se han descrito casos de proteínas reguladoras cuya expresión únicamente es detectada en un tipo celular (Raj et al., 2014). A pesar de la variabilidad respecto a la proporción de órganos distintos donde se expresa cada uno de estos péptidos, buena parte de ellos son referidos en la bibliografía como factores de *splicing* específicos de tejido. Por otro lado, aquellos factores con actividad en más de un tipo celular pueden ejercer actividades reguladoras distintas dependiendo de la presencia cambiante de cofactores en cada contexto celular (Vuong et al., 2016) (Fig. I4b). De hecho, esta combinatoria particular de factores en cada tejido, ligada a un estado regulador determinado, resulta muy similar a la descrita tradicionalmente para los factores de transcripción.

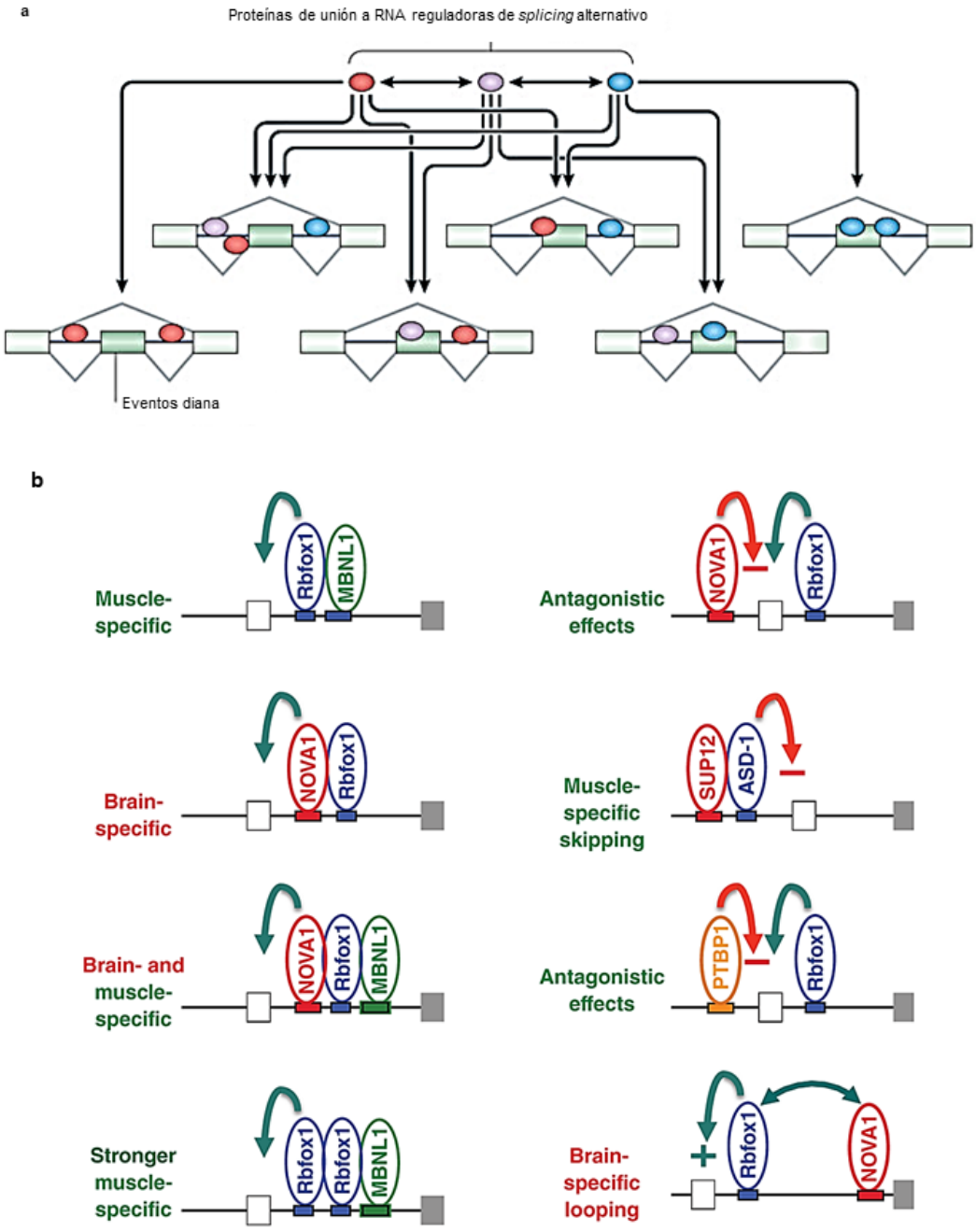

Figura I4 | (a) Adaptado de Vuong C.K. et al. 2016. Esquema sobre la cooperación específica en cada evento de distintos factores de splicing para generar el transcriptoma de un tipo cellular dado. **(b)** En inglés; adaptado de Gonvoy J. et al. 2017. Representación de las interacciones específicas de tejido que provocan la inclusion diferencial de distintos exones en cerebro, músculo o ambos. La flechas verdes simbolizan actividad potenciadora, mientras que las rojas son silenciadoras.

Factores de *splicing* alternativo involucrados en el desarrollo embrionario.

Mientras que algunos de estos factores regulan una cantidad notablemente reducida y específica de eventos de AS (Traunmuller et al., 2016), otros ejercen su impacto funcional sobre numerosas dianas. Debido a la influencia extensa de estos últimos casos sobre el transcriptoma celular, a menudo se hace referencia al conjunto de sus eventos regulados como programas de AS. Bajo esta nomenclatura también subyace la idea de que estos grupos de eventos sujetos a un regulador en *trans* determinado están frecuentemente involucrados en funciones celulares comunes. Según esta perspectiva, la expresión de un factor determinado en un contexto celular dado produciría las isoformas propicias para llevar a cabo procesos fisiológicos concretos (Vuong et al., 2016). Si bien este modelo puede pecar en ocasiones de excesivamente simplista o generalista, probablemente resulta acertado para subconjuntos amplios de los eventos diana. De esta forma, un factor dado puede estar implicado en más de un rol fisiológico determinado tanto en diferentes órganos como dentro de un mismo tipo celular (Raj and Blencowe, 2015). En esta línea, se han empezado a identificar familias de factores de *splicing* cuyas funciones están relacionadas con procesos del desarrollo variados, especialmente en organismos modelo.

Es el caso, por ejemplo, de las familias génicas *Nova* (neuro-oncological ventral antigen) y *RbFox* (RNA binding protein, Fox1-homolog). Los factores que forman parte de estas familias en mamíferos (*Nova1, Nova2, RbFox1, RbFox2* y *RbFox3*) se expresan durante el desarrollo del sistema nervioso en células cuyo destino celular ya ha sido determinado como neuronal (Jensen et al., 2000; Underwood et al., 2005). Entre los principales papeles funcionales descritos para la familia *Nova* en estos tejidos se encuentran la migración de progenitores mitóticos en la médula espinal, la laminación cortical o el disparo de las neuronas motoras (Gallego-Paez et al., 2017) (Fig. I5a). La familia *RbFox* está involucrada también en la arquitectura del córtex cerebral, así como en la formación de dendritas en neuronas excitatorias o el crecimiento del cerebelo (Gehman et al., 2012, 2011; Hamada et al., 2015). De hecho, ambos factores regulan el *splicing* de algunos eventos diana comunes, con interacciones tanto sinérgicas, como aditivas o antagónicas (Zhang et al., 2010). Por otro lado, estos genes también desempeñan roles fisiológicos en órganos no neurales de vertebrados. La família Nova está involucrada en termogénesis en

el tejido adiposo (Vernia et al., 2016), así como en la formación del lumen vascular durante la angiogénesis (Giampietro et al., 2015). Por su parte, algunos genes RbFox están implicados en procesos como la fusión de mioblastos (Singh et al., 2014) (Fig. I5b) o la función cardíaca (Gallagher et al., 2011; Gao et al., 2016).

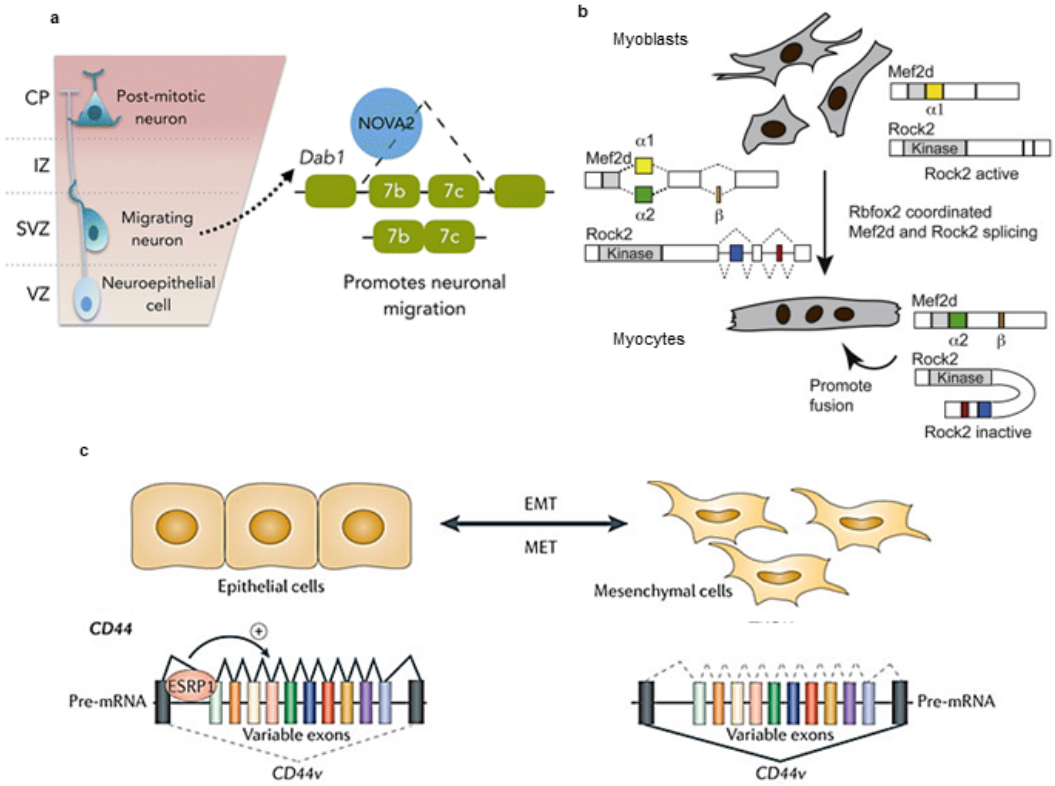

Figura I5 | En inglés. **(a)** Adaptado de Gallego-Paez L.M. et al. 2017. *Nova2* promueve la migración en la corteza cerebral de ratón de células ya determinadas como neuronas mediante la regulación de las isoformas del gen *Dab1*. **(b)** Adaptado de Singh R.K. et al. 2014. La actividad de *RbFox2* en mioblastos murinos en cultivo promueve la fusión de estas células para formar fibras musculares multinucleadas a través del *splicing* de los genes *Mef2d* y *Rock2*. **(c)** Adaptado de Kalsotra A. et al. 2011. El gen Esrp1 promueve el fenotipo epithelial en diversos cultivos celulares humanos mediante la regulación de la inclusion exónica en una batería de genes, como en el caso de CD44.

Otro tipo de variabilidad respecto la expresión tisular es la observada en famílias de factores de *splicing* como *Esrp*. Los dos parálogos encontrados en mamíferos, *Esrp1* y Esrp2, se expresan en ratón en múltiples órganos de manera muy dinámica durante el embrionario (Revil and Jerome-Majewska, 2013). Sin embargo, su expresión se ha

considerado específica de tipo celular en un sentido histológico, ya que se describió restringida a tejidos epiteliales. La función de ambos genes fue primeramente relacionada con la capacidad de influir en transiciones epitelio-mesénquima en cultivos celulares humanos (Warzecha et al., 2010). En estos estudios, una interrupción de la actividad de *Esrp1* produjo una pérdida de adhesión celular y un incremento en su motilidad (Fig. I5c). Coherentemente, muchos de los eventos de *splicing* regulados por estos factores suceden en genes involucrados en adhesión celular y migración (Dittmar et al., 2012). La generación reciente de mutantes murinos para *Esrp1* y *Esrp2*, tanto por separado como conjuntamente, ha revelado su implicación en múltiples procesos morfogenéticos (Bebee et al., 2015). Los fenotipos observados se han adjudicado presumiblemente a una distorsión de diversas interacciones organogenéticas entre tejidos epiteliales y mesenquimales.

La implicación de estos programas de AS en diversos procesos mediante la modulación de propiedades o roles celulares concretos, coloca a sus factores reguladores como miembros relevantes en las redes génicas del desarrollo. Puesto que la modificación de dichas redes es responsable del cambio estructural entre linajes, su comparativa puede aportar pistas sobre la base molecular de la evolución organísmica. Por tanto, es importante entender las similitudes y diferencias en la expresión y función ontogenética de los factores de *splicing* alternativo, así como entre los conjuntos de eventos que regulan a nivel transcriptómico. Este tipo de aproximación permitirá valorar tanto la plasticidad evolutiva de los programas de AS como su conexión con procesos celulares ligados al desarrollo de caracteres fenotípicos. Dicha perspectiva es capaz de conectar más comprensiblemente los distintos niveles de organización biológica en comparación con el inventariado de isoformas totales en cada especie.

Evolución y características de los organismos deuteróstomos.

La utilización de un conjunto de especies anidadas respecto a su separación cladística resulta conveniente para valorar la magnitud de los cambios evolutivos a diferentes escalas filogenéticas. Este uso estratégico de organismos pertenecientes a grupos relativamente lejanos pero relacionados permite también la inferencia de escenarios

macroevolutivos más precisos. Dado que la mayor parte de datos publicados para los factores de *splicing* pertenecen a animales vertebrados (y en especial, mamíferos), en la presente tesis se ha trabajado con especies de este grupo y de aquellos linajes más cercanos a ellos. De este modo, los organismos que forman parte del trabajo experimental son cordados y equinodermos. El grupo filogenético que incluye a estos dos filos y a los hemicordados, grupo hermano de los equinodermos, son los deuteróstomos (Deuterostomia), cuyo origen se haya probablemente en el periodo Ediacárico (635-542 Ma). Un esquema de las principales relaciones filogenéticas de este grupo puede visualizarse en la Figura I6 (Sansom et al., 2010).

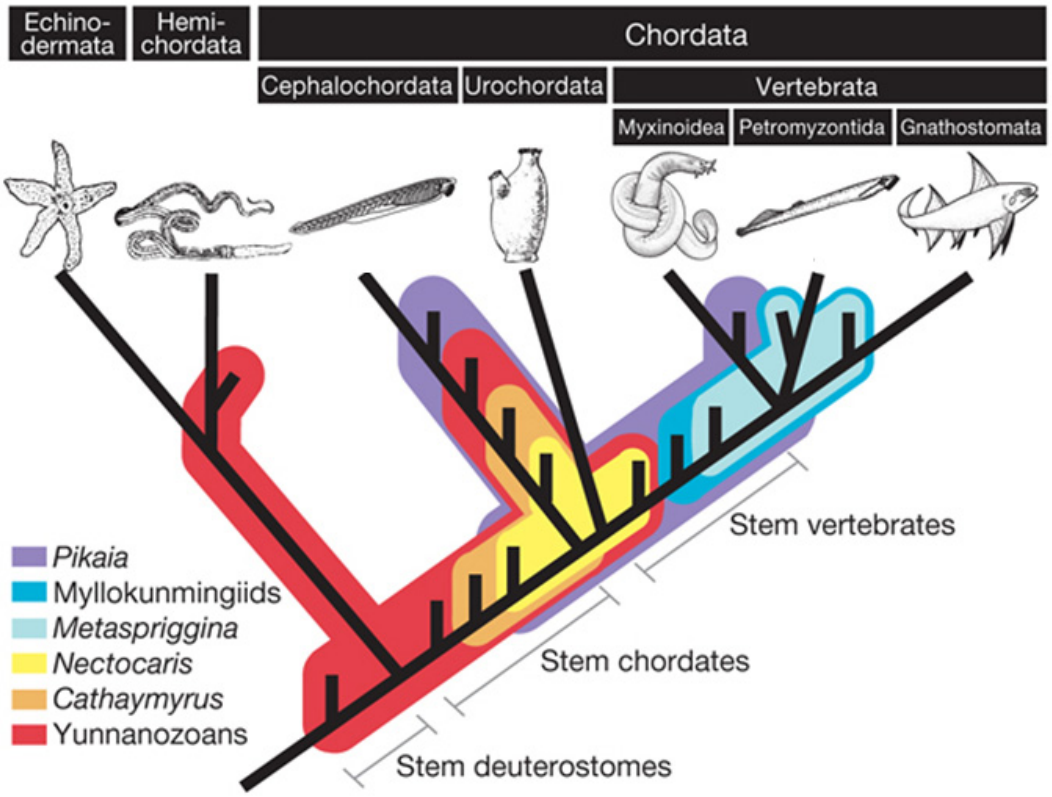

Figura I6 | En inglés; adaptado de Sansom R. et al 2010. Relaciones taxonómicas de los principales grupos de animales deuteróstomos. Las ramas cortas constituyen organismos extinguidos. Cada color representa la gama de posibles posiciones filogenéticas de diferentes fósiles cámbricos. Debido a esta incertidumbre, resulta complicado hacerse una idea precisa de muchos de los caracteres estructurales del ancestro de cada linaje.

La disparidad de planes corporales de los tres filos constituyentes complica la reconstrucción de las características corporales de su último ancestro común. Los deuteróstomos comparten la formación del ano a partir del blastoporo, motivo por el que recibieron su nombre taxonómico. No obstante, la deuterostomía ontogénica no constituye una característica única de este grupo, pues también está presente en algunos linajes de protóstomos e incluso se ha propuesto que podría representar la condición ancestral de bilaterales (Martín-Durán et al., 2012). Aun así, parece existir consenso al menos sobre un carácter sinapomórfico hallado en individuos adultos, embriones o fósiles de los tres clados: las hendiduras faríngeas. Se ha llegado incluso a relacionar este rasgo con un agrupamiento génico conservado de cuatro factores de transcripción expresados coordinadamente durante el desarrollo de la faringe en embriones de vertebrados y hemicordados (Simakov et al., 2015). Además, algunos autores establecen también un origen común entre el cartílago acelular faríngeo de hemicordados y anfioxo (Rychel et al., 2006). Otra estructura propuesta como homóloga entre cordados y hemicordados es el cordón nervioso dorsal, aunque esta relación está mucho más discutida (Kaul and Stach, 2010).

En general, numerosos caracteres no presentan una correspondencia anatómica clara entre los distintos filos de deuteróstomos. Sin embargo, ciertas estructuras difícilmente homologables entre grupos muestran una similitud notable respecto a sus bases moleculares subyacentes. Un caso interesante es el de las redes génicas descritas en las regiones que rodean los organizadores secundarios del sistema nervioso central de vertebrados (Pani et al., 2012). Muchos de los genes implicados parecen seguir una lógica reguladora muy parecida en torno a los límites de la proboscis, el collar y el tronco de embriones hemicordados. A pesar de haber sido reclutadas para la formación de estructuras distintas, es probable que un conjunto de interacciones génicas esenciales se haya mantenido estable para establecer fronteras morfológicas en el eje anteroposterior. Este caso ilustra la posibilidad de desacoplamiento entre programas genéticos razonablemente conservados y los caracteres organísmicos que producen en linajes evolutivos distantes.

A continuación, una breve descripción de los principales organismos deuteróstomos empleados en la presente tesis, incluyendo sus procesos ontogénicos más estudiados en el apartado experimental:

Strongylocentrotus purpuratus: Perteneciente al filo de los equinodermos, en esta tesis se ha trabajado con el erizo de mar púrpura (*Strongylocentrotus purpuratus),* cuya distribución natural se sitúa en las costas del Océano Pacífico norteamericano. Los individuos adultos presentan pentamerismo, con un fino epitelio recubriendo un endoesqueleto formado por carbonato cálcico. El esqueleto está formado por placas que se extienden desde la boca hasta el ano y que presentan múltiples agujeros a través de los que emergen los pies ambulacrales. Estos pies ambulacrales, revestidos de musculatura, forman parte de un sistema vascular hidráulico conectado al exterior a través del madreporito, ubicado cerca del ano. El órgano ambulacral confiere movilidad al animal, además de ayudarle a conducir los alimentos hasta la boca. Ésta, situada en la parte inferior, contiene un órgano masticatorio formado por una compleja estructura esquelética y muscular consistente en un armazón pentagonal, conocida como linterna de Aristóteles. Su sistema nervioso consiste en un anillo neural que rodea la boca del que surgen cinco nervios parejos a los canales radiales del sistema ambulacral (Fig. I7a).

Sin embargo, dicho plan corporal no aparece hasta pasado un proceso de metamorfosis, pues las primeras fases del desarrollo generan una larva con simetría bilateral. Este fenómeno es extensible a todas las clases de equinodermos, si bien cada clase presenta un tipo de larva particular en el sentido morfológico. En *Strongylocentrotus*, el zigoto se compartimentiza a través de divisiones celulares siguiendo un patrón radial. Aproximadamente hacia la sexta división, las capas germinales ya han sido especificadas. El estadio de blástula se alcanza hacia las 24 horas post-fertilización (hpf) a una temperatura de 15ºC. Hacia las 48hpf el embrión ha alcanzado un estadio de gástrula avanzado, y a las 72hpf ya es reconocible la estructura en forma de prisma característica de la larva pluteus.

Uno de los primeros procesos morfogenéticos reconocibles en el estadio de blástula es el ingreso de las células mesenquimales primarias (PMCs) en el blastocele mediante una

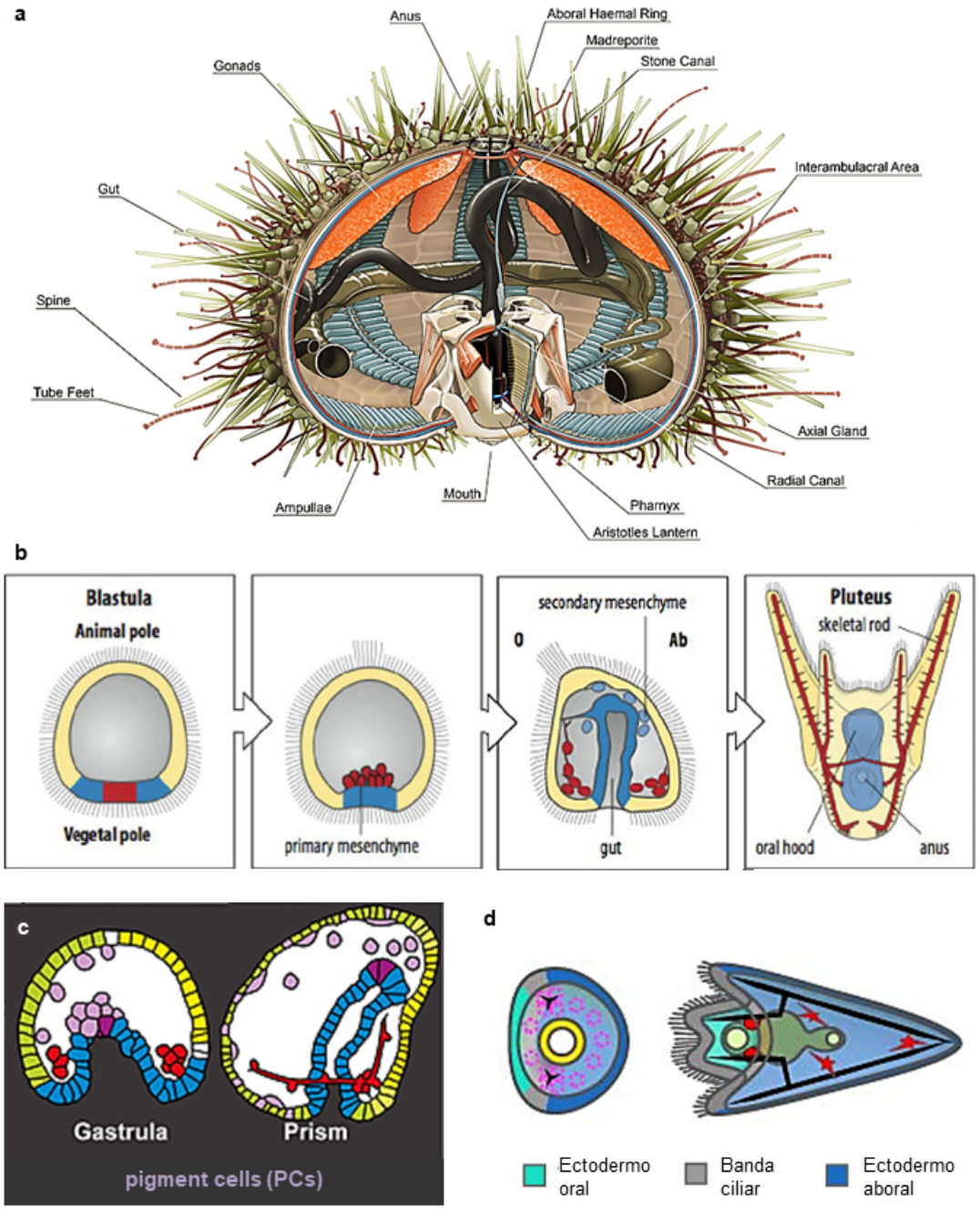

Figura I7 | (a) En inglés. Adaptado de Abiogenesis. Dibujo de los principales órganos de un erizo de mar adulto. **(b)** Adaptado de Staveley 2011. Esquema del desarrollo de un embrión euequinoideo. Las células rojas marcan el mesénquima primario, las azules, el secudario. O, oral; Ab, aboral **(c)** Adaptado de Gildor 2015. Dibujo que muestra la integración de las células pigmentarias (color malva) en el ectodermo aboral (color verde). **(d)** Adaptado de Lapratz et al. 2009. Representación por colores de las tres regiones primordiales del ectodermo en una gastrula y una larva plúteus.

transición de epitelio a mesénquima (Ettensohn, 2009). Una vez ingresadas, las PMCs forman un sincitio alrededor de la invaginación endodérmica y finalmente excretan una matriz biomineral que constituirá el esqueleto larvario (Fig. I7b). El resto de células mesodérmicas permanece en forma epitelial hasta que comienza la gastrulación, cuando ingresan también en el blastocele junto a la invaginación endodérmica y quedan dispuestos alrededor de la punta del arquénteron (McClay, 2011) (Fig. I7b). Este conjunto de tejidos, conocido como células mesenquimales secundarias (SMCs) o mesodermo no-esqueletogénico (NSM), se divide básicamente en cuatro grupos: precursores de células pigmentarias, blastocelares, de las bolsas celómicas, y miogénicas. Estas últimas, después de un proceso de fusión celular, forman las fibras musculares que rodean al esófago en la fase pluteus (Andrikou et al., 2013). Por su parte, las precursoras de las células pigmentarias migran durante las primeras fases de la gastrulación hacia el ectodermo aboral, en el que se integran mediante un proceso de transición mesénquima-a-epitelio (MET) (Gibson and Burke, 1985) (Fig. I7c). El ectodermo, que constituye la superficie del embrión, puede dividirse principalmente en aboral, oral, y banda ciliar (Lapraz et al., 2009). Esta última estructura se distribuye en forma de anillo en el estadio de blástula, separando a las dos otras regiones (Fig. I7d). En la banda ciliar se formarán las neuronas, así como los cilios que la larva usará para nadar. El ectodermo oral forma parte de la región donde se formará la apertura del tracto digestivo anterior, mientras que el ectodermo aboral constituirá la mayor superficie del embrión durante la fase pluteus.

Branchiostoma lanceolatum: El término anfioxo se aplica a aquellos animales pertenecientes al subfilo de los cefalocordados. Este grupo constituye una rama basal dentro de los cordados actuales puesto que los otros dos clados, los urocordados y los vertebrados, son grupos hermanos (Delsuc et al., 2006). La anatomía del anfioxo adulto presenta múltiples puntos de similitud respecto a la de un vertebrado, aunque de mayor simplicidad general (Fig. I8a). Estos animales poseen características típicas del prototipo cordado, como un cordón nervioso dorsal, una notocorda subyacente, un sistema digestivo ventral, perforaciones faríngeas, musculatura axial agrupada en bloques, o la cola post-anal. Además, también presentan órganos supuestamente homólogos a la glándula tiroides y la adenohipófisis de vertebrados, conocidos como el endostilo y la foseta pre-oral, respectivamente. Sin embargo, carecen de muchos de los órganos

compartidos por los vertebrados, como sistemas sensitivos pares (ojos, oídos), esqueleto interno o diversas estructuras derivadas de la cresta neural (cráneo).

Los anfioxos son animales filtradores que viven en zonas costeras en fondos arenosos. Durante su alimentación, a menudo adoptan una posición en la que entierran gran parte de su cuerpo, dejando al extremo más anterior sobresalir del bentos. Anatómicamente, un capuchón oral cubre la obertura anterior de la faringe, del que sobresalen los cirros bucales que impiden la entrada de grandes partículas. El aparato filtrador faríngeo presenta hendiduras para permitir la salida de una corriente de agua unidireccional hacia el atrio. Las partículas alimenticias se adhieren a una banda dorsal en el surco epibranquial mediante una sustancia mucosa, segregada por el endostilo y las células secretoras de las barras faríngeas. A continuación, el alimento pasa al tubo digestivo, donde es objeto de un proceso de desmenuzamiento mecánico. Los fragmentos más pequeños son conducidos a través de cilios hacia el ciego digestivo, donde se produce la absorción de los nutrientes, mientras que el material desechado sale al exterior a través del ano. El agua acumulada en el atrio es expulsada a través del atrioporo.

Los huevos del anfioxo contienen muy poco vitelo, motivo que favorece un proceso de segmentación aparentemente sencillo. Las divisiones de los blastómeros, cada vez menos sincrónicas, conducen a una blástula de 32 células que rodean al blastocele lleno de líquido. La gastrulación tiene lugar por la invaginación de la pared del polo vegetativo. El embrión transiciona de una capa de blastómeros a una doble capa laminar de células que forman el ectodermo y el endomesodermo (Fig. I8c). Por su lado, el epitelio ventral del arquénteron se replegará para formar el tracto digestivo, la faringe y otros derivados endodérmicos. A partir de evaginaciones del endomesodermo, se forman unos pares de saquitos mesodérmicos cuyas cavidades darán lugar al celoma (Terazawa and Satoh, 1997) . El mesodermo situado en la línea media dorsal entre los saquitos se diferencia en el cordomesodermo, que originará el primordio de la notocorda central y dos secciones laterales que darán lugar a los somitas (Mansfield et al., 2015) (Fig. I8d). El cordomesodermo estimula a su vez la generación de una placa neural en el ectodermo superpuesto, que se convertirá en un tubo neural después de que ambos lados epidérmicos se fusionen en la línea media durante la neurulación (Holland and Holland, 2001).

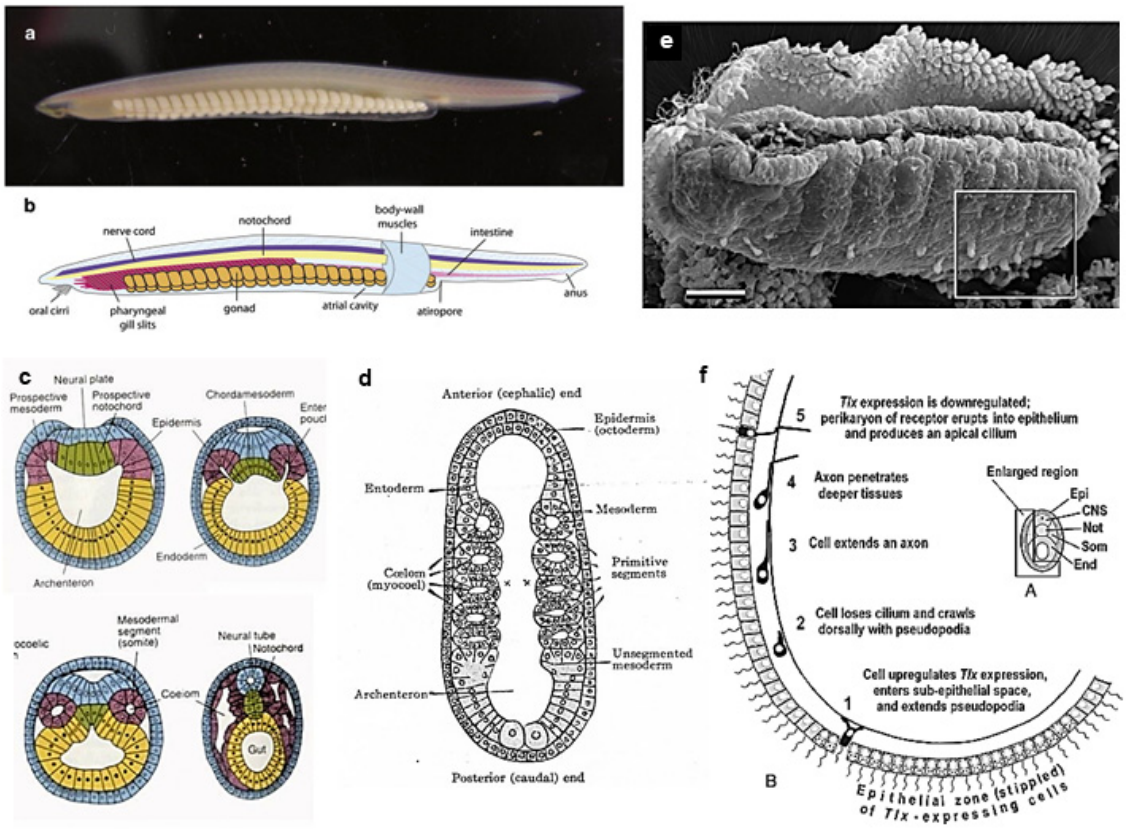

Figura I8 | En inglés. **(a,b)** Adaptado de Bertrand et al 2011. **(a)** Fotografía de un especímen de Branchiostoma lanceolatum. **(b)** Dibujo del plan corporal de un anfioxo adulto y sus principales órganos. **(c)** Adaptado de I. Stanek. Esquema representando el desarrollo y separación de las capas germinales en estadíos consecutivos de un embrión de anfioxo. El ectodermo está coloreado en azul, el endodermo en amarillo, el mesodermo somítico en rojo y la notocorda en verde. Los dibujos simulan un corte transversal. **(d)** Adaptado de Hatscheck 1881. Representación coronal de la disposición de las capas germinales en una néurula de anfioxo. **(e-f)** Adaptado de Kaltenbach et al. 2010. **(e)** Fotografía obtenida por microscopía electronica de barrido de una néurula de anfioxo que ha sido despojada de la epidermis. El recuadro marca las células procedentes del ectodermo ventral que migran hacia posiciones dorsales. **(f)** Representación gráfica del proceso de migración e integración de las células determinadas como neuronas epidérmicas sensoriales.

Uno de los procesos más peculiares durante la embriogénesis del anfioxo es la formación de las neuronas epidérmicas sensoriales, que formarían el sistema nervioso periférico. Los precursores de dicha población neuronal se originan en una zona del ectodermo ventral, delaminan al especio sub-ectodérmico y migran hacia regiones dorsales del embrión, donde se integran en la epidermis (Benito-Gutiérrez et al., 2005; Kaltenbach et al., 2009) (Figura I8e,f). Algunos autores que han estudiado el programa molecular

involucrado en el desarrollo de estas células han sugerido similitudes respecto a los mecanismos genéticos utilizados por poblaciones del sistema nervioso periférico en vertebrados, especialmente los derivados de las placodas (Lu et al., 2012).

El tubo neural del embrión de los cefalocordados no presenta las deformaciones complejas propias del sistema nervioso central (CNS) de los vertebrados, donde las diferentes partes exhiben diferencias morfológicas claras. También están ausentes los organizadores secundarios liberadores de morfógenos responsables de una parte importante de la diferenciación anatómica en vertebrados, como la ZLI (*zona limitans intrathalamica*) o el istmo (Irimia et al., 2010a). Sin embargo, un análisis detallado de la placa neural del estadío de néurula media de anfioxo ha revelado una alta complejidad en su genoarquitectura, incluyendo la conservación de la expresión relativa de diversos marcadores respecto al *bauplan* de vertebrados (Albuixech-Crespo et al., 2017) (artículo anexo 2). Una de las conclusiones más interesantes de dicho artículo es la identificación en anfioxo de una región homóloga al tálamo, el pretecho y el mesencéfalo, cuyo desarrollo depende de la ZLI y el istmo en vertebrados. Como se ha mencionado anteriormente, en hemicordados se han descrito programas moleculares muy similares a los de los organizadores secundarios de vertebrados (Pani et al., 2012). Además, se han encontrado *enhancers* del morfógeno de la ZLI (*sonic hedgehog*) en regiones genómicas homólogas en vertebrados y *Saccoglossus* que son funcionalmente intercambiables (Yao et al., 2016). Estos datos han alentado un debate sobre si los organizadores secundarios del CNS podrían haber estado presentes en el último ancestro de los cordados actuales y perdidos secundariamente en el linaje de los cefalocordados. De ser así, el sistema nervioso del anfioxo podría representar una simplificación estructural respecto a los cordados troncales.

Ciona intestinalis: Las ascidias son animales sésiles pertenecientes al subfilo de los urocordados, grupo hermano de los vertebrados. Una de las características más representativas de este clado es la túnica, una substancia parecida a la celulosa segregada por la epidermis que forma la pared del cuerpo en individuos adultos. Entre estas paredes se encuentran el cestillo branquial, una amplia cavidad atrial y las vísceras. Existe un sifón inhalante y otro exhalante para la entrada y salida respectivas de una corriente de

agua que circula por el animal y contiene el plancton del que se alimenta. Las hendiduras branquiales filtran el agua hacia el atrio, localizado entre el cestillo y la túnica. El endostilo, un surco medioventral del cestillo branquial, produce una sustancia mucosa a la que se adhieren las partículas en suspensión, de manera muy similar al anfioxo. Unas hileras de cilios recogen el moco cargado de alimento y lo conducen a la lámina dorsal, que a su vez la dirige al intestino. El sistema nervioso consiste en un ganglio cerebroideo situado entre los sifones del que parten nervios hacia éstos, las branquias y los órganos viscerales. Las bandas musculares lisas que corren a lo largo del cuerpo y de los sifones pueden contraerse para cambiar la forma y el tamaño del adulto.

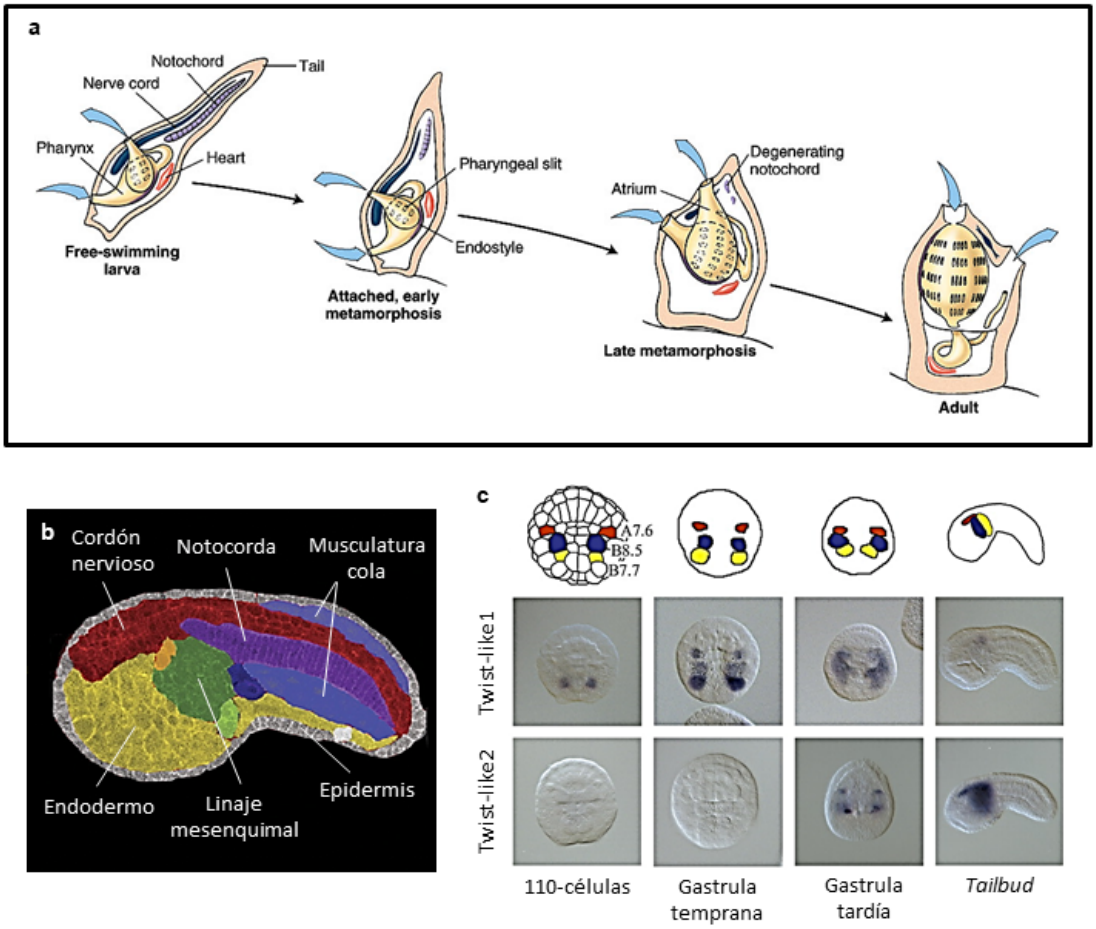

Figura I9 | (a) En inglés; adaptado de Hickman et al. 1993. Representación de la metaforfósis típica de las ascídias, que sucede después de que las larvas se hayan fijado a un sustrato. **(b)** Adaptado de Shi et al. 2005. Tejidos embrionarios de un embrión de *Ciona intestinalis* en el estadío de *tailbud* temprano. **(c)** Adaptado de Imai et al. 2003. Expresión en el linaje mesenquimal de los genes *Twist-like* de C. intestinalis durante las primeras fases del desarrollo embrionario. *Twist-like1* es el primero en iniciar su transcripción, y de hecho activa la expresión de Twist-like2 en gastrula tardía antes de dejar de transcribirse en el estadío *tailbud*.

Esta organización corporal puede recordar poco a la de un vertebrado o incluso al prototipo cordado. No obstante, la fase embrionaria de las ascidias resulta mucho más semejante (Passamaneck and Di Gregorio, 2005) (Fig. I9b). Estos animales presentan una larva planctónica con capacidad natatoria cuya función es la de encontrar un sustrato adecuado al que fijarse mediante unas papilas adhesivas. Los embriones desarrollan un tubo neural dorsal e incluso una vesícula sensorial, además de un órgano fotorreceptor (el ocelo) y un sensor de balance gravitatorio (el otolito). Estos órganos constituyen un supuesto equipo de navegación implicado en la orientación de la larva. Durante la ontogénesis, también presentan una notocorda turgente en la cola, que carece de células vacuoladas. Parejas a esta notocorda se ubican las células musculares estriadas, que se contraen a la vez a cada lado para doblar la cola. Una vez adheridas al sustrato, las larvas comienzan un proceso de metamorfosis absorbiendo las células de la cola, incluyendo los músculos, la notocorda, parte del cordón nervioso y la epidermis (Holland, 2016) (Fig I9a).

Recientemente, estudios embriológicos en *Ciona intestinalis* han revelado nuevos caracteres o tipos celulares en común con vertebrados, que se pensaban exclusivos de estos últimos. Por ejemplo, se han descrito células con doble función quimiosensorial y neurosecretora que son candidatas a provenir del mismo tipo celular ancestral que algunas neuronas derivadas de las placodas sensoriales de vertebrados (Abitua et al., 2015). También se ha propuesto que determinadas células del borde de la placa neural podrían constituir una cresta neural rudimentaria que da lugar tanto a células pigmentarias como a neuronas migratorias periféricas, de manera similar a vertebrados (Abitua et al., 2012; Stolfi et al., 2015). Por otro lado, las ascidias también presentan tipos celulares peculiares durante la embriogénesis, como el linaje mesenquimal (Fig. I9c). Dicho tejido proviene de tres pares de blastómeros en el estadio de 110 células (A7.6, B7.7 y B8.5) que comparten la expresión del factor de transcripción *Twist-like1* (Imai, 2003). Estas células se dividen en fases posteriores del desarrollo y forman tres subgrupos mesenquimales similares pero diferenciados (Tokuoka et al., 2004). Poco antes de cesar su expresión completamente en el estadio de *early tailbud*, *Twist-like1* promueve la transcripción de su homólogo *Twist-like2*, que permanece activado en el linaje mesenquimal durante unas cuantas fases ontogenéticas subsiguientes. Estas células migrarán posteriormente hacia la

parte anterior del tronco y formarán partes de diversos órganos del juvenil y el adulto (Tokuoka et al., 2005). Es interesante remarcar que, si bien *Twist-like1* es indispensable para la determinación celular, *Twist-like2* parece involucrado en conferir capacidad migratoria a las células (Abitua et al., 2012).

Danio rerio: El pez cebra es un teleósteo ciprínido de agua dulce, próximo filogenéticamente a carpas y barbos, originario del sudeste asiático. Se trata de una especie muy utilizada en biología del desarrollo debido a la facilidad en su estabulación, reproducción y manipulación de embriones. Este organismo pertenece al clado de los gnatóstomos, que junto con los ciclóstomos (lampreas y mixinos) constituyen el subfilo de los vertebrados. Dicho linaje presenta múltiples estructuras novedosas, como un cráneo que protege al cerebro, un esqueleto cartilaginoso u óseo conectado por una columna axial vertebral, o extremidades locomotoras que sobresalen del tronco en número parejo o impar. El sistema nervioso está altamente elaborado respecto a los otros grupos de cordados, compuesto por un encéfalo, médula espinal y numerosos ganglios y nervios. Asimismo, poseen diversos órganos sensoriales muy desarrollados agrupados en su mayoría en el cráneo, como ojos, oídos o el sistema olfactor. El origen evolutivo de este diseño corporal podría estar relacionado con un modo de vida activo, posiblemente consecuencia de una alimentación macrófaga ligada a la depredación.

El desarrollo embrionario del pez cebra comienza, después de una fecundación externa, con una segmentación en la región libre del abundante vitelo, el blastodisco (Kimmel et al., 1988) (Fig. I10a). Durante la gastrulación, se genera un movimiento de epibolia en el que las células internas migran hacia afuera para intercalarse con las externas, lo que provoca un adelgazamiento del blastodermo a la vez que éste se expande hacia el polo vegetal del embrión. La neurulación sucede mediante un proceso peculiar, donde las células de la placa se pliegan en la línea media para constituir la quilla neural, que después se abrirá internamente dando lugar a la característica estructura hueca del tubo neural (Lowery and Sive, 2004). A continuación, en el estadio de faríngula, comienza un período donde se formarán los principales órganos del embrión mediante procesos morfogenéticos. Muchos de estos procesos dependerán de la interacción señalizadora a nivel molecular entre distintos tejidos. Especialmente abundante durante el desarrollo es

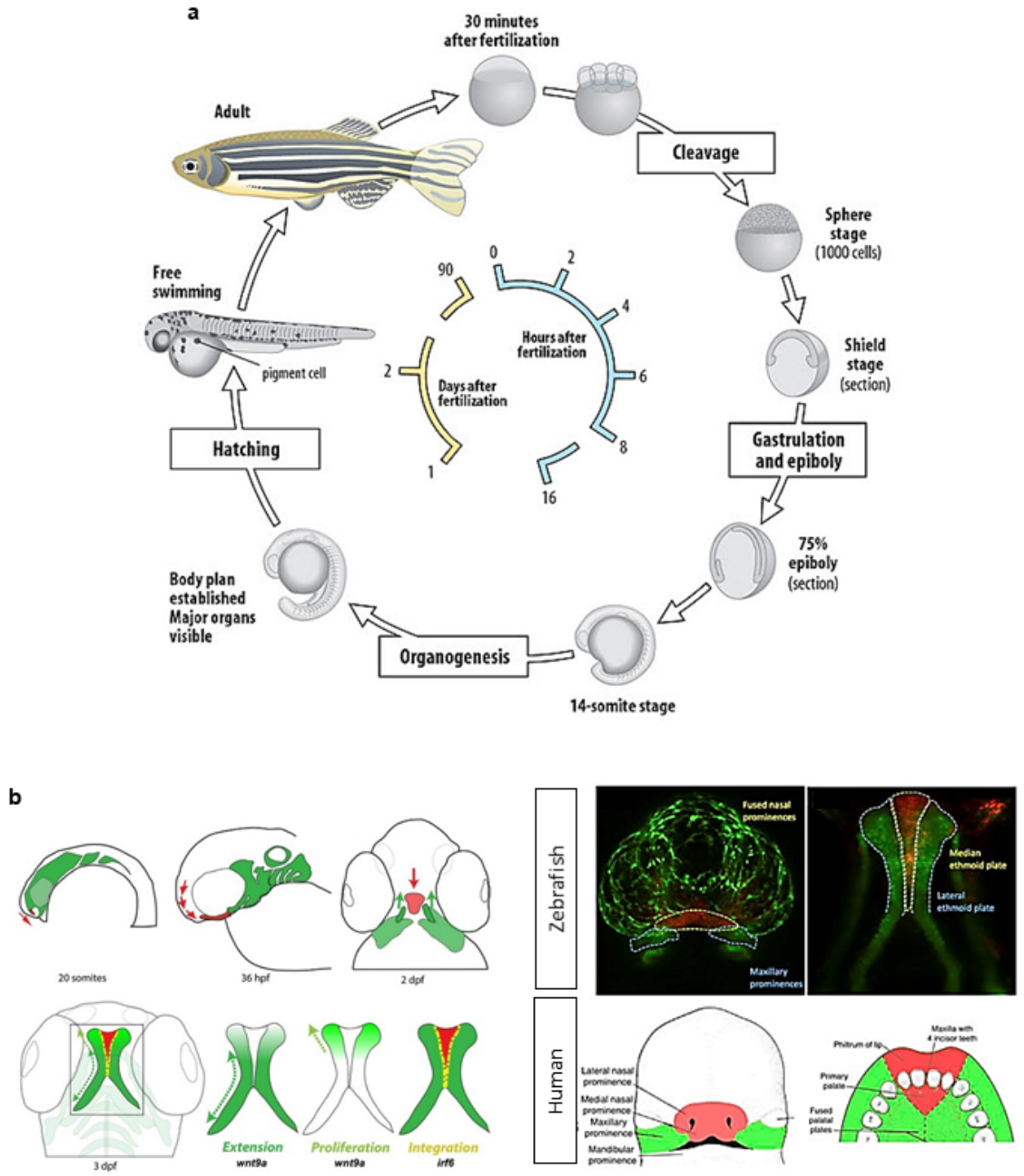

Figura I10 | En inglés. **(a)** Adaptado de D'Costa et al. 2009. Representación de los primeros estadíos embrionarios y el ciclo vital del pez cebra. **(b)** Adaptado de Dougherty et al. 2013. Izquierda, esquema que muestra los pasos ontogenéticos de la formación del paladar, incluyendo la migración e integración de una población de la cresta neural en la estructura cartilaginosa del hueso etmoides. Derecha, representación de las partes que componen el paladar en humano y pez cebra según su origen embriológico, que es equivalente en ambos organismos. La linea de pez utilizada contiene un *enhancer* del gen Sox10 controlando la expression de la proteína fotoconvertible Kaede, que ha sido alterada en la población migratoria supraocular mediante manipulación con un microscopio de fluorescencia.

neurulación (Klymkowsky et al., 2010). Estas células tienen la capacidad de migrar durante la ontogenia a diversas localizaciones corporales donde se diferencian en distintos tipos celulares como melanocitos, condrocitos o células de Schwann. De este modo, constituyen una parte relevante del material celular de diversos órganos, como el corazón, la señalización cruzada entre tipos celulares epiteliales y mesenquimales (Gilbert, 2013). Un ejemplo de estos casos es la interacción molecular entre la cresta apical ectodérmica, un epitelio localizado en la parte distal de la extremidad creciente, y las células mesenquimáticas del mesodermo subyacente (Zeller et al., 2009). Este intercambio de moléculas señalizadoras se ha revelado clave para la proliferación y diferenciación de las células esqueléticas y musculares que conforman las extremidades (Masselink et al., 2016).

Por otro lado, es interesante destacar que en los vertebrados muchos órganos se forman mediante el acoplamiento de poblaciones celulares diversas que pueden tener orígenes embrionarios diferentes. Una de las estructuras embrionarias que mejor ejemplifica dicho fenómeno es la cresta neural. También conocida como “la cuarta capa germinal”, la cresta neural proviene de las células del borde de la placa neural, que se localizan en la parte más dorsal del tubo nervioso una vez concluida lalos ganglios sensoriales o el cartílago craneal. En este último caso, un proceso morfogenético concreto relacionado con las células de la cresta ha sido especialmente estudiado: la formación del paladar (Mork and Crump, 2015). El paladar constituye el techo de la cavidad oral y está formado en un principio por condrocitos que se mineralizan en los vertebrados con huesos (teleóstomos). Tanto en peces como en mamíferos, uno de los procesos básicos durante la ontogenia del paladar es la integración de dos poblaciones distintas de la cresta neural craneal (Swartz et al., 2011) (Fig. I10b). Una de estas poblaciones se extiende bajo la vesícula óptica y forma las regiones laterales del paladar, mientras que una población distinta migra por encima del ojo y se integra en medio de esa estructura (Dougherty et al., 2013) (Figura I10).

OBJETIVOS

Durante la realización de la presente tesis, se han marcado los siguientes **objetivos** principales:

1.- Identificar aquellos exones alternativos con patrones de inclusión y exclusión diferencial en varios tejidos de organismos deuteróstomos. (Capítulo 1)

2.- A fin de inferir escenarios macroevolutivos de ensamblaje de programas de *splicing* alternativo:

a) Caracterizar la expresión y/o la función embrionaria de determinadas familias de factores reguladores de *splicing* en especies de cordados y equinodermos. (Capítulos 2 y 3)

b) Investigar la conexión entre los fenotipos obtenidos y la alteración de los programas post-transcripcionales derivados de la perturbación de dichos factores. (Capítulos 2 y 3)

c) Estudiar la evolución de los programas de splicing regulados por un mismo factor, tanto a nivel exónico como génico, en un contexto filogenético amplio. (Capítulo 3)

RESULTADOS

Capítulo 1

C1: Preliminary insights into the tissue-regulated alternative splicing landscape in deuterostome species

To begin unravelling macroevolutionary trends among AS patterns in the deuterostome lineage, we aimed to quantify the relative abundance of tissue-specific splicing events in distinct organs of two bony vertebrates, one chondrichthyan, one cephalochordate and one echinoderm. In particular, the species included in the analysis were: zebrafish (*Danio rerio*), human (*Homo sapiens*), elephant shark (*Callorhinchus milii*), amphioxus (*Branchiostoma lanceolatum*) and purple sea urchin (*Strongylocentrotus purpuratus*). We selected 7 tissues for each species, matched for homology when possible, specially within vertebrates (neural, muscle, male and female gonads, digestive tube and hepatic). For vertebrate species, we used publicly available RNA-seq data. For sea urchin, we generated deep coverage RNA-seq for radial nerve (neural), lantern (muscle) and gut, and used other tissues from public sources (Tu et al., 2012). For the amphioxus *B. lanceolatum*, we generated high-coverage RNA-seq samples from embryonic and dissected adult organs. Since this species lacks a published genome, we used these data, along with data coming from other labs, to annotate the *B. lanceolatum* genome pre-release using a combination of RNA-seq tools and EVidenceModeler (EVM) (see Methods).

Using the vast-tools pipeline, for each species, we first filtered our AS events that did not have enough read coverage in at least three out of the seven samples. Next, we defined alternative exons in coding genes as those with Percent Spliced In (PSI) value between 15% and 85% in at least one sample. Then, to characterize those exons with a tissue-biased inclusion and exclusion pattern, we quantified the number of exons with a differential PSI (ΔPSI = PSI in tissue A – PSI in tissue B) value greater than a given threshold in one tissue compared to all other samples. We used two different thresholds, ΔPSI > 15 and ΔPSI > 25, to check the effect of a more permissive and a more restrictive definition of tissue-specificity, respectively (Fig. R1 and Fig. R2). Using the most relaxed definition (ΔPSI >15), between 51 and 64% of exons showed tissue-biased regulation in all species. An increase of the specificity threshold (ΔPSI >25) reduced about half the percentage of tissue-biased exons in human, shark and sea urchin, while a softer decrease

Figure R1

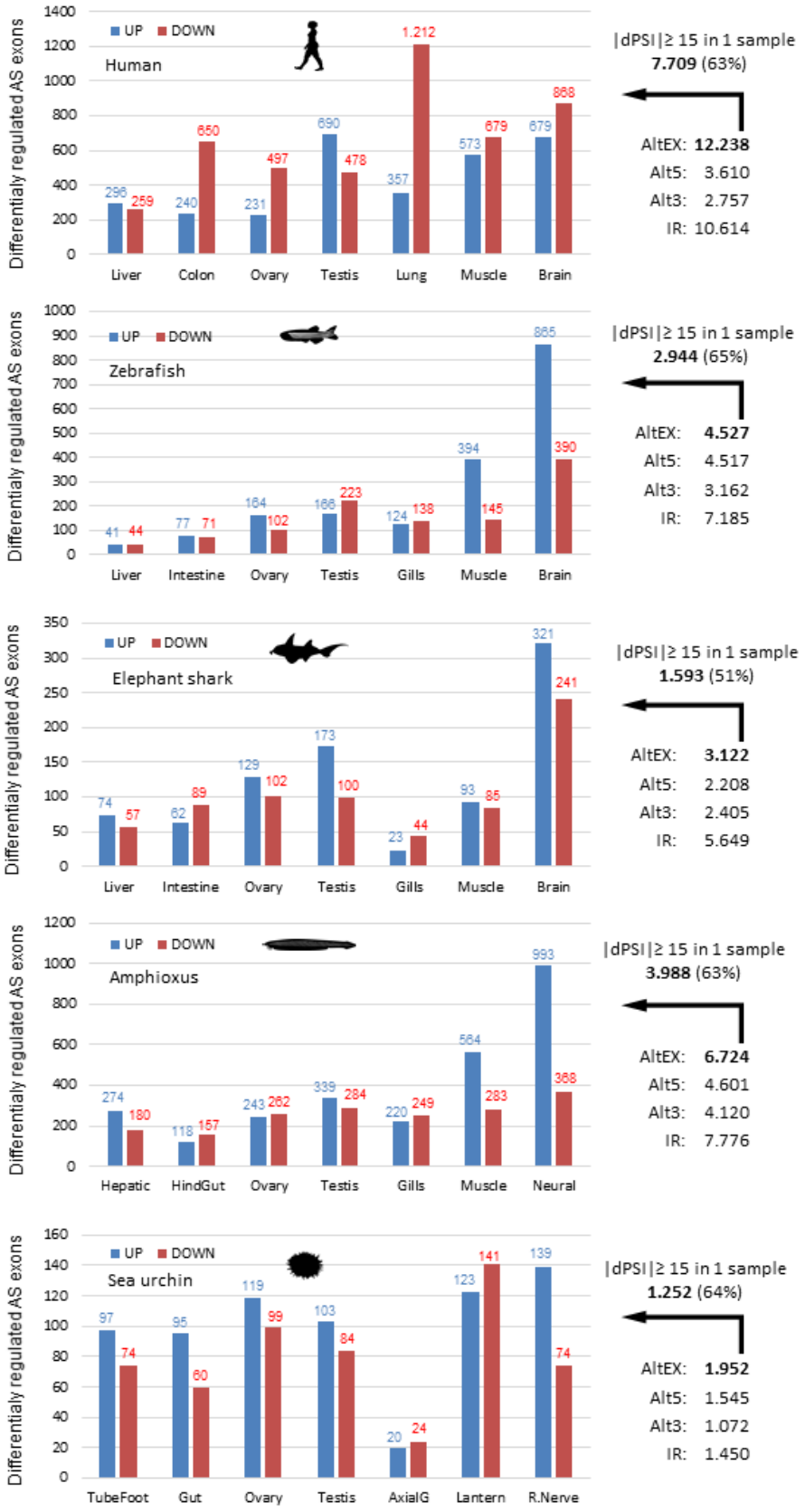
Differentialy regulated AS exons
UP
DOWN
Human
Liver
Colon
Ovary
Testis
Lung
Muscle
Brain
|dPSI|≥ 15 in 1 sample
7.709 (63%)
AltEX: 12.238
Alt5: 3.610
Alt3: 2.757
IR: 10.614
Zebrafish
Intestine
Gills
|dPSI|≥ 15 in 1 sample
2.944 (65%)
AltEX: 4.527
Alt5: 4.517
Alt3: 3.162
IR: 7.185
Elephant shark
|dPSI|≥ 15 in 1 sample
1.593 (51%)
AltEX: 3.122
Alt5: 2.208
Alt3: 2.405
IR: 5.649
Amphioxus
Hepatic
HindGut
Neural
|dPSI|≥ 15 in 1 sample
3.988 (63%)
AltEX: 6.724
Alt5: 4.601
Alt3: 4.120
IR: 7.776
Sea urchin
TubeFoot
Gut
AxialG
Lantern
R.Nerve
|dPSI|≥ 15 in 1 sample
1.252 (64%)
AltEX: 1.952
Alt5: 1.545
Alt3: 1.072
IR: 1.450

Figure R2

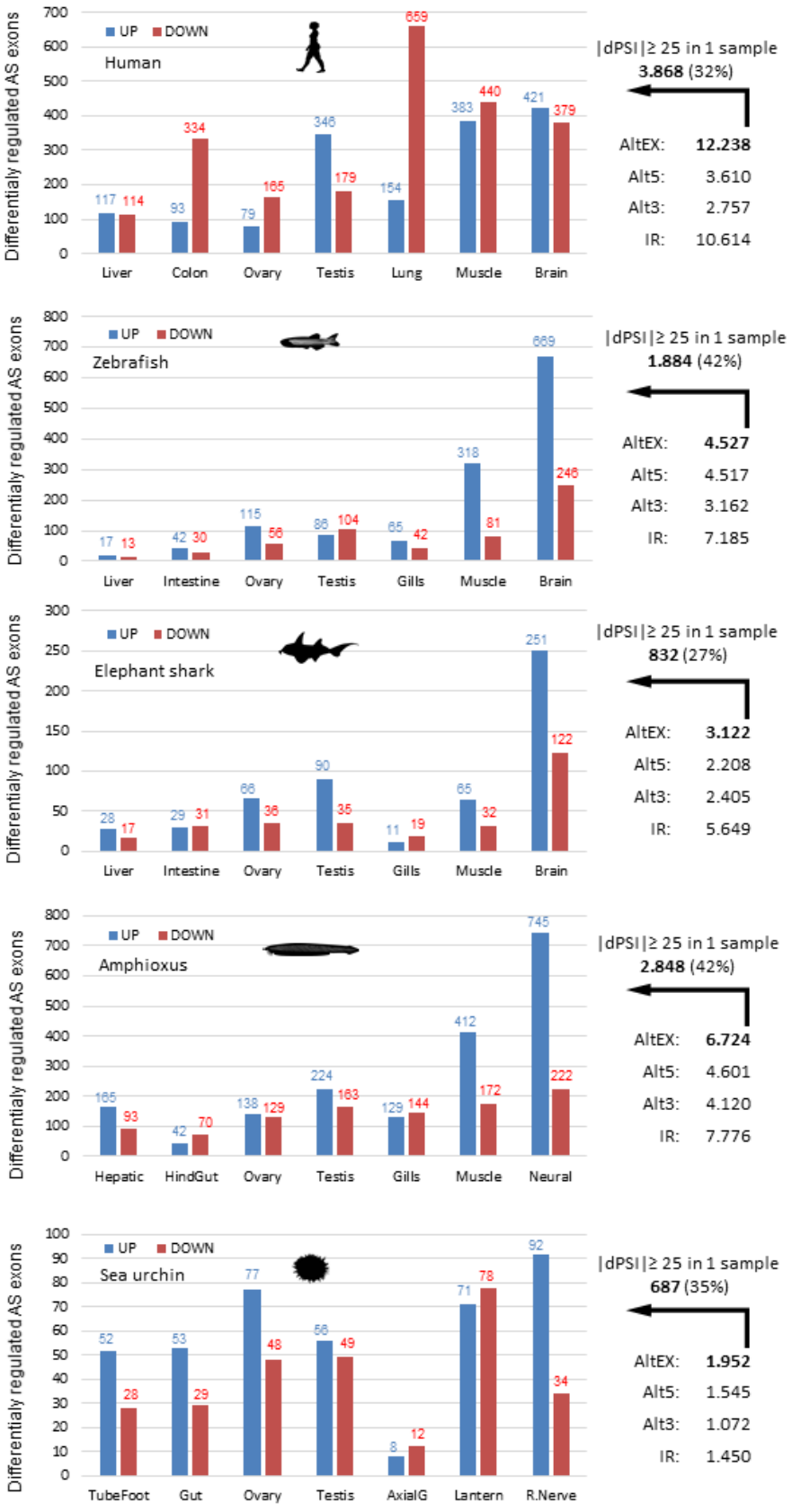
Differentialy regulated AS exons
UP
DOWN
Human
Liver
Colon
Ovary
Testis
Lung
Muscle
Brain
117
114
93
334
79
165
346
179
154
659
383
440
421
379
|dPSI|≥ 25 in 1 sample
3.868 (32%)
AltEX: 12.238
Alt5: 3.610
Alt3: 2.757
IR: 10.614
Zebrafish
Liver
Intestine
Ovary
Testis
Gills
Muscle
Brain
17
13
42
30
115
56
86
104
65
42
318
81
669
246
|dPSI|≥ 25 in 1 sample
1.884 (42%)
AltEX: 4.527
Alt5: 4.517
Alt3: 3.162
IR: 7.185
Elephant shark
Liver
Intestine
Ovary
Testis
Gills
Muscle
Brain
28
17
29
31
66
36
90
35
11
19
65
32
251
122
|dPSI|≥ 25 in 1 sample
832 (27%)
AltEX: 3.122
Alt5: 2.208
Alt3: 2.405
IR: 5.649
Amphioxus
Hepatic
HindGut
Ovary
Testis
Gills
Muscle
Neural
165
93
42
70
138
129
224
163
129
144
412
172
745
222
|dPSI|≥ 25 in 1 sample
2.848 (42%)
AltEX: 6.724
Alt5: 4.601
Alt3: 4.120
IR: 7.776
Sea urchin
TubeFoot
Gut
Ovary
Testis
AxialG
Lantern
R.Nerve
52
28
53
29
77
48
56
49
8
12
71
78
92
34
|dPSI|≥ 25 in 1 sample
687 (35%)
AltEX: 1.952
Alt5: 1.545
Alt3: 1.072
IR: 1.450

Figure R1 and R2 | Differentially regulated AS exons in a given organ detected with dPSI>15 (R1) and dPSI>25 (R2). Blue bars represent the number of exons with differentially regulated maximum inclusion in a given sample versus the rest (UP), while dark red bars represent those exons with a significant tissue-specific skipping (DOWN). In amphioxus, "Hepatic" sample refers to the digestive cecum organ, for simplicity. In sea urchin, AxialG refers to the axial gland, and R.Nerve to the radial nerve organ. IR, intron retention; Alt5, alternative 5' acceptor; Alt3, alternative 3' donor; AltEX, alternative exon cassette.

to 42% was observed in zebrafish and amphioxus.

Some common patterns were observed across all species. On one hand, comparison between the seven adult organs in each species revealed that the nervous system showed the highest number of exons with up-regulated inclusion using ΔPSI > 25 as cut-off (Table R1). However, the magnitude of this difference in the number of detected neural-enhanced exons versus other tissues was variable among species. The purple sea urchin, in particular, showed the more balanced levels of organ-specific exons, with samples presenting fold-differences below 1.5 (ΔPSI >15) or 2 (ΔPSI >25) relative to the radial nerve in all cases but in the axial gland. Interestingly, the restrictive analysis increased the distance between nervous system and most other organs, although proportions were generally maintained in muscle of chordates and most sea urchin tissues.

On the other hand, differentially down-regulated exons exhibited a more complex landscape. Those exons presented relatively similar numbers than enhanced ones in a given sample of non-human organisms, especially in ΔPSI >15 analysis. A recurrent exception to this pattern was observed for neural and muscle tissues in several species, that showed a substantial decrease in skipped versus included exons in most cases. Strikingly, human presented very high relative levels of organ-specific down-regulated exons. In this species, the lungs were detected as the most extreme sample, even exceeding the already elevated number of differentially skipped exons in both muscle and neural tissues. This result points to organ-specific skipping regulation as a more recurrent phenomenon in this primate organism relative to the other studied deuterostomes. However, these results may be confound by the use of different RNA-seq sources and lack of replicates, and it is therefore difficult to draw specific conclusions about the diversity of patterns observed for tissue-specific skipping.

Human	dPSI>15	dPSI>25
Muscle	1,18	1,09
Lung	1,9	2,73
Testis	0,98	1,2
Ovary	2,9	5,32
Colon	2,8	4,52
Liver	2,29	3,59

Zebrafish	dPSI>15	dPSI>25
Muscle	2,19	2,1
Gills	6,9	10,2
Testis	5,2	7,77
Ovary	5,2	5,8
Intestine	11,23	15,9
Liver	21	39

Elephant shark	dPSI>15	dPSI>25
Muscle	3,45	3,8
Gills	13,9	22,8
Testis	1,85	2,78
Ovary	2,48	3,8
Intestine	5,17	8,65
Liver	4,33	8,9

Amphioxus	dPSI>15	dPSI>25
Muscle	1,76	1,8
Gills	4,5	5,77
Testis	2,9	3,32
Ovary	4	5,3
HindGut	8,4	17,7
Hepatic	3,6	4,5

Sea urchin	dPSI>15	dPSI>25
Lantern	1,13	1,29
AxialG	6,95	11,5
Testis	1,34	1,64
Ovary	1,16	1,19
Gut	1,46	1,86
TubeFoot	1,43	1,76

Table R1 | This tables show the proportion of neural up-regulated exons relative to all other tissues (neural/given organ) in each species in both dPSI>15 and dPSI>25 analysis. Green color is for values above 2-fold. Yellow color is for values between 1,5 and 2-fold. Red color is for values between 1 and 1,5-fold. Blue color is for values below 1.

Capítulo 2

C2: Characterization of *RbFox* and *Nova* ontogenetic functions in sea urchin and the evolution of their expression patterns across distant species.

Characterization of differentially spliced events in multiple species is important for understanding the evolutionary dynamics regarding relative abundance of this regulatory mechanism in particular organs. Nevertheless, this approach is limited in terms of unveiling the organismic function of those sets of tissue-specific alternative isoforms. Regulation of alternative splicing events is usually performed by RNA-binding proteins that interact with the spliceosome to enhance or silence the inclusion of multiple exons in one or few tissues or cell-types. Investigating the expression and organismic roles of those factors can contribute to unveil the evolution and function of coordinated alternative splicing programs that are often deployed in coherent biological processes.

For example, *RbFox* and *Nova* splicing factors are involved in the development of certain structures, including the central nervous system, in studied bony vertebrates. On one hand, an evolutionary scenario leading to the assembly of neural-specific splicing programs regulated by *Nova* proteins in chordates has been proposed based on embryonic expression (Irimia et al., 2011a) (Annexed article 3). On the other hand, a similar macroevolutionary perspective for *RbFox* ontogenetic role is lacking, as reported analysis have been restricted to vertebrates and fast-evolving ecdisozoans. Furthermore, there is no functional data regarding the embryonic function of both gene families, neither their regulated splicing programs, in deuterostome organisms other than mouse or zebrafish.

Nova function is involved in gastrulation movements in sea urchin embryo.

To begin unravel the developmental function of *Nova* splicing factor in an organism closely related to the chordate phylum, we investigated its role in the purple sea urchin (*Strongylocentrotus purpuratus*). The sole *Nova* ortholog of this species was described to be expressed in an endomesodermal ring of cells surrounding the future blastopore in mesenchyme blastula embryos (24hpf) and subsequently restricted to the hindgut region during gastrula stages (36-48hpf) (Fig. R3a) (Irimia et al., 2011a). In fact, this pattern is very similar to the one previously described for the Mediterranean urchin *Paracentrotus lividus* (Röttinger et al., 2006), which suggests a certain degree of functional conservation

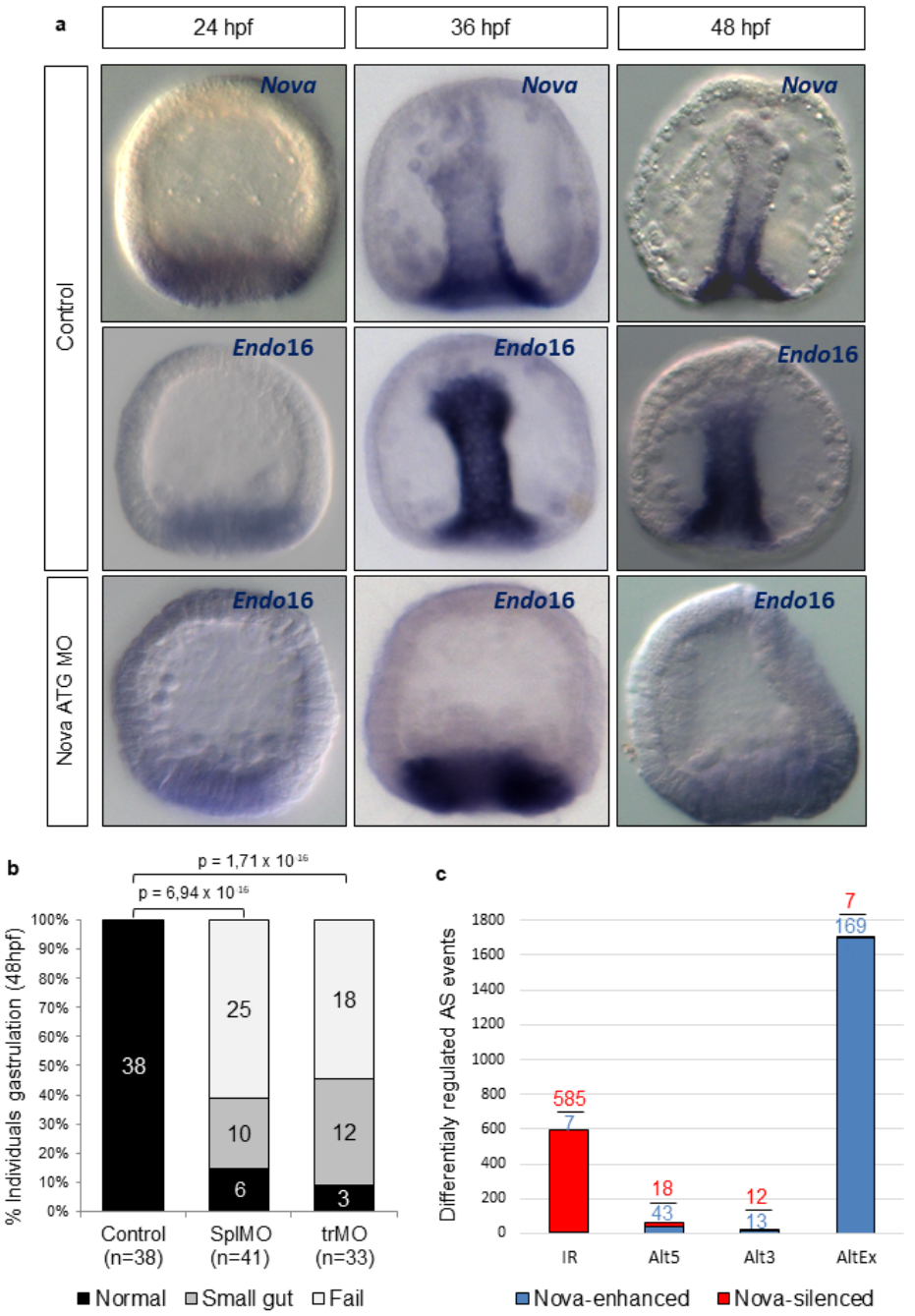

Figure R3 | Endoderm invagination is impaired during gastrulation in Nova knock-down embryos. (a) WISH using Nova and Endo16 anti-sense probes in *Strongylocentrotus purpuratus* embryos at three different developmental stages (24hpf, 36hpf, 48hpf). **(b)** Statistics regarding the gastrulation phenotype in 48hpf embryos injected with both splicing (SplMO) and translation (trMO) morpholinos. **(c)** Number of differentially regulated splicing events, classified by type, obtained by RNA-seq comparison between 3 replicates of control and trMO injected embryos. Blue color is used for those events whose inclusion is promoted by *Nova*, while red color represents those events with down-regulated inclusion by *Nova* factor. IR, intron retention; Alt5, alternative 5' acceptor; Alt3, alternative 3' donor; AltEX, alternative exon cassette.

for this gene within the Echinacea lineage.

We designed two morpholino molecules to knock-down *Nova* function in sea urchin embryos, one of them blocking translation (ATG-MO) and another one blocking the 3' splice site of exon 3 (Spl-MO). Eggs were injected separately with the two morpholinos to ensure the specificity of the experiment. In both cases, a significant fraction of injected embryos showed an impairment in the invagination movements of the endoderm tissue that occur during gastrulation. While some of embryos exhibited a reduced gut at 48hpf that did not reach the animal side of the gastrula, most of them presented an apparent fail in gastrulation initiation (Fig. R3b). A whole mount in situ hybridization (WMISH) of *Endo16*, a marker for endoderm specification, showed no change in expression at 24hpf and 36hpf (Fig. R3a). This suggests that the phenotype is not due to an error in cell lineage determination, but more probably related to morphogenetic disturbance.

To check the transcriptomic impact of *Nova* knock-down during sea urchin embryogenesis, we performed three independent replicas of RNA sequencing (RNA-seq) from control and ATG-MO injected embryos at 24hpf stage. Using vastools pipeline, we identified differentially-regulated splicing events (dPSI $\geq$ 10) between control and knock-down blastulas. We found 1.695 exon cassettes with down-regulated inclusion in Nova depleted embryos, suggesting a profound molecular affectation. Surprisingly, a great percentage of those exons (~66%) are constitutively included in a relatively complete set of developmental and adult public samples. Thus, a possible explanation for this result is that one or more of *Nova*-regulated alternative exon targets may produce a direct or indirect impairment of the constitutive spliceosomal function in knock-down embryos. Alternatively, *Nova* might act as protein co-factor needed to catalyse the inclusion of some of these constitutive exons in their expressing cells.

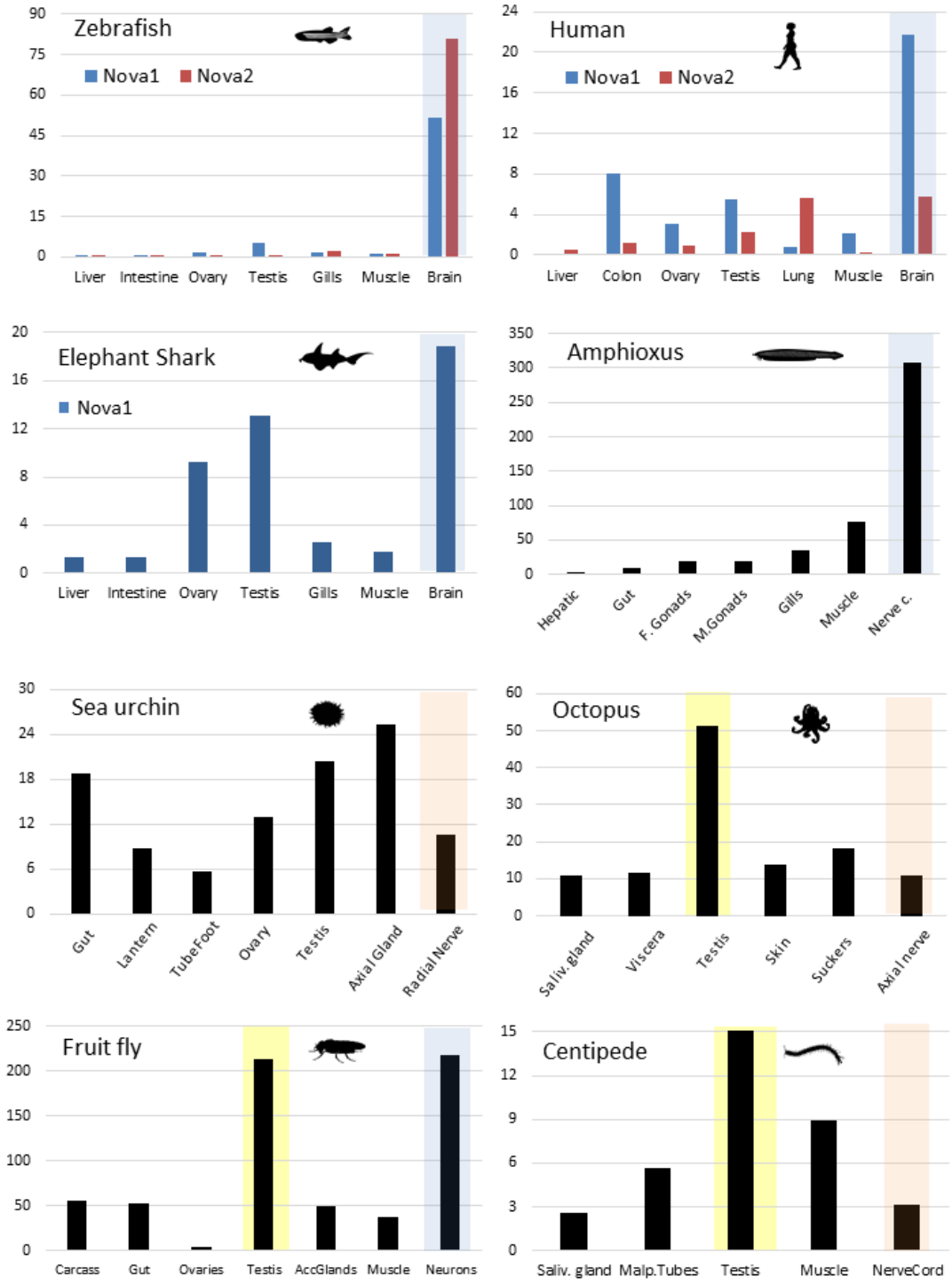

Figure R4 | *Nova* family gene expression in adult organs of deuterostome and protostome species (in cRPKMs). Gene expression values are obtained from RNA-seq samples measured in corrected Reads per Kilobase per Million reads (cRKPMs). Species shown in this figure are zebrafish (*Danio rerio*), human (*Homo sapiens*), elephant shark (*Callorhinchus milii*), European amphioxus (*Branchiostoma lanceolatum*), purple sea urchin (*Strongylocentrotus purpuratus*), octopus (*Octopus vulgaris*), fruit fly (*Drosophila melanogaster*) and the centipede (*Strigamia maritima*).

We also aimed to characterize relative *Nova* expression in adult organs of five deuterostomes and three protostome species using RNA-seq data (Fig. R4). We found high transcription of *Nova* genes in the central nervous system (CNS) in organisms from the chordate phylum. Nevertheless, while both paralogues of zebrafish exhibit a quite clear neural-specific pattern, human genes presented a less clean picture, with *Nova2* transcription exhibiting similar levels in brain and lungs (which are highly enriched in endothelial tissue). Along these lines, *Nova1* also showed elevated presence in male and female gonads in elephant shark. Moreover, fainter but noticeable expression was detected in amphioxus muscular tissue, as has been previously reported by qPCR data (Irimia et al., 2011a). Interestingly, the purple sea urchin showed a much less tissue-enriched pattern, with the radial nerve being one of the organs with lowest expression. Within the protostomes, the two arthropods and one cephalopod species presented higher abundance of *Nova* transcripts in the male gonads, although *Drosophila melanogaster* exhibited comparable expression levels in the nervous system. These results point to complex evolutionary trajectories of this gene family including scenarios of conservation and recruitment of *Nova* function in certain organs within distinct metazoan clades.

***RbFox* activity is conserved in the myogenic mesoderm and co-opted into lineage-specific developmental processes among deuterostomes.**

To unravel the evolution *RbFox* gene family expression patterns during development, we performed whole mount in situ hybridization (WISH) in several non-vertebrate deuterostome species. We found the sole *RbFox* homologues expressed in the embryonic mesoderm of all studied organisms (Figure R5). In the urochordate *Ciona intestinalis*, we observed expression in the tail in muscular and notochord tissues at tailbud stage. In *Branchiostoma lanceolatum*, a cephalochordate species, *RbFox* transcription was detected along dorsal mesoderm at mid-neurula stage. This tissue-specific pattern was maintained at late neurula stage, as individual somites derived from the adaxial mesoderm were stained. In *Strongylocentrotus purpuratus*, expression of *RbFox* was clearly detected in the skeletogenic mesenchyme at blastula stages (18hpf and 24hpf) and in the myogenic cell lineage in gastrula embryos (48hpf). In addition, transcription of this gene in other mesodermal non-skeletogenic tissues during blastula stage was also observed, although assays with additional markers would be further needed to unveil the precise cell lineage/s. In summary, these expression patterns suggest the possibility that *RbFox* gene family was expressed in the myogenic embryonic mesoderm of the last common ancestor of deuterostomes. Moreover, they also point to co-option of this gene family in the ingressing skeletogenic mesenchyme of at least one echinoid species and into brain development of bony vertebrates.

Next, to investigate the ontogenetic role of this splicing factor in a non-chordate species, we aimed to knock-down *RbFox* function during embryogenesis. We designed two different morpholino molecules to ensure the specificity of our experimental approach. A first morpholino was designed to block splicing of exon 5 (SplMO), which contains the sequence coding for the internal part of the only RNA Recognition Motif (RRM) domain of the encoded protein. Injected embryos collected at 24hpf showed missplicing of the targeted exon, with usage of a cryptic splice site located within the adjacent intron (Figure R6a). The transcript resulting from this experimental manipulation contained a premature stop codon (PTC), leading to the production of a non-functional peptide.

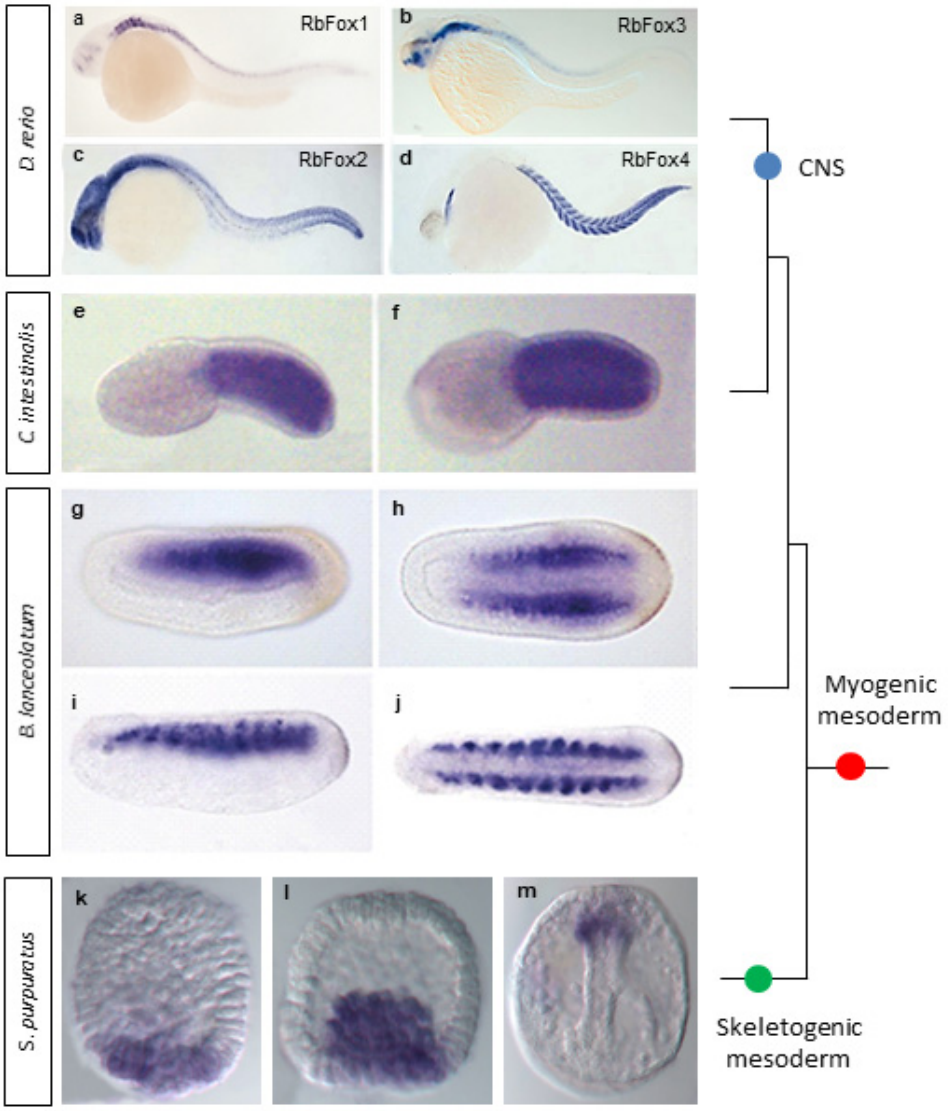

Figure R5 | RbFox genes are expressed in myogenic mesoderm of studied deuterostome species and also in developing CNS of vertebrate species. **(a-d)** Pictures adapted from Thisse 2004 and Gallagher et al. 2010. WISH for RbFox gene family members in zebrafish embryos around 32hpf show expression in central nervous system in case of RbFox1, RbFox2 and RbFox3 **(a,b)**, in myogenic cells in RbFox2 and RbFox4 **(c,d)**. **(e,f)** WISH of RbFox gene in mid-tailbud embryos of *Ciona intestinalis* show a strong expression pattern in the muscle cell lineage, located in the tail, along with slightly weaker expression in the notochord. **e** is lateral view, **f** is dorsal view. (**g-j**) WISH of RbFox ortholog in embryos of *Branchiostoma lanceolatum* at middle neurula stage **(g,h)** reveals transcription in paraxial mesoderm, that is maintained in the somites coming from this tissue in late neurulas **(i,j)**. **g** and **i** are lateral views; **h** and **j** are dorsal views. **(k-m)** WISH for RbFox transcripts in *Strongylocentrotus purpuratus* embryos at 18hpf **(k)**, 24hpf **(l)** and 48hpf **(m)** showed a mesodermal expression patterning, with clear staining of the primary mesenchyme during its ingression into the blastocele cavity **(l)** and in the myogenic lineage at gastrula stage **(m)**.

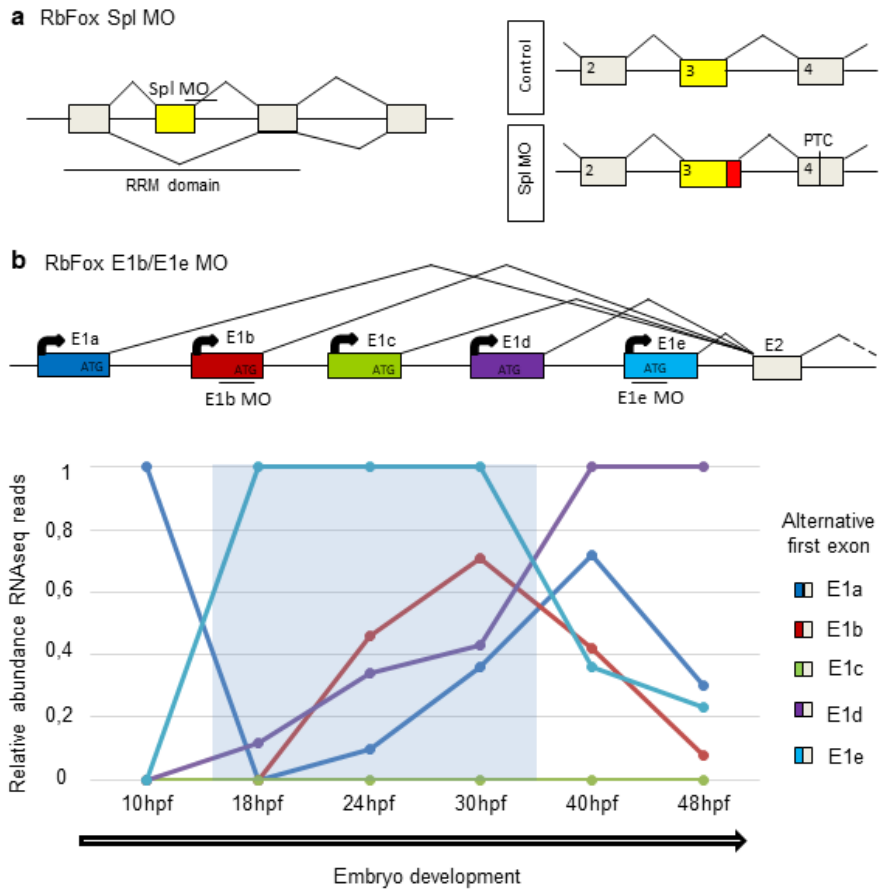

Figure R6 | RbFox knock-down in sea urchin embryos with two different morpholino molecules. (a) Left, schematic representation of the gene structure of RbFox gene of Strongylocentrotus purpuratus, with boxes representing exons, and horizontal lines representing introns. The binding region of the Spl MO is marked with a thicker line at the exon 5 donor site. Targeted exon codes for the internal part of the RRM domain. Right, transcriptional alteration produced by morpholino injection, with the included intronic region painted in red. PTC, premature termination codon. (b) Up, schematic representation of the multiple alternative first exons of RbFox gene in sea urchin, and their relative position relative to exon 2. Down, a graphic showing the relative abundance of RNA-seq reads from sea urchin embryo stages that map to the junction of each of the first annotated exons with exon 2. Blue column marks the developmental period when co-injection of both E1bMO and E1eMO is supposed to be more effective.

We then aimed to design a second morpholino in a region overlapping the ATG codon to block translation of the protein. However, similar to vertebrate's case, we found five alternative promoters containing in-frame ATG codons that may constitute translation initiators. To understand the differential usage of those promoters, we used publicly available RNA-seq data spanning 10hpf to 48hpf embryonic stages. We quantified the proportion of reads mapping to exon junctions formed by the sequence transcribed by

each promoter and the first constitutive exon of the transcript (Figure R6b). Obtained results pointed to a dynamic use of the different promoters during development. Exons E1b and E1e were the most frequently transcribed at 24hpf and 30hpf. On the other hand, exons E1a, and specially E1d, were predominant at 40hpf and 48hpf. Thus, to maximize down-regulation of *RbFox* gene expression around 24hpf, we designed two morpholinos blocking translation of the transcripts containing exons E1b (E1bMO) and E1e (E1eMO).

As *RbFox* gene is expressed in skeletogenic mesenchyme during blastula stage and in myogenic cells at gastrula stage, we checked the development of those organs in knock-down embryos at pluteus stage (Fig. R7). Embryos injected with SplMO developed into larvae with complete absence of skeletal structure (92,5%) or with very small rudimentary spicules (7,5%) at 72hpf. We observed the same phenotypes in embryos injected with both E1bMO and E1eMO, although in this case the proportion of pluteus larvae with rudimentary spicules was higher (73%) compared to the absolute lack of a calcium carbonate skeleton (25%). We also studied the development of the muscular circumesophageal ring tissue using an antibody against myosin heavy chain (MHC). This staining allowed us to quantify that most SplMO injected embryos presented an impaired circumesophageal ring (73%), with muscle cells not fused or disorganized, and even a noticeable percentage of larvae showed no ring presence at all (19%).

On contrary, E1bMO and E1eMO co-injection lead to a normal MHC ring in most cases (94%), while only a minority showed impairment of muscular structure (6%). This data seems to reflect differential promoter usage in mesodermal tissues. *RbFox* is strongly expressed in primary mesenchyme at 24hpf, when most active promoters produce isoforms containing exons E1b and E1e, and in the myogenic lineage at 48hpf, when transcripts mainly contain exons E1a and E1d. Thus, blocking the two most active promoters during primary mesenchyme ingression at 24hpf have wide structural consequences for the larvae skeleton, but not for the development of the muscular circumesophageal ring.

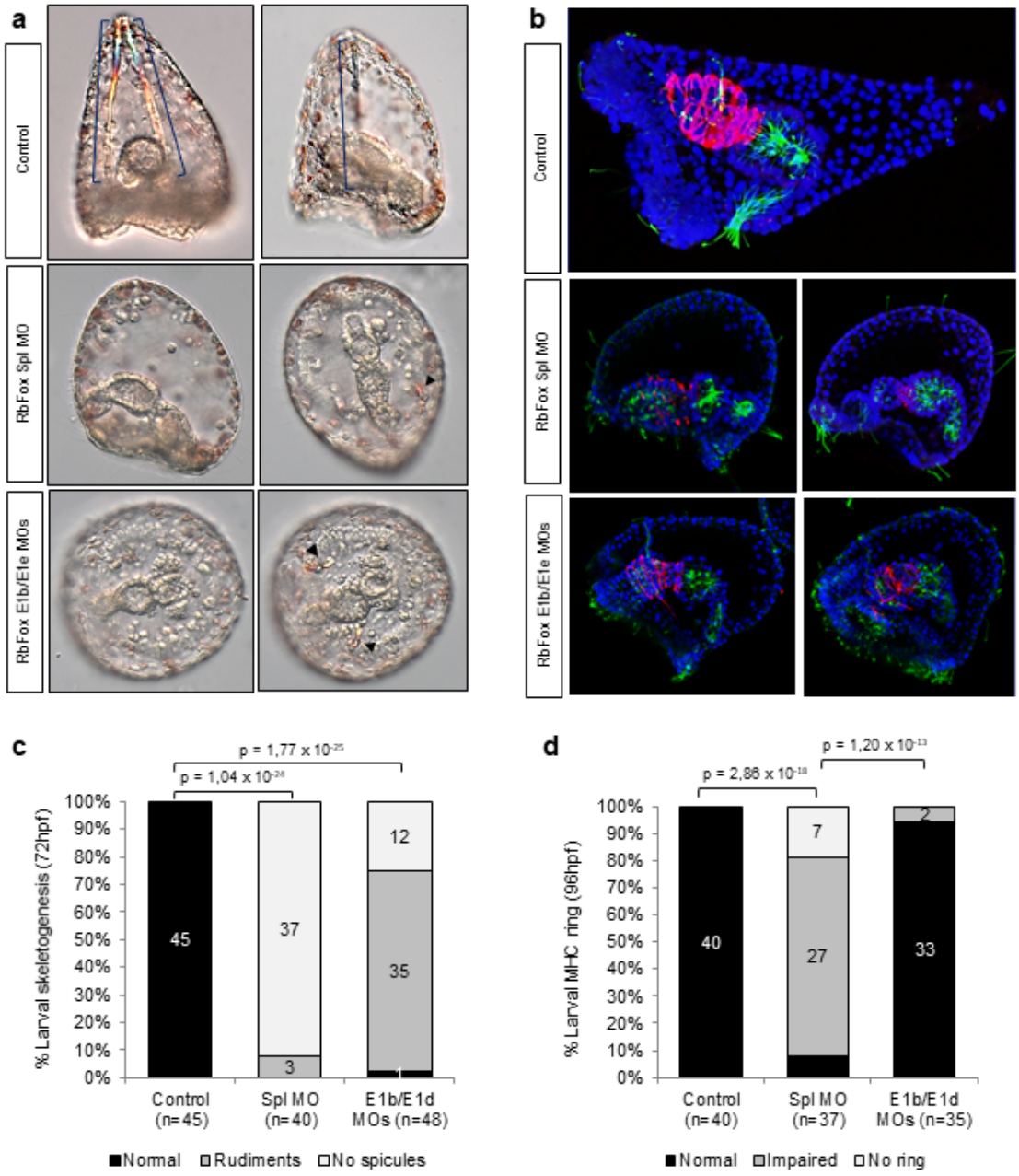

Figure R7 | RbFox gene is involved in the development of both larva skeleton and circumesophageal muscle in *Strongylocentrotus purpuratus* embryos. (a) DIC images of control and morpholino-injected early pluteus larvae at 72hpf showing skeletal spicules (blue claudators) or rudiments (black) arrowheads. In wild type, left picture is aboral view, and right picture shows lateral view. Both RbFox SplMO and E1bMO/E1eMO injection experiments produced some embryos with a stronger phenotype characterized by the absence of skeletal spicules (left), and other individuals that presented small rudiments (right). **(b)** Z-stacks from confocal microscope pictures of control and knock-down embryos stained with antibodies against MHC (red) and acetylated tubulin (green) at 96hpf. Cell nucleus were marked with DAPI (blue). All red signal from the embryos is included in the pictures. Control embryos show the proper morphology of continuous circumesophageal muscle rings. Embryos injected with SplMO showed an impairment of MHC rings structure, with non-fusined MHC-positive cells (left) or

even a complete absence of differentiated muscle cells surrounding the foregut (left). However, embryos with double E1b/E1e morpholino injection showed normal ring (left) or a softer impairment of the structure. **(c)** Statistics regarding the skeleton phenotype in the knockdown experiments show a stronger effect in case of SplMO injection. **(d)** Statistics regarding the muscular phenotype in the knockdown experiments show that the phenotype is greatly restricted to the SplMO injection.

To get insights into the molecular function of *RbFox* in purple sea urchin, we performed RNA-seq of 3 replicas of wild type and Spl-MO injected embryos at blastula stage (24hpf) (Fig R8). We identified multiple cases of differentially regulated splicing events: 204 exon cassettes, 49 alternative donor sites, 13 alternative acceptor sites and 29 intron retentions. Interestingly, among the obtained events, we detected an *RbFox*-silenced exon in *Fgfr1*, a member of the *Fgf* signalling receptor family. This gene was previously reported to be expressed in both the myogenic mesodermal lineage and in the ectodermal apical organ during early development. Moreover, a knock-down of Fgfr1 in sea urchin embryos revealed a very similar phenotype to that of *RbFox* in terms of muscle formation (Andrikou et al., 2015). We then performed an in-silico analysis that identified two canonical *RbFox* binding sites within the 160nt adjacent nucleotides of the upstream intron, suggesting direct regulation of this event by the splicing factor.

Finally, we also characterized the expression of *RbFox* family in multiple adult tissues from diverse species using the same RNA-seq samples as in the *Nova* analysis (Fig. R9). Surprisingly, all non-vertebrate organisms showed the highest relative levels of *RbFox* mRNA in the nervous system. This pattern was similar in general terms for vertebrate species, although maximum levels were observed in muscle for some homologs like human *RbFox1* or zebrafish *RbFox4*. Consistent with published data for mammals, *RbFox2* gene seems to present the more promiscuous expression among the different paralogs. These results point to three main conclusions: (i) *RbFox* family could be related to AS regulation in the adult nervous system since the origin of Bilateria; (ii) embryonic *RbFox* transcription is decoupled from adult pattern in terms of neural expression in non-vertebrate deuterostome species; (iii) *RbFox* paralogs from vertebrate organisms present notable evolutionary plasticity regarding their relative expression levels in distinct tissues.

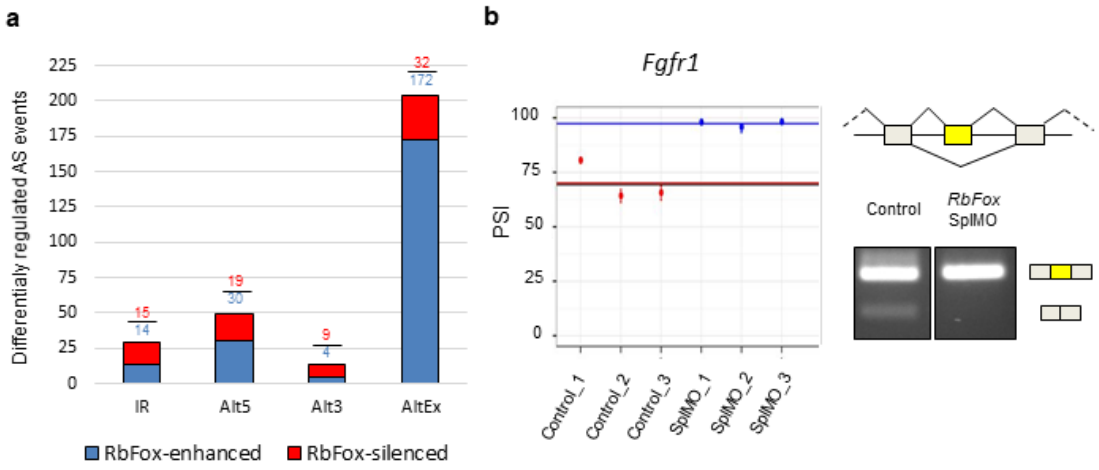

Figure R8 | Inclusion levels of numerous AS events in sea urchin blastula change upon *RbFox* knock-down, including one *Fgfr1* exon. (a) Number of differentially regulated splicing events, classified by type, obtained by RNA-seq comparison between 3 replicates of control and SplMO injected embryos. Blue color is used for events whose inclusion is promoted by *RbFox*, while red color represents those events with down-regulated inclusion by *RbFox* factor. IR, intron retention; Alt5, alternative 5' acceptor; Alt3, alternative 3' donor; AltEX, alternative exon cassette. (b) Left, a graphic showing the inclusion levels (PSI) of an *Fgfr1* exon in the three replicates of control and *RbFox* knock-down embryos in sea urchin embryos at 24hpf. Lines are drawn at the mean value for control (red) and SplMO injected (blue) samples. Right, Rt-PCRs showing the different isoform balance if *Fgfr1* splicing between control and SplMO cDNAs

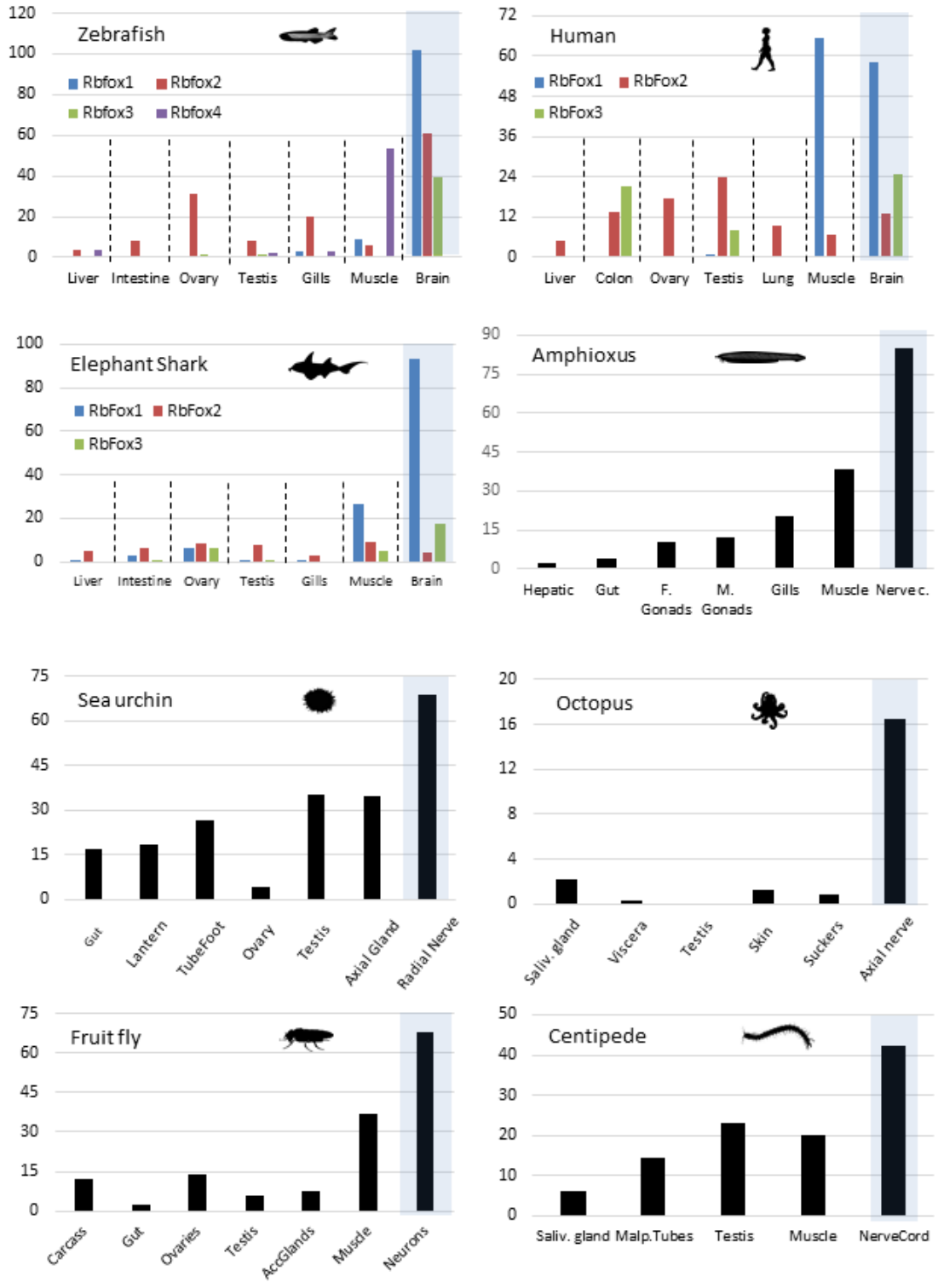

Figure R9 | RbFox gene family expression in adult organs is neural-enriched in diverse Bilateria organisms. GE values are expressed in corrected Reads per Kilobase per Million reads (cRKPMs). Species are the same already shown in R4.

Capítulo 3

C3: Evolutionary recruitment of flexible Esrp-dependent splicing programs into diverse embryonic morphogenetic processes

Epithelial-mesenchymal interplays are essential to many organogenetic processes in vertebrates (Gilbert, 2013; Wagner, 2014). These tissues often interact in morphogenetic interfaces through the exchange of cells and signaling molecules (Niswander et al., 1994; Thesleff et al., 1995). Despite the great diversity of cell types across the embryo, the majority can be classified as showing either mesenchymal or epithelial characteristics. This broad distinction, which is independent of tissue origin, has also been shown to be reflected in the patterns of gene expression and alternative splicing (AS) (Mallinjoud et al., 2014). Those transcriptomic programs confer partly antagonistic morphogenetic properties to epithelial and mesenchymal tissues by modulating certain cellular features, such as adhesion, motility and polarity.

Several morphogenesis-associated AS events are directly regulated by the *Epithelial Splicing Regulatory Protein* (*Esrp*) genes in mammalian species (Claude C Warzecha et al., 2009). *Esrp1* and *Esrp2* were originally identified as positive regulators of IIIb exon inclusion of the *Fgfr2* gene (Claude C. Warzecha et al., 2009). They encode RNA-binding proteins that are dynamically expressed mainly in a subset of epithelial tissues during mouse development (Revil and Jerome-Majewska, 2013), although mesenchymal expression has also been reported in chicken (Sagnol et al., 2016). Recently, double knockout (DKO) mice for both *Esrp* genes were shown to display severe organogenetic defects, and a complete shift to exon IIIc inclusion in *Fgfr1*, *Fgfr2* and *Fgfr3* (Bebee et al., 2015). In addition, many *Esrp* exon targets were identified in genes involved in cell-cell adhesion, cell polarity and migration (Warzecha et al., 2010). However, the degree of evolutionary conservation and diversity of *Esrp* morphogenetic functions and its regulated AS programs at a large phylogenetic scale remain unknown.

esrp1 and *esrp2* are involved in multiple morphogenetic processes in zebrafish development.

A broad phylogenetic analysis showed that *Esrp* predates the origin of metazoans and that a single copy of *Esrp* has been maintained in most metazoan groups with the exception

of the vertebrate lineage, in which two copies are present in all studied species (Supplementary Fig. R1 and R2). To investigate the evolution of *Esrp* roles, we first examined the expression and function of the two *Esrp* paralogs (*esrp1* and *esrp2*) in zebrafish. A highly dynamic expression pattern was observed for both genes during the development of zebrafish using whole-mount *in situ* hybridization (WMISH) (Fig. R10a and Supplementary Fig. R3a). At early stages, both genes displayed different expression patterns. *esrp1* transcripts were detected in the whole epidermis at 14 hours post-fertilization (hpf), but its expression was restricted to the posterior part of the embryo at 16hpf. On the other hand, *esrp2* was found only in the hatching gland rudiment at these stages. However, from 24hpf to 5 days post-fertilization (dpf), the expression of both genes converged in most territories. Their transcription was transiently activated during the development of multiple organs, including the olfactory epithelium, otic vesicle, pharynx, epidermis and notochord. *esrp2* showed expression in a few additional tissues such as pronephros, hatching gland, liver and heart.

Next, we used the CRISPR-Cas9 system to generate loss-of-function zebrafish mutant lines for *esrp1* and *esrp2*. We targeted single guide-RNAs to the first and third exons of *esrp1* and *esrp2*, respectively (Fig. R10b). For *esrp1*, we selected a mutant allele with a 168-bp deletion and 14-bp insertion that induced the usage of an upstream cryptic splice donor, resulting in skipping of the whole coding sequence of exon 1, including the start codon. For *esrp2*, we selected a mutant allele with a 17-bp frame-disrupting deletion that produced a premature stop codon before the translation of any RNA-binding domain and that was predicted to trigger non-sense mediated decay (Fig. R10b). To determine the functional impact of these mutations, we attempted to clone the full-length version of both mutant and wild type (WT) alleles in a pcDNA3.1 vector and transfect the construct into human 293T cells. Whereas expression of the WT allele of zebrafish *esrp1* was able to modify the splicing pattern of previously reported endogenous targets (*EXOC7*, *ARHGAP17* and *FGFR1*) in the same way as its human orthologue (Warzecha et al., 2010), expression of the mutant *esrp1* allele did not produce any measurable effect in exon inclusion levels (Supplementary Fig. R3m). We were unable to clone the full-length transcript of the mutant *esrp2* allele due to its very reduced expression (Supplementary Fig. R3n), supporting that the selected *esrp2* allele is also a functionally null mutant.

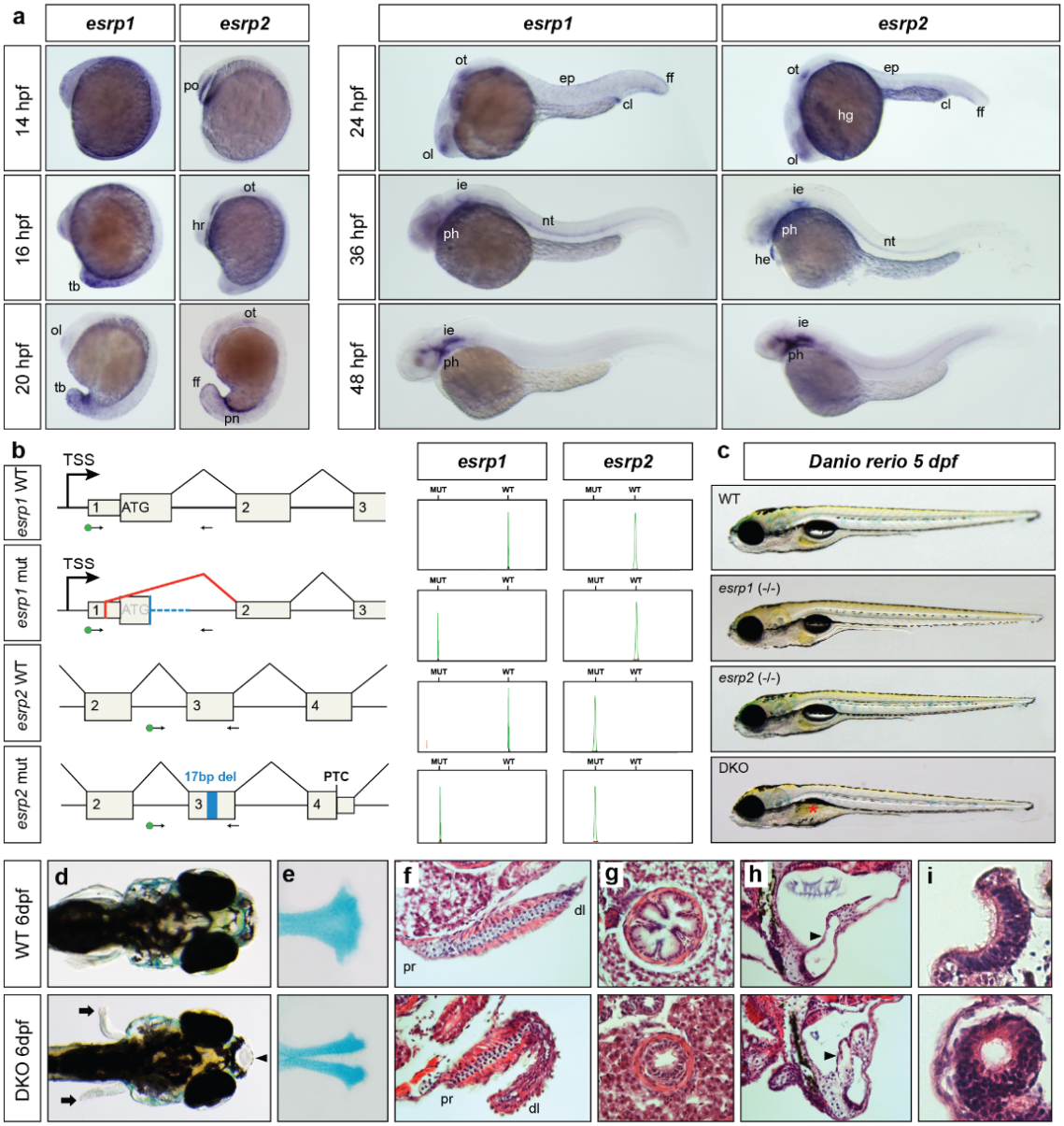

Figure R10 | Expression and developmental roles of *esrp1* and *esrp2* in zebrafish. (a) WMISH for *esrp1* and *esrp2* in *Danio rerio* wild type embryos. At 14hpf, *esrp1* transcripts were observed in embryonic epidermis, while *esrp2* expression was only detected in the polster (po). At 16hpf, *esrp1* was restricted to the posterior and tailbud (tb) epidermis, whereas *esrp2* persisted in the hatching gland rudiment (hr) and mild expression started to be detected in the otic placode (ot). By 20hpf, *esrp1* was found in the tailbud epidermis and more subtly in the olfactory placode (ol), while *esrp2* appeared in new territories such as pronephros (pn) and ectodermal cells of tailbud fin fold (ff). At 24hpf, expression of both paralogs presented a similar pattern including olfactory and otic placodes, cloaca (cl) and epidermis (ep), although *esrp2* was also observed in the hatching gland (hg). By 36hpf, both genes were detected in the inner ear epithelium (ie), notochord (nt), and phanynx (ph), and *esrp2* was also observed in the heart (he). At 48hpf, expression was found predominantly in inner ear and pharynx. **(b)** Left: Schematic representation of the genomic and

transcriptional impact of the selected *esrp1* and *esrp2* mutations. Blue boxes/lines represent genomic deletions in the mutants, while the red line depicts an altered splice junction in the *esrp1* mutant allele. TSS, transcription start site; PTC, premature stop codon; del, deletion. Standard and fluorescent (green dot) primers used during genotyping are represented by arrows. Right: genotyping of those embryos by fluorescent PCR distinguished between WT and KO alleles. **(c)** Representative 5dpf larvae for wild type (WT), *esrp1* knockout [*esrp1* (-/-)], *esrp2* knockout [(*esrp2* (-/-)] and double knockout (DKO) genotypes. Deflated swim bladder in the DKO embryo is indicated by an asterisk. **(d-i)** Phenotypic differences between 6dpf WT (top) and DKO (bottom) embryos in different embryonic structures. DKO larvae showed impaired fin formation (arrows) and cleft palate (arrowhead) **(d)**, including malformation of the ethmoid bone, as shown by alcian blue staining **(e)**. **(f-i)** Transversal histological sections stained with hematoxylin and eosin showing structural differences in pectoral fin **(f)**, esophagus **(g)**, inner ear **(h)** and olfactory epithelium **(i)**. Black arrowheads mark the dorso-lateral septum between semicircular canals in **(h)**. Proximal (pr) and distal (dl) parts of the fin are indicated in **(f)**.

Morphological examination of single *esrp1* or *esrp2* homozygous zebrafish mutants showed no apparent gross defects during development (Fig. R10c). Although *esrp2* knockout females were unable to produce eggs, both mutant lines grew normally in homozygosity and became seemingly healthy adults. However, double knockout (DKO) mutants presented multiple developmental abnormalities. Most larvae (28/37, 75.7%) died between 8 and 10dpf, and no fish survived beyond 14dpf. Phenotypic analysis of 6dpf DKO larvae showed multiple fully penetrant morphogenetic defects. All DKO larvae presented cleft palate (Fig. R10d), with the medial population of cartilage cells being absent in the ethmoid plate, as revealed by alcian blue staining (Fig. R10e). Fin development was also impaired, with evident dysgenesis of its distal endoskeletal part (Fig. R10f). Reduction in esophagus diameter and loss of its villous shape was observed (Fig. R10g). The volume of the inner ear was smaller compared to wild-type larvae, and the dorsolateral septum that separates the rostral and caudal semicircular canals was abnormally invaded by cellular and extracellular material (Fig. R10h). The posterior part of the olfactory epithelium formed a spherical internal lumen, instead of being open towards the embryo surface (Fig. R10i). Mutants also showed an abnormal arrangement of basibranchial pharyngeal cartilage (Supplementary Fig. R3p), in addition to a smaller and thicker swim bladder epithelium (Supplementary Fig. R3q), which failed to inflate in 24/35 (68,5%) of examined DKO embryos (Fig. R10c). Interestingly, *Esrp* genes in mouse are also required during development of structures homologous to some of these organs (Bebee et al., 2015), including several that exhibit distinct morphologies and

functions compared to zebrafish, such as the lungs/swim bladder, palate skeleton and pectoral limbs/fins.

To characterize the phenotype of the DKO embryos at the molecular level, we performed RNA-seq of two replicates of DKO 5dpf and age-matched WT larvae (see Methods). Differential gene expression analysis identified 248 and 609 down-regulated and up-regulated genes, respectively. Gene Ontology (GO) enrichment analysis showed functional categories that were highly consistent with some of the observed phenotypes, such as skeletal system development and sensory perception (Supplementary Fig. R3r). Interestingly, other significantly enriched categories pointed to specific impaired processes at the cellular level such as cell-cell adhesion, cell-matrix adhesion and cell component morphogenesis.

Esrp is able to modulate the motility of the mesenchymal cell lineage in vase tunicates.

To examine the diversity of roles that *Esrp* genes play during embryogenesis beyond the vertebrate clade, we first studied the ascidian *Ciona intestinalis*, a species belonging to its sister group, the tunicates (Delsuc et al., 2006). Expression of the single *Esrp* ortholog present in the *Ciona* genome was detected in the embryonic epidermis after neurulation, as in the case of vertebrates (Fig. R11). In addition, *Esrp* expression was also observed in a bilateral domain located within the mesenchymal lineage from early to late tailbud stage. *Ciona* mesenchymal cells derive from the *Twist-like1*-expressing A7.6 [trunk lateral cells], B7.7, and B8.5 blastomeres of the 110-cell stage embryo (Imai, 2003). As development proceeds, those cells divide and give rise to three mesenchymal sub-lineages that are located in a region of the trunk adjacent to the tail during mid-tailbud stages. *Twist-like1* enhances the transcription of several mesenchymal genes, including *Twist-like2*, before being downregulated around mid-tailbud stage (Imai, 2003; Tokuoka et al., 2004). In subsequent stages, a number of cells coming from the *Twist-like2*-positive lineage migrate towards the anterior part of the trunk to contribute to the formation of mesodermal organs (Tokuoka et al., 2005).

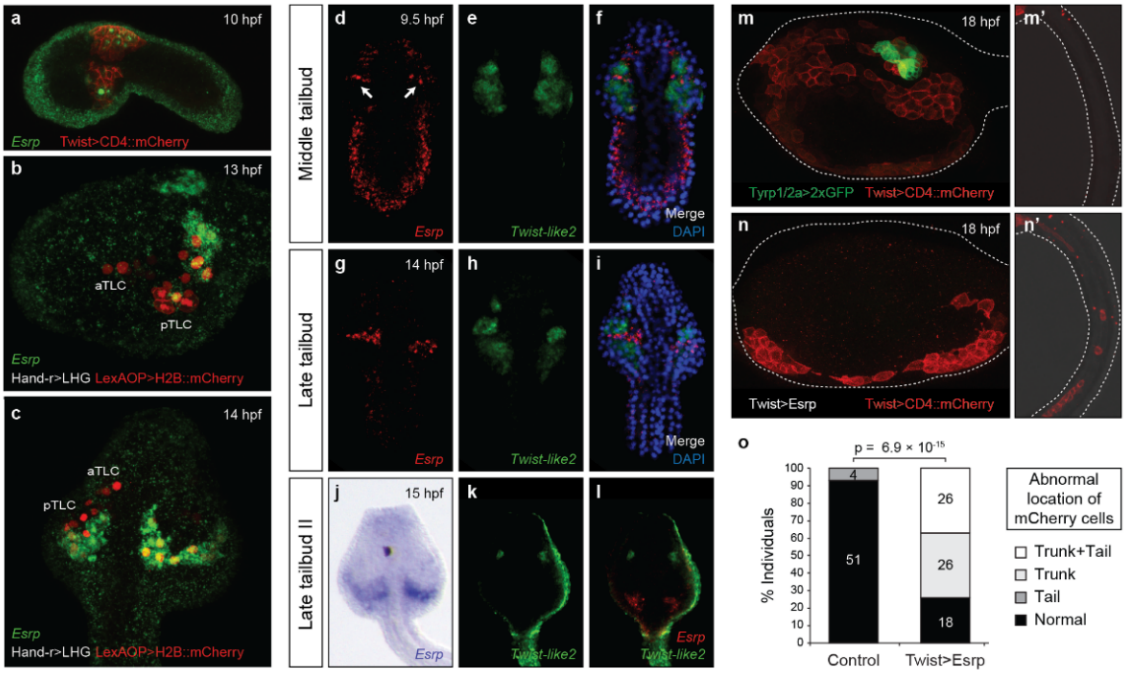

Figure R11 | *Esrp* is expressed in a subpopulation of TLCs in *Ciona* and is able to modulate cell motility in the mesenchymal lineage. (a) *Esrp* expression (green) is detected at 10hpf by fluorescent WMISH in the epidermis and in some cells within the mesenchymal lineage, as shown by co-staining with mCherry driven by the Twist promoter, which labels the *Twist-like1*-derived cell lineage. **(b-c)** *Esrp* (green) is expressed in the TLC lineage as shown by co-staining with Hand-r>LHG/LexAOP>H2B::mCherry (red) in 13hpf and 14hpf embryos in lateral (b) and dorso-lateral (c) views, respectively. aTLC: Anterior TLCs, pTLC: posterior TLCs. **(d-l)** Double fluorescent WMISH for *Esrp* (red) and *Twist-like2* (green), with the exception of (j), which corresponds to colorimetric *Esrp* mRNA staining (purple). At middle tailbud stage, *Esrp* expression is detected in both epidermis and mesenchymal cell lineage (the latter is marked by arrows). **(m-m')** Mesenchymal lineage in wild type larvae at 18hpf stained in red using the Twist>CD4::mCherry construct. Tyrp1/2a>2xGFP, which labeled pigment sensory organs in green, was used as co-electroporation control plasmid. **(n-n')** Mesenchymal lineage stained in larvae co-electroporated with Twist>CD4::mCherry and Twist>Esrp constructs. The trunk region is shown in (m-n), while tail segments are shown in (m'-n'). **(o)** Quantification of the different phenotypes of mesenchymal cell lineage motility observed in Twist>Esrp and control larvae. These included individuals with abnormal migration in the trunk ('Trunk'), with ectopic mCherry positive cells in the tail ('Tail') or both phenotypes ('Trunk + Tail'). P-values correspond to a two-sided Fisher Exact tests ('Normal' vs rest).

We confirmed the expression of *Esrp* within the mesenchymal lineage with a double-staining assay. Fertilized eggs were electroporated with a construct (Twist>CD4::mChe) carrying the *Twist-like1* promoter driving the expression of the membrane-targeted

Cherry (mChe) protein as a reporter (Gline et al., 2015). An anti-mChe antibody was used to track the mesenchymal cell lineage, while endogenous *Esrp* expression was visualized by fluorescent WMISH (Fig. R11a). A similar assay using a LexA/LexAop system driven by the *Hand-r* proximal enhancer (Tolkin and Christiaen, 2016) narrowed the identity of this *Esrp*-expressing domain down to a subset of posterior trunk lateral cells (Fig. R11b,c). This mesenchymal lineage contributes to the formation of specific organs like the oral siphon muscle and the epithelium of the $1^{st}/2^{nd}$ gill-slits (Tokuoka et al., 2005).

To unravel the dynamics of these *Twist-like1*-derived *Esrp*-positive cells, we next performed a double WMISH with probes for *Esrp* and *Twist-like2*. This showed that the expression of both genes is rapidly regulated during development and soon acquire a mutually exclusive expression pattern, which becomes evident by late tailbud stage (Fig. R11g-i). At late tailbud II stage, *Twist-like2* was restricted to anterior mesenchymal domains, while *Esrp* transcripts were only detected in the posterior-most part of the trunk (Fig. R11j-l).

The common developmental origin of these two cell populations, the function of *Twist-like2* as a key inducer of cellular migration (Abitua et al., 2012), and the described antagonistic roles of *Esrp* and *Twist* genes in mammalian cells (Shapiro et al., 2011) led us to hypothesize that *Esrp* may confer particular morphogenetic properties to the subset of cells within the mesenchymal lineage in which it is expressed. To test this possibility, we ectopically expressed *Esrp* in all mesenchymal cells (*Twist*>Esrp) during early stages, together with *Twist*>CD4::mChe to visualize them. We fixed embryos at larval stage, when a large part of the cell migration towards the anterior part of the trunk has occurred. We observed two main phenotypes associated with an abnormal mesenchymal distribution in 75% of individuals (n=70). In all affected embryos, migrating mChe-positive cells were found only in the lateral sides adjacent to the epidermis, but not through the middle part of the trunk (Fig. R11m-n,o). In addition, 35% of co-electroporated larvae also showed ectopic mChe-positive cells distributed along the tail, which were only very rarely observed in control individuals (Fig. R11o). Interestingly, a previous study found that some cells derived from B7.7 and B8.5 mesenchymal lineages, which normally do not express *Esrp,* localized in the tail of *Twist-like1* knockdown of

Ciona larvae, integrating muscular and endodermal tissues (Tokuoka et al., 2005). Altogether, our results thus suggest that *Esrp* may modulate motility properties of the mesenchymal cell lineage in ascidians, as well as compromise topological cellular fate when ectopically expressed.

Esrp expression in amphioxus embryos is associated with different morphogenetic processes.

We next investigated *Esrp* expression in the amphioxus *Branchiostoma lanceolatum*, a cephalochordate species that shares many developmental processes and a general bodyplan with vertebrates (Garcia-Fernàndez et al., 2009). Amphioxus *Esrp* showed a highly dynamic expression pattern during embryo development (Fig. R12). In early neurula embryos (14hpf), *Esrp* transcripts were observed in the border region, an ectodermal tissue adjacent to the neural plate (Fig. R12a). During neurulation, *Esrp* was strongly expressed along the ectodermal hinge points of neural tube closure (Fig. R12b-c). Right after neurulation (21hpf), transcription of *Esrp* was extended to the epidermis of the whole embryo (Fig. R12d). Finally, in pre-mouth larvae stages, the expression was restricted to the tailbud region, anterior ectoderm, and, strikingly, in a few cells near and within the dorsal epidermis (Fig. R12e-g). Because of their shape and location, the latter group of cells may correspond to a previously described population of epidermal sensory neurons (Benito-Gutiérrez et al., 2005; Kaltenbach et al., 2009; Lu et al., 2012). These cells have been reported to delaminate from the ventral ectoderm, migrate underneath the epithelium towards the dorsal part of the embryo and re-integrate into the ectoderm, where they become sensory cells. Based on its dorsal expression, we speculate that *Esrp* might contribute to the process of epithelial integration at the final migratory stages.

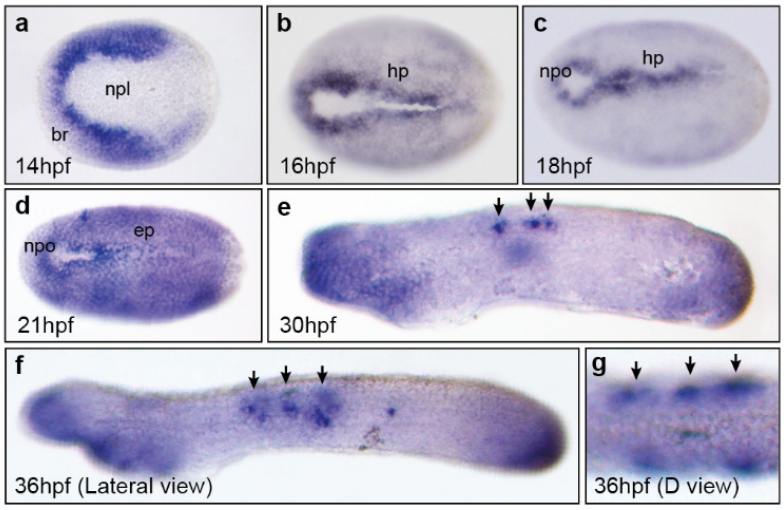

Figure R12 | *Esrp* is expressed dynamically in the non-neural ectoderm during amphioxus embryo development. WMISH of *Esrp* in *Branchiostoma lanceolatum* embryos. Anterior is to the left in all cases. **(a)** 14hpf early neurula (dorsal view) showing expression in the border region (br) next to the neural plate (npl). **(b,c)** 16hpf and 18hpf mid-neurula embryos (dorsal view) stained most strongly in the ectodermal cells next to the neural plate border and that form the hinge points (hp) during neural tube closure. The location of the neuropore (npo) is indicated. **(d)** In 21hpf late neurula (dorsal view), *Esrp* expression is extended throughout the whole epidermis (ep). **(e-f)** Early (30hpf) and late (36hpf) pre-mouth stages (lateral views) showing *Esrp*-positive cells in anterior ectoderm, tail bud epithelia and in a few cells that likely corresponding to migrating sensory cells during dorsal incorporation or already integrated into the epithelium (black arrows). **(g)** Dorsal (D) view shows the epidermal location those *Esrp*-positive cells.

Esrp is involved in ciliogenesis repression in ectodermal cells and the mesenchymal-to-epithelial transition of pigment cells in sea urchin.

We next investigated the functions of *Esrp* in the purple sea urchin *Strongylocentrotus purpuratus* (hereafter referred as 'sea urchin'). This organism belongs to Ambulacraria, a lineage closely related to chordates, with a transcriptome-based annotated genome and available genetic tools. Colorimetric WMISHs revealed *Esrp* expression in the ectoderm and mesoderm in one half of the embryo at blastula stage (24hpf) (Fig. R13a,b). At later stages (36hpf), expression became more complex in the mesoderm (Fig 4c). Expression was no longer detected at gastrula (48hpf) or early pluteus stage (72hpf). Fluorescent WMISH confirmed *Esrp* expression in the ectoderm and non-skeletogenic mesodermal

cells at 30hpf (Fig. R13d,e). To investigate the nature of the ectodermal expression, we performed double fluorescent WMISH with *Esrp* and *Hnf6*, a marker for the ciliary band (Poustka et al., 2004), the region where ciliary cells and neurons differentiate (Fig. R13f). No signal overlap was observed, indicating that *Esrp* expression is restricted to the non-neural ectoderm. Next, double WMISH with *Gcm*, a marker for aboral non-skeletogenic mesoderm (Andrikou et al., 2013), showed that *Esrp* expression in the ectodermal tissue corresponds to the aboral side (Fig. R13g-i). Interestingly, we observed co-expression of *Gcm* and *Esrp* in pigment cells precursors, a group of cells that migrate from the mesoderm towards the ectoderm, where they insert between epithelial cells becoming immunocytes (Gibson and Burke, 1985; Solek et al., 2013).

To explore the functions of *Esrp*, we generated gene knockdowns by injecting sea urchin zygotes with two different morpholinos (MO), one blocking translation and a second impairing splicing of intron 2. Efficiency of the splicing MO was assessed by RT-PCR (Fig. R13p). We observed two main phenotypic defects in both MO injections, supporting knockdown specificity (Fig R13q,r). First, a "chickenpox" phenotype was evident at gastrula (42hpf) (Fig. R13j,k and Supplemental Figure R4a) and prism/early pluteus (68hpf) stages (Fig. R13l-m,q). Whereas in control embryos most pigment cells were already located in the ectoderm at 42hpf and acquired a dendritic conformation by 68hpf, in knockdown embryos these cells were usually observed in the sub-ectodermal space at gastrula stage and maintained their roundish shape at prism stages ($p < 10^{-4}$ for all comparisons, Fisher Exact test). This failure in the complete integration of pigment cells into the ectoderm likely constitutes an impaired mesenchymal-to-epithelial transition. Second, knockdown embryos showed a "hairy" phenotype at gastrula and pluteus stage, consisting of ectopic long cilia on the aboral ectoderm, especially at the apex (Fig. R13j,k,n,o,r and Supplemental Fig R4b; $p < 10^{-6}$ for all comparisons, 3-way Fisher Exact test). In summary, these results demonstrate that *Esrp* in sea urchin is necessary for a complete integration of pigment cells into its destination epithelium and to avoid ciliogenesis in aboral ectodermal cells.

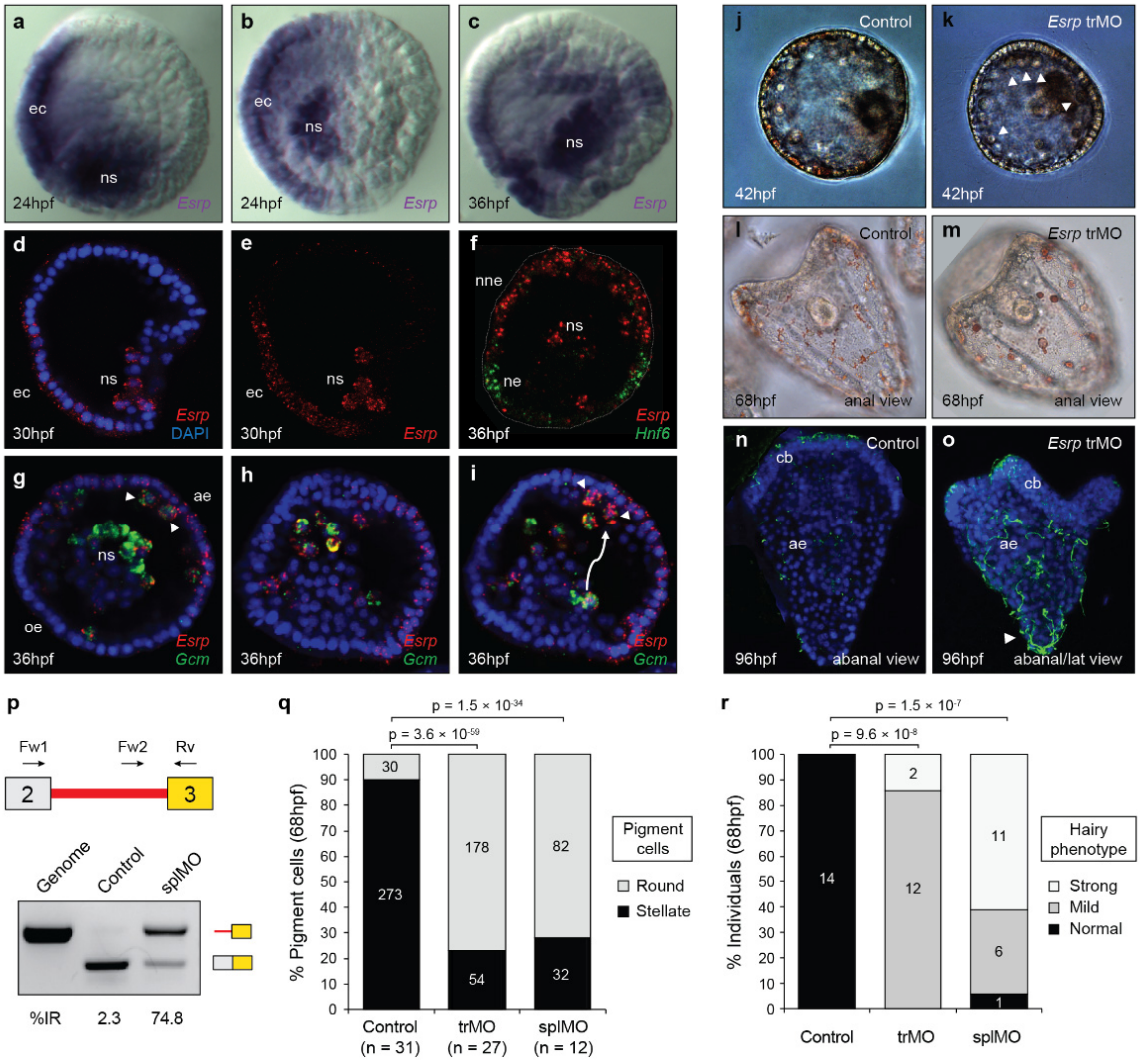

Figure R13 | *Esrp* represses cilia formation in aboral ectoderm and is necessary for complete MET of pigment cells. (a-c) Colorimetric WMISH of *Esrp* in *Strongylocentrotus purpuratus* embryos at 24hpf, in lateral (a) and dorsal (b) views showed expression in one side of the ectodermal territory (ec) and in some cells of the non-skeletogenic mesoderm (ns); signal at 36hpf, oral view (c), revealed a more complex pattern. **(d-e)** Fluorescent WMISH at 30hpf (lateral view) confirmed ectodermal and mesodermal expression of *Esrp*. **(f)** Double fluorescent WMISH showed that *Esrp* expression (red) was restricted to non-neuronal ectoderm (nne) at 36hpf (aboral view), since its signal did not overlap with the neurogenic ectoderm (ne) as labeled by *Hnf6* (green). **(g)** Double fluorescent WMISH of *Esrp* (red) and *Gcm* (green) at 36hpf (dorsal view) revealed that *Esrp* was expressed in the aboral ectoderm (ae) and in the pigment cell precursors. These cells are initially part of the aboral non-skeletogenic mesoderm and subsequently migrate towards the ectoderm. Some pigment cell precursors that are already in contact with the ectodermal epithelium are marked by arrowheads. Oral ectoderm (oe). **(h-i)** *Esrp* (green) and *Gcm* (red) at 36hpf in two different stacks from same embryo (lateral view). The arrow indicates a representative migratory path of pigment cells from mesoderm to ectoderm. **(j-k)** Early gastrula (42hpf) from uninjected control and *Esrp* trMO embryos showed marked differences in pigment cell location and cilia presence. Pigment cells in the sub-ectodermal space are indicated by white

arrowheads. **(l-m)** Early pluteus larvae (68hpf) in lateral view show marked differences in pigment cell morphology in control and *Esrp* trMO embryos (stellate and roundish, respectively). **(n,o)** Ectopic embryonic cilia stained with acetylated tubulin in the aboral ectoderm (ae) of 96hpf *Esrp*-trMO injected embryos. Apex is marked by a white arrowhead. Ciliary band (cb). **(p)** RT-PCRs showing the levels of intron 2 retention in *Esrp* transcripts from control and *Esrp* splMO embryos; genomic DNA was used as a reference for intron inclusion. **(q)** Quantification of pigment cell morphology in control, *Esrp* trMO and splMO knockdown 68hpf embryos (sum of 3 independent experiments). **(r)** Quantification of the 'hairy' phenotype in control, *Esrp* trMO and spMO knockdown 68hpf embryos (sum of 2 independent experiments). P-values correspond to 2-way (q) or 3-way (r) two-sided Fisher Exact tests.

To further characterize these developmental defects, we generated RNA-seq data for two replicates of SplMO-injected embryos at 24hpf and age-matched controls. These data confirmed our RT-PCRs results showing a high level of retention of *Esrp* intron 2 due to the morpholino effect (Supplementary Fig. R4c). Differential gene expression analysis identified 360 and 712 downregulated and upregulated genes, respectively. Interestingly, some enriched GO categories for these gene sets were similar to those found for the zebrafish DKO analysis, including cell-cell adhesion, cell component morphogenesis and ectoderm development (Supplementary Fig. R4d). We also observed a significant enrichment for functions related to nervous system development among the upregulated genes, consistent with a possible failure in proper non-neural ectoderm specification.

Evolutionary comparison of *Esrp*-dependent programs.

Next, we investigated the origin and evolution of alternative exon programs regulated by *Esrp* across multiple phylogenetic timescales using our zebrafish and sea urchin RNA-seq data, as well as previously published RNA-seq data for *Esrp* perturbations in mouse epidermis (Bebee et al., 2015) and three human cell cultures (Dittmar et al., 2012; Yang et al., 2016). Importantly, this approach detected both direct and indirect *Esrp*-regulated events, hereafter referred together as *Esrp*-dependent. We identified 188 differentially spliced cassette exons in sea urchin, 494 in zebrafish, 254 in mouse and 336 in human (see Methods for details). In all species, these exons were found enriched in genes associated to certain GO terms such as vesicle-mediated transport, GEF activity, and actin cytoskeleton cell components (Supplementary Fig. R5). Additionally, we detected lower numbers of other types of AS regulatory changes, such as alternative 5′ or 3′ splice site

choice and intron retention (Fig. R14a). RT-PCR assays validated all tested differentially regulated exons in zebrafish (ΔPSI correlation $R^2 = 0.90$, n=15) and in sea urchin ($R^2 = 0.89$, n=12) (Supplementary Fig. R6).

To understand the evolution of *Esrp*-dependent programs at the exon level, we performed automatic comparisons followed by manual curation to detect high confidence homologous coding cassette exons within conserved gene intron-exon structures (Supplementary File 2 and see Methods). A large fraction of alternative exons was detected as *Esrp*-dependent only in one of the studied species, ranging from 47.8% (110/232) in mouse to 99.5% (180/181) in sea urchin (Fig. R14b). However, comparisons between closely and distantly related organisms uncovered different scenarios with regards to the sources for exon recruitment. On the one hand, most non-overlapping *Esrp*-dependent exons in vertebrates could be found in the other species, ranging from 93% in mouse to 52% in zebrafish (Fig. R14b). On the other hand, we only detected homologous counterparts in any of the studied genomes for 21% of sea urchin non-overlapping exons.

When focusing on the full set of 308 human *Esrp*-dependent exons, 82.5% had a homologous exon in mouse, most of which were also alternatively spliced in the rodent species (Fig. R14c). Among the latter subset, 116 exons were also identified as *Esrp*-dependent in mouse. These events include numerous previously described *Esrp*-dependent exons in genes such as *Scrib, Nf2*, *Enah* and *Grhl1* (Bebee et al., 2015). From this set of shared mammalian targets, we found homologous exons in zebrafish for 70 cases (60%), most of which were also alternatively spliced in this species (Fig. R14c). Interestingly, we detected a core set of 22 homologous exons classified as *Esrp*-dependent in the three vertebrate species, including some in genes previously associated with morphogenetic processes (Warzecha and Carstens, 2012) (e.g. *Numb, p120-catenin*, *Arhgap17* or *Itga6*). However, most of these exons (90.9%) did not have a detected homologous counterpart in sea urchin, and the two exons identified in the echinoderm genome did not exhibit *Esrp*-dependent differential regulation (Fig. R14c). From the total set of *Esrp*-dependent exons in sea urchin, only one homologous exon showed changes in inclusion also in human (Fig. R14b), but was constitutively spliced in both mouse and zebrafish, suggesting that *Esrp*-dependent regulation was independently acquired.

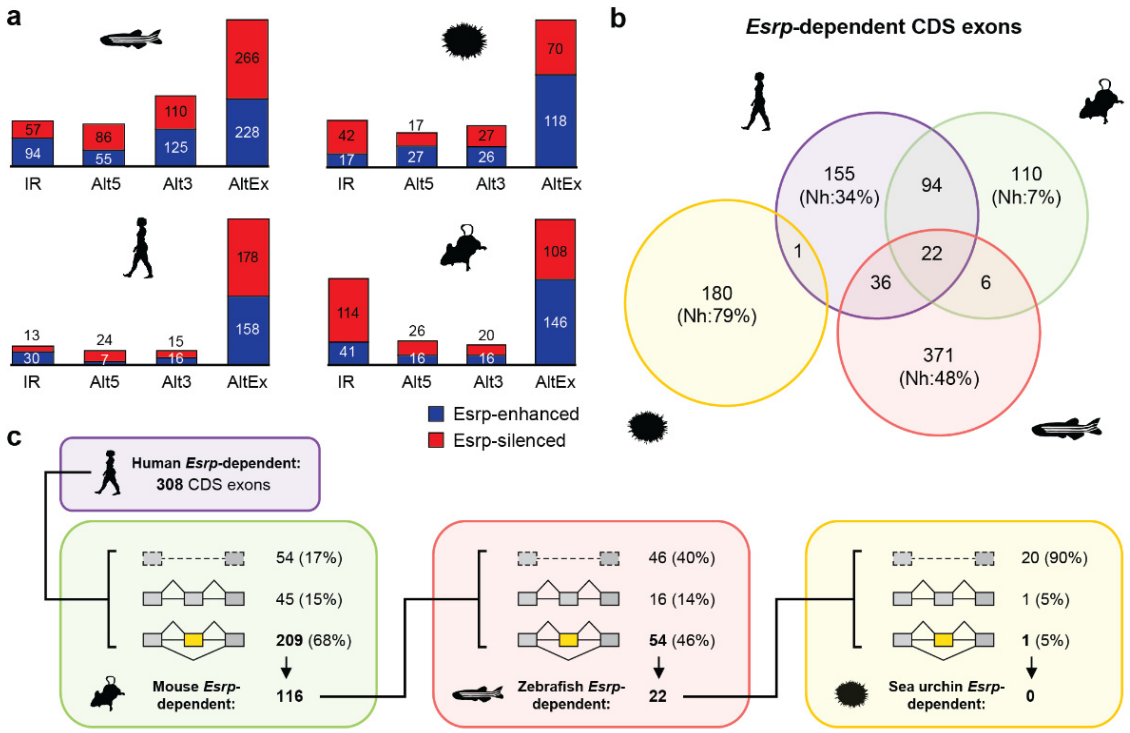

Figure R14 | Evolution of *Esrp*-dependent splicing programs. (a) Number *Esrp*-dependent AS events by type detected in zebrafish, sea urchin, human and mouse RNA-seq samples. Blue/red bars correspond to *Esrp*-enhanced/silenced inclusion of the alternative sequence. IR, intron retention; Alt5, alternative 5′ splice site choice; Alt3, alternative 3′ splice site choice; AltEx, alternative cassette exons. **(b)** Venn diagram showing the overlap among *Esrp*-dependent cassette exons in coding regions in the four species. For exons with clade-specific *Esrp*-dependent regulation, the percent of exons with no homology in any of the other species is provided (Nh). **(c)** Summary of conservation at the level of genomic presence, alternative splicing and *Esrp*-dependency for human *Esrp*-dependent coding exons in other species. Shared *Esrp*-dependent exons between the previous phylogenetic group is classified in the test species into three categories: (i) the exon is not detected in the genome (top row, discontinuous line); (ii) the homologous exon is detected in the genome, but it is constitutively spliced (middle row, grey exon); and (iii) the homologous exon is alternatively spliced (bottom row, yellow exon, bold numbers). Below this exon type classification, number of *Esrp*-dependent exons shared by the two species/lineages.

Along these lines, we also identified 49 orthologous genes whose alternative splicing was dependent on *Esrp* in at least two species, but in which the specific regulated exons were different (i.e. non-homologous). Twenty one of these cases involved sea urchin and at least one vertebrate, and impact genes related to diverse morphogenetic processes in metazoans (Boehlke et al., 2015; Bouchet et al., 2016; Jung et al., 2011; Laprise et al.,

2010; Zhao et al., 2013) (e.g. *Exoc7*, *Slain2*, *Epb41*, *Ift88* and *Scrib*). Moreover, we further observed a significant fraction of target genes with more than one *Esrp*-dependent exon, ranging from 5.2% in sea urchin to 19.1% in zebrafish. These observations highlight the evolutionary plasticity of some genes for multiple acquisition of AS regulation. An interesting case is *Cd44*, which acquired at least nine *Esrp*-dependent exons within the mammalian clade, and is involved in ureteric branching in mouse (Pohl et al., 2000), a process affected in *Esrp1* KO mice (Bebee et al., 2016).

Regulation of *Fgfr* AS by *Esrp* is conserved across the chordate phylum.

Among the 22 *Esrp*-dependent homologous AS event groups shared by the three vertebrate species, one case involved multiple paralogous genes of the *Fgfr* family. Evolutionary conservation of the mutually exclusive exons encoding the IgIII domain of *fgfr2* had been previously reported for zebrafish (Liu et al., 2011). As in mammals (Vainikka et al., 1992), we found homologous AS events also in *fgfr1a*, *fgfr1b* and *fgfr3,* but not in *fgfr4*. RT-PCR assays for those *Fgfr* genes showed a complete isoform switch towards the mesenchymal IIIc exons in zebrafish *esrp1* and *esrp2* DKO embryos (Fig. R15a). Interestingly, the *Fgfr* ortholog of sea urchin harbored only one exon homologous to those alternatively spliced in vertebrates and it was constitutively included in all transcripts (see below). Therefore, to assess when this AS event originated during evolution, we first turned to the chordate amphioxus. We found that the sole amphioxus *Fgfr* gene harbors exons homologous to IIIb and IIIc that are also alternatively spliced in a mutually exclusive manner. In addition, a cephalochordate-specific exon was found in this genomic region (exon IIIx; Fig R15b). RT-PCR assays on dissected adult tissues showed that *Esrp* expression was only strongly detected in the amphioxus skin, where the highest inclusion of exon IIIb was also observed (Fig R15b). An amphioxus-specific isoform including both exons IIIx and IIIc was also detected in this tissue, while inclusion of exon IIIc alone was nearly absent. On the other hand, the rest of the tissues express predominantly the isoform containing only the exon IIIc.

To gain further insights into the regulatory evolution of this event, we made two minigene constructs, one comprising the whole genomic region spanning the amphioxus *Fgfr* AS

event, and one lacking the amphioxus-specific exon IIIx (Fig. R15c). These minigenes were individually transfected into human 293T cells together with an expression vector containing the amphioxus or the zebrafish full-length *Esrp* transcripts. Remarkably, despite considerable mis-splicing of the minigenes in 293T cells, amphioxus *Esrp* acted as a major regulator of *Fgfr* AS, promoting inclusion of IIIb exon in both minigenes (Fig. R15c). On the other hand, zebrafish *esrp1* produced only very mild changes compared to the control, despite both amphioxus and zebrafish *Esrp* genes were able to modify the AS pattern of endogenous exon targets as the human *ESRP1* (Fig. R15d and Supplementary Fig. R7). Therefore, altogether, these results provide two main insights into the evolution of *Fgfr* AS regulation: (i) its mutually exclusive regulation by *Esrp* originated before the last common ancestor of chordates; and (ii) it acquired lineage-specific regulatory requirements in *trans* in cephalochordates.

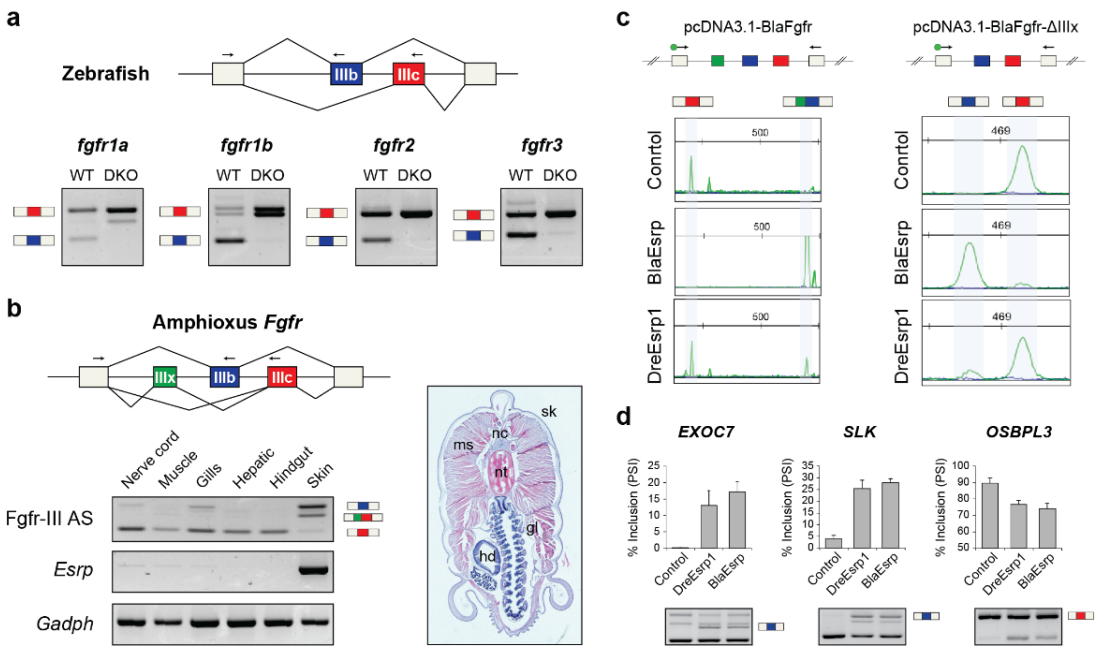

Figure R15 | *Fgfr* AS is regulated by *Esrp* genes in vertebrates and amphioxus. (a) RT-PCR assays showing differential *Fgfr* exon IIIb and IIIc inclusion in wild type versus DKO 5dpf zebrafish embryos. **(b)** RT-PCR assays for *Fgfr* AS in different amphioxus adult tissues, depicted in a transversal section. Nc, nerve cord, ms, muscle, gl, gills, hd, hepatic diverticulum, nt, notochord, sk, skin. Reverse primers were designed in both exons IIIb and IIIc (arrows) and used together in the same PCR reactions. **(c)** Top: schematic representation of pcDNA3.1-based minigene constructs containing the genomic region spanning the *Fgfr* AS event of *Branchiostoma lanceolatum*, with (pcDNA3.1-BlaFGFR) and without (pcDNA3.1-BlaFGFRΔIIIx) exon IIIx.

Bottom: relative intensity of fluorescent RT-PCR bands supporting differential inclusion of exons IIIb and IIIc when transfecting the minigenes alone (Control) or together with a plasmid containing either amphioxus or zebrafish full-length *Esrp* transcripts (BlaEsrp and DreEsrp1, respectively). Despite significant mis-splicing of the minigene in all conditions, only the amphioxus construct was able to induce a dramatic switch towards exon IIIb inclusion. Primers were designed in the neighboring constitutive exons (arrows). **(d)** RT-PCR assays for endogenous human AS events in the same control, BlaEsrp or DreEsrp1 transfected 293T cells showing that the amphioxus and zebrafish *Esrp* constructs are able to modulate endogenous *Esrp*-dependent events in a similar manner. *Esrp*-enhanced isoforms are marked with a black arrowhead.

Fgfr AS evolved independently in several Bilateria lineages.

Given the remarkable conservation across chordates (for over 550 million years of independent evolution), we next studied the evolution of *Fgfr* AS in further detail. A gene structure analysis for Bilateria species showed that vertebrate exons IIIb and IIIc are the result of a single tandem exon duplication that occurred at the base of the chordate phylum, before the split of its three main sub-phyla (Fig. R16). In contrast to chordates, the single pro-orthologous exon IIIb/IIIc is found as constitutively included in all observed transcripts from all studied non-chordate species. However, previous studies reported other AS events in the genomic locus encoding the region homologous to the IgIII domain in two non-vertebrate species (the purple sea urchin (McCoon et al., 1998; Mistry et al., 2003) and the red flour beetle (Sharma et al., 2015)), and we further show that a diverse array of AS events independently evolved in most studied lineages (Fig. R16). In particular, the previously reported alternative exon in sea urchin is located upstream of exon IIIb/c and exhibits no sequence similarity with its neighboring exons. Moreover, its inclusion was not detected as *Esrp*-dependent, which is consistent with the non-overlapping expression of *Fgfr* and *Esrp* genes during sea urchin's development (Andrikou et al., 2015). Remarkably, this exon is also present and alternatively spliced across the Ambulacraria clade, which comprises echinoderms and hemichordates phyla. In summary, our phylogenetic survey shows that this genomic region is a hotspot for recurrent AS evolution across Bilateria, likely due to its potential to modulate FGF signaling (Miki et al., 1992).

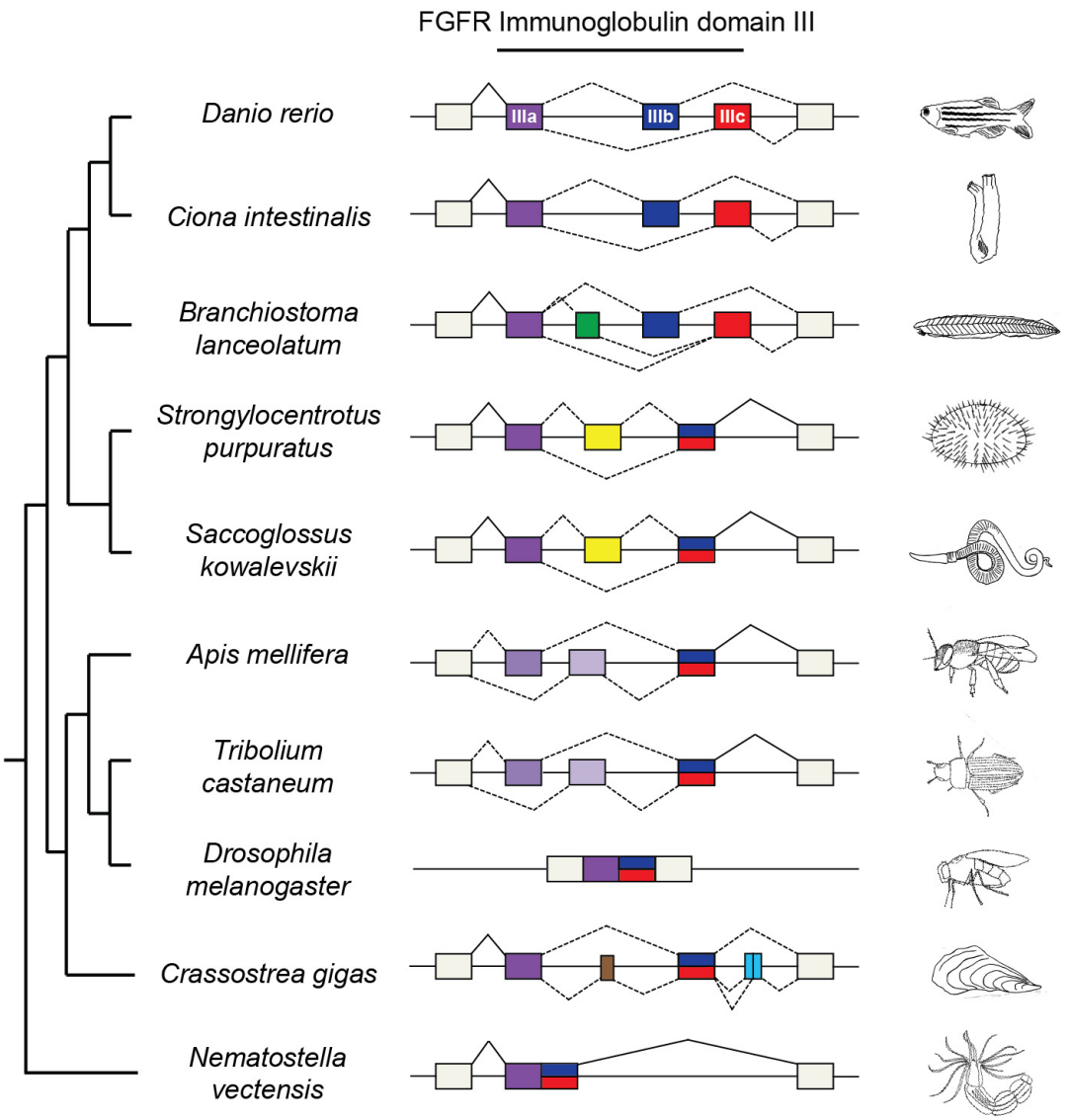

Figure R16 | Gene structure and AS at the IgIII domain of the *Fgfr* gene family in metazoans. Schematic representation of the AS diversity in the region encoding the homolog of the *Fgfr* IgIII domain for zebrafish (*Danio rerio*), vase tunicate (*Ciona intestinalis*), amphioxus (*Branchiostoma lanceolatum*), purple sea urchin (*Strongylocentrotus purpuratus*), acorn worm (*Saccoglossus kowalevskii*), honey bee (*Apis mellifera*), red flour beetle (*Tribolium castaneum*), fruit fly (*Drosophila melanogaster*), pacific oyster (*Crassostrea gigas*) and starlet sea anemone (*Nematostella vectensis*). Homologous to vertebrate exons IIIa, IIIb and IIIc are shown in purple, blue and red, respectively. The non-chordate pro-orthologous exon of exons IIIb and IIIc is colored half blue and half red. The amphioxus- and ambulacrarian-specific alternative exons are depicted in green and yellow, respectively. Light violet colors are used for the insect-specific mutually exclusive event involving exon IIIa, and brown and light blue for oyster-specific exons. Grey exons are constitutive in all species. Fruit fly orthologues (*heartless* and *branchless*) are intronless genes.

Figuras suplementarias

Supplementary Figure R1

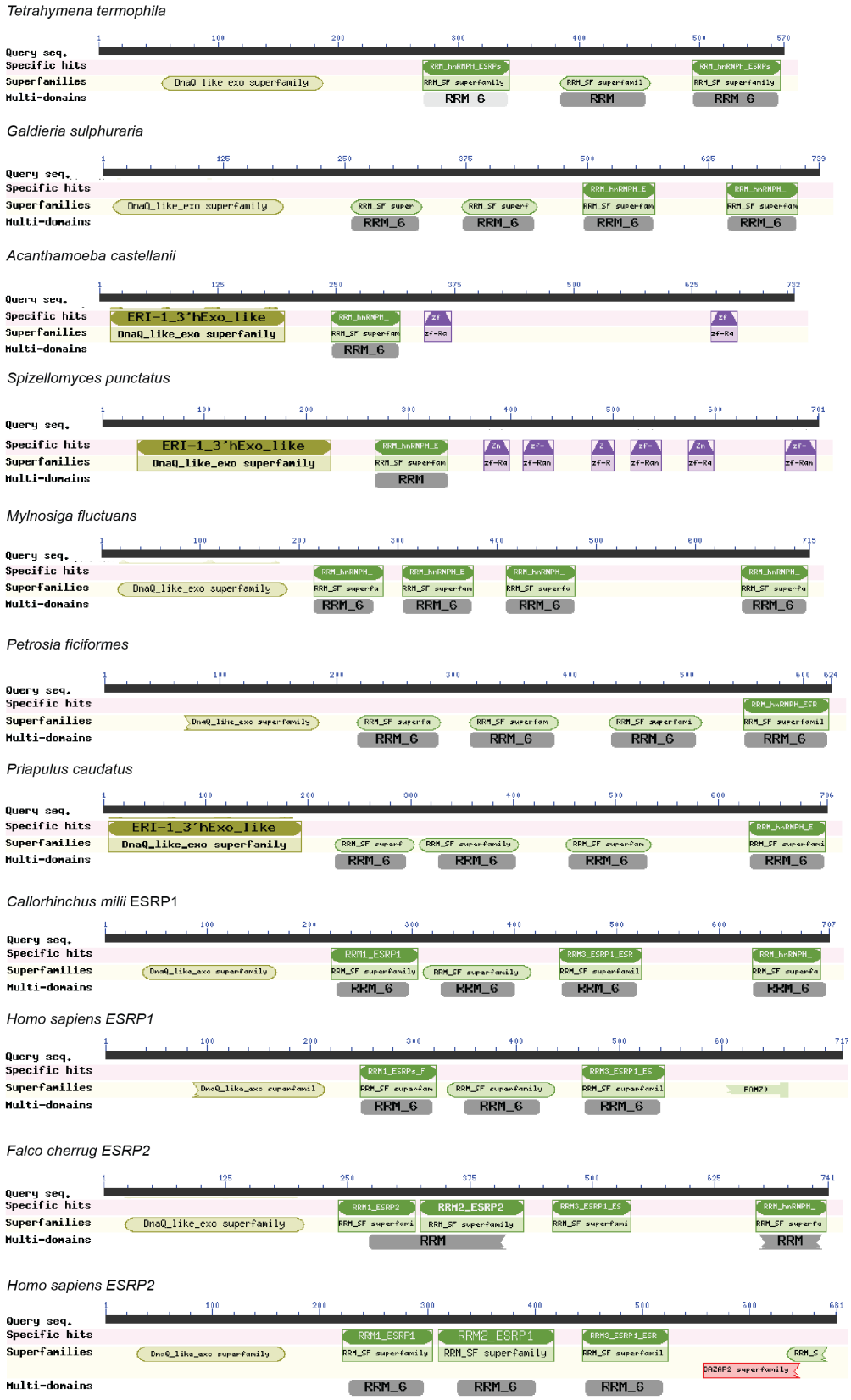

Supplementary Figure R1 | Protein domain composition of *Esrp* homologous genes in eukaryotic species.

All represented eukaryotes share a DnaQ-like exonuclease domain in their *Esrp* homologous genes. Variation arises from the number of RRM6 domains, a specific type of RNA-binding domain. The alveolata species *Tetrahymena termophila*, and the rodhophyte *Galdieria sulphuraria* have three and four RRM6 domains, respectively. In the amebozoan *Acanthamoeba castellanii* and the fungi *Spizellomyces punctatus*, more closely related to metazoans, only one RRM6 domain was found. Zinc finger domains were also detected in those species. Four RRM6 domains were found in orthologues from choanoflagelate and metazoan species. However, partial or no detection of a fourth RRM6 domain was observed in some species, especially in *Esrp1* genes from vertebrates. Partial DAZAP2 and FAM70 domains were also detected in human genes, but with low e-values. Other species in the figure are the choanoflagelate *Mylnosiga fluctuans,* the demosponge *Petrosia ficiformis*, the priapulid *Priapulus caudatus*, the chondrichthyan *Callorhincus milii*, the dinosaur *Falco cherrug* and the mammal *Homo sapiens*.

Supplementary Figure R2

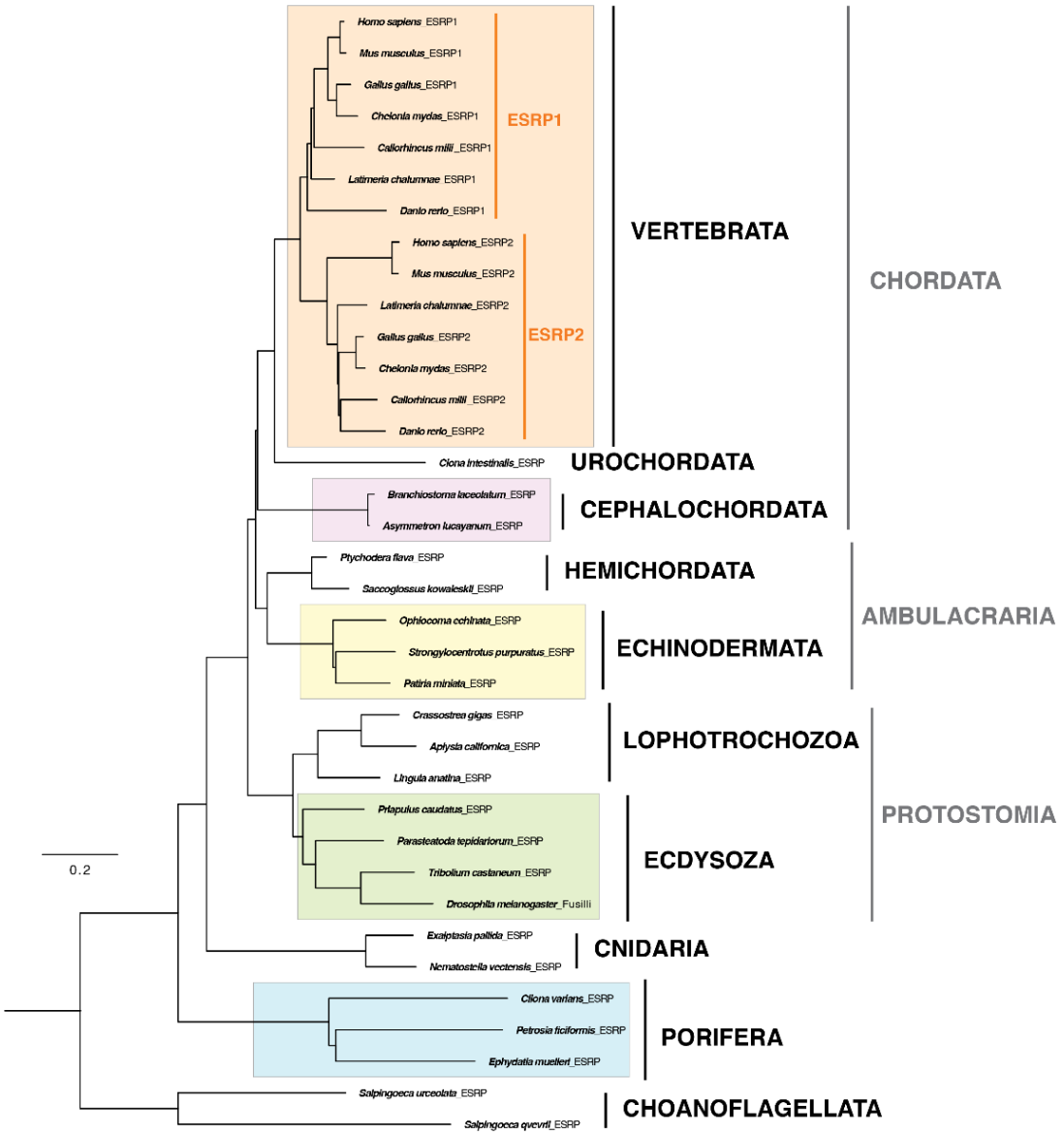

Supplementary Figure R2 | Phylogenetic analysis reveals a lineage-specific duplication of *Esrp* genes in vertebrates.

Most species shown in the tree belong to metazoan lineages, with the exception of choanoflagelates *Salpingoeca urceolata* and *Salpingoeca qvevrii*. Vertebrates: *Homo sapiens* (Hsa), *Mus musculus* (Mmu), *Gallus Gallus* (Gga), *Chelonia mydas* (Cmy), *Callorhincus milii* (Cmi), *Latimeria chalumnae* (Lch) and *Danio rerio* (Dre). Urochordates: *Ciona intestinalis* (Cin). Cephalochordates: *Branchiostoma lanceolatum* (Bla) and *Asymmetron lucayanum* (Alu). Hemichordates: *Ptycodera flava* (Pfl) and *Saccoglossus kowalevskii* (Sko). Echinoderms: *Ophiocoma echinata* (Oec), *Strongylocentrotus purpuratus* (Spu) and *Patiria miniata* (Pmi). Lophotrochozoans: *Crassostea gigas* (Cgi), *Aplysia californica* (Aca) and *Lingula anatina* (Lan). Ecdysozoans: *Priapulus caudatus* (Pca), Parasteatoda tepidariorum (Pte), Tribolium castaneum (Tca) and Drosophila melanogaster (Dre). Cnidarians: *Exaiptasia pallida (Epa) and Nematostella vectensis (Nve). Sponges: Cliona varians (Cva), Petrosia ficiformis (Pfi) and Ephydatia muelleri (Emu).*

Supplementary Figure R3

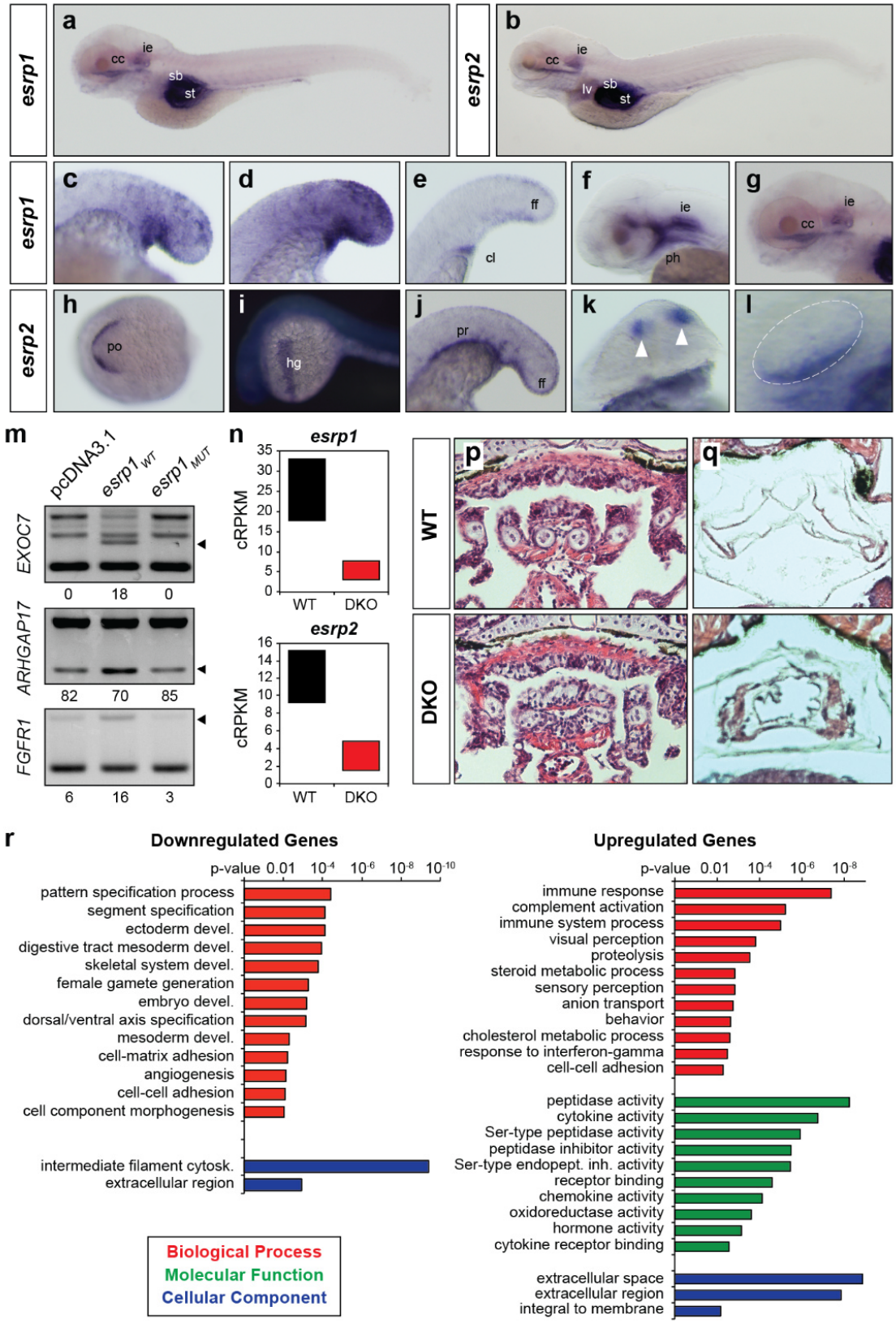

Supplementary Figure R3 | Developmental expression and impact of *Esrp* genes in zebrafish.

Additional details of WMISH for *esrp1* and *esrp2* in zebrafish embryos. **(a,b)** Similar expression of *esrp1* and *esrp2* was detected in 5dpf embryos in inner ear (ie) and craniofacial cartilaginous (cc) tissue. Signal was also observed in stomach (st) and swim bladder (sb), although non-specific staining of those hollow organs by NBT/BCIP precipitation could not be ruled out. *esrp2* was additionally found in the liver (lv). **(c-e)** Broad expression of *esrp1* in the tail bud ectoderm was maintained at 18hpf (c), reached its highest intensity by 20hpf (d), and became restricted to the median fin fold (ff) by 24hpf (e)**,** when it was also observed in cloaca (cl) tissue. **(f)** 48hpf embryo heads showed expression of *esrp1* predominantly in pharynx (ph) and inner ear (ie). **(g)** Detail of *esrp1* expression in the head of 5dpf embryos in craniofacial cartilague (cc) and inner ear (ie). **(h-l)** *esrp2* expression was also detected in a few territories where *esrp1* was not observed, including the polster (po) at 14hpf (h), that later develops into the hatching gland (hg) by 24hpf (i), and in the pronephros (pr) (j); it shared expression with *esrp1* in structures such as olfactory placode (white arrowheads) (k, 24hpf) and inner ear ventral epithelium (l, 32hpf). (**m**) Ectopic expression of wild type, but not mutant, zebrafish *esrp1* transcripts in human 293T cells produced splicing changes in endogenous *ESRP1* human targets. Black arrowheads indicate *Esrp*-enhanced isoforms. (**n**) Expression of *esrp1* and *esrp2* expression in 5dpf embryos quantified by RNA-seq shows a clear reduction in the steady-state mRNA levels of both genes in DKO embryos. Boxes represent the range of expression in the two replicates. (**p,q**) Phenotypic comparison of transversal sections stained with hematoxylin and eosin from 6dpf embryos shows impaired development of visceral skeleton (p) and swim bladder (q). (**r**) Significantly enriched GO terms for down- and up-regulated genes in DKO 5dpf embryos.

Supplementary Figure R4

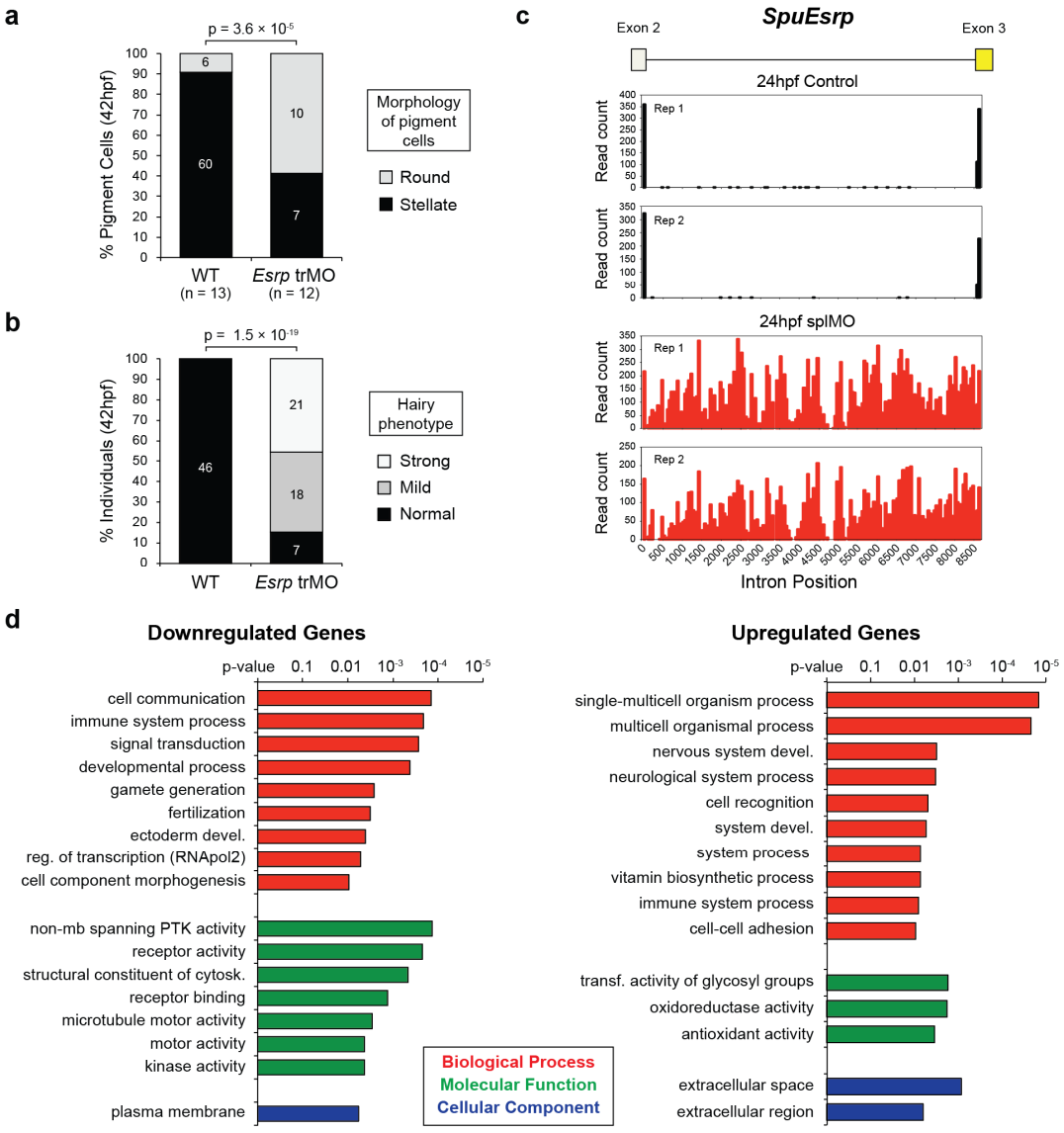

Supplementary Figure R4 | Developmental and transcriptomic impact of *Esrp* in sea urchin.

(a) Quantification of pigment cell morphology in control and *Esrp* trMO knockdown embryos at 42hpf. **(b)** Quantification of the 'hairy' phenotype in control and *Esrp* trMO knockdown embryos at 42hpf. P-values correspond to 2-way (a) or 3-way (b) two-sided Fisher Exact tests. (**c)** RNA-seq reads mapping to the genomic region spanning exons 2 and 3 of *Esrp* in control and SplMO injected embryos. **(d)** GO terms enriched in genes with down- and up-regulated expression in 24hpf embryos upon splMO treatment.

Supplementary Figure R5

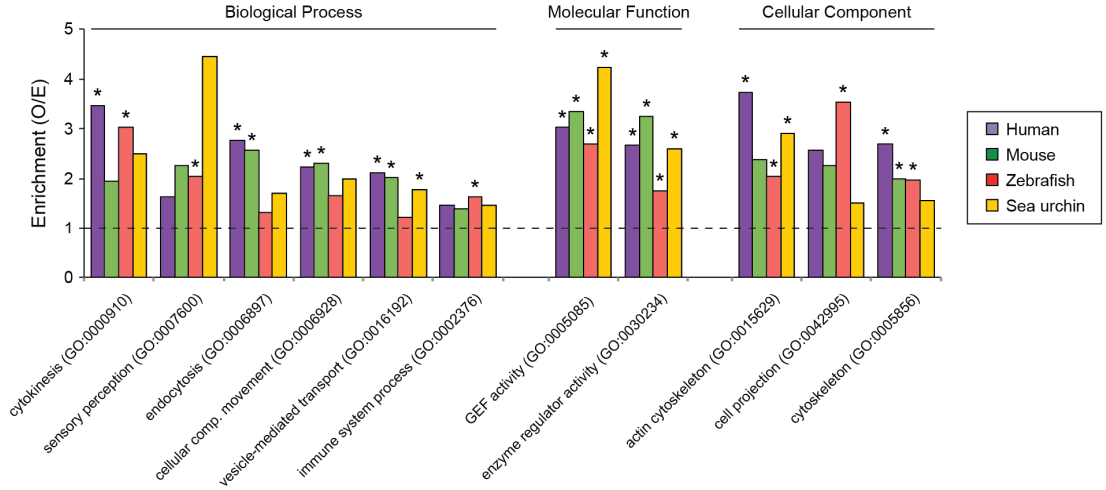

Supplementary Figure R5 | Gene Ontology enrichment of genes containing *Esrp*-dependent exons among all studied species.

GO Categories that were significantly over-represented in at least one species and showed an observed vs. expected enrichment ratio higher than 1.3 for all species. Asterisks indicate significant over-representation ($p<0.05$) in a given species, as calculated by PANTHER.

Supplementary Figure R6

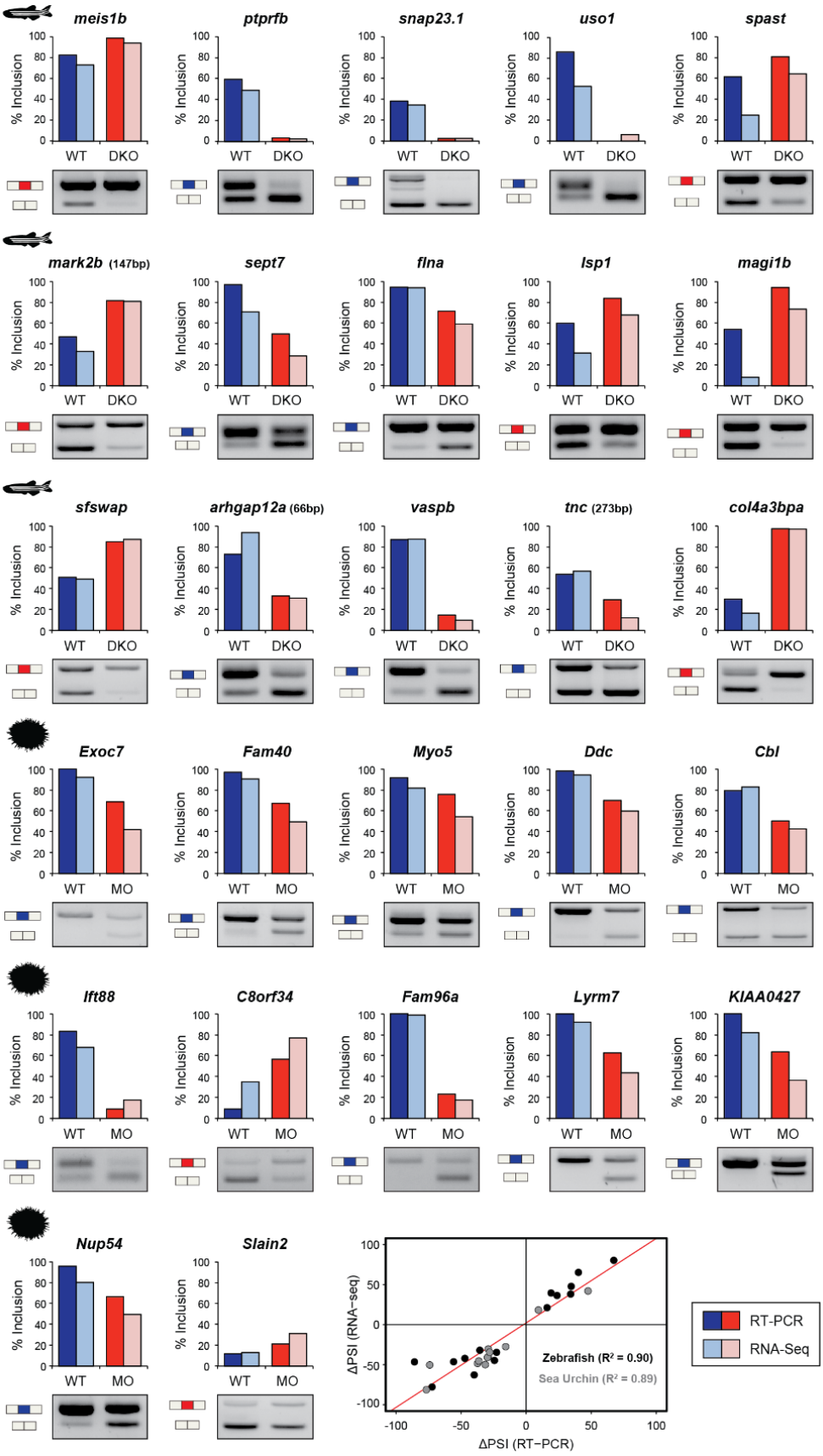

Supplementary Figure R6 | Validation of *Esrp*-dependent exons by RT-PCR.

RT-PCR (dark colors) and RNA-seq (light colors) based quantification of exon inclusion for a subset of 15 and 12 representative *Esrp*-dependent exons in wild type (blue) and *Esrp*-depleted (red) zebrafish and sea urchin embryos, respectively. Bottom-right: correlation between ΔPSI values obtained by RNA-seq and PCRs. Strong correlations are observed both in case of zebrafish (R^2=0.90, black dots) and sea urchin (R^2=0.89, grey dots).

Supplementary Figure R7

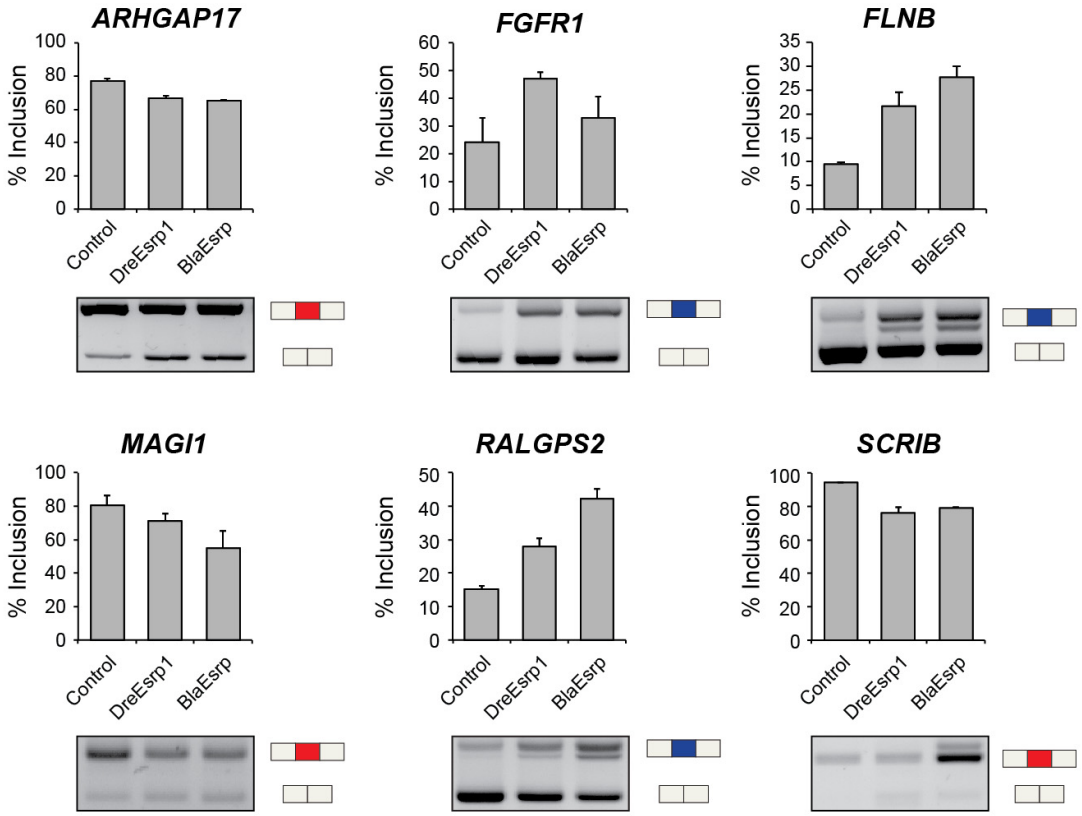

Supplementary Figure R7 | *Esrp* transcripts from amphioxus and zebrafish change the splicing pattern of endogenous human *Esrp*-dependent exons in 293T cells.

RT-PCR quantifications of ΔPSI changes in endogenous exons in 293T cells after transfection of expression vectors containing amphioxus (BlaEsrp) or zebrafish (DreEsrp1) ORF sequences. Error bars correspond to the standard error of three independent replicates.

MÉTODOS

Domain and phylogenetic analyses of *Esrp* genes. Putative *Esrp* orthologs for all organisms included in Supplementary Fig. 1 and 2 were identified by combining blastp and tblastn searches against NCBI databases and resources specific for sponges (Riesgo et al., 2014) and choanoflagellates *Salpingoeca urceolata, Salpingoeca qvevrii, and Mylnosiga Fluctuans* from unpublished transcriptomes provided by Daniel Richter. Domain detection was performed using the NCBI conserved domain search function (Marchler-Bauer et al., 2015) (https://www.ncbi.nlm.nih.gov/Structure/cdd/wrpsb.cgi). To reconstruct the phylogenetic relationships of *Esrp* genes among the Apoikozoa clade (Metazoa + Choanoflagellata), we first aligned protein sequences with MAFFT (Katoh and Standley, 2013). Neighbor-joining algorithm, as implemented by MEGA7 with default parameters and a JTT substitution model, was employed for tree reconstruction using only conserved positions of the multi-sequence alignment, as identified by MAFFT.

Zebrafish experimental procedures. Breeding zebrafish (*Danio rerio*) were maintained at 28°C on a 14 hours light/10 hours dark cycle as previously described. All protocols used have been approved by the Institutional Animal Care and Use Ethic Committee (PRBB–IACUEC), and implemented according to national and European regulations. All experiments were carried out in accordance with the principles of the 3Rs.

To investigate the expression of *Esrp* genes during development, embryos were raised at 28ºC for staging(Kimmel et al., 1995) and fixed overnight with 4% paraformaldehyde (PFA) in PBS at 4ºC. RNA probes were labeled with digoxigenin, and WMISH was performed as previously described(Thisse and Thisse, 2008). To create loss-of-function zebrafish lines for *esrp1* and *esrp2*, we used the CRISPR-Cas9 system. We first assessed the presence of multiple promoter in both genes looking at RNA-seq-based annotations and H3K4me3 Chip-seq peaks at their respective loci in the UCSC browser. Since each gene had only one promoter, we designed single guide RNAs (gRNAs) targeting the first and third exons of *esrp1* and *esrp2*, respectively. The genomic target sites were identified using a publicly available web tool (http://crispr.mit.edu/). Selected targeted gRNA sequences corresponded to: 5′-GGAGCAAGTGGGGATAAGTTGGG-3′ for *esrp1* and 5′-GGAGACCGGGCTCACTGCCGAGG-3′ for *esrp2*. The CRISPR-Cas9 approach was performed following the protocol from Chen and Wente laboratories, as previously

described for zebrafish (Jao et al., 2013). Engineered vectors were obtained from Addgene. One nl of a mixed solution containing gRNA (80 ng/µl) and purified Cas9 mRNA (150 ng/µl) was microinjected into one-cell stage zebrafish embryos. F0 founders were crossed with a wild type strain, and F1 individuals genotyped by fin clipping to select the appropriate mutations. We selected the following mutations for further analyses: a 168-bp deletion together with a 14-bp insertion that induced the usage of a cryptic splice donor upstream the start codon for *esrp1*, and a 17-bp frame-disrupting deletion for *esrp2* (Fig. 1c). Crosses between male and female heterozygous individuals carrying the same mutation were set to obtain single KO mutant lines in the F2 generation. In addition, individuals from these *esrp1* and *esrp2* F1 lines were crossed to obtain a F2 generation of double heterozygous. DKO embryos were obtained in subsequent F3 generations from intercrosses between F2 double heterozygous fish, at the expected Mendelian ratio. Sequences of the primers used for genotyping are provided in Supplementary Table 4.

For histological analysis, fixed embryos were progressively dehydrated in ethanol and xylol, embedded in paraffin, sectioned in transversal orientation with a microtome at 7-10 µm thickness, stained with haematoxilyn and eosin, and mounted with DPX (Eukitt). Alcian blue staining of chondrocytes at 6dpf embryos was performed according to the Zebrafish Book (Westerfield, 2007).

Vase tunicate experimental procedures. Adult *Ciona intestinalis* animals were collected from both the Gulf of Naples and M-REP (San Diego CA, USA). Ripe oocytes and sperm were collected surgically and kept separately until *in vitro* fertilization. We used chemical dechorionation to eliminate the chorion and follicular cells surrounding the eggs. Dechorionated eggs were then *in vitro* fertilized using sperm from various individuals. Fertilized eggs were washed in Millipore-filtered sea water, and transferred to a solution containing 0.77M Mannitol and 50–80mg of the plasmid DNA used for electroporation. Electroporation was carried out in Bio-Rad Gene Pulser 0.4 cm cuvettes, using Gene Pulser II (Bio-Rad). Each experiment was performed at least three times. Embryos were staged according to an standard developmental timeline (Hotta et al., 2007). A DIG-labelled probe for RbFox and *Esrp* and a fluorescein-labelled probe for *Twist-like2* were transcribed with Sp6 RNA polymerase (Roche) and purified with the

RNeasy Mini Kit (Qiagen). WMISH, antibody stainings and embryo manipulations were performed as previously described (Racioppi et al., 2014). To generate the *Twist>Esrp* construct, we cloned a genomic region upstream *Twist-like1* reported to be active in the mesenchymal lineage (Abitua et al., 2012). As transcripts for the predicted full-length *Esrp* locus were not detected using a mix of embryonic *Ciona* cDNAs, we cloned the most highly expressed isoform during development for overexpression experiments. This isoform lacks the exonuclease domain at the N-terminus as a result of splice-leader trans-splicing, but contains all RNA-binding domains.

Amphioxus experimental procedures. Adult *Branchiostoma lanceolatum* animals were collected in Banyuls (France) and Mataró (Catalonia). Spawning of reproductive individuals was done as previously reported (Fuentes et al., 2007). Embryos were cultured in filtered sea water at 17ºC and fixed in 4% PFA in MOPS buffer overnight at 4ºC. WMISH was performed with digoxigenin labeled RNA probes for *RbFox* and *Esrp* and performed as previously described (Irimia et al., 2010b). BM Purple (Sigma) was used as chromogenic substrate.

Sea urchin experimental procedures. Adult *Strongylocentrotus purpuratus* specimens were obtained from the Kerckhoff Marine Laboratory, California Institute of Technology, Pasadena CA, USA. Spawning was induced by vigorous shaking of animals, and embryos were cultured at 15ºC in diluted (9:10) stilled water with 0.22 μm filtered Mediterranean Sea water. Embryos were fixed in 4% PFA in MOPS buffer. RNA probes were differentially labelled with digoxigenin (*Esrp*) and fluorescein (*Hnf6*, *Gcm*) in double assays. *RbFox, Nova* and *Endo16* probes were al labelled with digoxinenin. Colorimetric and fluorescent WMISH and immunohistochemistry with anti-acetilated tubulin antibody were performed according to previous reports (Andrikou et al., 2013). For *Hnf6* and *Gcm* WMISH assays, we used previously published probes (Poustka et al., 2004; Ransick and Davidson, 2006). To knockdown *Esrp*, two different morpholinos were designed, one targeting the single annotated translation start site (5′-CCAGATAGTTAAACGCCATTTTTCC-3′) and one the 3′ splice site of the third exon in order to induce intron retention (5′- AGTTGTCAAGCTGCGAAAATGATGA-3′). Morpholinos were obtained from GeneTools and injected (about 6-8 pl per injection) in

zygotes at a 300 uM concentration in the presence of 0,12M KCl. Sequences of primers used to clone the *Esrp* probe and test intron 2 retention are provided in Supplementary Table 4.

RNA extraction, library preparation and RNA sequencing. RNA extractions were performed using the RNeasy Qiagen MiniKit (for zebrafish embryos) or the RNaquous (Ambion) (for sea urchin embryos). Trizol extraction (Invitrogen) according to manufacturer's instructions was employed to obtain total RNA from adult amphioxus tissues. All RNA samples were subjected to DNAse treatment. First-strand cDNAs for RT-PCR assays were generated using SuperScript III Reverse Transcriptase (Invitrogen). Libraries for Illumina high-throughput RNA sequencing were produced from poly-A selected RNA as described by the manufacturer, and Illumina HiSeq2500 machines in high yield mode were used for sequencing. Two replicates for DKO fish embryos and age-matched controls at 5dpf, and two replicates of splicing morpholino-treated sea urchin embryos at 24hpf and matched controls were sequenced, producing an average of ~145 and ~80 million 125-nucleotide paired-end reads per zebrafish and sea urchin sample, respectively. Raw sequence data were submitted to Gene Expression Omnibus (GSE97267). For human, we used RNA-seq from previous studies (Dittmar et al., 2012; Yang et al., 2016), including one replicate of a *ESRP1* mRNA knockdown (KD) in PNT2 cell line, three replicates of *ESRP1* and *ESRP2* knockdowns in H358 cells, and a replicate of overexpression (OE) of *ESRP1* in MB231 cell line. For mouse, we used previously published RNA-seq data for two replicates of embryonic epidermis from *Esrp1* and *Esrp2* DKO and control mice at the E18.5 stage (Bebee et al., 2015).

B. lanceolatum genome annotation. Dissection of several adult tissues and collection of different embryonic stages from *Branchiostoma lanceolatum* species was performed before RNA extraction of those biological samples. Obtained RNA-seq reads from each condition were aligned to an unpublished assembly of the genomic sequence (sequenced and assembled by Genoscope and Ferdinand Marletaz, respectively) using Tophat2. The corresponding BAM outputs were merged into a single file and processed by Cufflinks to produce gene structures. Independently, a de novo transcriptome assembly was performed using Trinity software separately for each RNA-seq sample. Obtained transcripts were

aligned to the genome using PASA. Both genome annotations were merged and filtered to obtain non-redundant transcripts. Finally, trandecoder tool was employed to classify those genes with a putative open reading frame, that were used in downstream analysis as protein coding genes.

Differential gene expression analysis. Gene expression levels for zebrafish and sea urchin were quantified from RNA-seq data using the cRPKM metrics (Labbé et al., 2012), which employs a single transcript per gene as reference and performs a length correction to account for non-uniquely mapped positions. We used Ensembl version 80 as zebrafish gene annotation (Zv10 assembly) and Spur-v3.1 for sea urchin, retrieved from EchinoBase (previously SpBase; http://www.echinobase.org/). To identify differentially expressed genes in *Esrp* loss-of-function embryos in each species, we first filtered out genes that did not have: (i) a minimal expression of cRPKM>2 in both replicates in at least one condition (control or loss-of-function); and (ii) at least 50 raw reads supporting expression in at least one sample. For the remaining genes, we required a minimum fold difference of 2 (for zebrafish) or 1.5 (for sea urchin) between the average expression levels in the two conditions, and a fold difference of at least 1.5 (for zebrafish) or 1.2 (for sea urchin) between all pairwise comparisons between each group's replicates.

Identification of *Esrp*-dependent exons from RNA-seq data. To quantify all major types of AS from RNA-seq data, we implemented *vast-tools* (Irimia et al., 2014) (https://github.com/vastgroup/vast-tools) for zebrafish and sea urchin. This software uses different modules to identify and quantify simple and complex exon skipping events, intron retention and alternative 5' and 3' splice site choices. It has been extensively used to identify differentially spliced AS events in human, mouse, chicken and planarians, providing high validation rates in RT-PCR assays (Braunschweig et al., 2014; Gueroussov et al., 2015; Solana et al., 2016). Associated VASTDB files to run *vast-tools* gene expression and AS analyses on zebrafish (species key "Dre") and sea urchin (species key "Spu") can be downloaded at http://vastdb.crg.eu/libs/vastdb.dre.10.03.17.tar.gz (Dre) and http://vastdb.crg.eu/libs/vastdb.spu.10.03.17.tar.gz (Spu). *vast-tools* was also used to quantify AS from human and mouse RNA-seq samples. For each AS event and processed sample in each species, *vast-tools* provided a table with the percent of alternative

sequence inclusion (using the metric 'Percent Splice In', PSI) and a score related to the number of reads supporting this PSI (Irimia et al., 2014) (N<VLOW<LOW<OK<SOK; see https://github.com/vastgroup/vast-tools for further details).

Next, to identify differentially spliced exons in each organism, we performed the following steps. For zebrafish, sea urchin and mouse we required that a given AS event had sufficient read coverage (score VLOW or higher in the *vast-tools* output) in all compared samples (two control and two loss-of-function replicates). Then, we required: (i) a minimum absolute PSI change (ΔPSI) between the averages of 15 (for zebrafish and mouse) or 10 (for sea urchin); and (ii) a minimum ΔPSI of 5 between all pairwise comparisons of control and *Esrp* loss-of-function samples. For IR, we further required that the binomial test for read imbalance (Braunschweig et al., 2014) was not significant ($p<0.05$) in any of the samples. For human, since we used three different sources, we produced a combined dataset consisting of AS events that were differentially spliced ($|\Delta PSI| > 15$ between the control and KD averages, and $|\Delta PSI| > 5$ for all pairwise replicate comparisons in the same direction) in either of the following groupings: (i) the three replicate pairs of the H358 KD experiment; (ii) the PNT2 KD single-replicate experiment and a merged sample of the H358 KD replicates (i.e. pulling all the reads for the three replicates together in each condition to increase read coverage); (iii) the PNT2 KD and MB231 *ESRP1* overexpression single-replicate data (the ΔPSI values should be in the opposite direction); and (iv) the merged H358 KD dataset and the MB231 *ESRP1* overexpression dataset (again with ΔPSI values in the opposite direction). All these comparisons were performed as implemented by the *vast-tools* module “compare”, using the following parameters: --min_dPSI 15 --min_range 5 --p_IR. Finally, cassette exons in a given species that had an homologous counterpart detected as *Esrp*-dependent in another species but that did not pass the initial read coverage filters were re-evaluated and were considered *Esrp*-dependent if: (i) the total number of reads supporting the PSI was at least five in each sample, and (ii) their PSI values fulfilled the cut-offs described above for the corresponding species.

Gene Ontology analysis. We used PANTHER statistical overrepresentation test (version 11.1 released 2016-10-24; http://www.pantherdb.org/) with default settings to investigate

functional gene enrichment for all species. Sea urchin gene identifiers from v3.1 (starting with WHL22) were converted to SPU identifiers using the conversion table provided by EchinoBase. For differentially expressed genes, we used as background all genes that passed the same initial quality filters (minimal expression of cRPKM>2 in both replicates of at least one condition and a minimum of 50 raw reads in at least one sample), corresponding to 10,666 genes for zebrafish and 13,574 for sea urchin. For differentially spliced exons, we used raw p-values and employed as background all multiexonic genes that fulfilled the same read coverage criteria described above. In total, this corresponded to 11,140 genes in human, 8,501 in mouse, 14,939 in zebrafish and 10,370 in sea urchin. Next, to compare enrichment of specific GO categories among all four species, we selected those categories that were significantly over-represented in at least one species (p-value < 0.05), and tested enrichment (ratio observed vs. expected) in the raw PANTHER outputs. GO categories that had a ratio > 1.3 in all four species were selected and plotted in Supplementary Fig. R5.

RT-PCR validations and quantitative fluorescent PCRs. Fluorescent PCRs were performed using forward oligonucleotides marked with a HEX fluorophore reporter (Sigma), with emission at 556 nm. Capillary electrophoresis was performed and analysis and quantification of the amplicons was made with GeneScan software. 500Rox from AppliedBiosystems (Life Technologies) was used as a standard size marker.

Building of homologous exon clusters. The clusters of homologous exons in coding regions were assembled according to the following steps. First, clusters of homologous human, mouse, zebrafish and sea urchin coding genes were built with information from OMA (Altenhoff et al., 2013), Multiparanoid (Alexeyenko et al., 2006) and BlastP, using the longest protein isoform for each protein-coding genes. For OMA and Multiparanoid, a pair of genes was considered to be homologous if they belong to the same gene cluster. For BlastP, genes were related if they were in the first three hits in a reciprocal manner between pair of species. Gene clusters were built from orthologous gene pairs that were supported at least by 2 out of the 3 aforementioned approaches, and employing a subsequent guilt-by-association approach. In parallel, aminoacid sequences of all *Esrp*-dependent exons were mapped to all protein isoforms of the harboring genes to obtain a

non-redundant set of proteins for each species that contain all *Esrp*-dependent exons. Then, those protein sequences were aligned in a pairwise manner to all isoforms of their gene homologous counterparts using MAFFT. Exon-intron structure information was introduced to the resulting alignment, by intercalating intron positions and their corresponding phase.

For each *Esrp*-dependent exon in species A, conservation in species B was assessed based on (i) local exon-intron structure, and (ii) exon sequence similarly. Conservation of upstream and/or downstream flanking introns in the aligned region was considered positive if there were two aligned intron positions in identical phase and a maximum deviation of 3 positions. Exon sequence conservation was considered significant if the pairwise similarity was higher than 20%. However, if an exon significantly aligned with more than one exon in the other species, local realignment with those exon sequences was performed, and the exon with the highest similarity was kept. With this information, a pair of homologous exons was automatically assigned if the pairwise sequence alignment of the alternative exon and at least one flanking constitutive exon was significant, and both flanking intron positions were conserved. Cases were manually evaluated if: (i) the sequence alignment of the alternative exon and at least one constitutive exon was significant, but at least one of the flanking intron positions was not detected automatically as conserved; or (ii) the upstream and downstream intron positions were conserved, but a low similarity score was obtained for the alternative exon. After this classification, for those exons in human, mouse and zebrafish with no detected homologous counterparts, an additional homology search was performed using liftOver software (http://genome.ucsc.edu/cgi-bin/hgLiftOver) followed by manual curation. Homologous exon clusters of *Esrp*-dependent exons were assembled based on these individually identified exon pairs using a guilt-by-association approach.

Amphioxus *Fgfr* AS minigenes and cell cultures. The full-length *Esrp* open reading frame (ORF) from *B. lanceolatum* and *esrp1* ORF from *D. rerio* were amplified from cDNA using iProof High Fidelity Polymerase (BioRad) and cloned into the pcDNA3.1 vector (Thermo Fisher Scientific). To generate the minigenes for the amphioxus *Fgfr* AS event, the *B. lanceolatum* genomic region spanning the AS event was amplified and

cloned into pcDNA3.1; the deletion to generate BlaFgfr-ΔIIIx was generated by PCR using iProof polymerase with reversed oligos in the flanking intronic regions and the wild type minigene as template. Human 293T cells were co-transfected with the minigenes plus a vector encoding amphioxus *Esrp*, zebrafish *esrp1* or an empty vector, using Lipofectamine 2000 (Invitrogen) according to manufacturer's instructions. Total RNA was extracted 24 hours after transfection using RNeasy Mini Kit (QIAGEN), cDNA was prepared using SuperScript III (Invitrogen) according to manufacturer's instructions. RT-PCRs for the endogenous AS events and the minigenes were performed using oligos annealing to the adjacent constitutive exons. Amphioxus *Fgfr* amplicons obtained from RT-PCRs were sequenced for isoform identification.

Genome sources and gene annotation. To understand the origins and evolution of the mutually exclusive exons IIIb and IIIc found in the *Fgfr* paralogs of vertebrates, we performed a comparative analysis in non-vertebrate species. First, we searched for *Fgfr* loci and transcripts in phylogenetically key species that have available genomic and transcriptomic information. Transcript isoforms were obtained by tblastn searches using the human *FGFR2* transcripts as query against public transcriptomes or ESTs databases. Genomic sequences were obtained from public genome databases for *Nematostella vectensis* (nemVec1, JGI), *Crassostrea gigas*, (oyster_v9, JGI), *Drosophila melanogaster* (dm6, FlyBase), *Tribolium castaneum* (triCas2, BeetleBase), *Apis mellifera* (apiMel2, Baylor College of Medicine), *Saccoglossus kowalevskii* (Skow_1.1, Baylor College of Medicine), *Strongylocentrotus purpuratus* (Spur_v3.1, EchinoBase), *Ciona intestinalis* (ci2, Aniseed) and *Danio rerio* (danRer10, Ensembl). Sequencing of amplicons from genomic DNA and tissue-specific cDNA was also carried out for *Branchiostoma lanceolatum*. With this information, Genewise software (http://www.ebi.ac.uk/Tools/psa/genewise/) was employed to annotate gene structures for each species. Finally, to compare intron/exon structures of the homologous regions to vertebrate's *Fgfr* IgIII domain, we performed interspecific multiple protein alignments with MAFFT, which were manually curated using intron position information and summarized in Fig. R16.

DISCUSIÓN

Patrones macroevolutivos del splicing específico de tejido en deuteróstomos

Recientemente, el desarrollo de las técnicas de secuenciación masiva ha permitido realizar las primeras aproximaciones globales a las dinámicas transcriptómicas en los principales organismos modelo. Uno de los procesos moleculares que afecta a las diferencias reguladoras entre distintos órganos, tejidos o tipos celulares es el *splicing* alternativo. Sin embargo, la todavía abrumadora falta de datos o análisis transcriptómicos para muchos linajes filogenéticos dificulta la compresión de los patrones macroevolutivos de este mecanismo regulador. En la presente tesis se ha realizado un intento inicial de comparar los paisajes post-transcripcionales de unos pocos deuteróstomos, incluyendo organismos no vertebrados. La detección de eventos de splicing con regulación específica de tejido está condicionada por los parámetros que definen dicha especificidad, al ser las diferencias entre los niveles de inclusión en distintos órganos altamente cuantitativas en general.

La utilización de un ΔPSI mayor de 15 entre el valor de inclusión máximo o mínimo de una muestra respecto a todas las demás consigue clasificar casi dos tercios de los exones alternativos totales como diferencialmente regulados en un órgano concreto en cuatro de las cinco especies estudiadas. Sin embargo, un aumento del umbral de detección hasta un ΔPSI mayor de 25 reduce esta proporción hasta un tercio en varios organismos. Curiosamente, este descenso no es igual de marcado en pez cebra y anfioxo, apuntando a una mayor abundancia de patrones específicos pronunciados en algunos organismos. Resulta interesante destacar que un análisis similar publicado en *Drosophila* reveló hasta un 63% de exones alternativos con inclusión/exclusión específica de tejidos adultos exhibiendo un ΔPSI mayor de 50. (Gibilisco et al., 2016). En este díptero, la mitad de la producción de isoformas totales se concentra en tan solo 42 genes (James B. Brown et al., 2014). Dichos genes, algunos con la capacidad potencial de generar cientos de tránscritos alternativos, presentan un patrón de expresión sesgado hacia un solo tejido. Por tanto, las diferencias entre especies en la proporción de AS regulado diferencialmente en un órgano concreto podrían ser debidas en parte a la distribución génica de los eventos con regulación intra-tisular.

Aquellos exones no detectados como diferencialmente regulados en una muestra respecto

al resto presentan por tanto patrones de inclusión y exclusión más balanceados. Existen diversos factores que pueden ser causa de este fenómeno. Los distintos transcriptomas de un organismo emergen desde el nivel celular, con lo que órganos formados por diferentes tipos celulares pueden enmascarar la regulación específica de exones en tejidos con identidades celulares minoritarias o muy variadas. Además, se han descrito eventos con inclusión variable dentro de un mismo tipo celular dependiendo de su estado fisiológico concreto (Gu et al., 2012). Por otro lado, también hay órganos distintos que poseen tipos celulares cercanos, ontogenética o funcionalmente, que pueden presentar programas de *splicing* similares, anulando la especificidad a nivel de órgano. Podría ser el caso, por ejemplo, de tejidos con abundancia de células epiteliales, que compartirían la inclusión o exclusión diferencial de ciertos exones relacionados con propiedades como la adhesión celular (Mallinjoud et al., 2014). Finalmente, también se han descrito casos donde tejidos biológicos distintos co-regulan ciertos exones alternativos de manera muy similar. Por estos motivos, un porcentaje probablemente elevado de eventos funcionales de *splicing* alternativo no presenta especificidad reguladora de tipo celular o tejido cuando se realizan aproximaciones transcriptómicas desde órganos enteros.

En la presente tesis se ha observado un mayor número de exones diferencialmente incluidos en el sistema nervioso respecto al resto de órganos seleccionados en nueve de diez comparaciones (5 especies y 2 parámetros de dPSI distintos). Sin embargo, la distancia respecto a la cantidad detectada de exones "específicos" en otros órganos resulta variable entre organismos. El mamífero *Homo sapiens* y el equinoideo *Strongylocentrotus purpuratus* muestran niveles similares de inclusión diferencial entre algunos o la mayoría de órganos no neurales, respectivamente. Por un lado, estos datos apuntan a la hipótesis de que tejidos como el músculo y los testículos aumentaron sustancialmente su proporción de exones diferencialmente incluídos dentro de un clado sarcopterígio indeterminado que contiene el linaje de los primates. Por otro lado, las diferencias aún menos sesgadas en erizo de mar abren la puerta a dos escenarios simplificados: (i) algunas especies o linajes de deuteróstomos podrían haber reducido notablemente su proporción de exones específicos neurales respecto al resto de tejidos; (ii) un aumento significativo en los niveles de inclusión diferencial neural sucedió durante el origen de los cordados. La determinación de la probabilidad de estos escenarios está ligada al éxito en la

reconstrucción de las características transcriptómicas del ancestro de los deuteróstomos. Análisis ampliados a otros grupos filogenéticos podrían contribuir tanto a discernir la probabilidad de los escenarios mencionados, como a dibujar patrones y tendencias macroevolutivas generales de la regulación específica de tejido mediante *splicing* alternativo.

Las comparaciones entre las cantidades absolutas de exones alternativos en cada especie son tentadoras. Sin embargo, la confrontación directa de estos valores debe realizarse con cautela debido a múltiples sesgos inherentes en los análisis. Entre los factores que afectan a la identificación de exones alternativos están el ensamblaje y la anotación genómica, los niveles de polimorfismo, o la calidad y profundidad de cubrimiento (*coverage*) de las muestras de RNA-seq. De este modo, organismos como la especie humana con una anotación genómica muy cuidada presentan implícitamente una capacidad de detección de eventos alternativos más elevada que el resto de especies. No obstante, organismos como pez cebra o anfioxo muestran un número mayor de exones diferencialmente incluídos en el sistema nervioso. Por tanto, dentro de los cordados, los elevados niveles de inclusión exónica específica del sistema nervioso adulto parecen estar más ligados a la fisiología de los circuitos y tipos neurales que a la elaboración estructural del órgano en el que se integran.

Los motivos funcionales de todo este *splicing* alternativo específico de tejido en el sistema nervioso constituyen una incógnita. Actualmente no existe una explicación clara y contundente, puesto que una comprensión profunda de la funcionalidad organísmica de estos eventos alternativos requiere un trabajo detallado de cada caso particular. Por el tipo de genes que presentan *splicing* alternativo en mamíferos, una parte importante podría estar asociada a procesos dinámicos propios de los circuitos neuronales, como la plasticidad sináptica o la excitabilidad neuronal. Resulta interesante mencionar que diversos mecanismos de regulación post-transcripcional parecen estar especialmente activos en células neurales de distintos clados animales (Kiebler et al., 2013), como la edición de RNA en ganglios cerebrales de cefalópodos coloideos (Liscovitch-Brauer et al., 2017).

Por otro lado, la especie humana es el único de los cinco organismos estudiados en este

trabajo que presenta más exones diferencialmente excluídos que incluídos en el conjunto total de los órganos estudiados. Esta predominancia relativa de la exclusión exónica en ciertos linajes ha sido descrita en casos particulares como la familia *Cerkl*, cuyos ortólogos de humano y ratón codifican para más de veinte y treinta isoformas, mayoritariamente mediante la exclusión de exones conservados (Garanto et al., 2011). Sin embargo, otros linajes de vertebrados producen entre dos y cinco tránscritos a través de promotores alternativos, inclusión de exones no conservados, y algún caso de *skipping* (Riera et al., 2013) (artículo anexo 4). A nivel transcriptómico general, análisis suplementarios en otras especies de vertebrados son necesarias para revelar tanto el origen evolutivo de esta "transición" en humanos a mayores niveles de exclusión diferencial como su frecuencia filogenética en otros clados. Algunos análisis han apuntado a los primates como el linaje animal con mayores niveles de producción de isoformas mediante splicing alternativo (Barbosa-Morais et al., 2012), aunque la recolección de datos genómicos y transcriptómicos de alta calidad en un conjunto amplio de grupos filogenéticos es necesaria para la confirmación de este escenario.

Es importante tener en cuenta que no todos los elementos que forman parte del transcriptoma son resultado de procesos de selección positiva o negativa. Es probable que un porcentaje no negligible de isoformas generadas por AS en un contexto celular concreto no presente una función específica. Estos elementos pueden ser producidos tanto por fallos en la maquinaria de *splicing*, o como un subproducto relativamente constante, aunque sin propósito, del ambiente molecular. Dicho tipo de variaciones transcripcionales, si bien pueden resultar muy abundantes en un organismo dado, tenderían a presentar una trayectoria evolutiva breve si no son objeto de un proceso selectivo en algún linaje. Por otro lado, resulta interesante especular sobre las implicaciones de este tipo de ruido transcriptómico bajo la luz de la teoría jerárquica de la selección de especies. En este sentido, aquellos linajes que a escala organísmica puedan soportar un ruido más elevado dispondran también de un número mayor de elementos transcriptómicos co-optables durante procesos macroevolutivos determinantes como la especiación.

Evolución de la expresión y función ontogénica de los factores *RbFox* y *Nova*

La expresión y/o función de un número cada vez más elevado de familias génicas que codifican proteínas de unión a RNA y tienen la capacidad de modular el *splicing* alternativo de múltiples eventos ha sido descrita en mamíferos o peces. Muchas de estas familias presentan uno o más de sus miembros expresados en células neurales, hecho que podría explicar los elevados niveles relativos de regulación diferencial en este tejido. Entre estos factores se encuentran las familias *Nova* y *RbFox*, con la mayoría de sus parálogos fuertemente expresados en el sistema nervioso central de humano, ratón y pez cebra (Jensen et al., 2000; Underwood et al., 2005). Paralelamente, se han descrito roles fisiológicos adicionales para ambos factores en algunas de esas especies, como en el músculo esquelético y el corazón en caso de genes *RbFox* o en el tejido adiposo en caso de Nova (Gallagher et al., 2011; Vernia et al., 2016).

Con el propósito de comprender las trayectorias macroevolutivas de ambas familias génicas, en la presente tesis se han caracterizado los niveles relativos de expresión de dichos factores en varios tejidos adultos de distintos organismos bilaterales. Los resultados obtenidos reflejan escenarios diferentes en cuanto al origen del patrón neural descrito en vertebrados. Por un lado, los miembros de la familia *Nova* están expresados mayormente en el sistema nervioso de los vertebrados estudiados, anfioxo y *D. melanogaster*, pero no en las especies estudiadas de erizo de mar, el pulpo o el ciempiés. Por tanto, el escenario más parsimonioso bajo estos datos sería el de una potenciación de los niveles de expresión neural tanto en la base de los cordados como en algún ancestro de la mosca no compartido con el miriápodo *Strigamia*. Por otro lado, exceptuando algún parálogo en vertebrados, los genes *RbFox* sí presentan los niveles de transcripción más elevados en el órgano nervioso de todos los organismos analizados. Así, resulta plausible proponer un origen ancestral y una conservación general de la actividad reguladora de RbFox en el sistema nervioso de protóstomos y deuteróstomos.

En mamíferos, las dos famílias parecen tener roles fisiológicos ligados a procesos sinápticos propios del tejido neuronal. Por ejemplo, *RbFox1* está implicado en la regulación del *splicing* de muchos componentes sinápticos excitatorios, mientras que el

gen *Nova2* influye en el balance de isoformas de varios genes involucrados en conexiones neuronales inhibidoras, presentando fenotipos acordes en los dos casos (Gehman et al., 2011; Jensen et al., 2000). Interesantemente, estudios muy recientes han descrito que la expresión neuronal de ambos genes potencia la memoria en *Drosophila*, en el caso de *RbFox* a través del control de la excitación neuronal (Guven-Ozkan et al., 2016). En consecuencia, resulta tentador especular sobre la posibilidad de que los genes *RbFox* presenten funciones relacionadas con excitación neuronal en otros clados de animales bilaterales. Si bien el programa post-transcripcional regulado por *RbFox* en neuronas de la mosca de la fruta no ha sido investigado, *Nova* parece ejercer su función principalmente a través de la regulación de un evento de retención intrónica en el gen *Orb2A* (Gill et al., 2017). Aclarar el origen de esta conexión reguladora podría proporcionar una mejor comprensión de los pasos evolutivos que facilitan ganancias de función a través de eventos particulares de *splicing* alternativo.

Otros órganos aparte del sistema nervioso presentan patrones de expresión consistentes dentro de algunos clados para miembros de ambas familias de factores. Es el caso de las gónadas masculinas de protóstomos en el caso de *Nova*, o de los niveles relativamente elevados en el músculo esquelético de cordados para diferentes homólogos *RbFox.* Además, algunas especies exhiben niveles de expresión relativamente altos de manera particular en varios órganos. Estas observaciones sugieren que ambas familias presentan múltiples funciones organísmicas en distintos linajes evolutivos, apoyando una alta frecuencia de co-opción de estos reguladores post-transcripcionales en tejidos adultos a diversas escalas evolutivas. En consecuencia, la nomenclatura clásica que se refiere a estos factores como “específicos de tejido” puede resultar confusa o desfasada en muchos casos, puesto que parecen tener roles relevantes en múltiples órganos.

Un estudio anterior reveló los patrones de expresión de la familia *Nova* durante el desarrollo embrionario de diversos metazoos (Irimia et al., 2011a) (artículo anexo 3). Entre las conclusiones principales de dicho trabajo se encuentra la aparición de una expresión neural significativa en la base de los cordados. Este escenario resulta similar respecto a la expresión relativa de los genes *Nova* caracterizada en los tejidos de diversos organismos en estadio reproductivo en el presente trabajo. Sin embargo, el análisis de los

patrones de expresión de la familia *RbFox* en diversos deuteróstomos ha revelado un escenario más discordante entre las etapas embrionaria y adulta. De este modo, mientras que todos los estadios embrionarios de los cordados y el equinodermo estudiados presentan expresión en el linaje celular miogénico, tan solo se ha observado un patrón neural en algunos parálogos de organismos vertebrados. La interpretación más parsimoniosa apunta a una función embrionaria ancestral en el mesodermo muscular, mientras que la actividad de la familia *RbFox* habría sido intercalada en el desarrollo del sistema nervioso durante la evolución de los vertebrados.

El análisis de la función embrionaria de *Nova* en el erizo de mar ha desvelado su implicación en los movimientos de invaginación que sufre el endodermo en el polo vegetal al inicio de la gastrulación. Este rol ontogénico dista mucho de aquellos descritos para sus ortólogos en otros organismos, como la migración neuronal en el córtex de mamíferos, la formación del lumen vascular en pez cebra o la estructuración y secreción apical de las glándulas salivares de *Drosophila* (Giampietro et al., 2015; Hamada et al., 2016; Seshaiah et al., 2001). No obstante, es lícito recalcar que las funciones descritas durante el desarrollo en las especies estudiadas, incluyendo erizo, constituyen mayormente procesos morfogenéticos. De hecho, se han detectado problemas de polaridad celular colectiva tanto en fenotipos de vertebrados como en *D. melanogaster*. A pesar de que estas similitudes a nivel celular deben tomarse con precaución, constituyen una propuesta sobre un posible rol de *Nova* compartido a esa escala por embriones de distintos filos. Una investigación sobre los mecanismos celulares que impiden la gastrulación en *S. purpuratus* podría aportar más evidencia a favor o en contra de esa hipótesis.

No existen muchos datos sobre la función embrionaria de los factores *RbFox* en el linaje muscular exceptuando unos pocos estudios en pez cebra, donde se han descrito fenotipos relacionados con la organización miofibrilar, incluyendo afectaciones ultraestructurales en los sarcómeros (Gallagher et al., 2011). Los resultados obtenidos en erizo de mar muestran que *RbFox* también es necesario para el desarrollo de la musculatura de origen mesodérmico en este organismo. La formación alrededor del esófago de los anillos de miosina del tipo II (*MHC*), proteína codificada por el gen de diferenciación terminal

MHC18, se ve alterada cuando la expresión de todas las isoformas de *RbFox* está perturbada. No obstante, con los datos disponibles es complicado determinar si este fallo se debe a problemas en la determinación del destino celular o en el proceso de diferenciación donde suceden las transformaciones morfogenéticas propias de la población muscular. Entre estas últimas, se encuentra la fusión de los mioblastos en la fase pluteus para formar las bandas musculares (Andrikou et al., 2013). Resulta interesante remarcar que el gen *RbFox2* de ratón está implicado en la fusión celular que acontece durante la miogénesis en cultivos de mioblastos (Singh et al., 2014). Por otro lado, el receptor de señalización celular *Fgfr1* está relacionado con la especificación muscular en este organismo a través de la activación de factores de transcripción que bloquean la determinación celular y potencian la expresión de marcadores de diferenciación (Andrikou et al., 2015). La identificación de *Fgfr1* como una probable diana directa de *RbFox* en el erizo de mar apunta a un posible rol de este factor de *splicing* en la red de especificación-diferenciación.

El músculo embrionario es una de las poblaciones celulares que expresan factores de la familia *RbFox* en el nemátodo *C. elegans*. Resulta interesante remarcar que la regulación por *RbFox* de varios eventos de *splicing* musculares en esta especie se lleva a cabo a través de su co-operación física con otra proteína, llamada s*up-12* (*Rbm24/38* en vertebrados) (Mackereth, 2014). Este factor pertenece a una familia de reguladores maestros del *splicing* alternativo del tejido muscular tanto en *C. elegans* como en vertebrados, donde su actividad es necesaria para la diferenciación miogénica y la formación de sarcómeros (Grifone et al., 2014; Kuroyanagi et al., 2007). Resulta interesante recalcar que el patrón de expresión embrionaria de los homólogos de *Rbm24/38* en anfioxo y *C. intestinalis* también exhiben un patrón predominantemente muscular (datos no mostrados). Además, la interacción protéica entre miembros de la familia *RbFox* y *Rbm24/38* ha sido descrita en humano en ensayos experimentales (Lim et al., 2006). En definitiva, esta interacción podría ser un mecanismo molecular conservado entre deuteróstomos y protóstomos que permitiría la regulación específica diferencial de eventos de splicing mediante la co-operación de *RbFox* y *Rbm24/38* en el tejido muscular.

Además de su papel durante la miogénesis, *S. purpuratus* ha reclutado la actividad de *RbFox* durante la ingresión en el blastocele del mesénquima primario, el tejido que acaba formando el esqueleto larvario. A pesar de que tanto los euechinoideos, como los cidaroideos y las ofiuras poseen un esqueleto larvario, tan sólo los primeros presentan un mesénquima primario derivado de micrómeros, convirtiendo a este ingreso celular en una apomorfía morfogenética (Ettensohn, 2009). La función necesaria de *RbFox* durante el estadío de blástula en el desarrollo del esqueleto larvario revela otro caso de reclutamiento de un factor regulador de *splicing* para un proceso ontogénico específico de linaje. Por otro lado, en vertebrados se han descrito múltiples roles de la familia *RbFox* durante el desarrollo del sistema nervioso, como la laminación cortical o la migración de neuronas Purkinje en el cerebelo (Gallego-Paez et al., 2017). En resumen, los miembros de esta familia de factores de *splicing* han sido co-optados independientemente para la morfogénesis de distintas estructuras embrionarias en varios linajes de deuteróstomos.

En la presente tesis, se han detectado múltiples eventos de *splicing* diferencialmente regulados en la fase de blástula del equinodermo *S. purpuratus* tras la inyección de morpholinos noqueadores de la expresión de *Nova* y *RbFox*. Obviamente, estos conjuntos de eventos contienen tanto dianas directas, con las que el factor interacciona físicamente, como dianas indirectas donde la alteración del patrón de *splicing* es debida al desbarajuste transcriptómico derivado de los cambios en la regulación directa. Por un lado, la cantidad de exones diferencialmente regulados tras la manipulación de la expresión de *RbFox* en embriones ha sido cuantificada alrededor de los doscientos casos. Paralelamente, la reducción de la actividad de *Nova* ha identificado más de mil setecientos. Esta diferencia espectacular en el número de exones dependientes podría reflejar un alto número de casos indirectos para *Nova*, la mayor parte de los cuales serían incluso constitutivos en condiciones normales. Entre las explicaciones más plausibles para este fenómeno se encuentran: (i) uno o múltiples eventos regulados directa o indirectamente por *Nova* que afecten la función de algún elemento de la maquinaria spliceosomal; (ii) la co-opción de *Nova* en el endodermo como un miembro spliceosomal auxiliar que asegura la inclusión exónica en múltiples casos; (iii) un efecto no-específico del morpholino inyectado que provocaría una perturbación de varios procesos constitutivos de *splicing*, independientemente de la función de *Nova*.

Reclutamiento de programas de splicing dependientes de los factores *Esrp* en diversos procesos morfogenéticos de deuteróstomos

Los genes *Esrp1* y *Esrp2* han sido descritos en mamíferos como factores de *splicing* específicos de tipos celulares epiteliales (Claude C Warzecha et al., 2009). Su función ha sido relacionada en este clado con la regulación de propiedades celulares antagónicas entre tejidos epiteliales y mesenquimales, como la adhesión o la motilidad celular (Dittmar et al., 2012). En el presente trabajo, se ha observado una expresión muy dinámica de esta familia génica en los embriones de todas las especies de deuteróstomos estudiadas. En pez cebra, el patrón transcripcional de ambos genes resulta muy similar al de ratón en múltiples estructuras epiteliales homólogas, sugiriendo un grado de conservación generalmente elevado de las funciones de *Esrp* entre ambos linajes de vertebrados (Revil and Jerome-Majewska, 2013). Sin embargo, parece haber diferencias respecto a los requerimientos ontogenéticos de ambos parálogos en ratón y pez cebra. Mientras que los ratones mutantes para *Esrp1* presentan múltiples defectos morfológicos y mortalidad neonatal (Bebee et al., 2015), los peces KO para su ortólogo en cebrita no muestran ningún fenotipo evidente. Por otro lado, los mutantes para *Esrp2* de ratón son viables y reproductores, mientras que las hembras de los teleósteos noqueados son aparentemente estériles. Así, tan solo los mutantes dobles de pez cebra exhiben anomalías morfogenéticas graves en su desarrollo. Este resultado refleja niveles de solapamiento funcional diferentes entre ambos parálogos en los dos organismos, que serían notablemente mayores en pez cebra.

La expresión de genes *Esrp* también ha sido reclutada por algunas estructuras específicas de linaje dentro de los vertebrados, como los folículos pilosos y los esbozos mamarios en mamíferos o la glándula de eclosión en teleósteos. Además, algunas estructuras conservadas presentan expresión clara solamente de uno de los parálogos, como el hígado post-natal de ratón, donde *Esrp2* está involucrado en la diferenciación terminal y la competencia funcional de los hepatocitos (Bhate et al., 2015). También se ha observado expresión de factores *Esrp* en la notocorda y corazón del cebrita, aunque no se ha podido determinar si ésta se da en los componentes mesenquimales o epiteliales de esos órganos. Resulta interesante destacar que se han empezado a describir patrones de expresión

mesenquimales para miembros *Esrp* en organismos vertebrados, por ejemplo en las células indiferenciadas de la musculatura lisa gastrointestinal del pollo, tejido en el que *Esrp1* promueve la proliferación (Sagnol et al., 2016). Por tanto, parece adecuado asumir una gama funcional en vertebrados más allá del control de la adhesión celular y motilidad en tejidos epiteliales.

El presente trabajo ha revelado una expresión ontogénica dinámica de la familia *Esrp* en el ectodermo no neural de todos los deuteróstomos estudiados. Así, los cordados exhiben un claro incremento en la detección de tránscritos en la epidermis justo al final de la neurulación. En comparación, los embriones de erizo de mar presentan un patrón sesgado hacia el ectodermo aboral tanto previa como paralelamente a la gastrulación. A pesar de las diferencias heterocrónicas y de identidad celular, esto sugiere la posibilidad de un rol primitivo en el ectodermo no neural del ancestro deuteróstomo. Sin embargo, merece la pena ser precavidos respecto a esta afirmación, puesto que los roles ontogénicos descritos en estos tejidos en ratón y erizo difieren enormemente y podrían ser consecuencia de reclutamientos génicos independientes.

Por otro lado, la expresión y/o la función de factores *Esrp* ha sido detectada en estos organismos en células mesenquimales involucradas en procesos morfogenéticos. En *S. purpuratus*, células pigmentarias mesodérmicas que expresan *Esrp* se integran en el ectodermo mediante una transición mesénquima-a-epitelio, un proceso que se ve alterado tras la perturbación de dicho factor. Una función similar podría explicar la expresión de *Esrp* en un presunto conjunto de precursores neuronales migradores que se incorporan al ectodermo dorsal en anfioxo. De todos modos, la identificación definitiva de esas células está pendiente de confirmación experimental. En *C. intestinalis*, *Esrp* parece modular propiedades relacionadas con la motilidad celular en poblaciones concretas del linaje mesenquimal. En vertebrados, las células migradoras provenientes de la cresta neural que se integran en la parte anteromedial del paladar están ausentes en dicha estructura en los dobles mutantes de ratón y cebrita. Este fenotipo podría estar relacionado con un fallo en el proceso de integración de esas poblaciones celulares en el cartílago craneal. A favor de esta hipótesis está el hecho de que la familia *Esrp* ha sido frecuentemente relacionada con cambios en la adhesión celular y transiciones epitelio-a-mesénquima en cultivos celulares

humanos y cáncer (Shapiro et al., 2011). Sin embargo, la confirmación definitiva de que estos factores regulan procesos de este tipo durante la embriogénesis de vertebrados requerirá de análisis experimentales adicionales.

A pesar de este uso evolutivo recurrente de *Esrp* en procesos morfogenéticos relacionados con propiedades o interfaces epitelio-mesenquimales, muchos de los exones cuya inclusión depende de estos factores muestran una regulación específica de linaje. El ejemplo más extremo se da entre el erizo de mar y los organismos vertebrados, donde no se han detectado exones alternativos regulados por *Esrp* conservados en ambos filos. Estas observaciones son consistentes con una divergencia intercladal rápida respecto a la regulación de los eventos particulares de *splicing* alternativo (Barbosa-Morais et al., 2012; Julien et al., 2016; Merkin et al., 2012). Aun así, merece la pena tener en cuenta que la cantidad de exones homólogos regulados compartidos entre especies representa una infraestimación con toda seguridad. Los datos transcriptómicos utilizados provienen de fuentes biológicas profundamente heterogéneas: monocultivos de tres tipos celulares en humano, epidermis embrionaria de ratón, larvas de cebrita y blástulas de erizo de mar. La actividad de los factores de *splicing* depende frecuentemente del contexto celular en el que se encuentran, por lo que es posible que exones que no son detectados como diferencialmente regulados en una muestra determinada sí lo sean en otra. Además, no todos los eventos investigados presentan un cubrimiento (coverage) de *reads* suficiente en todas las réplicas para determinar con seguridad su porcentaje de inclusión. Por otro lado, los resultados obtenidos mediante secuenciación de embriones enteros muy probablemente contengan una proporción significativamente incrementada de dianas indirectas respecto aquellas muestran que provienen de un solo tejido celular. La discriminación entre exones regulados directa e indirectamente utilizando técnicas como el CLIP-seq, aclararía las posibles diferencias entre los niveles de conservación de ambos conjuntos.

Dentro de vertebrados, los eventos dependientes de *Esrp* no compartidos entre especies proceden mayoritariamente de exones pre-existentes, que serían usualmente alternativos en los otros organismos analizados. Resulta interesante constatar que algunos linajes presentan tasas más elevadas de reclutamiento de exones huérfanos que otras, como

evidencia el caso humano en comparación con ratón. Por el contrario, sólo una quinta parte de los exones diferencialmente regulados en erizo presentan homólogos en vertebrados. Estos datos sugieren que el ensamblaje de los programas de splicing en los clados de metazoos más distantes procede frecuentemente mediante el reclutamiento de exones específicos de linaje. De todos modos, sí se ha detectado regulación por *Esrp* en múltiples dianas homólogas a nivel de gen entre todos los organismos. Si bien el escenario evolutivo responsable de dicha situación resulta incierto, esta observación podría explicar las semejanzas funcionales interfiléticas descritas a escala celular.

A pesar de la acumulación de profundas diferencias estructurales entre actinopterígios y sarcopterígios desde su separación filogenética en el Silúrico, algunos roles morfogenéticos de *Esrp* se han revelado conservados entre estos clados. Dicha afirmación se fundamenta en la similitud apreciable de los fenotipos descritos en ratón y pez cebra para múltiples caracteres homólogos (Bebee et al., 2015). Esta situación tiene un reflejo a nivel molecular por un conjunto de al menos 22 exones homólogos que presentan niveles de inclusión diferencial dependientes de *Esrp* en las tres especies de vertebrados analizadas. La lista incluye a miembros de la familia *Fgfr,* que codifican para receptores de la vía de señalización celular FGF. De hecho, la mayoría de las estructuras afectadas en los mutantes de *Esrp* en ratón y cebrita expresan genes *Fgfr*, e incluso presentan fenotipos similares a los descritos en mutantes condicionales para la isoforma epitelial de *Fgfr2* en el roedor (De Moerlooze et al., 2000). Esta relación es consistente con el descubrimiento de que, igual que sus ortólogos de ratón, los factores *Esrp* de pez cebra son necesarios para la inclusión del exón epitelial IIIb en tejidos embrionarios. Por lo tanto, una de las principales causas moleculares de los fenotipos observados en los dobles mutantes es probablemente la interrupción de la señalización FGF cruzada entre epitelios y mesénquima durante el desarrollo de los órganos afectados. De hecho, esta conexión reguladora podría explicar el pronunciado sesgo de expresión en tejidos epiteliales de la familia *Esrp* en vertebrados. Curiosamente, el ratón mutante condicional para *Fgfr2b*, que no expresa ninguna de las dos isoformas en tejidos epiteliales, no desarrolla extremidades en absoluto. Contrariamente, la mayoría de los dobles mutantes para los factores *Esrp* exhiben aletas pectorales o extremidades anteriores con una desestructuración acentuada especialmente en la parte más distal. Esta observación sugiere que la regulación del

splicing alternativo del receptor *Ffgr2* no es imprescindible para el crecimiento inicial de la extremidad, pero sí para su desarrollo posterior.

Finalmente, se ha podido determinar que la regulación del *splicing* alternativo dependiente de *Esrp* en los genes *Fgfr* se originó en el ancestro de los cordados tras la duplicación en tándem de un exón pro-homólogo de los exones IIIb y IIIc. En consecuencia, los cordados evolucionaron una manera única de utilizar la vía FGF a través de la inclusión diferencial del exón IIIb en tejidos que expresan *Esrp*. Este sistema ha sido explotado recurrentemente por los vertebrados en múltiples procesos morfogenéticos, que han reclutado la señalización FGF para regular las interacciones moleculares entre epitelio y mesénquima requeridas durante el desarrollo de diversos órganos. Sorprendentemente, varios eventos de *splicing* alternativo han evolucionado independientemente en ortólogos *Fgfr* en regiones homólogas que codifican para dominios immunoglobulina en otros filos. Parece lícito especular con que muchos de estos eventos podrían contribuir a modular la afinidad del receptor por distintos ligandos *Fgf*. De todos modos, su rol organísmico dependerá de la lógica reguladora del *splicing* en cada linaje. Por ejemplo, de acuerdo a los resultados obtenidos en esta tesis, los embriones de erizo de mar producirían diferentes isoformas de *Fgfr1* en el mesodermo muscular y el ectodermo neural mediante la expresión de *RbFox* en el primero. Por último, este caso ilustra como mutaciones en la estructura génica probablemente neutrales en el momento de su aparición pueden tener un impacto a largo plazo. En el ejemplo estudiado, la ganancia de un intrón en medio de un exón codificante generó un *hotspot* genómico con un gran potencial macroevolutivo en los Bilateria.

Reflexión general sobre la evolución de los programas de *splicing* alternativo

Como se ha descrito en esta tesis y en otros tantos trabajos anteriores, la regulación precisa de diferentes programas de AS resulta esencial durante el desarrollo embrionario animal. Esta afirmación se halla respaldada por los fallos morfológicos y fisiológicos descritos en mutantes para factores de *splicing* con expresión restringida a contextos o procesos celulares concretos. De todos modos, parece sensato mostrar cautela a la hora de atribuir toda la causalidad de los fenotipos observados a perturbaciones en eventos de

AS. En el fondo, estos factores reguladores constituyen proteínas de unión a RNA, y como tales tienen la capacidad potencial de controlar múltiples procesos post-transcripcionales más allá del *splicing*. En neuronas, por ejemplo, se han publicado diversos casos que demuestran un papel relevante para varios de estos péptidos en el transporte de mRNAs hacia las sinápsis. También se ha detectado un número elevado de dianas génicas para varios factores a través de la poliadenilación alternativa o la estabilidad del tránscrito mediante unión a las UTRs (Dittmar et al., 2012).

Resultaría interesante investigar la cantidad de eventos diana de AS cuya desregulación en los mutantes y *knockdowns* realmente provoca los fenotipos observados. Es imaginable que la flexibilidad evolutiva asociada al AS pueda estar relacionada con un impacto funcional variable de los diferentes eventos regulados en una especie dada. Dentro de esta lógica, es probable que cada programa de splicing contenga un número reducido de dianas centrales, generalmente más conservadas, que serían las responsables troncales de los procesos afectados. Contrariamente, muchos de los eventos regulados tendrían una participación pequeña y no imprescindible que podría ser fácilmente eliminada o sustituida evolutivamente conforme a las necesidades organísmicas circunstanciales. A nivel molecular, estudios de la conexión entre el mapa genotípico y los valores de PSI de eventos particulares han aportado luz sobre la enorme sensibilidad del splicing alternativo a mutaciones puntuales (Julien et al., 2016).

Por otro lado, los reguladores de *splicing* alternativo son frecuentemente co-optados en diferentes clados para contribuir en procesos ontogénicos diversos. Resulta interesante especular acerca de las etapas a través de las que procede dicha exaptación molecular. Una de las posibilidades es que el regulador sea aprovechado para cambiar o fortalecer el balance de isoformas de uno o unos pocos eventos particulares, aprovechando su capacidad de unión al tránscrito inmaduro debido a su conexión reguladora ancestral en otro contexto celular. Otra opción es que la ganancia de función se ejecute mediante la interacción proteica con la maquinaria spliceosomal u algún co-factor concreto del nuevo ambiente en el que se ha inserido, como se ha descrito recientemente para un sub-conjunto de eventos influenciados por *RbFox* (Damianov et al., 2016). En ambos casos, la expansión de su actividad reguladora podría proceder a través de la ganancia progresiva

de secuencias de unión en la vecindad genómica de exones alternativos, constitutivos o crípticos cuyos niveles de inclusión sea conveniente modular o reforzar.

Ciertamente, la aparición de elementos moleculares novedosos puede proporcionar un impulso importante hacia la materialización de nuevos caracteres o funciones. Sin embargo, en múltiples ocasiones simplemente constituyen una manera alternativa de ejercer roles fisiológicos o construir estructuras previamente existentes. De este modo, muchos cambios moleculares en elementos funcionales pueden llegar a fijarse debido a su capacidad de suplir a componentes primitivos. Por ejemplo, hay trabajos que sugieren que las secuencias reguladoras de *splicing* podrían cambiar rápidamente entre especies a pesar del mantenimiento de los niveles de inclusión (Julien et al., 2016). Por tanto, es importante recalcar que no todas las sinapomorfias funcionales genómicas o transcriptómicas de un linaje particular tienen por qué estar ligadas a novedades evolutivas propias de ese grupo.

CONCLUSIONES

Conclusiones:

1) La cuantificación de casos de inclusión exónica diferencial en órganos adultos de las especies investigadas muestran una mayor proporción en general en el sistema nervioso de cordados, mientras que el erizo de mar púrpura presenta niveles más balanceados entre tejidos.
2) La especie humana exhibe una mayor cantidad de exones con exclusión diferencial en el conjunto de eventos con regulación específica de tejido, en comparación con los casos de inclusión, respecto al resto de especies estudiadas.
3) Los genes *Nova* presentan un paralelismo entre embriones y organismos adultos respecto a la ganancia de expresión neural en el origen de los cordados.
4) El ortólogo *Nova* de *S. purpuratus* está involucrado en la ejecución de los movimientos celulares de invaginación del endodermo durante la gastrulación.
5) La actividad en el sistema nervioso adulto de la familia *RbFox* representa probablemente una plesiomorfía de organismos bilaterales. Sin embargo, es posible que la función embrionaria ancestral en deuteróstomos estuviese relacionada con el desarrollo miogénico.
6) El ortólogo de *RbFox* de erizo de mar está implicado en la formación tanto del esqueleto larvario como del tejido muscular mesodérmico. Esta última función podría estar relacionada con la regulación del splicing alternativo del gen *Fgfr1*.
7) La función de la familia de factores de splicing *Esrp* ha sido co-optada por múltiples estructuras o tejidos celulares en los distintos linajes de deuteróstomos.
8) La familia *Esrp* presenta roles biológicos diversos en las especies estudiadas, pero usualmente ligados a morfogénesis. A nivel celular, su actividad morfogenética parece frecuentemente asociada a la regulación de propiedades celulares como la adhesión y la motilidad celular.
9) *Esrp1* y *2* coordinan en vertebrados la señalización molecular entre epitelio y mesénquima en diversos procesos organogenéticos a través la regulación de un evento de *splicing* en genes *Ffgr* que se originó en un ancestro de los cordados.

BIBLIOGRAFÍA

BIBLIOGRAFÍA

Abitua, P.B., Gainous, T.B., Kaczmarczyk, A.N., Winchell, C.J., Hudson, C., Kamata, K., Nakagawa, M., Tsuda, M., Kusakabe, T.G., Levine, M., 2015. The pre-vertebrate origins of neurogenic placodes. Nature 524, 462–465. doi:10.1038/nature14657

Abitua, P.B., Wagner, E., Navarrete, I.A., Levine, M., 2012. Identification of a rudimentary neural crest in a non-vertebrate chordate. Nature 492, 104–7. doi:10.1038/nature11589

Albuixech-Crespo, B., López-Blanch, L., Burguera, D., Maeso, I., Sánchez-Arrones, L., Moreno-Bravo, J.A., Somorjai, I., Pascual-Anaya, J., Puelles, E., Bovolenta, P., Garcia-Fernàndez, J., Puelles, L., Irimia, M., Ferran, J.L., 2017. Molecular regionalization of the developing amphioxus neural tube challenges major partitions of the vertebrate brain. PLOS Biol. 15, e2001573. doi:10.1371/journal.pbio.2001573

Alexeyenko, A., Tamas, I., Liu, G., Sonnhammer, E.L.L., 2006. Automatic clustering of orthologs and inparalogs shared by multiple proteomes, in: Bioinformatics. doi:10.1093/bioinformatics/btl213

Altenhoff, A.M., Gil, M., Gonnet, G.H., Dessimoz, C., 2013. Inferring Hierarchical Orthologous Groups from Orthologous Gene Pairs. PLoS One 8. doi:10.1371/journal.pone.0053786

Andrikou, C., Iovene, E., Rizzo, F., Oliveri, P., Arnone, M.I., 2013. Myogenesis in the sea urchin embryo: the molecular fingerprint of the myoblast precursors. Evodevo 4, 33. doi:10.1186/2041-9139-4-33

Andrikou, C., Pai, C.Y., Su, Y.H., Arnone, M.I., 2015. Logics and properties of a genetic regulatory program that drives embryonic muscle development in an echinoderm. Elife 4, 1–22. doi:10.7554/eLife.07343

Barbosa-Morais, N.L., Irimia, M., Pan, Q., Xiong, H.Y., Gueroussov, S., Lee, L.J., Slobodeniuc, V., Kutter, C., Watt, S., Colak, R., Kim, T., Misquitta-Ali, C.M., Wilson, M.D., Kim, P.M., Odom, D.T., Frey, B.J., Blencowe, B.J., 2012. The evolutionary landscape of alternative splicing in vertebrate species. Science (80-.). 338, 1587–1593. doi:10.1126/science.1230612

Bebee, T.W., Park, J.W., Sheridan, K.I., Warzecha, C.C., Cieply, B.W., Rohacek, A.M., Xing, Y., Carstens, R.P., 2015. The splicing regulators Esrp1 and Esrp2 direct an epithelial splicing program essential for mammalian development. Elife 4. doi:10.7554/eLife.08954

Bebee, T.W., Sims-Lucas, S., Park, J.W., Bushnell, D., Cieply, B., Xing, Y., Bates, C.M., Carstens, R.P., 2016. Ablation of the epithelial-specific splicing factor Esrp1 results in ureteric branching defects and reduced nephron number. Dev. Dyn. 245, 991–1000. doi:10.1002/dvdy.24431

Bell, G., Mooers, A.O., 1997. Size and complexity among multicellular organisms. Biol. J.

Linn. Soc. 60, 345–363. doi:10.1111/j.1095-8312.1997.tb01500.x

Benito-Gutiérrez, È., Illas, M., Comella, J.X., Garcia-Fernàndez, J., 2005. Outlining the nascent nervous system of Branchiostoma floridae (amphioxus) by the pan-neural marker AmphiElav, in: Brain Research Bulletin. pp. 518–521. doi:10.1016/j.brainresbull.2005.03.007

Bhate, A., Parker, D.J., Bebee, T.W., Ahn, J., Arif, W., Rashan, E.H., Chorghade, S., Chau, A., Lee, J.-H., Anakk, S., Carstens, R.P., Xiao, X., Kalsotra, A., 2015. ESRP2 controls an adult splicing programme in hepatocytes to support postnatal liver maturation. Nat. Commun. 6, 8768. doi:10.1038/ncomms9768

Boehlke, C., Janusch, H., Hamann, C., Powelske, C., Mergen, M., Herbst, H., Kotsis, F., Nitschke, R., Kuehn, E.W., 2015. A cilia independent role of Ift88/polaris during cell migration. PLoS One 10. doi:10.1371/journal.pone.0140378

Bouchet, B.P., Noordstra, I., van Amersfoort, M., Katrukha, E.A., Ammon, Y.-C., ter Hoeve, N.D., Hodgson, L., Dogterom, M., Derksen, P.W.B., Akhmanova, A., 2016. Mesenchymal Cell Invasion Requires Cooperative Regulation of Persistent Microtubule Growth by SLAIN2 and CLASP1. Dev. Cell 1–16. doi:10.1016/j.devcel.2016.11.009

Braunschweig, U., Barbosa-Morais, N.L., Pan, Q., Nachman, E.N., Alipanahi, B., Gonatopoulos-Pournatzis, T., Frey, B., Irimia, M., Blencowe, B.J., 2014. Widespread intron retention in mammals functionally tunes transcriptomes. Genome Res. 24, 1774–1786. doi:10.1101/gr.177790.114

Brown, J.B., Boley, N., Eisman, R., May, G.E., Stoiber, M.H., Duff, M.O., Booth, B.W., Wen, J., Park, S., Suzuki, A.M., Wan, K.H., Yu, C., Zhang, D., Carlson, J.W., Cherbas, L., Eads, B.D., Miller, D., Mockaitis, K., Roberts, J., Davis, C.A., Frise, E., Hammonds, A.S., Olson, S., Shenker, S., Sturgill, D., Samsonova, A.A., Weiszmann, R., Robinson, G., Hernandez, J., Andrews, J., Bickel, P.J., Carninci, P., Cherbas, P., Gingeras, T.R., Hoskins, R.A., Kaufman, T.C., Lai, E.C., Oliver, B., Perrimon, N., Graveley, B.R., Celniker, S.E., 2014. Diversity and dynamics of the Drosophila transcriptome. Nature 512, 393–399. doi:10.1038/nature12962

Brown, J.B., Boley, N., Eisman, R., May, G.E., Stoiber, M.H., Duff, M.O., Booth, B.W., Wen, J., Park, S., Suzuki, A.M., Wan, K.H., Yu, C., Zhang, D., Carlson, J.W., Cherbas, L., Eads, B.D., Miller, D., Mockaitis, K., Roberts, J., Davis, C. a, Frise, E., Hammonds, A.S., Olson, S., Shenker, S., Sturgill, D., Samsonova, A. a, Weiszmann, R., Robinson, G., Hernandez, J., Andrews, J., Bickel, P.J., Carninci, P., Cherbas, P., Gingeras, T.R., Hoskins, R. a, Kaufman, T.C., Lai, E.C., Oliver, B., Perrimon, N., Graveley, B.R., Celniker, S.E., 2014. Diversity and dynamics of the Drosophila transcriptome. Nature 512, 1–7.

doi:10.1038/nature12962

Buckley, P.T., Khaladkar, M., Kim, J., Eberwine, J., 2014. Cytoplasmic intron retention, function, splicing, and the sentinel RNA hypothesis. Wiley Interdiscip. Rev. RNA. doi:10.1002/wrna.1203

Buckley, P.T., Lee, M.T., Sul, J.Y., Miyashiro, K.Y., Bell, T.J., Fisher, S.A., Kim, J., Eberwine, J., 2011. Cytoplasmic Intron Sequence-Retaining Transcripts Can Be Dendritically Targeted via ID Element Retrotransposons. Neuron 69, 877–884. doi:10.1016/j.neuron.2011.02.028

Calo, E., Wysocka, J., 2013. Modification of Enhancer Chromatin: What, How, and Why? Mol. Cell. doi:10.1016/j.molcel.2013.01.038

Chen, L., Bush, S.J., Tovar-Corona, J.M., Castillo-Morales, A., Urrutia, A.O., 2014. Correcting for differential transcript coverage reveals a strong relationship between alternative splicing and organism complexity. Mol. Biol. Evol. 31, 1402–1413. doi:10.1093/molbev/msu083

Collén, J., Porcel, B., Carré, W., Ball, S.G., Chaparro, C., Tonon, T., Barbeyron, T., Michel, G., Noel, B., Valentin, K., Elias, M., Artiguenave, F., Arun, A., Aury, J.-M., Barbosa-Neto, J.F., Bothwell, J.H., Bouget, F.-Y., Brillet, L., Cabello-Hurtado, F., Capella-Gutiérrez, S., Charrier, B., Cladière, L., Cock, J.M., Coelho, S.M., Colleoni, C., Czjzek, M., Da Silva, C., Delage, L., Denoeud, F., Deschamps, P., Dittami, S.M., Gabaldón, T., Gachon, C.M.M., Groisillier, A., Hervé, C., Jabbari, K., Katinka, M., Kloareg, B., Kowalczyk, N., Labadie, K., Leblanc, C., Lopez, P.J., McLachlan, D.H., Meslet-Cladiere, L., Moustafa, A., Nehr, Z., Nyvall Collén, P., Panaud, O., Partensky, F., Poulain, J., Rensing, S.A., Rousvoal, S., Samson, G., Symeonidi, A., Weissenbach, J., Zambounis, A., Wincker, P., Boyen, C., 2013. Genome structure and metabolic features in the red seaweed *Chondrus crispus* shed light on evolution of the Archaeplastida. PNAS 110, 5247–52. doi:10.1073/pnas.1221259110

Coschigano, K.T., Wensink, P.C., 1993. Sex-specific transcriptional regulation by the male and female doublesex proteins of Drosophila. Genes Dev. 7, 42–54. doi:10.1101/gad.7.1.42

Csuros, M., Rogozin, I.B., Koonin, E. V., 2011. A detailed history of intron-rich eukaryotic ancestors inferred from a global survey of 100 complete genomes. PLoS Comput. Biol. 7. doi:10.1371/journal.pcbi.1002150

Curtis, B.A., Tanifuji, G., Burki, F., Gruber, A., Irimia, M., Maruyama, S., Arias, M.C., Ball, S.G., Gile, G.H., Hirakawa, Y., Hopkins, J.F., Kuo, A., Rensing, S.A., Schmutz, J., Symeonidi, A., Elias, M., Eveleigh, R.J.M., Herman, E.K., Klute, M.J., Nakayama, T., Oborník, M., Reyes-Prieto, A., Armbrust, E.V., Aves, S.J., Beiko, R.G., Coutinho, P., Dacks, J.B., Durnford, D.G., Fast, N.M., Green, B.R., Grisdale, C.J., Hempel, F.,

Henrissat, B., Höppner, M.P., Ishida, K.-I., Kim, E., Kořený, L., Kroth, P.G., Liu, Y., Malik, S.-B., Maier, U.G., McRose, D., Mock, T., Neilson, J.A.D., Onodera, N.T., Poole, A.M., Pritham, E.J., Richards, T.A., Rocap, G., Roy, S.W., Sarai, C., Schaack, S., Shirato, S., Slamovits, C.H., Spencer, D.F., Suzuki, S., Worden, A.Z., Zauner, S., Barry, K., Bell, C., Bharti, A.K., Crow, J.A., Grimwood, J., Kramer, R., Lindquist, E., Lucas, S., Salamov, A., McFadden, G.I., Lane, C.E., Keeling, P.J., Gray, M.W., Grigoriev, I. V., Archibald, J.M., 2012. Algal genomes reveal evolutionary mosaicism and the fate of nucleomorphs. Nature 492, 59–65. doi:10.1038/nature11681

Damianov, A., Ying, Y., Lin, C.H., Lee, J.A., Tran, D., Vashisht, A.A., Bahrami-Samani, E., Xing, Y., Martin, K.C., Wohlschlegel, J.A., Black, D.L., 2016. Rbfox Proteins Regulate Splicing as Part of a Large Multiprotein Complex LASR. Cell 165, 606–619. doi:10.1016/j.cell.2016.03.040

De Moerlooze, L., Spencer-Dene, B., Revest, J.M., Hajihosseini, M., Rosewell, I., Dickson, C., Amaya, E., Musci, T., Kirschner, M., Araki, K., Araki, M., Miyazaki, J.-I., Vassalli, P., Arman, E., Haffner-Krausz, R., Chen, Y., Heath, J.K., Lonai, P., Bellusci, S., Grindley, J., Emoto, H., Itoh, N., Hogan, B.L.M., Cardoso, W. V., Itoh, A., Nogawa, H., Mason, I., Brody, J.S., Carstens, R., Mckeehan, W., Garcia-Blanco, M., Carstens, R.P., Eaton, J. V., Krigman, H.R., Walther, P.J., Garciablanco, M.A., Celli, G., Larochelle, W.J., MacKem, S., Sharp, R., Merlino, G., Ciruna, B.G., Schwartz, L., Harpal, K., Yamaguchi, T.P., Rossant, J., Colvin, J.S., Bohne, B.A., Harding, G.W., McEwen, D.G., Ornitz, D.M., Crossley, P.H., Minowada, G., MacArthur, C.A., Martin, G.R., Gatto, F. Del, Plet, A., Gesnel, M.-C., Fort, C., Breathnach, R., DeMoerlooze, L., Dickson, C., Deng, C., Wynshaw, B.A., Zhou, F., Kuo, A., Leder, P., Deng, C.X., Bedford, M., Li, C.L., Xu, X.L., Yang, X., Dunmore, J., Leder, P., Deng, C.X., Wynshaw-Boris, A., Shen, M.M., Daugherty, C., Ornitz, D.M., Leder, P., DeVore, D.L., Horvitz, H.R., Stern, M.J., Ericson, J., Norlin, S., Jessell, T.M., Edlund, T., Fantl, V., Stamp, G., Andrews, A., Rosewell, I., Dickson, C., Finch, P., Cunha, G., Rubin, J., Wong, J., Ron, D., Gilbert, E., Gatto, F. Del, Gesnel, M.-C., Fort, C., Breathnach, R., Gu, H., Zou, Y.-R., Rajewsky, K., Guo, L., Degenstein, L., Fuchs, E., Igarashi, M., Finch, P., Aaronson, S., Jackson, D., Bresnick, J., Rosewell, I., Crafton, T., Poulsom, R., Stamp, G., Dickson, C., Johnson, D., Williams, L., Kettunen, P., Karavanova, I., Thesleff, I., Laird, P., Zijderveld, A., Linders, K., Rudnicki, M., Jaenisch, R., Berns, A., Mahmood, R., Bresnick, J., Hornbruch, A., Mahony, C., Morton, N., Colquhoun, K., Martin, P., Lumsden, A., Dickson, C., Mason, I., Mansour, S.L., Goddard, J.M., Capecchi, M.R., Mason, I., Fuller-Pace, F., Smith, R., Dickson, C., Mathieu, M., Chatelain, E., Ornitz, D., Bresnick, J., Mason, I., Kiefer, P., Dickson, C.,

McKeehan, W.L., Wang, F., Kan, M., McLeod, M., Miki, T., Bottaro, D., Fleming, T., Smith, C.L., Burgess, W., Chan, A., Aaronson, S., Min, H., Danilenko, D., Scully, S., Bolon, B., Ring, B., Tarpley, J., DeRose, M., Simonet, W., Ohuchi, H., Nakagawa, T., Yamamoto, A., Araga, A., Ohata, T., Ishimaru, Y., Yoshioka, H., Kuwana, T., Nohno, T., Yamasaki, M., Itoh, N., Noji, S., Ornitz, D.M., Xu, J.S., Colvin, J.S., McEwen, D.G., MacArthur, C.A., Coulier, F., Gao, G.X., Goldfarb, M., Orr-Urtreger, A., Bedford, M., Burakova, T., Arman, E., Zimmer, Y., Yayon, A., Givol, D., Lonai, P., Peters, K., Werner, S., Chen, G., Williams, L., Peters, K., Werner, S., Liao, X., Wert, S., Whitsett, J., Williams, L., Qiao, J., Uzzo, R., Obara-Ishihara, T., Degenstein, L., Fuchs, E., Herzlinger, D., Reichman-Fried, M., Shilo, B.Z., Robinson, M.L., MacMillan-Crow, L.A., Thompson, J.A., Overbeek, P.A., Satokata, I., Maas, R., Sekine, K., Ohuchi, H., Fujiwara, M., Yamasaki, M., Yoshizawa, T., Sato, T., Yagishita, N., Matsui, D., Koga, Y., Itoh, N., Kato, S., Thesleff, I., Sharpe, P., Treier, M., Gleiberman, A., O'Connell, S., Szeto, D., McMahon, J., McMahon, A., Rosenfeld, M., Vogel, A., Rodriguez, C., Izpisua-Belmonte, J.C., Weinstein, M., Xu, X.L., Ohyama, K., Deng, C.X., Werner, S., Smola, H., Liao, X., Longaker, M., Krieg, T., Hofschneider, P., Williams, L., Werner, S., Weinberg, W., Liao, X., Peters, K., Blessing, M., Yuspa, S., Weiner, R., Williams, L., Wilkinson, D., Bhatt, S., McMahon, A., Xu, X.L., Weinstein, M., Li, C.L., Naski, M., Cohen, R.I., Ornitz, D.M., Leder, P., Deng, C.X., Yamaguchi, F., Saya, H., Bruner, J.M., Morrison, R.S., Yamaguchi, T.P., Rossant, J., Yamasaki, M., Miyake, A., Tagashira, S., Itoh, N., 2000. An important role for the IIIb isoform of fibroblast growth factor receptor 2 (FGFR2) in mesenchymal-epithelial signalling during mouse organogenesis. Development 127, 483–492. doi:10.1016/0092-8674(91)90616-7

Delsuc, F., Brinkmann, H., Chourrout, D., Philippe, H., 2006. Tunicates and not cephalochordates are the closest living relatives of vertebrates. Nature 439, 965–968. doi:10.1038/nature04336

Dittmar, K.A., Jiang, P., Park, J.W., Amirikian, K., Wan, J., Shen, S., Xing, Y., Carstens, R.P., 2012. Genome-Wide Determination of a Broad ESRP-Regulated Posttranscriptional Network by High-Throughput Sequencing. Mol. Cell. Biol. 32, 1468–1482. doi:10.1128/MCB.06536-11

Djebali, S., Davis, C.A., Merkel, A., Dobin, A., Lassmann, T., Mortazavi, A., Tanzer, A., Lagarde, J., Lin, W., Schlesinger, F., Xue, C., Marinov, G.K., Khatun, J., Williams, B.A., Zaleski, C., Rozowsky, J., Röder, M., Kokocinski, F., Abdelhamid, R.F., Alioto, T., Antoshechkin, I., Baer, M.T., Bar, N.S., Batut, P., Bell, K., Bell, I., Chakrabortty, S., Chen, X., Chrast, J., Curado, J., Derrien, T., Drenkow, J., Dumais, E., Dumais, J., Duttagupta, R.,

Falconnet, E., Fastuca, M., Fejes-Toth, K., Ferreira, P., Foissac, S., Fullwood, M.J., Gao, H., Gonzalez, D., Gordon, A., Gunawardena, H., Howald, C., Jha, S., Johnson, R., Kapranov, P., King, B., Kingswood, C., Luo, O.J., Park, E., Persaud, K., Preall, J.B., Ribeca, P., Risk, B., Robyr, D., Sammeth, M., Schaffer, L., See, L.-H., Shahab, A., Skancke, J., Suzuki, A.M., Takahashi, H., Tilgner, H., Trout, D., Walters, N., Wang, H., Wrobel, J., Yu, Y., Ruan, X., Hayashizaki, Y., Harrow, J., Gerstein, M., Hubbard, T., Reymond, A., Antonarakis, S.E., Hannon, G., Giddings, M.C., Ruan, Y., Wold, B., Carninci, P., Guigó, R., Gingeras, T.R., 2012. Landscape of transcription in human cells. Nature 489, 101–108. doi:10.1038/nature11233

Doolittle, F., Brunet, T.D.P., Linquist, S., Gregory, T.R., 2014. Distinguishing between "Function" and "Effect" in genome biology. Genome Biol. Evol. doi:10.1093/gbe/evu098

Dougherty, M., Kamel, G., Grimaldi, M., Gfrerer, L., Shubinets, V., Ethier, R., Hickey, G., Cornell, R. a, Liao, E.C., 2013. Distinct requirements for wnt9a and irf6 in extension and integration mechanisms during zebrafish palate morphogenesis. Development 140, 76–81. doi:10.1242/dev.080473

Ellis, J.D., Barrios-Rodiles, M., Çolak, R., Irimia, M., Kim, T.H., Calarco, J.A., Wang, X., Pan, Q., O'Hanlon, D., Kim, P.M., Wrana, J.L., Blencowe, B.J., 2012. Tissue-Specific Alternative Splicing Remodels Protein-Protein Interaction Networks. Mol. Cell 46, 884–892. doi:10.1016/j.molcel.2012.05.037

Ettensohn, C.A., 2009. Lessons from a gene regulatory network: echinoderm skeletogenesis provides insights into evolution, plasticity and morphogenesis. Development 136, 11–21. doi:10.1242/dev.023564

Finlay, B.J., Esteban, G.F., 2009. Can Biological Complexity Be Rationalized? Bioscience 59, 333–340. doi:10.1525/bio.2009.59.4.11

Fu, X.-D., Ares, M., 2014. Context-dependent control of alternative splicing by RNA-binding proteins. Nat. Rev. Genet. 15, 689–701. doi:10.1038/nrg3778

Fuentes, M., Benito, E., Bertrand, S., Paris, M., Mignardor, A., Godoy, L., Jimenez-Delgado, S., Oliveri, D., Candiani, S., Hirsinger, E., D'Aniello, S., Pascual-Anaya, J., Maeso, I., Pestarino, M., Vernier, P., Nicolas, J., Schubert, M., Laudet, V., Geneviere, A.M., Albalat, R., Garcia-Fernàndez, J., Holland, N.D., Escrivà, H., 2007. Insights Into Spawning Behavior and Development of the European Amphioxus (Branchiostoma lanceolatum). J. Exp. Zool. B. Mol. Dev. Evol. 308, 484–493. doi:10.1002/jez.b

Gallagher, T.L., Arribere, J.A., Geurts, P.A., Exner, C.R.T., McDonald, K.L., Dill, K.K., Marr, H.L., Adkar, S.S., Garnett, A.T., Amacher, S.L., Conboy, J.G., 2011. Rbfox-regulated alternative splicing is critical for zebrafish cardiac and skeletal muscle functions. Dev.

Biol. 359, 251–261. doi:10.1016/j.ydbio.2011.08.025

Gallego-Paez, L.M., Bordone, M.C., Leote, A.C., Saraiva-Agostinho, N., Ascens??o-Ferreira, M., Barbosa-Morais, N.L., 2017. Alternative splicing: the pledge, the turn, and the prestige: The key role of alternative splicing in human biological systems. Hum. Genet. 1–28. doi:10.1007/s00439-017-1790-y

Gao, C., Ren, S., Lee, J., Qiu, J., Chapski, D.J., Rau, C.D., Zhou, Y., Abdellatif, M., Nakano, A., Vondriska, T.M., Xiao, X., Fu, X., Chen, J., Wang, Y., 2016. RBFox1-mediated RNA splicing regulates cardiac hypertrophy and heart failure. J. Clin. Invest. 126, 195–206. doi:10.1172/JCI84015DS1

Garanto, A., Riera, M., Pomares, E., Permanyer, J., de Castro-Miró, M., Sava, F., Abril, J.F., Marfany, G., Gonzàlez-Duarte, R., 2011. High transcriptional complexity of the retinitis pigmentosa CERKL gene in human and mouse. Investig. Ophthalmol. Vis. Sci. 52, 5202–5214. doi:10.1167/iovs.10-7101

Garcia-Fernàndez, J., Jiménez-Delgado, S., Pascual-Anaya, J., Maeso, I., Irimia, M., Minguillón, C., Benito-Gutiérrez, È., Gardenyes, J., Bertrand, S., D'Aniello, S., 2009. From the American to the European amphioxus: Towards experimental Evo-Devo at the origin of chordates. Int. J. Dev. Biol. doi:10.1387/ijdb.072436jg

Ge, Y., Porse, B.T., 2014. The functional consequences of intron retention: Alternative splicing coupled to NMD as a regulator of gene expression. BioEssays 36, 236–243. doi:10.1002/bies.201300156

Gehman, L.T., Meera, P., Stoilov, P., Shiue, L., O'Brien, J.E., Meisler, M.H., Ares, M., Otis, T.S., Black, D.L., 2012. The splicing regulator Rbfox2 is required for both cerebellar development and mature motor function. Genes Dev. 26, 445–460. doi:10.1101/gad.182477.111

Gehman, L.T., Stoilov, P., Maguire, J., Damianov, A., Lin, C.-H., Shiue, L., Ares, M., Mody, I., Black, D.L., 2011. The splicing regulator Rbfox1 (A2BP1) controls neuronal excitation in the mammalian brain. Nat. Genet. 43, 706–711. doi:10.1038/ng.841

Geisler, S., Coller, J., 2013. RNA in unexpected places: long non-coding RNA functions in diverse cellular contexts. Nat. Rev. Mol. Cell Biol. 14, 699–712. doi:10.1038/nrm3679

Gempe, T., Hasselmann, M., Schiøtt, M., Hause, G., Otte, M., Beye, M., 2009. Sex determination in honeybees: Two separate mechanisms induce and maintain the female pathway. PLoS Biol. 7. doi:10.1371/journal.pbio.1000222

Giampietro, C., Deflorian, G., Gallo, S., Di Matteo, A., Pradella, D., Bonomi, S., Belloni, E., Nyqvist, D., Quaranta, V., Confalonieri, S., Bertalot, G., Orsenigo, F., Pisati, F., Ferrero, E., Biamonti, G., Fredrickx, E., Taveggia, C., Wyatt, C.D.R., Irimia, M., Di Fiore, P.P.,

Blencowe, B.J., Dejana, E., Ghigna, C., 2015. The alternative splicing factor Nova2 regulates vascular development and lumen formation. Nat. Commun. 6, 8479. doi:10.1038/ncomms9479

Gibilisco, L., Zhou, Q., Mahajan, S., Bachtrog, D., 2016. Alternative Splicing within and between Drosophila Species, Sexes, Tissues, and Developmental Stages. PLoS Genet. 12. doi:10.1371/journal.pgen.1006464

Gibson, a W., Burke, R.D., 1985. The origin of pigment cells in embryos of the sea urchin Strongylocentrotus purpuratus. Dev. Biol. 107, 414–419.

Gilbert, S.F., 2013. Developmental Biology. Dev. Biol.

Gill, J., Park, Y., McGinnis, J.P., Perez-Sanchez, C., Blanchette, M., Si, K., 2017. Regulated Intron Removal Integrates Motivational State and Experience. Cell 169, 836–848.e15. doi:10.1016/j.cell.2017.05.006

Gline, S., Kaplan, N., Bernadskaya, Y., Abdu, Y., Christiaen, L., 2015. Surrounding tissues canalize motile cardiopharyngeal progenitors towards collective polarity and directed migration. Development 142, 544–54. doi:10.1242/dev.115444

Gonzalez, I., Munita, R., Agirre, E., Dittmer, T.A., Gysling, K., Misteli, T., Luco, R.F., 2015. A lncRNA regulates alternative splicing via establishment of a splicing-specific chromatin signature. Nat. Struct. Mol. Biol. doi:10.1038/nsmb.3005

Gracheva, E.O., Cordero-Morales, J.F., González-Carcacía, J.A., Ingolia, N.T., Manno, C., Aranguren, C.I., Weissman, J.S., Julius, D., 2011. Ganglion-specific splicing of TRPV1 underlies infrared sensation in vampire bats. Nature 476, 88–91. doi:10.1038/nature10245

Gregory, T.R., 2004. Macroevolution, hierarchy theory, and the C-value enigma. Paleobiology 30, 179–202. doi:10.1666/0094-8373(2004)030<0179:MHTATC>2.0.CO;2

Grifone, R., Xie, X., Bourgeois, A., Saquet, A., Duprez, D., Shi, D.L., 2014. The RNA-binding protein Rbm24 is transiently expressed in myoblasts and is required for myogenic differentiation during vertebrate development. Mech. Dev. 134, 1–15. doi:10.1016/j.mod.2014.08.003

Grosso, A.R., Gomes, A.Q., Barbosa-Morais, N.L., Caldeira, S., Thorne, N.P., Grech, G., von Lindern, M., Carmo-Fonseca, M., 2008. Tissue-specific splicing factor gene expression signatures. Nucleic Acids Res. 36, 4823–4832. doi:10.1093/nar/gkn463

Gu, Y., Barry, J., McDougel, R., Terman, D., Gu, C., 2012. Alternative splicing regulates Kv3.1 polarized targeting to adjust maximal spiking frequency. J. Biol. Chem. 287, 1755–1769. doi:10.1074/jbc.M111.299305

Gueroussov, S., Gonatopoulos-Pournatzis, T., Irimia, M., Raj, B., Lin, Z.-Y., Gingras, A.-C., Blencowe, B.J., 2015. An alternative splicing event amplifies evolutionary differences

between vertebrates. Science (80-.). 349, 868–873. doi:10.1126/science.aaa8381

Guven-Ozkan, T., Busto, G.U., Schutte, S.S., Cervantes-Sandoval, I., O'Dowd, D.K., Davis, R.L., 2016. MiR-980 Is a Memory Suppressor MicroRNA that Regulates the Autism-Susceptibility Gene A2bp1. Cell Rep. 14, 1698–1709. doi:10.1016/j.celrep.2016.01.040

Hahn, M.W., Wray, G.A., 2002. The g-value paradox. Evol. Dev. 4, 73–75. doi:10.1046/j.1525-142X.2002.01069.x

Hamada, N., Ito, H., Iwamoto, I., Morishita, R., Tabata, H., Nagata, K., 2015. Role of the cytoplasmic isoform of RBFOX1/A2BP1 in establishing the architecture of the developing cerebral cortex. Mol. Autism 6, 56. doi:10.1186/s13229-015-0049-5

Hamada, N., Ito, H., Nishijo, T., Iwamoto, I., Morishita, R., Tabata, H., Momiyama, T., Nagata, K.-I., 2016. Essential role of the nuclear isoform of RBFOX1, a candidate gene for autism spectrum disorders, in the brain development. Sci. Rep. 6, 30805. doi:10.1038/srep30805

Holland, L.Z., 2016. Tunicates. Curr. Biol. 26, R146–R152. doi:10.1016/j.cub.2015.12.024

Holland, L.Z., Holland, N.D., 2001. Evolution of neural crest and placodes: amphioxus as a model for the ancestral vertebrate? J. Anat. doi:10.1046/j.1469-7580.2001.19910085.x

Hotta, K., Mitsuhara, K., Takahashi, H., Inaba, K., Oka, K., Gojobori, T., Ikeo, K., 2007. A web-based interactive developmental table for the Ascidian Ciona intestinalis, including 3D real-image embryo reconstructions: I. From fertilized egg to hatching larva. Dev. Dyn. 236, 1790–1805. doi:10.1002/dvdy.21188

Imai, K.S., 2003. A Twist-like bHLH gene is a downstream factor of an endogenous FGF and determines mesenchymal fate in the ascidian embryos. Development 130, 4461–4472. doi:10.1242/dev.00652

Irimia, M., Blencowe, B.J., 2012. Alternative splicing: Decoding an expansive regulatory layer. Curr. Opin. Cell Biol. doi:10.1016/j.ceb.2012.03.005

Irimia, M., Denuc, A., Burguera, D., Somorjai, I., Martín-Durán, J.M., Genikhovich, G., Jimenez-Delgado, S., Technau, U., Roy, S.W., Marfany, G., Garcia-Fernàndez, J., 2011a. Stepwise assembly of the Nova-regulated alternative splicing network in the vertebrate brain. Proc. Natl. Acad. Sci. U. S. A. 108, 5319–24.

Irimia, M., Maeso, I., Burguera, D., Hidalgo-Sanchez, M., Puelles, L., Roy, S.W., Garcia-Fernàndez, J., Ferran, J.L., 2011b. Contrasting 5′ and 3′ evolutionary histories and frequent evolutionary convergence in Meis/hth gene structures. Genome Biol. Evol. 3, 551–564.

Irimia, M., Pineiro, C., Maeso, I., Gomez-Skarmeta, J.L., Casares, F., Garcia-Fernandez, J., Piñeiro, C., Maeso, I., Gómez-Skarmeta, J.L., Casares, F., Garcia-Fernàndez, J., 2010a. Conserved developmental expression of Fezf in chordates and Drosophila and the origin of the Zona Limitans Intrathalamica (ZLI) brain organizer. Evodevo 1, 7. doi:10.1186/2041-

9139-1-7

Irimia, M., Piñeiro, C., Maeso, I., Gómez-Skarmeta, J.L., Casares, F., Garcia-Fernàndez, J., 2010b. Conserved developmental expression of Fezf in chordates and Drosophila and the origin of the Zona Limitans Intrathalamica (ZLI) brain organizer. Evodevo 1, 7. doi:10.1186/2041-9139-1-7

Irimia, M., Roy, S.W., 2014. Origin of spliceosomal introns and alternative splicing. Cold Spring Harb. Perspect. Biol. 6. doi:10.1101/cshperspect.a016071

Irimia, M., Roy, S.W., 2008. Spliceosomal introns as tools for genomic and evolutionary analysis. Nucleic Acids Res. doi:10.1093/nar/gkn012

Irimia, M., Rukov, J.L., Penny, D., Vinther, J., Garcia-Fernandez, J., Roy, S.W., 2008. Origin of introns by “intronization” of exonic sequences. Trends Genet. doi:10.1016/j.tig.2008.05.007

Irimia, M., Weatheritt, R.J., Ellis, J.D., Parikshak, N.N., Gonatopoulos-Pournatzis, T., Babor, M., Quesnel-Vallières, M., Tapial, J., Raj, B., O’Hanlon, D., Barrios-Rodiles, M., Sternberg, M.J.E., Cordes, S.P., Roth, F.P., Wrana, J.L., Geschwind, D.H., Blencowe, B.J., 2014. A highly conserved program of neuronal microexons is misregulated in autistic brains. Cell 159, 1511–1523. doi:10.1016/j.cell.2014.11.035

Jao, L.-E., Wente, S.R., Chen, W., 2013. Efficient multiplex biallelic zebrafish genome editing using a CRISPR nuclease system. Proc. Natl. Acad. Sci. U. S. A. 110, 13904–9. doi:10.1073/pnas.1308335110

Jensen, K.B., Dredge, B.K., Stefani, G., Zhong, R., Buckanovich, R.J., Okano, H.J., Yang, Y.Y.L., Darnell, R.B., 2000. Nova-1 Regulates Neuron-Specific Alternative Splicing and Is Essential for Neuronal Viability. Neuron 25, 359–371. doi:10.1016/S0896-6273(00)80900-9

Jonas, S., Izaurralde, E., 2015. Towards a molecular understanding of microRNA-mediated gene silencing. Nat. Rev. Genet. 16, 421–433. doi:10.1038/nrg3965

Julien, P., Miñana, B., Baeza-Centurion, P., Valcárcel, J., Lehner, B., 2016. The complete local genotype–phenotype landscape for the alternative splicing of a human exon. Nat. Commun. 7, 11558. doi:10.1038/ncomms11558

Jung, Y., Kissil, J.L., McCarty, J.H., 2011. ??8 integrin and band 4.1B cooperatively regulate morphogenesis of the embryonic heart. Dev. Dyn. 240, 271–277. doi:10.1002/dvdy.22513

Kalsotra, A., Xiao, X., Ward, A.J., Castle, J.C., Johnson, J.M., Burge, C.B., Cooper, T. a, 2008. A postnatal switch of CELF and MBNL proteins reprograms alternative splicing in the developing heart. Proc. Natl. Acad. Sci. U. S. A. 105, 20333–20338. doi:10.1073/pnas.0809045105

Kaltenbach, S.L., Yu, J.K., Holland, N.D., 2009. The origin and migration of the earliest-developing sensory neurons in the peripheral nervous system of amphioxus. Evol. Dev. 11, 142–151. doi:10.1111/j.1525-142X.2009.00315.x

Kanapin, A.A., Mulder, N., Kuznetsov, V.A., 2010. Projection of gene-protein networks to the functional space of the proteome and its application to analysis of organism complexity. BMC Genomics 11 Suppl 1, S4+. doi:10.1186/1471-2164-11-S1-S4

Katoh, K., Standley, D.M., 2013. MAFFT multiple sequence alignment software version 7: Improvements in performance and usability. Mol. Biol. Evol. 30, 772–780. doi:10.1093/molbev/mst010

Kaul, S., Stach, T., 2010. Ontogeny of the collar cord: Neurulation in the hemichordate Saccoglossus Kowalevskii. J. Morphol. 271, 1240–1259. doi:10.1002/jmor.10868

Kelemen, O., Convertini, P., Zhang, Z., Wen, Y., Shen, M., Falaleeva, M., Stamm, S., 2013. Function of alternative splicing. Gene. doi:10.1016/j.gene.2012.07.083

Kiebler, M., Scheiffele, P., Ule, J., 2013. What, where, and when: the importance of post-transcriptional regulation in the brain. Front. Neurosci. doi:10.1038/nrg3141

Kimmel, C.B., Ballard, W.W., Kimmel, S.R., Ullmann, B., Schilling, T.F., 1995. Stages of embryonic development of the zebrafish. Dev. Dyn. 203, 253–310. doi:10.1002/aja.1002030302

Kimmel, C.B., Sepich, D.S., Trevarrow, B., 1988. Development of segmentation in zebrafish. Development 104 Suppl, 197–207.

Klymkowsky, M.W., Rossi, C.C., Artinger, K.B., 2010. Mechanisms driving neural crest induction and migration in the zebrafish and Xenopus laevis. Cell Adhes. Migr. doi:10.4161/cam.4.4.12962

Kuroyanagi, H., Ohno, G., Mitani, S., Hagiwara, M., 2007. The Fox-1 Family and SUP-12 Coordinately Regulate Tissue-Specific Alternative Splicing In Vivo. Mol. Cell. Biol. 27, 8612–8621. doi:10.1128/MCB.01508-07

Labbé, R.M., Irimia, M., Currie, K.W., Lin, A., Zhu, S.J., Brown, D.D.R., Ross, E.J., Voisin, V., Bader, G.D., Blencowe, B.J., Pearson, B.J., 2012. A Comparative transcriptomic analysis reveals conserved features of stem cell pluripotency in planarians and mammals. Stem Cells 30, 1734–1745. doi:10.1002/stem.1144

Lapraz, F., Besnardeau, L., Lepage, T., 2009. Patterning of the dorsal-ventral axis in echinoderms: Insights into the evolution of the BMP-chordin signaling network. PLoS Biol. 7. doi:10.1371/journal.pbio.1000248

Laprise, P., Paul, S.M., Boulanger, J., Robbins, R.M., Beitel, G.J., Tepass, U., 2010. Epithelial Polarity Proteins Regulate Drosophila Tracheal Tube Size in Parallel to the Luminal

Matrix Pathway. Curr. Biol. 20, 55–61. doi:10.1016/j.cub.2009.11.017

Lev Maor, G., Yearim, A., Ast, G., 2015. The alternative role of DNA methylation in splicing regulation. Trends Genet. doi:10.1016/j.tig.2015.03.002

Lim, J., Hao, T., Shaw, C., Patel, A.J., Szabo, G., Rual, J.F., Fisk, C.J., Li, N., Smolyar, A., Hill, D.E., Barabasi, A.L., Vidal, M., Zoghbi, H.Y., 2006. A protein-protein interaction network for human inherited ataxias and disorders of Purkinje cell degeneration. Cell 125, 801–814. doi:10.1016/j.cell.2006.03.032

Liscovitch-Brauer, N., Alon, S., Porath, H.T., Elstein, B., Unger, R., Ziv, T., Admon, A., Levanon, E.Y., Rosenthal, J.J.C., Eisenberg, E., 2017. Trade-off between Transcriptome Plasticity and Genome Evolution in Cephalopods. Cell 169, 191–202.e11. doi:10.1016/j.cell.2017.03.025

Liu, D.W., Hsu, C.H., Tsai, S.M., Hsiao, C. Der, Wang, W.P., 2011. A variant of Fibroblast growth factor receptor 2 (Fgfr2) regulates left-right asymmetry in Zebrafish. PLoS One 6. doi:10.1371/journal.pone.0021793

Lowery, L.A., Sive, H., 2004. Strategies of vertebrate neurulation and a re-evaluation of teleost neural tube formation. Mech. Dev. doi:10.1016/j.mod.2004.04.022

Lu, T.-M., Luo, Y.-J., Yu, J.-K., 2012. BMP and Delta/Notch signaling control the development of amphioxus epidermal sensory neurons: insights into the evolution of the peripheral sensory system. Development 139, 2020–2030. doi:10.1242/dev.073833

Mackereth, C.D., 2014. Splicing factor SUP-12 and the molecular complexity of apparent cooperativity. Worm 3, e991240. doi:10.4161/21624054.2014.991240

Mallinjoud, P., Villemin, J.P., Mortada, H., Espinoza, M.P., Desmet, F.O., Samaan, S., Chautard, E., Tranchevent, L.C., Auboeuf, D., 2014. Endothelial, epithelial, and fibroblast cells exhibit specific splicing programs independently of their tissue of origin. Genome Res. 24, 511–521. doi:10.1101/gr.162933.113

Mansfield, J.H., Haller, E., Holland, N.D., Brent, A.E., 2015. Development of somites and their derivatives in amphioxus, and implications for the evolution of vertebrate somites. Evodevo 6, 21. doi:10.1186/s13227-015-0007-5

Marchler-Bauer, A., Derbyshire, M.K., Gonzales, N.R., Lu, S., Chitsaz, F., Geer, L.Y., Geer, R.C., He, J., Gwadz, M., Hurwitz, D.I., Lanczycki, C.J., Lu, F., Marchler, G.H., Song, J.S., Thanki, N., Wang, Z., Yamashita, R.A., Zhang, D., Zheng, C., Bryant, S.H., 2015. CDD: NCBI's conserved domain database. Nucleic Acids Res. 43, D222–D226. doi:10.1093/nar/gku1221

Marquez, Y., H??pfler, M., Ayatollahi, Z., Barta, A., Kalyna, M., 2015. Unmasking alternative splicing inside protein-coding exons defines exitrons and their role in proteome plasticity.

Genome Res. 25, 995–1007. doi:10.1101/gr.186585.114

Martín-Durán, J.M., Janssen, R., Wennberg, S., Budd, G.E., Hejnol, A., 2012. Deuterostomic development in the protostome Priapulus caudatus. Curr. Biol. 22, 2161–2166. doi:10.1016/j.cub.2012.09.037

Masselink, W., Cole, N.J., Fenyes, F., Berger, S., Sonntag, C., Wood, A., Nguyen, P.D., Cohen, N., Knopf, F., Weidinger, G., Hall, T.E., Currie, P.D., 2016. A somitic contribution to the apical ectodermal ridge is essential for fin formation. Nature 535, 542–546. doi:10.1038/nature18953

McClay, D.R., 2011. Evolutionary crossroads in developmental biology: sea urchins. Development 138, 2639–48. doi:10.1242/dev.048967

McCoon, P.E., Blackstone, E., Angerer, R.C., Angerer, L.M., 1998. Sea urchin FGFR muscle-specific expression: posttranscriptional regulation in embryos and adults. Dev. Biol. 200, 171–81. doi:10.1006/dbio.1998.8943

Merkin, J., Russell, C., Chen, P., Burge, C.B., 2012. Evolutionary dynamics of gene and isoform regulation in Mammalian tissues. Science 338, 1593–9. doi:10.1126/science.1228186

Merkin, J.J., Chen, P., Alexis, M.S., Hautaniemi, S.K., Burge, C.B., 2015. Origins and impacts of new Mammalian Exons. Cell Rep. 10, 1993–2006. doi:10.1016/j.celrep.2015.02.058

Miki, T., Bottaro, D.P., Fleming, T.P., Smith, C.L., Burgess, W.H., Chan, a M., Aaronson, S. a, 1992. Determination of ligand-binding specificity by alternative splicing: two distinct growth factor receptors encoded by a single gene. Proc. Natl. Acad. Sci. U. S. A. 89, 246–250. doi:10.1073/pnas.89.1.246

Mirsky, a E., Ris, H., 1951. The desoxyribonucleic acid content of animal cells and its evolutionary significance. J. Gen. Physiol. 34, 451–462. doi:10.1085/jgp.34.4.451

Mistry, N., Harrington, W., Lasda, E., Wagner, E.J., Garcia-Blanco, M. a, 2003. Of urchins and men: evolution of an alternative splicing unit in fibroblast growth factor receptor genes. RNA 9, 209–217. doi:10.1261/rna.2470903

Moore, G.P., 1984. The C-value paradox. Bioscience 34, 425–429. doi:10.2307/1309631

Mork, L., Crump, G., 2015. Zebrafish Craniofacial Development. A Window into Early Patterning, in: Current Topics in Developmental Biology. pp. 235–269. doi:10.1016/bs.ctdb.2015.07.001

Ner-Gaon, H., Halachmi, R., Savaldi-Goldstein, S., Rubin, E., Ophir, R., Fluhr, R., 2004. Intron retention is a major phenomenon in alternative splicing in Arabidopsis. Plant J. 39, 877–885. doi:10.1111/j.1365-313X.2004.02172.x

Niswander, L., Jeffrey, S., Martin, G.R., Tickle, C., 1994. A positive feedback loop coordinates growth and patterning in the vertebrate limb. Nature 371, 609–612. doi:10.1038/371609a0

Niu, D.K., Jiang, L., 2013. Can ENCODE tell us how much junk DNA we carry in our genome? Biochem. Biophys. Res. Commun. doi:10.1016/j.bbrc.2012.12.074

Pani, A.M., Mullarkey, E.E., Aronowicz, J., Assimacopoulos, S., Grove, E.A., Lowe, C.J., 2012. Ancient deuterostome origins of vertebrate brain signalling centres. Nature 483, 289–294. doi:10.1038/nature10838

Passamaneck, Y.J., Di Gregorio, A., 2005. Ciona intestinalis: Chordate development made simple. Dev. Dyn. doi:10.1002/dvdy.20300

Pickrell, J.K., Pai, A.A., Gilad, Y., Pritchard, J.K., 2010. Noisy splicing drives mRNA isoform diversity in human cells. PLoS Genet. 6, 1–11. doi:10.1371/journal.pgen.1001236

Pirvola, U., Spencer-Dene, B., Xing-Qun, L., Kettunen, P., Thesleff, I., Fritzsch, B., Dickson, C., Ylikoski, J., 2000. FGF/FGFR-2(IIIb) signaling is essential for inner ear morphogenesis. J Neurosci 20, 6125–6134. doi:20/16/6125 [pii]

Pohl, M., Sakurai, H., Stuart, R.O., Nigam, S.K., 2000. Role of hyaluronan and CD44 in in vitro branching morphogenesis of ureteric bud cells. Dev. Biol. 224, 312–325. doi:10.1006/dbio.2000.9783

Poustka, A.J., Kühn, A., Radosavljevic, V., Wellenreuther, R., Lehrach, H., Panopoulou, G., 2004. On the origin of the chordate central nervous system: Expression of onecut in the sea urchin embryo. Evol. Dev. 6, 227–236. doi:10.1111/j.1525-142X.2004.04028.x

Price, D.C., Egizi, A., Fonseca, D.M., 2015. The ubiquity and ancestry of insect doublesex. Sci. Rep. 5, 13068. doi:10.1038/srep13068

Racioppi, C., Kamal, A.K., Razy-Krajka, F., Gambardella, G., Zanetti, L., di Bernardo, D., Sanges, R., Christiaen, L.A., Ristoratore, F., 2014. Fibroblast growth factor signalling controls nervous system patterning and pigment cell formation in Ciona intestinalis. Nat. Commun. 5, 4830. doi:10.1038/ncomms5830

Raj, B., Blencowe, B.J., 2015. Alternative Splicing in the Mammalian Nervous System: Recent Insights into Mechanisms and Functional Roles. Neuron 87, 14–27. doi:10.1016/j.neuron.2015.05.004

Raj, B., Irimia, M., Braunschweig, U., Sterne-Weiler, T., O'Hanlon, D., Lin, Z.Y., Chen, G.I., Easton, L.E., Ule, J., Gingras, A.C., Eyras, E., Blencowe, B.J., 2014. A global regulatory mechanism for activating an exon network required for neurogenesis. Mol. Cell 56, 90–103. doi:10.1016/j.molcel.2014.08.011

Ransick, A., Davidson, E.H., 2006. cis-regulatory processing of Notch signaling input to the sea urchin glial cells missing gene during mesoderm specification. Dev. Biol. 297, 587–602. doi:10.1016/j.ydbio.2006.05.037

Revil, T., Jerome-Majewska, L.A., 2013. During Embryogenesis, Esrp1 Expression Is Restricted

to a Subset of Epithelial Cells and Is Associated With Splicing of a Number of Developmentally Important Genes. Dev. Dyn. 242, 281–290. doi:10.1002/dvdy.23918

Riera, M., Burguera, D., Garcia-Fernàndez, J., Gonzàlez-Duarte, R., 2013. CERKL Knockdown Causes Retinal Degeneration in Zebrafish. PLoS One 8.

Riesgo, A., Farrar, N., Windsor, P.J., Giribet, G., Leys, S.P., 2014. The analysis of eight transcriptomes from all poriferan classes reveals surprising genetic complexity in sponges. Mol. Biol. Evol. 31, 1102–1120. doi:10.1093/molbev/msu057

Röttinger, E., Besnardeau, L., Lepage, T., 2006. Expression pattern of three putative RNA-binding proteins during early development of the sea urchin Paracentrotus lividus. Gene Expr. Patterns 6, 864–872. doi:10.1016/j.modgep.2006.02.006

Rychel, A.L., Smith, S.E., Shimamoto, H.T., Swalla, B.J., 2006. Evolution and development of the chordates: Collagen and pharyngeal cartilage. Mol. Biol. Evol. doi:10.1093/molbev/msj055

Sagnol, S., Marchal, S., Yang, Y., Allemand, F., de Santa Barbara, P., 2016. Epithelial Splicing Regulatory Protein 1 (ESRP1) is a new regulator of stomach smooth muscle development and plasticity. Dev. Biol. doi:10.1016/j.ydbio.2016.04.015

Sansom, R.S., Gabbott, S.E., Purnell, M.A., 2010. Non-random decay of chordate characters causes bias in fossil interpretation. Nature 463, 797–800. doi:10.1038/nature08745

Schmitz, J., Brosius, J., 2011. Exonization of transposed elements: A challenge and opportunity for evolution. Biochimie. doi:10.1016/j.biochi.2011.07.014

Seb??-Pedr??s, A., Irimia, M., del Campo, J., Parra-Acero, H., Russ, C., Nusbaum, C., Blencowe, B.J., Ruiz-Trillo, I., 2013. Regulated aggregative multicellularity in a close unicellular relative of metazoa. Elife 2013. doi:10.7554/eLife.01287

Seshaiah, P., Miller, B., Myat, M.M., Andrew, D.J., 2001. pasilla, the Drosophila Homologue of the Human Nova-1 and Nova-2 Proteins, Is Required for Normal Secretion in the Salivary Gland. Dev. Biol. 239, 309–322. doi:10.1006/dbio.2001.0429

Shapiro, I.M., Cheng, A.W., Flytzanis, N.C., Balsamo, M., Condeelis, J.S., Oktay, M.H., Burge, C.B., Gertler, F.B., 2011. An emt-driven alternative splicing program occurs in human breast cancer and modulates cellular phenotype. PLoS Genet. 7. doi:10.1371/journal.pgen.1002218

Sharma, R., Beer, K., Iwanov, K., Schmöhl, F., Beckmann, P.I., Schröder, R., 2015. The single fgf receptor gene in the beetle Tribolium castaneum codes for two isoforms that integrate FGF8-and Branchless-dependent signals. Dev. Biol. 402, 264–275. doi:10.1016/j.ydbio.2015.04.001

Shukla, J.N., Nagaraju, J., 2010. Doublesex: A conserved downstream gene controlled by

diverse upstream regulators. J. Genet. doi:10.1007/s12041-010-0046-6

Simakov, O., Kawashima, T., Marlétaz, F., Jenkins, J., Koyanagi, R., Mitros, T., Hisata, K., Bredeson, J., Shoguchi, E., Gyoja, F., Yue, J.-X., Chen, Y.-C., Freeman, R.M., Sasaki, A., Hikosaka-Katayama, T., Sato, A., Fujie, M., Baughman, K.W., Levine, J., Gonzalez, P., Cameron, C., Fritzenwanker, J.H., Pani, A.M., Goto, H., Kanda, M., Arakaki, N., Yamasaki, S., Qu, J., Cree, A., Ding, Y., Dinh, H.H., Dugan, S., Holder, M., Jhangiani, S.N., Kovar, C.L., Lee, S.L., Lewis, L.R., Morton, D., Nazareth, L. V., Okwuonu, G., Santibanez, J., Chen, R., Richards, S., Muzny, D.M., Gillis, A., Peshkin, L., Wu, M., Humphreys, T., Su, Y.-H., Putnam, N.H., Schmutz, J., Fujiyama, A., Yu, J.-K., Tagawa, K., Worley, K.C., Gibbs, R.A., Kirschner, M.W., Lowe, C.J., Satoh, N., Rokhsar, D.S., Gerhart, J., 2015. Hemichordate genomes and deuterostome origins. Nature 527, 459–465. doi:10.1038/nature16150

Singh, R.K., Xia, Z., Bland, C.S., Kalsotra, A., Scavuzzo, M.A., Curk, T., Ule, J., Li, W., Cooper, T.A., 2014. Rbfox2-coordinated alternative splicing of Mef2d and Rock2 controls myoblast fusion during myogenesis. Mol. Cell 55, 592–603. doi:10.1016/j.molcel.2014.06.035

Solana, J., Irimia, M., Ayoub, S., Orejuela, M.R., Zywitza, V., Jens, M., Tapial, J., Ray, D., Morris, Q., Hughes, T.R., Blencowe, B.J., Rajewsky, N., 2016. Conserved functional antagonism of CELF and MBNL proteins controls stem cell-specific alternative splicing in planarians. Elife 5. doi:10.7554/eLife.16797.001

Solek, C.M., Oliveri, P., Loza-Coll, M., Schrankel, C.S., Ho, E.C.H., Wang, G., Rast, J.P., 2013. An ancient role for Gata-1/2/3 and Scl transcription factor homologs in the development of immunocytes. Dev. Biol. 382, 280–292. doi:10.1016/j.ydbio.2013.06.019

Stolfi, A., Ryan, K., Meinertzhagen, I.A., Christiaen, L., 2015. Migratory neuronal progenitors arise from the neural plate borders in tunicates. Nature 527, 371–374. doi:10.1038/nature15758

Swartz, M.E., Sheehan-Rooney, K., Dixon, M.J., Eberhart, J.K., 2011. Examination of a palatogenic gene program in zebrafish. Dev. Dyn. 240, 2204–2220. doi:10.1002/dvdy.22713

Terazawa, K., Satoh, N., 1997. Formation of the chordamesoderm in the amphioxus embryo: Analysis with Brachyury and fork head/HNF-3 genes. Dev. Genes Evol. 207, 1–11. doi:10.1007/s004270050086

Thesleff, I., Vaahtokari, A., Partanen, A.M., 1995. Regulation of organogenesis. Common molecular mechanisms regulating the development of teeth and other organs. Int. J. Dev. Biol.

Thisse, C., Thisse, B., 2008. High-resolution in situ hybridization to whole-mount zebrafish embryos. Nat. Protoc. 3, 59–69. doi:10.1038/nprot.2007.514

Tokuoka, M., Imai, K.S., Satou, Y., Satoh, N., 2004. Three distinct lineages of mesenchymal cells in Ciona intestinalis embryos demonstrated by specific gene expression. Dev. Biol. 274, 211–224. doi:10.1016/j.ydbio.2004.07.007

Tokuoka, M., Satoh, N., Satou, Y., 2005. A bHLH transcription factor gene, Twist-like1, is essential for the formation of mesodermal tissues of Ciona juveniles. Dev. Biol. 288, 387–396. doi:10.1016/j.ydbio.2005.09.018

Tolkin, T., Christiaen, L., 2016. Rewiring of an ancestral Tbx1/10-Ebf-Mrf network for pharyngeal muscle specification in distinct embryonic lineages, bioRxiv. doi:10.1101/039289

Traunmuller, L., Gomez, A.M., Nguyen, T.-M., Scheiffele, P., 2016. Control of neuronal synapse specification by a highly dedicated alternative splicing program. Science (80-.). 352, 982–986. doi:10.1126/science.aaf2397

Tu, Q., Cameron, R.A., Worley, K.C., Gibbs, R.A., Davidson, E.H., 2012. Gene structure in the sea urchin Strongylocentrotus purpuratus based on transcriptome analysis. Genome Res. 22, 2079–2087. doi:10.1101/gr.139170.112

Turner, N., Grose, R., 2010. Fibroblast growth factor signalling: from development to cancer. Nat. Rev. Cancer 10, 116–129. doi:10.1038/nrc2780

Underwood, J.G., Boutz, P.L., Dougherty, J.D., Stoilov, P., Black, D.L., 2005. Homologues of the Caenorhabditis elegans Fox-1 Protein Are Neuronal Splicing Regulators in Mammals. Mol. Cell. Biol. 25, 10005–10016. doi:10.1128/MCB.25.22.10005-10016.2005

Vainikka, S., Partanen, J., Bellosta, P., Coulier, F., Birnbaum, D., Basilico, C., Jaye, M., Alitalo, K., 1992. Fibroblast growth factor receptor-4 shows novel features in genomic structure, ligand binding and signal transduction. EMBO J. 11, 4273–80.

Vernia, S., Edwards, Y.J.K., Han, M.S., Cavanagh-Kyros, J., Barrett, T., Kim, J.K., Davis, R.J., 2016. An alternative splicing program promotes adipose tissue thermogenesis. Elife 5. doi:10.7554/eLife.17672

Vuong, C.K., Black, D.L., Zheng, S., 2016. The neurogenetics of alternative splicing. Nat. Rev. Neurosci. 17, 265–281. doi:10.1038/nrn.2016.27

Wagner, G., 2014. Homology, Genes, and Evolutionary Innovation, Uma {é}tica para quantos? doi:10.1017/CBO9781107415324.004

Wahl, M.C., Will, C.L., Lührmann, R., 2009. The Spliceosome: Design Principles of a Dynamic RNP Machine. Cell. doi:10.1016/j.cell.2009.02.009

Wang, E.T., Sandberg, R., Luo, S., Khrebtukova, I., Zhang, L., Mayr, C., Kingsmore, S.F.,

Schroth, G.P., Burge, C.B., 2008. Alternative isoform regulation in human tissue transcriptomes. Nature 456, 470–476. doi:10.1038/nature07509

Wang, Y., Liu, J., Huang, B.O., Xu, Y.-M., Li, J., Huang, L.-F., Lin, J., Zhang, J., Min, Q.-H., Yang, W.-M., Wang, X.-Z., 2015. Mechanism of alternative splicing and its regulation. Biomed. reports 3, 152–158. doi:10.3892/br.2014.407

Warzecha, C.C., Carstens, R.P., 2012. Complex changes in alternative pre-mRNA splicing play a central role in the epithelial-to-mesenchymal transition (EMT). Semin. Cancer Biol. doi:10.1016/j.semcancer.2012.04.003

Warzecha, C.C., Jiang, P., Amirikian, K., Dittmar, K. a, Lu, H., Shen, S., Guo, W., Xing, Y., Carstens, R.P., 2010. An ESRP-regulated splicing programme is abrogated during the epithelial-mesenchymal transition. EMBO J. 29, 3286–3300. doi:10.1038/emboj.2010.195

Warzecha, C.C., Sato, T.K., Nabet, B., Hogenesch, J.B., Carstens, R.P., 2009. ESRP1 and ESRP2 Are Epithelial Cell-Type-Specific Regulators of FGFR2 Splicing. Mol. Cell 33, 591–601. doi:10.1016/j.molcel.2009.01.025

Warzecha, C.C., Shen, S., Xing, Y., Carstens, R.P., 2009. The epithelial splicing factors ESRP1 and ESRP2 positively and negatively regulate diverse types of alternative splicing events. RNA Biol. 6, 546–562. doi:10.4161/rna.6.5.9606

Westerfield, M., 2007. The Zebrafish Book. A Guide for the Laboratory Use of Zebrafish (Danio rerio), 5th Edition. Univ. Oregon Press. Eugene.

Yang, Y., Park, J.W., Bebee, T.W., Warzecha, C.C., Guo, Y., Shang, X., Xing, Y., Carstens, R.P., 2016. Determination of a Comprehensive Alternative Splicing Regulatory Network and Combinatorial Regulation by Key Factors during the Epithelial-to-Mesenchymal Transition. Mol Cell Biol 36, 1704–1719. doi:10.1128/MCB.00019-16

Yao, Y., Minor, P.J., Zhao, Y.-T., Jeong, Y., Pani, A.M., King, A.N., Symmons, O., Gan, L., Cardoso, W. V, Spitz, F., Lowe, C.J., Epstein, D.J., 2016. Cis-regulatory architecture of a brain signaling center predates the origin of chordates. Nat. Genet. 48. doi:10.1038/ng.3542

Zeller, R., López-Ríos, J., Zuniga, A., 2009. Vertebrate limb bud development: moving towards integrative analysis of organogenesis. Nat. Rev. Genet. 10, 845–858. doi:10.1038/nrg2681

Zhang, C., Frias, M.A., Mele, A., Ruggiu, M., Eom, T., Marney, C.B., Wang, H., Licatalosi, D.D., Fak, J.J., Darnell, R.B., 2010. Integrative Modeling Defines the Nova Splicing-Regulatory Network and Its Combinatorial Controls. Science (80-.). 329, 439–443. doi:10.1126/science.1191150

Zhao, Y., Liu, J., Yang, C., Capraro, B., Baumgart, T., Bradley, R., Ramakrishnan, N., Xu, X., Radhakrishnan, R., Svitkina, T., Guo, W., 2013. Exo70 generates membrane curvature for

morphogenesis and cell migration. Dev. Cell 26, 266–278. doi:10.1016/j.devcel.2013.07.007

Zhou, H.L., Luo, G., Wise, J.A., Lou, H., 2014. Regulation of alternative splicing by local histone modifications: Potential roles for RNA-guided mechanisms. Nucleic Acids Res. 42, 701–713. doi:10.1093/nar/gkt875

ANEXO

Artículo anexo 1

Contrasting 5′ and 3′ Evolutionary Histories and Frequent Evolutionary Convergence in *Meis/hth* Gene Structures

Manuel Irimia*,†,§,[1,2], Ignacio Maeso‡,§,[1], Demián Burguera[1],§, Matías Hidalgo-Sánchez[3], Luis Puelles[4], Scott W. Roy[2], Jordi Garcia-Fernàndez[1], and José Luis Ferran[4]

[1]Department of Genetics, School of Biology, University of Barcelona, Barcelona, Spain

[2]Department of Biology, Stanford University, Stanford, California

[3]Department of Cell Biology, School of Science, University of Extremadura, Badajoz, Spain

[4]Department of Human Anatomy and Psychobiology, School of Medicine, University of Murcia, Murcia, Spain

†Present address: Banting and Best Department of Medical Research, Donnelly Centre, University of Toronto, Toronto, Ontario, Canada

‡Present address: Department of Zoology, University of Oxford, South Parks Road, Oxford, OX1 3PS, UK

§These authors contributed equally to this work

*Corresponding author: E-mail: mirimia@gmail.com; scottwroy@gmail.com; jordigarcia@ub.edu; jlferran@um.es.

Accepted: 4 June 2011

Abstract

Organisms show striking differences in genome structure; however, the functional implications and fundamental forces that govern these differences remain obscure. The intron–exon organization of nuclear genes is involved in a particularly large variety of structures and functional roles. We performed a 22-species study of *Meis/hth* genes, intron-rich homeodomain-containing transcription factors involved in a wide range of developmental processes. Our study revealed three surprising results that suggest important and very different functions for *Meis* intron–exon structures. First, we find unexpected conservation across species of intron positions and lengths along most of the *Meis* locus. This contrasts with the high degree of structural divergence found in genome-wide studies and may attest to conserved regulatory elements residing within these conserved introns. Second, we find very different evolutionary histories for the 5′ and 3′ regions of the gene. The 5′-most 10 exons, which encode the highly conserved Meis domain and homeodomain, show striking conservation. By contrast, the 3′ of the gene, which encodes several domains implicated in transcriptional activation and response to cell signaling, shows a remarkably active evolutionary history, with diverse isoforms and frequent creation and loss of new exons and splice sites. This region-specific diversity suggests evolutionary "tinkering," with alternative splicing allowing for more subtle regulation of protein function. Third, we find a large number of cases of convergent evolution in the 3′ region, including 1) parallel losses of ancestral coding sequence, 2) parallel gains of external and internal splice sites, and 3) recurrent truncation of C-terminal coding regions. These results attest to the importance of locus-specific splicing functions in differences in structural evolution across genes, as well as to commonalities of forces shaping the evolution of individual genes along different lineages.

Key words: intron–exon structures, alternative splicing, homeobox transcription factors, convergent evolution.

Introduction

Intron–exon structures are highly variable both between and within species. Within metazoans, some species such as humans have an average of ~9 introns per gene, whereas others, such as flies, have nearly three times less (Roy and Irimia 2009b). A large number of genome-wide interspecies comparisons of intron–exon structures have revealed the history of change and stasis in intron–exon structures underlying these differences. Modern differences largely reflect orders-of-magnitude differences in the rates of intron creation and loss between species (Roy and Penny 2006). At one extreme, orthologous genes from deeply diverged species including vertebrates, the cnidarian *Nematostella*, and the placozoan *Trichoplax* have nearly identical intron–exon structures within conserved coding regions, indicating a striking dearth of intron creation and loss changes across hundreds of millions of years (Roy et al. 2003; Coulombe-Huntington and Majewski 2007a; Putnam et al. 2007; Srivastava et al. 2008). At the other extreme,

intron positions in lineages such as urochordates and *Caenorhabditis* nematodes only rarely correspond to intron positions in other lineages, indicating wholesale intron loss and gain (Seo et al. 2001; Rogozin et al. 2003; Edvardsen et al. 2004; Coulombe-Huntington and Majewski 2007b; Putnam et al. 2008).

While powerful for understanding general evolutionary trends, such studies may overlook differences in evolutionary mode between different genes or different introns within the same species. Intron–exon structures vary dramatically across genes: within humans, intron numbers range from hundreds of intronless genes to the 363-exon *TITIN* gene (Bang et al. 2001), and intron lengths span four orders-of-magnitude (from ~100 bp to ~1 Mbp). It is known that splicing encodes a large number of locus-specific functions (production of specific alternative transcripts, regulation of specific genes by production of sterile transcripts by splicing, etc. [e.g., Schmucker et al. 2000; Irimia et al. 2010]); as such, intron function and level of dispensability is likely to vary considerably across genes and introns within the same species. Systematic evolutionary differences have also been observed, often related to transcript position. For instance, in some species, the first (5′-most) intron within a coding sequence tends to be longer, and to exhibit more interspecific sequence conservation, consistent with greater frequencies of functional elements (Bergman and Kreitman 2001; Marais et al. 2005; Hughes et al. 2008). Striking differences in the incidence and lengths of introns are also observed between translated and untranslated regions of genes (Hong et al. 2006; Scofield et al. 2007; Hughes et al. 2008), also suggesting different evolutionary dynamics in different classes of introns. However, genome-wide studies tend to average across introns of different modes and levels of functionality, perhaps inaccurately sketching a portrait of intron evolution as a largely stochastic and random process.

Here, we employ an alternative approach, using many-species studies of an individual gene family to try to discern commonalities of evolution across species and differences between introns within the same genome. We studied myeloid ecotropic viral integration site homologue (*Meis*) genes (Moskow et al. 1995, called *homothorax* [*hth*] in *Drosophila* [Rieckhof et al. 1997]). In contrast to most homeobox genes, which contain one or no introns, *Meis* genes contain 10 or 11 introns in most metazoans. *Meis* are deeply conserved homeodomain-containing transcription factors of the TALE (three-amino acid loop extension) superclass, involved in a wide variety biological processes, ranging from hematopoiesis (Hisa et al. 2004; Azcoitia et al. 2005) to limb development and regeneration (Mercader et al. 1999; Mercader et al. 2005). *Meis1* and *Meis2* have overlapping but distinct dynamic expression domains in the developing central nervous system, related to patterning of the developing telencephalon (Toresson et al. 2000), pretectum (Ferran et al. 2007), and hindbrain (Dibner et al. 2001; Choe et al. 2002; Wassef et al. 2008). In *Drosophila*, *hth* has also been implicated in several biological processes, some of them in common with vertebrates (Pai et al. 1998; Mercader et al. 1999).

Most vertebrates contain three paralogs of *Meis* (Nakamura et al. 1996; Sánchez-Guardado et al. 2011), dating to the two rounds of whole-genome duplication (WGD) at the base of vertebrates (Dehal and Boore 2005; Putnam et al. 2008). Adding to MEIS protein diversity, *Meis* genes have been shown to be alternatively spliced. For instance, exon "12a" of the vertebrate *Meis1* gene is alternatively spliced: the *Meis1A* isoform contains exon 12a (fig. 1*A*), but the *Meis1B* isoform does not, leading to an alternative C-terminus, encoded by the downstream exon 12b, and to higher transcriptional activator capacities than both *Meis1A*- and the *Meis*-related *pknox1* gene, especially in response to protein kinase A (PKA) and TrichostatinA (TSA) (Maeda et al. 2001; Huang et al. 2005). Alternative splicing (AS) of exons homologous to 12a, as well as other AS events, have been reported for the *Meis2* and *Meis3* genes in vertebrates (Oulad-Abdelghani et al. 1997; Yang et al. 2000; Williams et al. 2005; Shim et al. 2007; Hyman-Walsh et al. 2010; Sánchez-Guardado et al. 2011).

Here we investigate the evolution of intron–exon structures and AS of *Meis* genes across metazoans. We find very different evolutionary histories for the 5′ and 3′ regions of the gene. Intron–exon structures of the 5′-most region, corresponding to the first ~1,000 nt of the coding sequence, are highly similar across species, with the positions and relative sizes of the first 9 intron positions being highly conserved across studied species. Unexpectedly, this conservation extends to metazoan groups with intron–exon structures that are generally very divergent, such as flies, nematodes and tunicates, suggesting functional constraints opposing intron loss. On the other hand, the C-terminal coding regions exhibit a complex and surprising history marked by creation and loss of introns and exons, gain and loss of AS of various gene regions, and a remarkable variety of cases of parallel evolution at the levels of genome, gene transcripts, and gene function. These differences in the evolution of intron–exon structures and splicing across *Meis* genes are likely to reflect, at least in part, qualitatively different protein and regulatory functions encoded by different genic regions. These results underscore the utility of many-species studies for understanding the functional genomics of introns and splicing.

Materials and Methods

Genome Sources and Gene Annotation

We used the following genome sequence assemblies and expression data (expressed sequence tags [ESTs]) from the following sources: *Trichoplax adhaerens* Grell-BS-1999

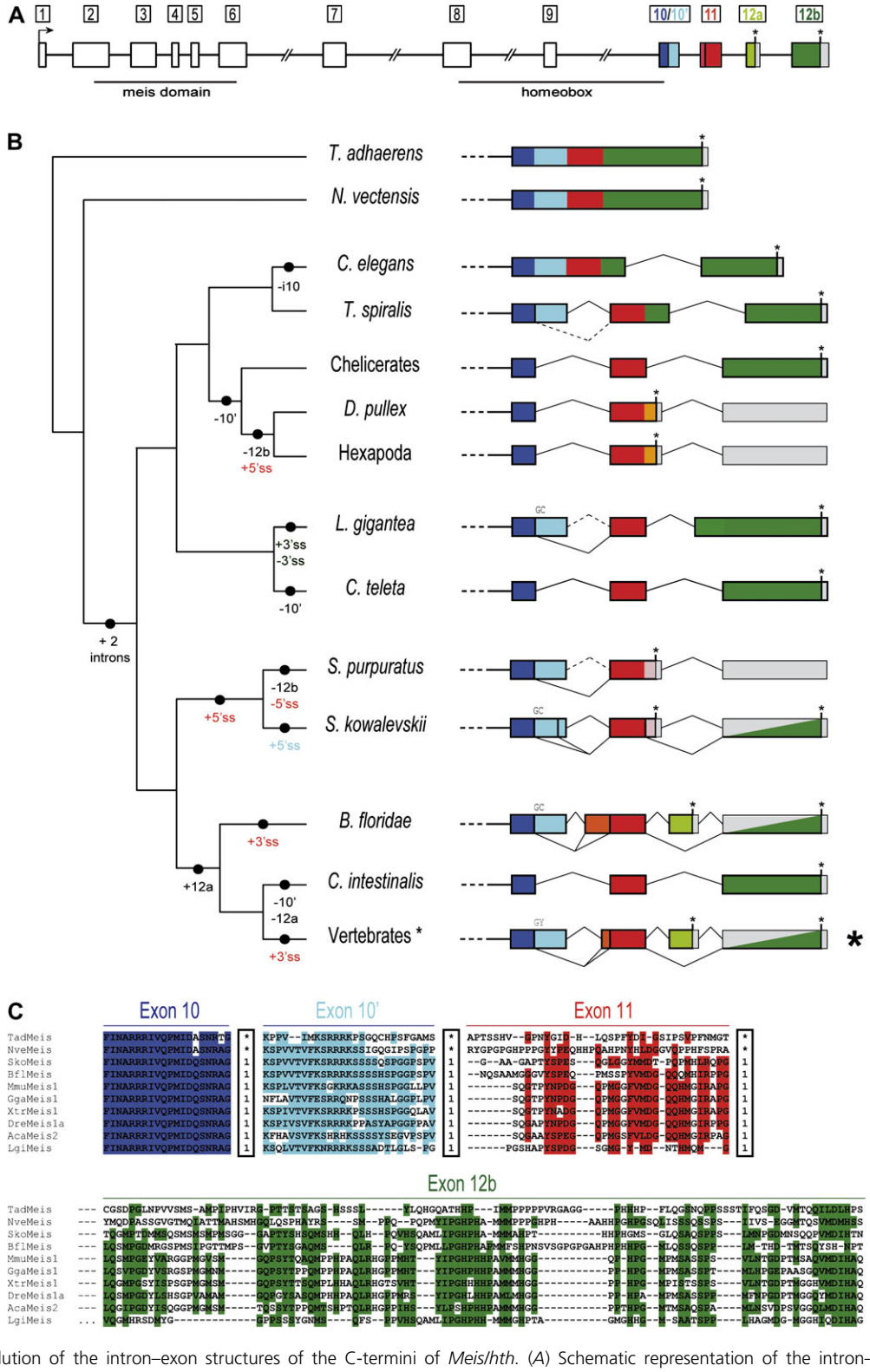

Fig. 1.—Evolution of the intron–exon structures of the C-termini of *Meis/hth*. (*A*) Schematic representation of the intron–exon structure of a prototypical vertebrate *Meis* gene. The conserved long size of introns 6–9 are indicated by a double slash. Homologous coding regions (exons) in the 3′ are indicated by colors: 10 (dark blue), 10′ (light blue), 11 (red), 12a (light green), and 12b (dark green). (*B*) Diversity of intron–exon structures of exons 10–12b in metazoans. The different genomic gains (+) and losses (−) of regions or splice sites (5′ splice site (SS) or 3′ ss, colored according to the exon), assuming parsimony, are indicated in the branches of the schematic tree on the left-hand side. Solid vertical bars between colors represent a conserved 5′ ss, and GC 5′ ss are indicated above each line. Asterisks represent termination codons and gray blocks indicate UTR exons. Split gray/colored boxes

v1.0 (Srivastava et al. 2008), *N. vectensis* v1.0 (Putnam et al. 2007), *Branchiostoma floridae* v1.0 (Putnam et al. 2008), *Ciona intestinalis* v2.0 and v1.0 (Dehal et al. 2002), *Takifugu rubripes* v4.0, *Xenopus tropicalis* v4.1 (Hellsten et al. 2010), *Daphnia pulex* v1.0, *Helobdella robusta* v1.0, *Lottia gigantea* v1.0 and *Capitella teleta* v1.0, at DOE Joint Genome Institute (JGI) Web page (http://genome.jgi-psf.org/euk_home.html), and of *Strongylocentrotus purpuratus* Build 2.1 (Sea Urchin Genome Sequencing Consortium et al. 2006), *Apis mellifera* Amel_4.0, *Tribolium castaneum* Build 2.1 (Tribolium Genome Sequencing Consortium et al. 2008), *Drosophila melanogaster* Build Fb5.3 (Adams et al. 2000), *Danio rerio* Zv8, *Gallus gallus* v2.1 (Chicken Genome Sequencing Consortium 2004), *Anolis carolinensis* AnoCar1.0, *Homo sapiens* Build GRCh37 (Lander et al. 2001; Venter et al. 2001), *Mus musculus* Build 37.1 (Waterston et al. 2002), and *Acyrtosiphon pisum* Build 1.1, at the NCBI Web page (http://www.ncbi.nlm.nih.gov/blast/Blast.cgi) and/or Ensembl Web page (http://www.ensembl.org), *Trichinella spiralis* at the NCBI Web page for unfinished eukaryotic genomes (http://www.ncbi.nlm.nih.gov/sutils/genom_table.cgi?organism=eukaryotes), *Brugia malayi BMA1* (*Ghedin et al. 2007*) at *TIGR Web page* (http://blast.jcvi.org/er-blast/index.cgi?project=bma1*), Caenorhabditis elegans WS213* (*Caenorhabditis elegans Sequencing Consortium 1998*) *at WormBase* (http://www.wormbase.org), and *Saccoglossus kowalevskii* 09 December 2008 scaffolds at HGSC Baylor College of Medicine Web page (http://blast.hgsc.bcm.tmc.edu/blast.hgsc?organism=20).

Additional sequences from arthropods without available genome resources (those included in supplementary fig. S1) were retrieved through TBlastN searches against the nucleotide collection database at the NCBI Web page. In more poorly annotated genomes, *Meis* candidates were searched by TBlastN and gene annotation was then performed by downloading the whole associated genomic region and identifying each exon by mapping available expression data and/or by similarity of sequence using ClustalW and Blast2seq. Available automatic gene predictions were also used. Combining the different sources of data, most exon boundaries could be determined unambiguously (supplementary table S1). Introns and exons were named following the vertebrate nomenclature (exons 12 and 13 were named 12a and 12b [Sánchez-Guardado et al. 2011] and insect-specific exons between ancestral exons 7 and 8 were not counted [supplementary fig. S1]). Intron–exon structures of the 5′ untranslated regions (UTRs) are not described here due to the lack of expression data for most species and difficulty to assess intron position conservation in noncoding sequences over long phylogenetic ranges.

Median, average and average excluding the top 5% intron lengths and intergenic distances (supplementary table S2) were calculated for each genome using custom Perl scripts on GTF (Ensemble), GFF (JGI), or GBK (NCBI) files or obtained from Irimia, Maeso, and Garcia-Fernandez (2008).

Phylogenetic Analyses

Meis/hth protein sequences from multiple species were aligned using MAFFT (Katoh et al. 2002, 2005) as implemented in Jalview 2.4 (Waterhouse et al. 2009), and the alignments were manually curated by using information on intron positions (Irimia and Roy 2008). Two different phylogenetic analyses were performed. First, to establish orthology of all studied *Meis/hth* genes, we used an alignment containing only the highly conserved Meis and Homeobox domains and including several *Meis*-related *pknox* proteins as outgroups (supplementary fig. S2A). Second, to allow confident assignment of paralogy relationships within vertebrates, the number of positions included in the alignment was increased using the whole protein sequence (except exon 1 and the alternatively spliced 3′ regions [exons 10′ to 12b]), and fast-evolving species were excluded (supplementary fig. S2B). Phylogenetic trees were generated by the Bayesian method with MrBayes 3.1.2 (Huelsenbeck and Ronquist 2001; Ronquist and Huelsenbeck 2003) using two independent runs (each with four chains). Model selection using ProtTest (Drummond and Strimmer 2001; Guindon and Gascuel 2003; Abascal et al. 2005), convergence determination, burn-in, and consensus tree calculations were done as previously described (D'Aniello et al. 2008).

cDNA Samples and Reverse Transcription–Polymerase Chain Reaction of Alternative Splicing Events

RNA from adult and/or embryonic vertebrate (*D. rerio*, *X. tropicalis*, *A. carolinensis*, *G. gallus*, and *M. musculus*) tissues and different amphioxus (*B. lanceolatum*) developmental stages was extracted using RNeasy Mini Kit (Qiagen), and retrotranscriptions were done using SuperScript III Reverse Transcriptase (Invitrogen), according to manufacturer. One *A. carolinensis* adult animal was bought in a local pet shop. All animals were sacrificed following standard and ethically approved procedures by the European Union and the Spanish government for laboratory animals.

←
indicate regions that are either translated or 3′ UTR depending on splice form. (*C*) Sequence alignment for some representative bilaterians and the two nonbilaterians showing sequence conservation at each exon. Within the boxes, "1" indicates a phase 1 intron, and an asterisk represents absence of an intron at that position. Highlighted positions correspond to 60% of similar amino acid types across studied genes, as generated by BioEdit.

For reverse transcription–polymerase chain reaction (RT-PCR) analyses, we designed two sets of primers for each gene in each studied species (*S. purpuratus*, *B. lanceolatum*, *D. rerio*, *X. tropicalis*, *A. carolinensis*, *G. gallus*, and *M. musculus*). The first set spans exons 10, 10′, and 11 and the second one exons 11, 12a (when present), and12b, to yield all isoforms of the 3′ region present in the studied set of tissues. All primer sequences are provided in supplementary table S3. RT-PCR were done trying to minimize the number of cycles and at least 3′ of elongation to diminish the PCR bias for short isoforms (Rukov et al. 2007), except for those probing exon 10′ inclusion (supplementary fig. S3), for which we used 36 cycles in each of two rounds of amplification.

Results

Meis Gene Complements in Metazoans

We studied 7 vertebrate and 15 invertebrate genomes, spanning all major metazoan clades (deuterostomes, protostomes, lophotrochozoans, and non-bilaterians). In most studied invertebrates, we found only 1 *Meis/hth* ortholog, including the basal branching non-bilaterians *T. adhaerens* and *N. vectensis*. However, we found four *Meis* genes in the lophotrochozoan *H. robusta*; in addition, two paralogs have been described in two distantly related spiders (Prpic et al. 2003; Pechmann and Prpic 2009), *Cupiennius salei* and *Acanthoscurria geniculata*, for which full genome sequences are not yet available. Among vertebrates, *Meis*

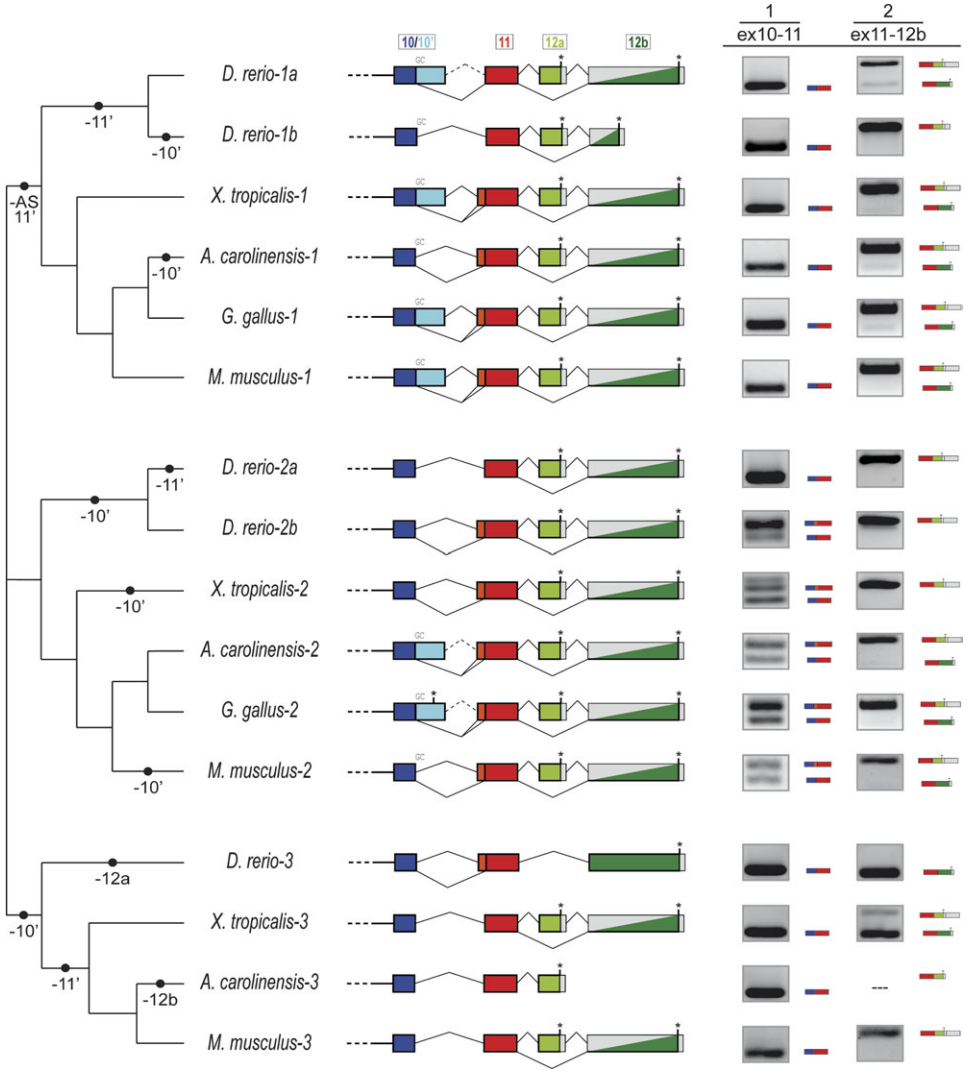

Fig. 2.—Evolution of intron–exon structures and alternative splicing of the 3′ end of vertebrate Meis genes. Diversity of intron–exon structures of exons 10–12b in vertebrates. The different genomic gains (+) and losses (–) of regions, assuming parsimony, are indicated in the branches of the schematic tree on the left-hand side. Solid vertical bars between colors represent a conserved 5′ splice site (SS), and GC 5′ ss are indicated above each line. Asterisks represent termination codons and gray blocks indicate UTR exons. Split gray/colored boxes indicate regions that are either translated or 3′ UTR depending on splice form. RT-PCR results for each event are shown on the right-hand side.

Table 1

Length of Each Intron and Species Median, Average, and Average Excluding the Longest 5% Introns

	Median	Average	Average − 5%	Intron 1	Intron 2	Intron 3	Intron 4	Intron 5	Intron 6	Intron 7	Intron 8	Intron 9	Intron 10	Intron 11	Intron 12	Mean
H. sapiens Meis1	1,419	5,787	2,792	1,868	1,879	577	801	1,437	*21,060*	*47,928*	*35,648*	*19,433*	1,155	293	2,100	11,182
H. sapiens Meis2				1,255	1,536	674	986	796	*9,695*	*46,811*	*86,413*	*53,637*	1,366	338	2,257	17,147
H. sapiens Meis3				1,719	214	101	1,550	109	5,169	188	1,961	107	361	—	2,906	13,08
M. musculus Meis1	1,290	4738	2,260	1,861	1,741	567	771	1,394	*22,862*	*46,463*	*35,893*	*20,037*	1,116	304	2,065	11,256
M. musculus Meis2				671	1,595	719	1,116	733	*9,432*	*48,807*	*78,382*	*52,868*	1,411	364	2,292	16,533
M. musculus Meis3				1,824	135	92	733	155	*2,940*	*167*	*1,322*	*170*	538	729	539	779
G. gallus Meis1	806	2,616	1,332	?	?	?	?	>849	*>6,084*	*25,232*	*25,453*	*16,211*	1,271	188	1,919	11,712
G. gallus Meis2				?	>967	222	1,734	791	*10,760*	*34,904*	*59,559*	*54,586*	1,439	422	3,103	16,752
T. rubripes Meis1.1	147	568	315	1,491	999	219	425	1,010	*7,736*	*15,920*	*13,058*	*10,547*	1,832	677	—	4,901
T. rubripes Meis1.2				1,061	388	243	78	70	*114*	*1,051*	*1,388*	*1,016*	373	145	—	539
T. rubripes Meis2				225	1,604	233	326	371	*7,877*	*18,177*	*18,491*	*14,252*	912	368	3,260	5,508
T. rubripes Meis3				2,027	301	93	87	84	*79*	*138*	*371*	*817*	87	—	90	379
C. intestinalis	333	545	365	2,488	4,548	1,349	1,357	363	*4,275*	*4,147*	*2,197*	*6,648*	101	—	242	2,520
B. floridae	730	1,460	973	177	412	633	701	1,231	*3,513*	*9,733*	*9,140*	*9,863*	2,580	503	2,552	3,420
S. kowalevskii	n.d.	n.d.	n.d.	274	453	697	1,289	1,943	*5,390*	*9,712*	*6,089*	*11,058*	1,815	—	—	3,872
S. purpuratus	748	1,624	1,015	297	850	1,965	901	10,371	*36,100*	*29,274*	*3,725*	*11,805*	6,788	—	—	10,208
D. melanogaster	74	1,123	394	7,616	2,154	9,190	2,091	5,480	*23,710*	*40,688*	*6,727*	*2,450*	221	—	—	10,033
A. mellifera	120	1,177	334	14,086	8,857	8,878	20,587	9,010	*69,950*	*13,9655*	*63,262*	*73,730*	21,383	—	—	42,940
T. castaneum	54	1,312	553	4,989	9,963	14,951	1,722	3,163	*5,821*	*28,551*	*3,236*	*6,276*	629	—	—	7,930
D. pulex	294	491	333	2,689	1845	4,383	1394	1,334	*10,586*	*26,222*	*1,323*	*14,569*	618	—	—	64,96
I. scapularis	n.d.	n.d.	n.d.	?	18,062	8,679	2356	17,775	*63,774*	*10,0420*	*31,473*	*46,591*	3,458	—	2,754	29,534
C. elegans	65	302	204	1,411	318	47	—	558	*1,122*	*1,128*	*312*	*3,973*	—	643	100	961
T. spiralis	n.d.	n.d.	n.d.	922	522	57	134	683	*669*	*1,037*	*1,436*	*5,423*	193	—	60	1,012
L. gigantea	552	965	662	129	536	1,608	931	804	*17,612*	*17,709*	*10,687*	*18,634*	1,330	–	182	6,378
C. teleta	299	553	386	1,502	169	505	533	2,883	*5,995*	*13,235*	*2,197*	*5,760*	124	–	3,361	3,297
N. vectensis	591	961	723	?	304	183	249	381	*1,062*	*3,494*	*2,409*	*4,920*	—	—	—	16,25
T. adhaerens	278	419	320	?	?	?	2,306	7,825	*3,181*	?	*267*	*904*	—	—	—	2,897
Average bilaterians	495	1,662	851	2,373	2,651	2,520	1,944	2,742	*14,340*	*26,633*	*16,421*	*16,843*	2,208	434	1,695	8,620

Note.—"?" indicates that the size could not be determined, ">"minimum size, and "—" intron absence. For genome-wide data, "n.d." indicates that statistics could not be determined due to lack of genome-wide annotation. Introns 6–9 are shown in italics to highlight their consistently longer lengths across bilaterians.

complement ranged from two paralogs in birds (Sánchez-Guardado et al. 2011) to five in zebrafish (dating to the extra round of WGD that occurred at the base of teleosts), with three genes in most tetrapods. Phylogenetic analysis using Bayesian inference strongly supports the orthology of all identified genes (supplementary fig. S2).

High Level of Conservation of 5′ Intron–Exon Structures of Meis across Metazoans

To compare intron-exon structures of *Meis* across animal lineages, we mapped intron positions onto alignments of translated coding sequences. We found very different general patterns for the 5′ and 3′ portions of the gene (fig. 1*A*). The first 9 intron positions and phases were conserved in all studied metazoans, with the two exceptions of the loss of intron 4 in *C. elegans* and of intron 3 in a divergent paralog in the leech *H. robusta* and intron gain events splitting exon 6 independently in *B. malayi* and another paralog of *H. robusta*. This extreme conservation is in striking contrast to the general patterns found in genome-wide studies, in which intron positions in a variety of lineages, notably arthropods, nematodes, and tunicates, show very little correspondence, attesting to large amounts of intron loss and gain (Logsdon 2004; Rogozin et al. 2003; Edvardsen et al. 2004; Putnam et al. 2008). The finding of widespread intron position correspondence in the 5′ regions of *Meis* genes thus suggests that locus-specific forces opposing loss of ancestral introns and gain of new ones are acting across a wide variety of metazoan lineages.

In addition, we found that the relative sizes of introns are widely conserved across species. In nearly all studied species, introns 6–9 are the longest ($P < 0.0001$ in a Kolmogorov–Smirnov comparison between introns 6 and 9 vs. the rest), with sizes usually 10–30 times larger than the species average intron length, reaching ~100 times as long as the average in some extreme cases (table 1). This pattern is observed both in vertebrates and invertebrates and in large and compact genomes. For instance, out of only ~500 introns longer than 10 Kb in the compact genome of the pufferfish *T. rubripes* (Aparicio et al. 2002), 6 are found in 2 *Meis* paralogs. Long introns are often associated with regulatory signals contained within intronic sequences; a regulatory role for these long introns could explain the lack of intron loss in diverse lineages (see below).

Interestingly, the only cases in which introns 6–9 are not long relative to species average occur in vertebrates. This could possibly reflect relaxed constraint on intronic regulatory functions following gene duplication. Consistent with this notion, vertebrate paralogs with short introns show more restricted developmental expression domains than do other vertebrate *Meis* genes (e.g., *Meis3* [Waskiewicz et al. 2001; Ng et al. 2009]). Perhaps relatedly, these same paralogs show reduced intergenic lengths. Whereas *Meis* genes are often found in large genomic regions with extended intergenic regions across animal phylogeny (supplementary table S2), paralogs with shortened introns also show highly reduced intergenic distances relative to other *Meis* genes. Together these results suggest general loss of regulatory motifs in noncoding regions following gene duplication.

Complex and Convergent Evolution of Meis 3′ Intron-Exon Structures

In contrast to widespread conservation of intron–exon structures in the 5′ region of the gene, the 3′ of metazoan *Meis* genes showed a much more volatile evolutionary history (fig. 1*B*); 3′ intron–exon structures differ between bilaterian and non-bilaterian genes: the entire region is encoded by a single exon in both studied non-bilaterians, *N. vectensis* and *T. adhaerens*, but is divided into multiple exons in all studied bilaterians. The orthologous sequence in most bilaterians is divided into three exons: one exon which we call exon 10 + 10′ (see below), exon 11, and exon 12b (often called 13, fig. 1). The simplest explanation for this difference is two intron gains at the base of bilaterians.

The region also shows remarkable diversity within bilaterians (fig. 1*B*). First, the 10th exon is alternatively spliced in diverse bilaterian lineages, with usage of an alternative splice site within the exon. (We refer to the upstream constitutive region as exon 10 and the downstream alternatively spliced region as 10′.) Interestingly, in many bilaterian lineages, the upstream 5′ splice site is a rare GC (accounting for 46% of splice boundaries at this position in studied genes; indicated in Figures 1 and 2). Whereas exon 10 is present in all transcripts, splicing of 10′ varies widely across groups, with 4 observed patterns: 1) 10′ is included in all available transcripts (nematodes), 2) a significant fraction of the transcripts show 10′ inclusion (amphioxus and hemichordates, based on RT-PCR and/or EST count), 3) despite clear conservation of exon sequence and coding meaning in the genome, inclusion of 10′ occurs at very low levels (some vertebrate genes) or could not be observed at all in either ESTs or RT-PCR experiments (sea urchin, supplementary fig. S3), and 4) the sequence encoding 10′ have been lost from the genome (some vertebrates, *C. teleta*, *C. intestinalis*, and arthropods). (Specifically, sequence clearly homologous to exon 10 is found, but the downstream sequence shows no similarity to the 10′ region, indicating loss of coding potential.) Strikingly, the loss of 10′ at the genomic level (case 4, above) has independently occurred at least nine times in the evolution of the studied genes (figs. 1 and 2).

Second, different *Meis* genes have undergone recurrent truncation at the transcript and genomic level. In each case, truncation has occurred by the introduction of a STOP codon within a novel exonic region upstream of the exon containing the putative ancestral protein terminus (exon 12b; novel

and ancestral STOPs are indicated by asterisks in figs. 1 and 2). 1) In some groups, the inferred ancestral situation has been maintained, with the terminal exon constitutively encoding the STOP codon (*C. intestinalis*, lophotrochozoans, some vertebrates, some ecdysozoans). 2) In chordates, a new alternative STOP-containing exon has arisen by an unknown mechanism (exon 12a, light green in figs. 1 and 2). The new exon is alternatively spliced; its inclusion leads to premature termination, leaving the ancestral exon 12b as 3′ untranslated region (3′ UTR, depicted as half grey). 3) In Ambulacraria (sea urchin and hemichordates), a new downstream splice site has evolved for exon 11, which is alternatively spliced. Use of the new 5′ splice site introduces "extra" downstream sequence (pink), which includes a new STOP codon; as in the case of exon 12a the resulting MEIS protein has a novel C-terminus, and all of exon 12b lies downstream of the STOP codon as 3′ UTR. Interestingly, in sea urchin, the ancestral exon 11 splice site has been lost, implying constitutive use of the new STOP codon and protein truncation. RT-PCR analyses throughout the early development of sea urchin confirmed that only the new terminal isoform is expressed (supplementary fig. S3). 4) Finally, in Pancrustacea (insects and crustaceans [*D. pulex*]), we found a situation similar to sea urchin: the termination codon is located in a downstream extension of exon 11, and no 12b coding meaning is recognized in the untranslated downstream exon. Importantly, in the last three cases (2–4), the protein sequence, structure, and function of C-terminus of *Meis*, which harbors the capacities for transcriptional activation and *Hox* interaction (Yang et al. 2000; Huang et al. 2005; Williams et al. 2005; Hyman-Walsh et al. 2010), are likely to be highly modified relative to the ancestral protein.

Other specific molecular elaborations have also evolved in several lineages (fig. 1*B*). For instance, the hemichordate *S. kowalevskii* shows an additional alternative 5′ splice site within the exon 10′ region (i.e., three alternative splice sites for the same exon 10 + 10′), producing an exon with an intermediate length (42 nucleotides less than the entire 10 + 10′ exon). On the other hand, exon 11 in chordates has evolved a 5′ extension of different lengths across species by emergence of an alternative upstream 3′ splice site, resulting in an extended alternative coding sequence (previously described for mammalian *Meis2* (Oulad-Abdelghani et al. 1997)). Similarly, in the lophotrochozoan *L. gigantea*, exon 12b has a constitutive (i.e., not alternative) 5′ extension of ~35 codons, consistent with loss of the ancestral 3′ splice site and use of a novel upstream site. Finally, nematodes exhibit loss and gain of introns, with loss of the ancestral phase 1 intron between exons 11 and 12b, and gain of a new phase 2 intron at a nearby site in a common ancestor of *Trichinella*, *Brugia*, and *Caenorhabditis*, and subsequent loss of the intron between exons 10′ and 11 in *Caenorhabditis* (fig. 1*B*). In stark contrast to this 3′ diversity, only little transcriptional variation was found in the 5′ of the gene. AS in insects and vertebrates produce homeodomain-less proteins (which are, indeed, C-terminal truncations) with distinct functions (Yang et al. 2000; Noro et al. 2006); similarly, alternative acceptor site choice within exon 6 in the vertebrate-derived paralog *Meis3* results in a protein without a meis domain (Hyman-Walsh et al. 2010). In addition, the annelid *C. teleta* has a mutually exclusive tandem exon duplication of exon 9 which results in two proteins that differ by only 5 aa substitutions (supplementary table S1), and insects and arthropods harbor 1–3 lineage-specific exons between the ancestral exons 7 and 8 (supplementary fig. S1).

Evolution of Alternative Splicing in Chordate *Meis* Genes

We next focused on chordates, studying the different AS events of the 3′ regions of *Meis* genes within 17 genes in 6 chordate species, both in silico and by RT-PCR (fig. 2) and supplementary figs. S4–6. We designed two sets of primers, one spanning exons 10, 10′, and 11 and the other spanning exons 11, (12a), and 12b (see Materials and Methods), and performed RT-PCRs for all *Meis* genes from six species (amphioxus, zebrafish, *X. tropicalis*, the anole lizard *A. carolinensis*, chicken, and mouse), a total of 34 AS events.

For exon 10 + 10′, we found that exon 10′ is included at very low levels in *Meis* of different vertebrates, only detectable using 10′-specific primers and a high number of PCR cycles for most species and tissues (supplementary fig. S4, see Materials and Methods). This is consistent with observations in human patients (Xiong et al. 2009) and in available ESTs (27/27 and 6/6 ESTs in humans and mouse shown exclusion of exon 10′). Perhaps relatedly, exon 10′ coding meaning has been lost at the genomic level at least 6 times in vertebrate *Meis* genes, including all *Meis3* genes, the *Meis2* genes of zebrafish, *Xenopus*, and mammals, the *Meis1* gene of lizard, the *Meis1.2* gene of zebrafish; in addition, in-frame STOP codons interrupt this region in chicken *Meis2* (fig. 2), suggesting a process of ongoing loss of this region from the gene.

For exon 11, we observed complex patterns for the 5′ extension (orange blocks). This extension with conserved coding meaning (often 21 nt) is found in a wide variety of vertebrate genes, suggesting emergence of an alternative upstream splice site in chordate ancestors. As with exon 10′, the phylogenetic distribution of this alternative splice site is highly punctate, with 4 parallel losses—in zebrafish *Meis1.1*/.2, zebrafish *Meis2.1*, tetrapod *Meis3* (fig. 2), and *C. intestinalis Meis*. In addition, although the genomic sequences of both *Meis1* and *Meis2* genes contain the potential splice site and conserved coding sequence, use of the splice site was only observed in *Meis2* genes (fig. 2). The frequency of usage in *Meis2* is conserved both across species

and development (~50% in various vertebrates, and throughout different tissues of several vertebrate species [supplementary fig. S5 and Sánchez-Guardado et al. 2011], similar to the pattern in amphioxus [supplementary fig. S6A]).

For exons 12a/12b, exon 12a shows very high levels of inclusion in nearly all paralogs of all vertebrate species; the only exceptions are *Xenopus Meis3*, which show more moderate levels of inclusion, and zebrafish and human *Meis3*, which have lost the exon entirely (fig. 2 and supplementary fig. S5). *Meis1* paralogs seem to have slightly lower levels of inclusion of exon 12a than *Meis2*, although the inclusion level is still higher than 90% (fig. 2). The high exon 12a inclusion level was found in a wide range of different tissues in several vertebrate species (supplementary fig. S5), in accordance with previous reports (Azcoitia et al. 2005; Williams et al. 2005; Sánchez-Guardado et al. 2011). Nonetheless, the possibility that a specific cell type in a particular developmental stage show a different splicing pattern cannot be ruled out (e.g. (Oulad-Abdelghani et al. 1997)). However, despite the fact that frequent inclusion of exon 12a may imply only infrequent translation of exon 12b, the ancestral coding meaning of exon 12b has been highly conserved in the vast majority of vertebrate *Meis* genes; the only exceptions are anole lizard *Meis3*, which seems to have lost the entire exon, and zebrafish *Meis1.2*, which has a much shorter sequence. Interestingly, the basal invertebrate chordate amphioxus shows significantly lower levels of exon 12a inclusion (i.e., higher levels of the ancestral isoform [supplementary fig. S6B]).

Discussion

We report the broadest evolutionary comparison of splicing diversity in a homeobox gene family to date. Three aspects of our 22-species comparison of metazoan *Meis* genes are of particular note: 1) conservation of intron positions and relative sizes across bilaterians, 2) striking differences in diversity and evolutionary patterns between the 5′ and 3′ regions of the gene, suggesting very different functions for introns and splicing for the two regions, and 3) convergent evolution of a variety of features of the alternative transcriptome of the 3′ region, suggesting similar selective forces acting on gene function across widely diverged species. These results show the utility of many-species studies for revealing modes of constraint and innovation acting at individual intronic loci and suggest a general strategy for comparative genomic analysis of splicing function.

Intron–Exon Structures and the Conservation-Implies-Function Paradigm

Comparative genomics has contributed a tremendous amount to our understanding of genome function. Arguably, the most productive paradigm has been "conservation implies function": in the face of ongoing mutation, only functional genomic features maintained by purifying selection will be retained over long evolutionary times (although for exceptions to this paradigm and a contrasting discussion, see Monroe 2009; Alexander et al. 2010). In the context of base pair substitutions and other small-scale sequence mutations, searches for conservation have utilized baseline mutation rates estimated from rates of changes for various classes of putatively neutral sites (e.g., synonymous or intronic sites) in order to identify slow-evolving and thus putatively functional sequences. While formally applicable to

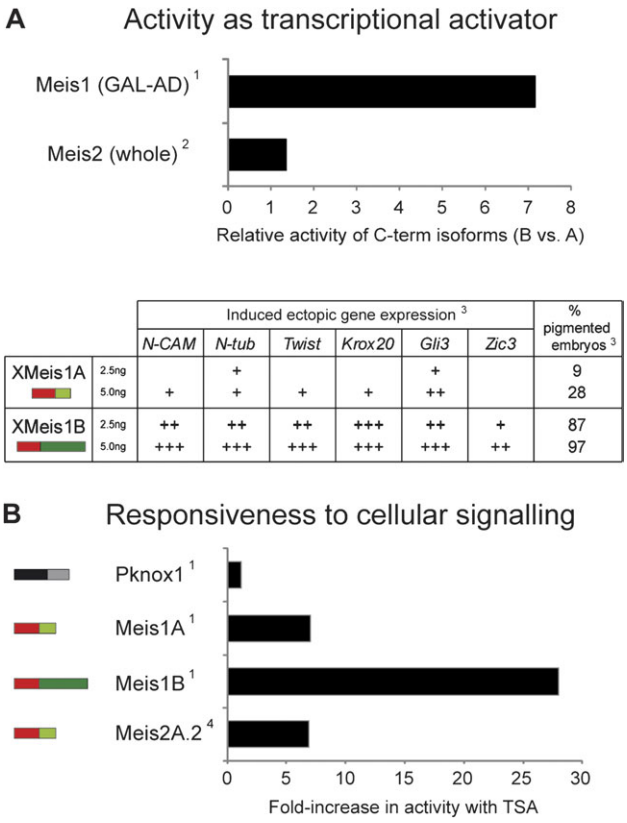

		Induced ectopic gene expression [3]						% pigmented embryos [3]
		N-CAM	*N-tub*	*Twist*	*Krox20*	*Gli3*	*Zic3*	
XMeis1A	2.5ng		+			+		9
	5.0ng	+	+	+	+	++		28
XMeis1B	2.5ng	++	++	++	+++	++	+	87
	5.0ng	+++	+++	+++	+++	+++	++	97

Fig. 3.—Summary of previous studies showing the different functional properties of C-terminal isoforms. (*A*) Differences in activity as transcriptional activators between C-terminal isoforms within each paralogous Meis gene in mammals. Top: histogram showing the ratio for activity of B (excluding 12a) versus A (including 12a) isoforms. Data for *Meis1* correspond to a protein fusion of the activation domain (AD, C-terminus) from each of the isoforms. *Meis2* data correspond to comparisons of full-length proteins and averaging the values for isoforms derived of inclusion/exclusion of exon 11′. Bottom: table summarizing the phenotypic results after injecting two different concentrations of full-length Meis1A or Meis1B isoforms in Xenopus embryos. Note that the intensity of the effect is not only isoform dependent but also concentration dependent. (*B*) Different C-terminal isoforms have different responses to TSA treatment. Histogram showing the fold-increase in transcriptional activation after TSA treatment for each *Meis1* isoform, Meis2A.2 (excluding 11′ but including 12a) and the related *pknox1* gene. References: (1) Huang et al. (2005), (2) Yang et al. (2000), (3) Maeda et al. (2001), and (4) Shim et al. (2007).

intron–exon structures, this strategy has met with complications in practice. First, there is no clear subset of putatively neutrally evolving introns; indeed, there is no consensus as to whether introns are generally beneficial, neutral, or deleterious or how the impact of introns on fitness might vary across lineages (Doolittle 1978; Lynch 2002). Second, the relevant molecular mutational mechanisms—in particular, those that lead to intron creation and loss from the genome—remain obscure and are known to be diverse (Llopart et al. 2002; Roy and Gilbert 2005; Stajich and Dietrich 2006; Irimia, Rukov, et al. 2008; Li et al. 2009; Roy and Irimia 2009a; Worden et al. 2009). Third, the genome-wide near absence of intron loss and gain over many millions of years in a variety of different groups of eukaryotes (e.g., vertebrates, and some genera of apicomplexans and fungi) suggests the possibility that intron loss and/or gain mutations simply do not occur in some lineages (Roy and Hartl 2006; Roy et al. 2006), in which case evolutionary conservation would not imply function.

The availability of many full genomes from diverse species allows us to circumvent these obstacles, at least in part. Here, we report the case of *Meis* homeobox genes. In contrast to the large amounts of intron loss and gain in some animal species observed in genome-wide comparisons (Seo et al. 2001; Rogozin et al. 2003; Edvardsen et al. 2004; Coulombe-Huntington and Majewski 2007b; Putnam et al. 2008), *Meis* genes have experienced almost no intron loss or gain in any studied species, particularly within the first ten exons of the gene. Unexpected conservation extends to the size of conserved introns: although intron size is thought to be relatively labile and not to persist over long evolutionary distances, *Meis* genes show clear conservation of relative intron sizes across genomically diverse species. Interestingly, long introns are known to show higher sequence conservation than short introns (Bergman and Kreitman 2001; Parsch 2003; Haddrill et al. 2005; Marais et al. 2005; Halligan and Keightley 2006; Parsch et al. 2010). The negative correlation between intron length and sequence divergence holds even within the set of longest introns, suggesting that the density of conserved sequence elements within introns may increase with intron length (Halligan and Keightley 2006). Thus, one possible explanation for the conserved long introns in *Meis/hth* is that they contain regulatory elements important for gene expression (Bergman and Kreitman 2001). *Meis/hth* genes are known to harbor the largest (or one of the largest) sets of associated highly conserved noncoding regions (HCNRs) in both vertebrates and in flies (Sandelin et al. 2004; Woolfe et al. 2005; Engstrom et al. 2007), with nearly a hundred associated HCNRs, depending on the study. Many of these HCNRs lie within these long introns (Engstrom et al. 2007; Visel et al. 2007; Dong et al. 2009; Xiong et al. 2009) and, in some cases, show even higher sequence conservation than the surrounding coding exons (Engstrom et al. 2007). Importantly, some of these elements have been shown to drive positive enhancer expression in reporter assays in mammals (Visel et al. 2007) or even to be involved in posttranscriptional regulation in dipterans (Glazov et al. 2005). Together, the conservation at the levels of intron loss/gain and intron size suggests that the introns in the 5′ region of *Meis* could encode conserved regulatory functions, leading to their retention across metazoans. Interestingly, the notion of *Meis* genes as hot spots for long-scale regulatory landscapes could extend beyond the transcribed regions: we also found that *Meis* genes are associated with large intergenic regions devoid of other genes (i.e., gene deserts) upstream and/or downstream *Meis/hth* genes in all studied metazoans (supplementary table S2), with the exceptions of some vertebrate *Meis* paralogs discussed above. As with intron lengths, longer intergenic regions are known to show less sequence divergence across species (Halligan and Keightley 2006).

Very Different Evolutionary Histories for 5′ and 3′ Regions of Meis Genes: Functional Causes and Consequences

In addition to general contrasts between *Meis* and genome-wide gene structure evolution, we found contrasting evolutionary histories for intron–exon structures of the 5′ and 3′ regions of *Meis* family genes (fig. 1*A*). As discussed above, the first 10 exons show remarkable conservation, with positions and relative sizes of the first 9 introns conserved across metazoans; by contrast, the 3′ of the gene shows a remarkable diversity of structures, evidencing intron and exon creation and loss, and great flexibility in AS patterns. These patterns echo findings in gene sequence evolution, in which different regions of the same protein may show opposed patterns of constraint or positive selection.

As with coding sequences, regional differences in protein function provide insight into the organismal functions undergoing potentially adaptive evolution. The conserved 5′ region encodes the highly conserved *Pbx*-interacting Meis (hth) domain and DNA-binding homeobox (Berthelsen et al. 1998; Mukherjee and Bürglin 2007), and the intervening introns may be implicated in developmental transcriptional regulation. By contrast, the variable 3′ region encodes interaction domains including the transcriptional activation domain and regulatory modules that modify protein transcriptional activity and response to cell signaling (Yang et al. 2000; Huang et al. 2005). For instance, regions within exons 11, 12a, and 12b affect transcriptional activator activity of human Meis1 proteins by mediating responsiveness to PKA and TSA (Huang et al. 2005; Shim et al. 2007), and inclusion of exon 12a lowers transcriptional activation in frogs and mammals (Yang et al. 2000; Maeda et al. 2001; Huang et al. 2005); (fig. 3). Shifting combinations of different isoforms and paralogs could thus allow subtle spatiotemporal control of Meis1 protein

transcriptional activity (Huang et al. 2005; Heine et al. 2008; Sánchez-Guardado et al. 2011). Such modulation would be particularly powerful given MEIS proteins' ability to enhance cell proliferation by transcriptional activation of cell cycle genes (Bessa et al. 2008; Heine et al. 2008): the quantitative combination of isoforms and paralogs present in each cell will likely affect the level of transcriptional activation of the target genes, and thus the proliferation rates. The 3′ region would therefore be a rich substrate for the evolution of different elaborations that could provide functional regulatory potential. Interestingly, this adaptation was likely aided by the gain of two introns in early bilaterians, splitting a single exon into three, allowing for a larger palette of potentially adaptive splicing-related mutations.

Deeply Conserved Splicing Functions in Bilaterians

Notably, our results show that *Meis/hth* genes harbor several cases of deeply conserved AS (Irimia et al. 2009). The AS of exon 10′ is a bilaterian innovation and has been maintained in some lineages since the very origin of bilaterians, representing one of the most ancestral AS events described to date (e.g., Mistry et al. 2003; Kalyna et al. 2006; Damianov and Black 2010). In addition, AS of exons 11 and 12a have likely arisen within chordate ancestors and have been conserved between amphioxus and vertebrates for some 600 My. This deep conservation of alternatively spliced sequences differs from the general low conservation of AS in different metazoan groups (reviewed in Irimia et al. 2009).

Frequent Gene Structural Convergence in Bilaterian Meis Evolution

Another striking result is the large number of cases of convergent evolution by identical or very similar sequence changes in different species in 3′ *Meis* regions. As with convergent protein changes in multiple lineages, these parallel changes suggest similar selective pressures acting in very different species; that these changes are restricted to the post-transcriptional regulatory domains of MEIS proteins suggests that evolution may have "used" and reused a finite set of accessible mechanisms for modulation of *Meis* function.

Recurrent Loss of Conserved Ancestral Sequence. We find several cases of convergent loss of conserved ancestral sequences. First, the sequence of 3′ end of exon 10 (which we call 10′) is highly conserved across a wide variety of bilaterian and non-bilaterian genes (fig. 1*C*), indicating function; yet, this region has been independently lost from genomic copies of *Meis* genes at least nine times and is only very infrequently observed in transcripts of some genes that do contain it, begging the question of this sequence region's mode of function. Similarly, the coding sequence of exon 12b is conserved between studied non-bilaterians and various bilaterians but has been lost by constitutive protein truncations in three independent lineages (Pancrustacea, sea urchin and *Meis3* in *Anolis*). In a third case, an ancestral vertebrate 5′ extension of exon 11 has been retained in many vertebrate genes but lost in 4 genic lineages; and the ancestral chordate AS exon 12a has been lost twice. Notably, these losses of conserved ancestral sequence have affected both putatively constitutively and alternatively spliced ancestral *Meis* gene regions.

Recurrent Evolution of Truncated C-Termini in Bilaterians. One of the most striking observations concerns the regulation of the novel alternative exon 12a in vertebrates. Exon 12a is nearly constitutive in most vertebrate *Meis* genes, which is surprising because inclusion of this exon significantly attenuates transcriptional activation in vertebrate MEIS proteins, especially for *Meis1* (Yang et al. 2000; Maeda et al. 2001; Huang et al. 2005). The scarce use of the most active, ancestral isoform may suggest that the emergence of exon 12a in chordates could have been associated with increasingly strict regulatory control of *Meis* target genes. This observation fits with postulates of the cybernetic theory of control in complex systems, which hold that the prevalence of negative regulatory mechanisms over positive ones increases system's stability (Wiener 1948). Notably, Ambulacraria and arthropods have independently achieved an equivalent situation by a different mechanism: evolution of constitutive 3′ extensions of exon 11 including premature stop codons. Insofar as these truncations also attenuate activator activity, these convergent patterns hint at an evolutionary trend towards more strictly regulated MEIS proteins in bilaterians.

The Fitness Effects of Introns and the Origins of Genome Complexity

Much discussion of spliceosomal introns has emphasized perspectives in which introns are neutral or slightly deleterious elements, potentially leading to evolutionary histories that are dominated by differences in mutation rates or effective population sizes (Lynch 2007). This study provides potential examples of two types of exceptions to this paradigm. First, widespread conservation of 5′ *Meis* intron–exon structures suggests strong purifying selection acting against intron loss in these regions. Second, the recurrent generation of very similar structures in the 3′ gene region suggests that alteration of intron–exon structures has been a frequent mechanism for adaptation. These findings join an increasingly long list of intronic loci encoding important organismal functions. Nonetheless, given the sheer number of introns in many metazoan genomes—reaching 200,000 in human and other vertebrate genomes—the proportion of introns whose loss is opposed by selection remains very much an open question, with answers ranging from a small minority

to a clear majority still being well within the realm of possibility.

Concluding Remarks

The diversity of structures, functions, and mechanisms associated with transcript splicing, and uncertainty about the general fitness consequences of introns, complicate efforts to understand the function of individual introns. The current report details a case in which the evolution of one gene family contrasts strikingly with genome-wide patterns, suggesting purifying selection on intron–exon structures and suggesting functional roles for splicing in these genes. These results indicate the utility of many-species comparisons between introns within a genome. Future research should research toward explicit models for divergence in intron–exon structures among large sets of metazoans, to allow for systematic prediction of intron functionality across lineages and loci.

Supplementary Material

Supplementary figure S1–S6 and tables S1–S3 are available at *Genome Biology and Evolution* online (http://www.oxfordjournals.org/our_journals/gbe/).

Acknowledgments

We thank Salvatore D'Aniello for kindly helping with the experiments, José L. Gómez-Skarmeta for the *X. tropicalis* samples and Maria Ina Arnone for the *S. purpuratus* samples. M.I., I.M., and J.G.F. were funded by grants BFU2005-00252 and BMC2008-03776 from the Spanish Ministerio de Educación y Ciencia; M.I. and I.M. held FPI and FPU fellowships, respectively; M.H.S., by FUNDESALUD-PRIS09043 and BFU2010-19461; and L.P. and J.L.F. by BFU2008-04156 and SENECA Foundation contract 04548/GERM/06-10891.

Literature Cited

Abascal F, Zardoya R, Posada D. 2005. ProtTest: selection of best-fit models of protein evolution. Bioinformatics. 21:2104–2105.

Adams MD, et al. 2000. The genome sequence of Drosophila melanogaster. Science. 287:2185–2195.

Alexander RP, Fang G, Rozowsky J, Snyder M, Gerstein MB. 2010. Annotating non-coding regions of the genome. Nat Rev Genet. 11:559–571.

Aparicio S, et al. 2002. Whole-genome shotgun assembly and analysis of the genome of Fugu rubripes. Science. 297:1301–1310.

Azcoitia V, Aracil M, Martínez-A C, Torres M. 2005. The homeodomain protein Meis1 is essential for definitive hematopoiesis and vascular patterning in the mouse embryo. Dev Biol. 280:307–320.

Bang ML, et al. 2001. The complete gene sequence of titin, expression of an unusual approximately 700-kDa titin isoform, and its interaction with obscurin identify a novel Z-line to I-ban linking system. Circ Res. 89:1065–1072.

Bergman CM, Kreitman M. 2001. Analysis of conserved noncoding DNA in Drosophila reveals similar constraints in intergenic and intronic sequences. Genome Res. 11:1335–1345.

Berthelsen J, Zappavigna V, Mavilio F, Blasi F. 1998. Prep1, a novel functional partner of Pbx proteins. EMBO J. 17:1423–1433.

Bessa J, et al. 2008. meis1 regulates cyclin D1 and c-myc expression, and controls the proliferation of the multipotent cells in the early developing zebrafish eye. Development. 135:799–803.

Choe SK, Vlachakis N, Sagerström CG. 2002. Meis family proteins are required for hindbrain development in the zebrafish. Development. 129:585–595.

Caenorhabditis elegans Sequencing Consortium. 1998. Genome sequence of the nematode C. elegans: a platform for investigating biology. Science. 282:2012–2018.

Chicken Genome Sequencing Consortium. 2004. Sequence and comparative analysis of the chicken genome provide unique perspectives on vertebrate evolution. Nature. 432:695–716.

Sea Urchin Genome Sequencing Consortium et al. 2006. The genome of the sea urchin Strongylocentrotus purpuratus. Science. 314:941–952.

Tribolium Genome Sequencing Consortium et al. 2008. The genome of the model beetle and pest Tribolium castaneum. Nature. 452:949–955.

Coulombe-Huntington J, Majewski J. 2007a. Characterization of intron loss events in mammals. Genome Res. 17:23–32.

Coulombe-Huntington J, Majewski J. 2007b. Intron loss and gain in drosophila. Mol Biol Evol. 24:2842–2850.

D'Aniello S, et al. 2008. Gene expansion and retention leads to a diverse tyrosine kinase superfamily in amphioxus. Mol Biol Evol. 25:1841–1854.

Damianov A, Black DL. 2010. Autoregulation of Fox protein expression to produce dominant negative splicing factors. RNA. 16:405–416.

Dehal P, Boore JL. 2005. Two rounds of whole genome duplication in the ancestral vertebrate. PLoS Biol. 3:e314.

Dehal P, et al. 2002. The draft genome of Ciona intestinalis: insights into chordate and vertebrate origins. Science. 298:2157–2167.

Dibner C, Elias S, Frank D. 2001. XMeis3 protein activity is required for proper hindbrain patterning in Xenopus laevis embryos. Development 128:3415–3426.

Dong X, Fredman D, Lenhard B. 2009. Synorth: exploring the evolution of synteny and long-range regulatory interactions in vertebrate genomes. Genome Biol. 10:R86.

Doolittle WF. 1978. Genes in pieces: were they ever together? Nature. 272:581–582.

Drummond A, Strimmer K. 2001. PAL: an object-oriented programming library for molecular evolution and phylogenetics. Bioinformatics. 17:662–663.

Edvardsen RB, et al. 2004. Hypervariable and highly divergent intron/exon organizations in the chordate Oikopleura dioica. J Mol Evol. 59:448–457.

Engstrom PG, Ho Sui SJ, Drivenes O, Becker TS, Lenhard B. 2007. Genomic regulatory blocks underlie extensive microsynteny conservation in insects. Genome Res. 17:1898–1908.

Ferran JL, Sánchez-Arrones L, Sandoval JE, Puelles L. 2007. A model of early molecular regionalization in the chicken embryonic pretectum. J Comp Neurol. 505:379–403.

Ghedin E, et al. 2007. Draft genome of the filarial nematode parasite Brugia malayi. Science. 317:1756–1760.

Glazov EA, Pheasant M, McGraw EA, Bejerano G, Mattick JS. 2005. Ultraconserved elements in insect genomes: a highly conserved intronic sequence implicated in the control of homothorax mRNA splicing. Genome Res. 15:800–808.

Guindon S, Gascuel O. 2003. A simple, fast, and accurate algorithm to estimate large phylogenies by maximum likelihood. Syst Biol. 52:696–704.
Haddrill PR, Charlesworth B, Halligan DL, Andolfatto P. 2005. Patterns of intron sequence evolution in Drosophila are dependent upon length and GC content. Genome Biol. 6:R67.
Halligan DL, Keightley PD. 2006. Ubiquitous selective constraints in the Drosophila genome revealed by a genome-wide interspecies comparison. Genome Res. 16:875–884.
Heine P, Dohle E, Bumsted-O'Brien K, Engelkamp D, Schulte D. 2008. Evidence for an evolutionary conserved role of homothorax/Meis1/2 during vertebrate retina development. Development. 135:805–811.
Hellsten U, et al. 2010. The genome of the Western clawed frog Xenopus tropicalis. Science. 328:633–636.
Hisa T, et al. 2004. Hematopoietic, angiogenic and eye defects in Meis1 mutant animals. EMBO J. 23:450–459.
Hong X, Scofield DG, Lynch M. 2006. Intron size, abundance, and distribution within untranslated regions of genes. Mol Biol Evol. 23:2392–2404.
Huang H, et al. 2005. MEIS C termini harbor transcriptional activation domains that respond to cell signaling. J Biol Chem. 280:10119–10127.
Huelsenbeck JP, Ronquist F. 2001. MRBAYES: Bayesian inference of phylogenetic trees. Bioinformatics. 17:754–755.
Hughes SS, Buckley CO, Neafsey DE. 2008. Complex selection on intron size in Cryptococcus neoformans. Mol Biol Evol. 25:247–253.
Hyman-Walsh C, Bjerke GA, Wotton D. 2010. An autoinhibitory effect of the homothorax domain of Meis2. FEBS J. 277:2584–2597.
Irimia M, Maeso I, Garcia-Fernandez J. 2008. Convergent evolution of clustering of Iroquois homeobox genes across metazoans. Mol Biol Evol. 25:1521–1525.
Irimia M, Maeso I, Gunning PW, Garcia-Fernandez J, Roy SW. 2010. Internal and external paralogy in the evolution of Tropomyosin genes in metazoans. Mol Biol Evol. 27:1504–1517.
Irimia M, Roy SW. 2008. Spliceosomal introns as tools for genomic and evolutionary analysis. Nucleic Acids Res. 36:1703–1712.
Irimia M, et al. 2008. Origin of introns by 'intronization' of exonic sequences. Trends Genet. 24:378–381.
Irimia M, Rukov JL, Roy SW, Vinther J, Garcia-Fernandez J. 2009. Quantitative regulation of alternative splicing in evolution and development. Bioessays. 31:40–50.
Kalyna M, Lopato S, Voronin V, Barta A. 2006. Evolutionary conservation and regulation of particular alternative splicing events in plant SR proteins. Nucleic Acids Res. 34:4395–4405.
Katoh K, Kuma K, Toh H, Miyata T. 2005. MAFFT version 5: improvement in accuracy of multiple sequence alignment. Nucleic Acids Res. 33:511–518.
Katoh K, Misawa K, Kuma K, Miyata T. 2002. MAFFT: a novel method for rapid multiple sequence alignment based on fast Fourier transform. Nucleic Acids Res. 30:3059–3066.
Lander ES, et al. 2001. Initial sequencing and analysis of the human genome. Nature. 409:860–921.
Li W, Tucker AE, Sung W, Thomas WK, Lynch M. 2009. Extensive, recent intron gains in Daphnia populations. Science. 326:1260–1262.
Llopart A, Comeron JM, Brunet FG, Lachaise D, Long M. 2002. Intron presence-absence polymorphism in Drosophila driven by positive Darwinian selection. Proc Natl Acad Sci U S A. 99:8121–8126.
Logsdon J. 2004. Worm genomes hold the smoking guns of intron gain. Proc Natl Acad Sci U S A. 101:11195–11196.
Lynch M. 2007. The Origins of Genome Architecture. Sunderland (MA): Sinauer Associates.
Lynch M. 2002. Intron evolution as a population-genetic process. Proc Natl Acad Sci U S A. 99:6118–6123.
Maeda R, et al. 2001. Xmeis1, a protooncogene involved in specifying neural crest cell fate in Xenopus embryos. Oncogene. 20:1329–1342.
Marais G, Nouvellet P, Keightley PD, Charlesworth B. 2005. Intron size and exon evolution in Drosophila. Genetics. 170:481–485.
Mercader N, et al. 1999. Conserved regulation of proximodistal limb axis development by Meis1/Hth. Nature. 402:425–429.
Mercader N, Tanaka EM, Torres M. 2005. Proximodistal identity during vertebrate limb regeneration is regulated by Meis homeodomain proteins. Development. 132:4131–4142.
Mistry N, Harrington W, Lasda E, Wagner EJ, Garcia-Blanco MA. 2003. Of urchins and men: evolution of an alternative splicing unit in fibroblast growth factor receptor genes. RNA. 9:209–217.
Monroe D. 2009. Genetics. Genomic clues to DNA treasure sometimes lead nowhere. Science. 325:142–143.
Moskow JJ, Bullrich F, Huebner K, Daar IO, Buchberg AM. 1995. Meis1, a PBX1-related homeobox gene involved in myeloid leukemia in BXH-2 mice. Mol Cell Biol. 15:5434.
Mukherjee K, Bürglin TR. 2007. Comprehensive analysis of animal TALE homeobox genes: new conserved motifs and cases of accelerated evolution. J Mol Evol. 65:137–153.
Nakamura T, Jenkins NA, Copeland NG. 1996. Identification of a new family of Pbx-related homeobox genes. Oncogene. 13:2235–2242.
Ng L, et al. 2009. An anatomic gene expression atlas of the adult mouse brain. Nat Neurosci. 12:356–362.
Noro B, Culi J, McKay DJ, Zhang W, Mann RS. 2006. Distinct functions of homeodomain-containing and homeodomain-less isoforms encoded by homothorax. Genes Dev. 20:1636–1650.
Oulad-Abdelghani M, et al. 1997. Meis2, a novel mouse Pbx-related homeobox gene induced by retinoic acid during differentiation of P19 embryonal carcinoma cells. Dev Dyn. 210:173–183.
Pai CY, et al. 1998. The homothorax homeoprotein activates the nuclear localization of another homeoprotein, extradenticle, and suppresses eye development in Drosophila. Genes Dev. 12:435–446.
Parsch J. 2003. Selective constraints on intron evolution in Drosophil. Genetics. 165:1843–1851.
Parsch J, Novozhilov S, Saminadin-Peter SS, Wong KM, Andolfatto P. 2010. On the utility of short intron sequences as a reference for the detection of positive and negative selection in Drosophila. Mol Biol Evol. 27:1226–1234.
Pechmann M, Prpic NM. 2009. Appendage patterning in the South American bird spider Acanthoscurria geniculata (Araneae: mygalomorphae). Dev Genes Evol. 219:189–198.
Prpic NM, Janssen R, Wigand B, Klingler M, Damen WG. 2003. Gene expression in spider appendages reveals reversal of exd/hth spatial specificity, altered leg gap gene dynamics, and suggests divergent distal morphogen signaling. Dev Biol. 264:119–140.
Putnam N, et al. 2008. The amphioxus genome and the evolution of the chordate karyotype. Nature. 453:1064–1071.
Putnam NH, et al. 2007. Sea anemone genome reveals ancestral Eumetazoan gene repertoire and genomic organization. Science. 317:86–94.
Rieckhof GE, Casares F, Ryoo HD, Abu-Shaar M, Mann RS. 1997. Nuclear translocation of extradenticle requires homothorax, which encodes an extradenticle-related homeodomain protein. Cell. 91:171–183.
Rogozin IB, Wolf YI, Sorokin AV, Mirkin BG, Koonin EV. 2003. Remarkable interkingdom conservation of intron positions and massive, lineage-specific intron loss and gain in eukaryotic evolution. Curr Biol. 13:1512–1517.

Ronquist F, Huelsenbeck JP. 2003. MrBayes 3: Bayesian phylogenetic inference under mixed models. Bioinformatics. 19:1572–1574.
Roy SW, Fedorov A, Gilbert W. 2003. Large-scale comparison of intron positions in mammalian genes shows intron loss but no gain. Proc Natl Acad Sci U S A. 100:7158–7162.
Roy SW, Gilbert W. 2005. The pattern of intron loss. Proc Natl Acad Sci U S A. 102:713–718.
Roy SW, Hartl DL. 2006. Very little intron loss/gain in Plasmodium: intron loss/gain mutation rates and intron number. Genome Res. 16:750–756.
Roy SW, Irimia M. 2009a. Mystery of intron gain: new data and new models. Trends Genet. 25:67–73.
Roy SW, Irimia M. 2009b. Splicing in the eukaryotic ancestor: form, function and dysfunction. Trends Ecol Evol. 24:447–455.
Roy SW, Irimia M, Penny D. 2006. Very little intron gain in Entamoeba histolytica genes laterally transferred from prokaryotes. Mol Biol Evol. 23:1824–1827.
Roy SW, Penny D. 2006. Large-scale intron conservation and order-of-magnitude variation in intron loss/gain rates in apicomplexan evolution. Genome Res. 16:1270–1275.
Rukov JL, et al. 2007. High qualitative and quantitative conservation of alternative splicing in Caenorhabditis elegans and Caenorhabditis briggsae. Mol Biol Evol. 24:909–917.
Sánchez-Guardado LÓ, et al. 2011. Distinct and redundant expression and transcriptional diversity of Meis gene paralogs during chicken development. Dev Dyn. 240:1475–1492.
Sandelin A, et al. 2004. Arrays of ultraconserved non-coding regions span the loci of key developmental genes in vertebrate genomes. BMC Genomics. 5:99.
Schmucker D, et al. 2000. Drosophila Dscam is an axon guidance receptor exhibiting extraordinary molecular diversity. Cell. 101:671–684.
Scofield DG, Hong X, Lynch M. 2007. Position of the final intron in full-length transcripts: determined by NMD? Mol Biol Evol. 24:896–899.
Seo H-C, et al. 2001. Miniature genome in the marine chordate Oikopleura dioica. Science. 294:2506.
Shim S, Kim Y, Shin J, Kim J, Park S. 2007. Regulation of EphA8 gene expression by TALE homeobox transcription factors during development of the mesencephalon. Mol Cell Biol. 27:1614–1630.
Srivastava M, et al. 2008. The Trichoplax genome and the nature of placozoans. Nature. 454:955–960.
Stajich JE, Dietrich FS. 2006. Evidence of mRNA-mediated intron loss in the human-pathogenic fungus Cryptococcus neoformans. Eukaryot Cell. 5:789–793.
Toresson H, Parmar M, Campbell K. 2000. Expression of Meis and Pbx genes and their protein products in the developing telencephalon: implications for regional differentiation. Mech Dev. 94:183–187.
Venter JC, et al. 2001. The sequence of the human genome. Science. 291:1304–1351.
Visel A, Minovitsky S, Dubchak I, Pennacchio LA. 2007. VISTA Enhancer Browser—a database of tissue-specific human enhancers. Nucleic Acids Res. 35:D88–D92.
Waskiewicz AJ, Rikhof HA, Hernandez RE, Moens CB. 2001. Zebrafish Meis functions to stabilize Pbx proteins and regulate hindbrain patterning. Development. 128:4139–4151.
Wassef MA, et al. 2008. Rostral hindbrain patterning involves the direct activation of a Krox20 transcriptional enhancer by Hox/Pbx and Meis factors. Development. 135:3369–3378.
Waterhouse AM, Procter JB, Martin DM, Clamp M, Barton GJ. 2009. Jalview version 2—a multiple sequence alignment editor and analysis workbench. Bioinformatics. 25:1189–1191.
Waterston R, et al. 2002. Initial sequencing and comparative analysis of the mouse genome. Nature. 420:520–562.
Wiener N. 1948. Cybernetics or control and communication in the animal and the machine. New York: John Wiley & Sons Inc.
Williams TM, Williams ME, Innis JW. 2005. Range of HOX/TALE superclass associations and protein domain requirements for HOXA13:MEIS interaction. Dev Biol. 277:457–471.
Woolfe A, et al. 2005. Highly conserved non-coding sequences are associated with vertebrate development. PLoS Biol. 3:e7.
Worden AZ, et al. 2009. Green evolution and dynamic adaptations revealed by genomes of the marine picoeukaryotes micromonas. Science. 324:268–272.
Xiong L, et al. 2009. MEIS1 intronic risk haplotype associated with restless legs syndrome affects its mRNA and protein expression levels. Hum Mol Genet. 18:1065–1074.
Yang Y, et al. 2000. Three-amino acid extension loop homeodomain proteins Meis2 and TGIF differentially regulate transcription. J Biol Chem. 275:20734–20741.

Associate editor: John Archibald

Artículo anexo 2

PLOS BIOLOGY

RESEARCH ARTICLE

Molecular regionalization of the developing amphioxus neural tube challenges major partitions of the vertebrate brain

Beatriz Albuixech-Crespo[1], Laura López-Blanch[2,3☯], Demian Burguera[1,2,3☯], Ignacio Maeso[4], Luisa Sánchez-Arrones[5], Juan Antonio Moreno-Bravo[6], Ildiko Somorjai[7,8], Juan Pascual-Anaya[9], Eduardo Puelles[6], Paola Bovolenta[5], Jordi Garcia-Fernàndez[1]*, Luis Puelles[10,11]*, Manuel Irimia[2,3]*, José Luis Ferran[10,11]*

1 Department of Genetics, School of Biology, and Institut de Biomedicina (IBUB), University of Barcelona, Barcelona, Spain, **2** Centre for Genomic Regulation (CRG), Barcelona Institute of Science and Technology (BIST), Barcelona, Spain, **3** Universitat Pompeu Fabra (UPF), Barcelona, Spain, **4** Centro Andaluz de Biología del Desarrollo (CSIC/UPO/JA), Sevilla, Spain, **5** Centro de Biología Molecular Severo Ochoa CSIC-UAM and CIBERER, ISCIII, Madrid, Spain, **6** Instituto de Neurociencias, UMH-CSIC, Campus de San Juan, Sant Joan d'Alacant, Alicante, Spain, **7** The Scottish Oceans Institute, University of St Andrews, St Andrews, Fife, Scotland, United Kingdom, **8** Biomedical Sciences Research Complex, University of St Andrews, Fife, Scotland, United Kingdom, **9** Evolutionary Morphology Laboratory, RIKEN, Kobe, Japan, **10** Department of Human Anatomy and Psychobiology, School of Medicine, University of Murcia, Murcia, Spain, **11** Institute of Biomedical Research of Murcia (IMIB), Virgen de la Arrixaca University Hospital, University of Murcia, Murcia, Spain

☯ These authors contributed equally to this work.
* mirimia@gmail.com (MI); jordigarcia@ub.edu (JGF); puelles@um.es (LP); jlferran@um.es (JLF)

Citation: Albuixech-Crespo B, López-Blanch L, Burguera D, Maeso I, Sánchez-Arrones L, Moreno-Bravo JA, et al. (2017) Molecular regionalization of the developing amphioxus neural tube challenges major partitions of the vertebrate brain. PLoS Biol 15(4): e2001573. https://doi.org/10.1371/journal.pbio.2001573

Academic Editor: Marianne Bronner, California Institute of Technology, United States of America

Received: November 14, 2016

Accepted: March 22, 2017

Published: April 19, 2017

Data Availability Statement: All relevant data are within the paper and its Supporting Information files.

Funding: Spanish Ministry of Economy and Competitiveness and European FEDER funds (grant number BFU2014-57516-P). To Luis Puelles and Jose Luis Ferran. The funder had no role in study design, data collection and analysis, decision to publish, or preparation of the manuscript. European Research Council (grant number ERC-

Abstract

All vertebrate brains develop following a common Bauplan defined by anteroposterior (AP) and dorsoventral (DV) subdivisions, characterized by largely conserved differential expression of gene markers. However, it is still unclear how this Bauplan originated during evolution. We studied the relative expression of 48 genes with key roles in vertebrate neural patterning in a representative amphioxus embryonic stage. Unlike nonchordates, amphioxus develops its central nervous system (CNS) from a neural plate that is homologous to that of vertebrates, allowing direct topological comparisons. The resulting genoarchitectonic model revealed that the amphioxus incipient neural tube is unexpectedly complex, consisting of several AP and DV molecular partitions. Strikingly, comparison with vertebrates indicates that the vertebrate thalamus, pretectum, and midbrain domains jointly correspond to a single amphioxus region, which we termed Di-Mesencephalic primordium (DiMes). This suggests that these domains have a common developmental and evolutionary origin, as supported by functional experiments manipulating secondary organizers in zebrafish and mice.

Author summary

According to textbooks, vertebrate brains develop from a neural tube that rapidly becomes regionalized into the forebrain (which includes the secondary prosencephalon and

StG-LS2-637591). To Manuel Irimia. The funder had no role in study design, data collection and analysis, decision to publish, or preparation of the manuscript. Spanish Ministry of Economy and Competitiveness (grant number SEV-2012-0208). Centro de Excelencia Severo Ochoa (to CRG, Manuel Irimia). The funder had no role in study design, data collection and analysis, decision to publish, or preparation of the manuscript. Spanish Ministry of Economy and Competitiveness (grant number BFU2014-58908-P). To Jordi Garcia-Fernadez. The funder had no role in study design, data collection and analysis, decision to publish, or preparation of the manuscript. Seneca Foundation, Comunidad de Murcia (grant number 19904/GERM/15). To Luis Puelles. The funder had no role in study design, data collection and analysis, decision to publish, or preparation of the manuscript. Generalitat de Catalunya (grant number). ICREA Academia Prize to Jordi Garcia-Fernandez. The funder had no role in study design, data collection and analysis, decision to publish, or preparation of the manuscript. Spanish Ministry of Economy and Competitiveness (grant number BFU2013-43213-P). To Paola Bovolenta. The funder had no role in study design, data collection and analysis, decision to publish, or preparation of the manuscript. Spanish Ministry of Economy and Competitiveness (grant number BFU2014-55076-P). To Manuel Irimia. Including an FPI PhD fellowship to Laura Lopez-Blanch. The funder had no role in study design, data collection and analysis, decision to publish, or preparation of the manuscript. Marine Alliance for Science and Technology Scotland (MASTS) (grant number). To Ildiko Somorjai. The funder had no role in study design, data collection and analysis, decision to publish, or preparation of the manuscript.

Competing interests: The authors have declared that no competing interests exist.

Abbreviations: 4MO, quadruple morpholino; AP, anteroposterior; ARCH, archencephalic prototagma; CNS, central nervous system; DEU, deuteroencephalic prototagma; DiMes, Di-Mesencephalic primordium; DV, dorsoventral; Evo-Devo, evolutionary developmental biology; hpf, h post fertilization; HH5, Hamburger–Hamilton 5; HyPTh, hypothalamo-prethalamic primordium; IsO, isthmic organizer; KO, knockout; MHB, Midbrain–Hindbrain Boundary; p1, pretectum diencephalic prosomere; p2, thalamus diencephalic prosomere; p3, prethalamus diencephalic prosomere; PHy, peduncular hypothalamic prosomere; RhSp, Rhombencephalo-Spinal primordium; THy, terminal hypothalamic prosomere; ZLI, zona limitans intrathalamica.

diencephalon), midbrain, and hindbrain. These regions are then further subdivided; in particular, the diencephalon gives rise to the prethalamus, thalamus, and pretectum. However, embryological manipulations of brain signaling centers showed that the prethalamus behaves very differently than the thalamus and pretectum, which largely share their developmental potential with the midbrain. Therefore, this classic partition scheme might not be fully consistent from a developmental perspective. To better understand the origin and evolution of the regionalization of the vertebrate brain, we built a comprehensive molecular model of the incipient neural tube of amphioxus, an invertebrate chordate that shares multiple features with its vertebrate relatives. This model shows that the amphioxus nervous system is unexpectedly complex, sharing its basic blueprint with that of vertebrates. However, a single undivided region in amphioxus, which we termed Di-Mesencephalic primordium (DiMes), unambiguously corresponds to the region encompassing the thalamus, pretectum, and midbrain in vertebrates, indicating that these regions are also more closely related evolutionarily. Therefore, the diencephalon as a neuroanatomical compartment as well as the classic separation between forebrain and midbrain in vertebrates seem inconsistent from both an evolutionary and developmental perspective.

Introduction

The vertebrate brain is arguably the most complex structure in nature. All vertebrates show a highly conserved construction plan, or Bauplan, of their central nervous system (CNS), which involves several major anatomical and genetic partitions and their subsequent subdivisions [1]. Understanding how this Bauplan has originated during evolution has been a matter of intense research and debate, but there is still no satisfactory answer. Do homologues to major vertebrate brain partitions exist in invertebrate species? Have new vertebrate partitions originated by subdivision and specialization of preexisting structures? Did positional genetic patterning mechanisms predate the origin of recognizable neuroanatomical regions, or did both originate concomitantly?

These and related questions have been investigated mainly from an evolutionary developmental (Evo-Devo) perspective, since early developing brains have not yet undergone complex morphogenetic deformations and are thus more amenable to evolutionary comparisons between distantly related species. In the case of vertebrates, the CNS arises very early in embryonic development via neural induction. The neuroectodermal plate represents the earliest CNS primordium, which then folds into a closed tube during neurulation. Already at neural plate stages, the CNS becomes regionalized molecularly into large anteroposterior (AP) regions. According to the prosomeric model [2–4], this Bauplan includes the secondary prosencephalon and diencephalon proper (forebrain), midbrain, hindbrain, and spinal cord (Fig 1A and 1B). These primary regions are further partitioned into smaller transverse AP units, identified as brain segments or neuromeres (Fig 1B). Two lineal neuroepithelial signal sources known as **secondary organizers** are crucial for this process: the zona limitans intrathalamica (ZLI or mid-diencephalic organizer) and the isthmic organizer (IsO, located in the Midbrain–Hindbrain Boundary, MHB; Fig 1B). These organizers are characterized by the release of diffused morphogen signals (SHH and FGF8/WNT1, respectively) and are involved in AP regionalization and differential specification of the diencephalic, mesencephalic, and some rostral rhombencephalic neuromeres [5–13].

Furthermore, along the neural tube, each neuromere is composed of four continuous dorsoventral (DV) domains: roof, alar, basal, and floor plate regions (Fig 1A–1D). Importantly,

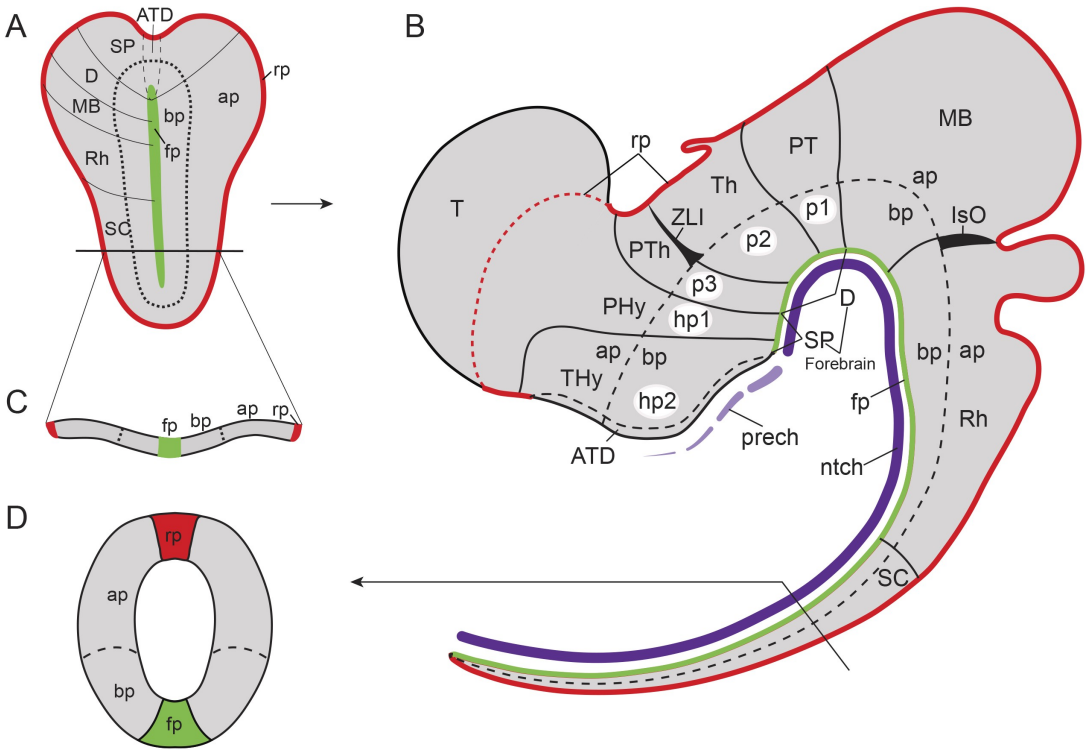

Fig 1. Bauplan of the vertebrate central nervous system (CNS). Schematic representation of the Bauplan of the vertebrate CNS according to the updated prosomeric model (Puelles and Rubenstein, 2015) at neural plate and early neural tube closure stages. **(A)** Schematic dorsal view of a representative neural plate of vertebrates depicting the components that define the longitudinal axis: floor plate (fp, in green) and parallel basal (bp), alar (ap) and roof (rp, in red) plates. Note that the fp does not reach the rostral boundary of the neural plate, whereas the bp, ap, and rp go around the fp; a similar phenomena can be observed in the caudal end of the neural plate. This peculiarity defines a rostral-most dorsoventral (DV) region termed acroterminal domain (ATD). From this domain, several anteroposterior (AP) partitions can be defined molecularly from rostral to caudal: secondary prosencephalon (SP) and diencephalon proper (D) (classic forebrain components), midbrain (MB), rhombencephalon (Rh), and spinal cord (SC) regions. **(B)** Schematic lateral view of an early closed neural tube in a more advanced stage of regionalization. Longitudinal components are indicated as fp (green), bp, ap, and rp (red). At this stage, the vertebrate neural tube is characterized by several definitive neuromeric units (i.e., AP partitions with all the DV components). The forebrain is subdivided into SP, with peduncular and terminal prosomeres (hp1 and hp2, respectively), which include the hypothalamic region, telencephalon (Tel), and the optic vesicles, and D (with prosomeres 1, 2, and 3 [p1–p3], which are represented at the ap level by pretectum [PT], thalamus [Th], and prethalamus [PTh], respectively). More caudally, MB, Rh, and SC regions are identified (for simplicity, their respective neuromeric components are not depicted). The secondary organizers zona limitans intrathalamica (ZLI) and the isthmic organizer (IsO) are located between the PTh and Th regions, and the MB and Rh regions, respectively. **(C)** The transversal section throughout the open neural plate in **(A)**, showing the main longitudinal components (fp, bp, ap, and rp) arranged medio-laterally at this stage. **(D)** Cross section through the closed neural tube, showing the DV relationships of the same longitudinal components highlighted in (**C**).

https://doi.org/10.1371/journal.pbio.2001573.g001

the prospective DV pattern is already observed at neural plate stages, corresponding to its mediolateral dimension (Fig 1A, 1C and 1D): the future floor corresponds to the neural plate midline, whereas the future roof lies at the border of the neural plate. The rostral end of the neural plate is thus morphologically singular because the floor does not reach the anterior border of the plate but ends rostrally at the prospective mamillary hypothalamic region, in coincidence with the underlying rostral tip of the notochord [14]; therefore, the roof, alar, and basal plates concentrically cross the midline at the terminal wall (future acroterminal domain), curving around the rostral end of the floor plate (Fig 1A, [2,4,15]).

An important breakthrough in the study of comparative neuroanatomy and the evolutionary origin of CNSs has been the observation that each established AP and DV anatomical

partition in a given species is characterized by the differential expression of specific gene markers early in development in a combinatorial code that we refer to as genoarchitecture [14]. These molecular codes create clear-cut molecular boundaries between the neuromeres, and often correspond with visible external bulges due to the differential proliferation of the progenitors because of their distinct genoarchitectonic profiles [3,15]. Strikingly, the number of neuromeric units and their associated genoarchitecture is highly conserved in all vertebrate groups, including the basal-branching agnathans [16–34]. This implies that a fundamentally conserved anatomical CNS Bauplan and its corresponding genetic blueprint have existed at least since the last common ancestor of vertebrates.

Therefore, a major approach to understanding the origins of this Bauplan has been to investigate the expression of orthologs of key gene markers in chordate and nonchordate invertebrate species. Remarkably, a subset of these markers show fixed relative AP positions, suggesting that some of the regional genoarchitectonic codes of vertebrates were established prior to the origin of the vertebrate brain Bauplan. For example, the transverse genetic boundaries defined by the abutting expression of *Fezf/Irx* and *Otx/Gbx*—which in vertebrates correspond to the anatomical positions in which the ZLI and IsO secondary organizers will develop, respectively—are observed in the CNSs of species as diverged as amphioxus and fruit flies [35–37]; although, these sites lack the expression of the morphogens responsible for the organizer activity in vertebrates [38–41]. Moreover, some markers expressed in the annelid *Platynereis dumeilii* show remarkable topologic similarity with the mediolateral and AP molecular pattern in vertebrates [42–44]. In one of the most striking cases of genetic patterning conservation observed between vertebrates and invertebrates, the diffuse epidermal nervous system of hemichordates displays multiple vertebrate-like AP genetic codes, including a ZLI-like domain with equivalent relative expression of *hh*, *six3*, *fng*, *otx*, and *wnt8* orthologs and an IsO-like region coexpressing *fgf8/17/18* and *wnt1*, suggesting conservation of the underlying genetic programs despite the fact that they are patterning divergent structures in the two lineages [45–48].

Altogether, these studies thus suggest that multiple defining genetic programs that pattern the vertebrate brain predate its evolutionary emergence. However, the major limitation of these nonchordate model systems to investigate the origin of the vertebrate brain Bauplan is the lack of an unambiguous anatomical and topological reference system. Even under the assumption that the nervous systems of these invertebrate phyla are truly homologous to the vertebrate CNS, each one has its own set of clade-specific characters and thus correspond to different variational modalities of CNSs [49]. This impedes direct topological comparisons, leaving similarities of gene expression patterns as the only support for any hypothesized homology assignment. For this reason, the cephalochordate amphioxus has traditionally been the most studied invertebrate species for comparative analyses with vertebrates. Unlike nonchordates, amphioxus develops its tubular CNS from a neural plate in the same way that vertebrates do, thus allowing direct topological comparisons of prospective brain regions. Furthermore, unlike tunicates, cephalochordates have undergone slow evolutionary rates, both genomically and morphologically [50,51]. Multiple studies on this organism have shown, for instance, that the *Otx/Gbx* and *Fez/Irx* genetic boundaries [36,37,52] as well as part of its neural *Hox* AP patterning [53–57] are conserved with vertebrates. Similarly, orthologs of many other key vertebrate genes have been implicated in neural function and development in amphioxus (see S1 Table for a list of previously described gene expression patterns in amphioxus with relevance to CNS development that have been used in this study). These reports, together with multiple comprehensive and integrating reviews [41,58–64], have provided important insights on the presence of molecularly-defined partitions in the developing amphioxus CNS. Nonetheless, these studies have been performed by different research groups, using different amphioxus species, and usually focused on the expression of a single gene at multiple

embryonic stages. This has made the systematic integration and accurate combinatorial analyses of these expression patterns a complex task.

To address these difficulties, we mapped here 48 genes with well-known roles in vertebrate CNS patterning on a single amphioxus developmental stage, the 7-somite mid-neurula, in which a wide spectrum of orthologs of vertebrate neural gene markers is expressed. With these data, we propose an integrative model of the molecular regionalization of the amphioxus developing CNS that is consistent and comparable with the prosomeric model of the vertebrate CNS Bauplan. Our results show that, at the mid-neurula stage, the amphioxus CNS primordium has an unexpectedly complex genoarchitecture, with three major molecularly distinguishable AP divisions (and some secondary subdivisions) and a set of standard DV zones. Strikingly, direct topological comparison between the molecular models of the two lineages, as well as extensive novel and previously reported functional data, suggest that the vertebrate territory comprising the diencephalic neuromeric units corresponding to thalamus and pretectum (prosomeres p2, p1), but not the prethalamus (p3), share with the midbrain a common ontogenetic and evolutionary origin, and, altogether, are homologous to a nonregionalized *Pax4/6*-positive domain in amphioxus, which we termed Diencephalo-Mesencephalic primordium (DiMes). Whether resulting from an increase in complexity in vertebrates or, alternatively, a simplification in amphioxus compared to the last common ancestor of chordates, these results suggest that the differences in AP Bauplan complexity between the two lineages are likely linked to the secondary organizers of vertebrates (ZLI and IsO), which are absent in amphioxus. Experimental abrogation and manipulation of these organizers in vertebrate species generate phenotypic defects that are consistent with this hypothesis.

Results

Molecular markers define and regionalize the amphioxus floor plate

AP and DV subdivisions in developing chordate neural tubes are defined according to axial references. Conventionally, such references are provided in vertebrates by the axial mesoderm (the notochord), the floor plate, roof plate, and alar–basal boundary within the lateral walls of the neural tube, all of which are topologically parallel to each other (Fig 1). Amphioxus has a notochord, which extends singularly beyond the forebrain [65], and a floor plate [66–70]. As previously reported for the Floridan amphioxus *Branchiostoma floridae* [71,72], we observed in the European amphioxus *B. lanceolatum* that the gene *FoxA2-1* is a selective marker of the notochord (Fig 2A–2A‴, 2E and 2F), while *Nkx2.1* seems to be a general floor plate marker at the 7-somite neurula stage (Fig 2B–2B‴). As in vertebrates, in which its expression in the floor plate is transient [73], *Nkx2.1* expression is highly dynamic during amphioxus CNS development (S1 Fig). *Nkx2.1* is observed along the entire presumptive floor plate at early- and mid-larval stages, but it subsequently becomes restricted rostralwards.

Since the whole neural tube of amphioxus sits on top of the notochord, it should be, in theory, regarded as topographically epichordal. Thus, as the floor plate is induced vertically by the notochord [74–76], we a priori expected the amphioxus floor plate to extend all along the acroterminal neural midline (up to the neuropore), in contrast to the vertebrate floor plate, which stops at the mamillary pouch of the hypothalamus, coinciding with the approximate position of the rostral tip of the notochord (Fig 1A and 1B; [2,4]). Instead, we observed that the floor plate, defined by *Nkx2.1* expression, does not reach the anterior neural border, but it ends in a slightly expanded median patch that recalls the mamillary hypothalamic ending observed in vertebrates (Fig 2B and 2B′ insets, K; see also [66]). Interestingly, *Hedgehog (Hh)*, which is a well-established floor plate marker in vertebrates [74,77,78], and *Nkx6* are also expressed in the amphioxus floor plate, but their anterior limit of expression is more caudal than that of

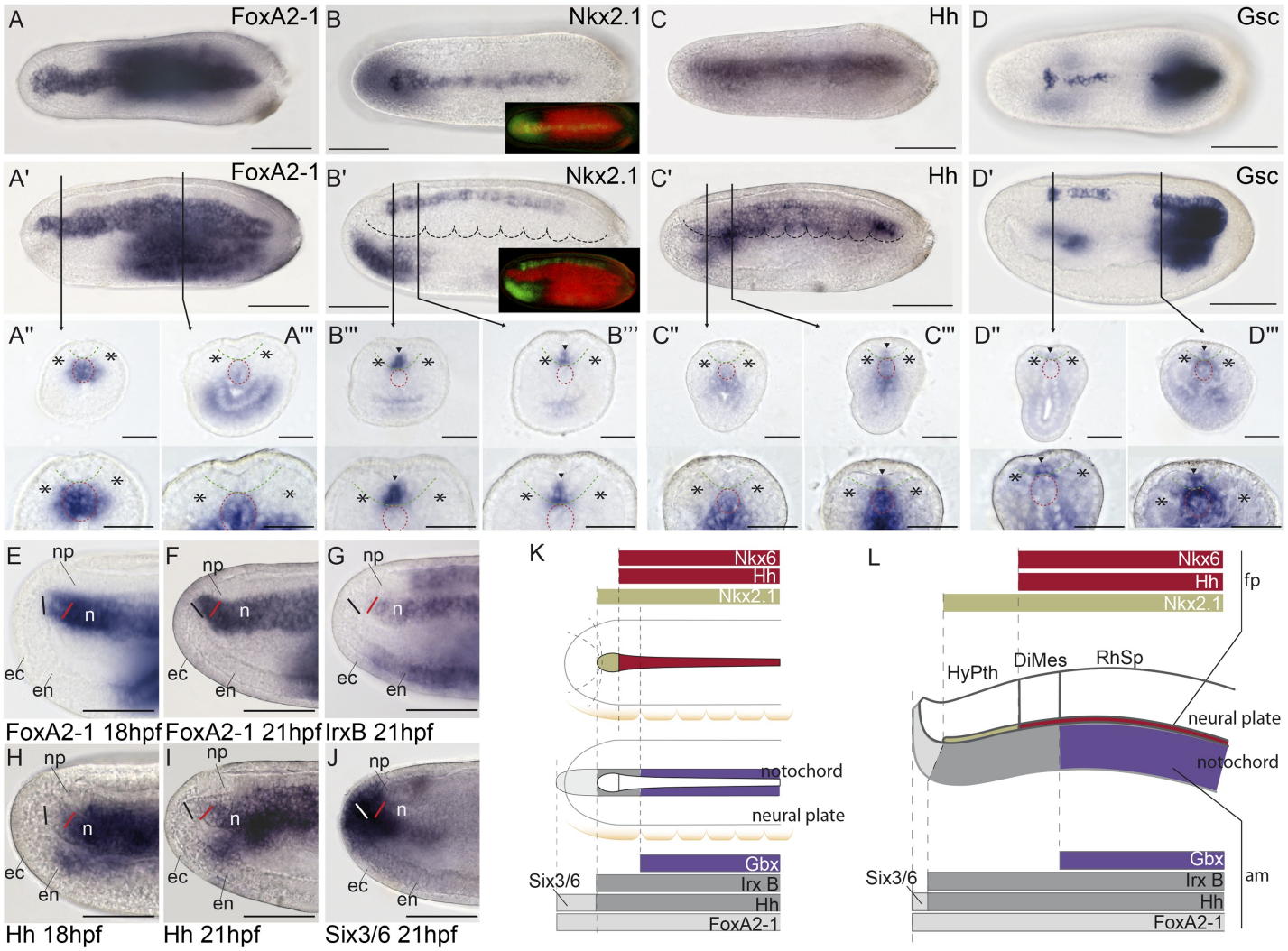

Fig 2. Molecular regionalization of the amphioxus floor plate and axial mesoderm. (A-A‴) *FoxA2-1* is expressed throughout the notochord, as shown by whole-mount in situ hybridization in dorsal **(A)** and lateral **(A′)** views and in situ hybridization in cryostat transversal sections **(A″,A‴)**. **(B-B‴)** *Nk2.1* mRNA is expressed throughout the entire floor plate, as observed in dorsal **(B)** and lateral **(B′)** views, and in cryostat transversal sections (**B″,B‴**). Insets in (**B**) and (**B′**) show the combined *FoxA2-1* and *Nkx2.1* expression patterns using pseudocolors, indicating that *Nkx2.1* is expressed above the notochord but does not reach its rostral boundary. (**C-C‴**) *Hh* mRNA is detected in most of the floor plate, with exception of the rostral-most portion (hypothalamo-prethalamic primordium [HyPTh] floor plate) as observed in dorsal **(C)** and lateral **(C′)** views, and in cryostat transversal sections (**C″, C‴**)**. (D-D‴)** *Gsc* expression is observed in different rostro-caudal patches in dorsal **(D)** and lateral **(D′)** views and in cryostat transversal sections **(D″, D‴)**. **E-J)** Detailed analysis of the rostral end of the notochord using whole-mount data at 18 h post fertilization (hpf) and 21 hpf stages further supports that *FoxA2-1* **(E,F)** is present throughout the entire length of the notochord; *IrxB* **(G)** and *Hh* **(H,I)** are absent rostrally and expressed caudally, and *Six3/6* **(I)** is expressed only in the rostral tip. (**K,L**) The rostral molecular code (*Six3/6* and *FoxA2-1* positive, but *IrxB* and *Hh* negative) is summarized in dorsal (**K**) and lateral (**L**) schematic representations. In cryostat sections, asterisks mark somites, and arrowheads indicate neural expression; red and green dotted lines delineate the notochord and neural plate, respectively. Abbreviations: np, neural plate; ec, ectoderm; en, endoderm; n, notochord; fp, floor plate; am, axial mesoderm. Scale bar: 50 μm.

https://doi.org/10.1371/journal.pbio.2001573.g002

Nkx2.1 (Figs 2C–2C‴, 2K, 2L and 7D–7D″; a similar expression for *Hh* has been reported in *B. floridae* [69]). *Goosecoid* (*Gsc*) is also expressed in the floor plate (in contrast to previous reports [79]) in a variable and patchy pattern that might reflect cyclic dynamic changes (Fig 2D–2D‴). These markers differentiate two major floor plate AP regions: (i) a rostral-most median floor domain characterized by only *Nkx2.1* expression, which corresponds to the floor plate of the forebrain region that we refer to as the amphioxus hypothalamo-prethalamic

primordium (HyPTh; see below and Fig 2K and 2L); and (ii) the rest of the floor plate, defined by *Hh*, *Gsc*, *Nkx6*, and *Nkx2.1* expression.

Molecular heterogeneity of the amphioxus axial mesoderm: Notochord and a possible prechordal primordium

We next examined the genoarchitecture of the amphioxus axial mesoderm to assess the existence of a putative prechordal plate homolog. According to the updated prosomeric model [2,4], the latter tissue lies topologically rostral to the neural primordium and the notochord (Fig 1B). As mentioned above, *FoxA2-1* labels the whole amphioxus prospective notochord (Fig 2A–2A‴). On the other hand, the expression of both *Hh* and *IrxB* in the axial notochordal tissue does not reach the rostral tip of the *FoxA2-1*–positive domain, stopping beneath the rostral end of the *Nkx2.1*–positive HyPTh floor plate (Fig 2L, 2E–2J; it should be noted, however, that *IrxB* expression seems to reach the anterior tip of the notochord in *B. floridae* [80]). Moreover, in the amphioxus axial mesoderm, *Six3/6* expression was observed exclusively in the rostral tip of the *FoxA2-1*–positive domain, beyond the *Hh/IrxB*–positive part of the notochord (Fig 2K, 2L and 2J; see also [81]). Interestingly, this *Six3/6* expression is maintained at later stages, when the notochord is fully formed [81], indicating that its rostral tip has a distinct molecular signature compared to the rest of the notochord. Remarkably, in vertebrates, *Six3* is expressed in the prechordal plate but not in the notochord at any level [24]; therefore, the rostral notochordal tip of amphioxus might represent a possible prechordal plate homologue, previously unrecognized due to its histologic similarity to the notochord proper (see Discussion).

Finally, we found that *Gbx* expression appears restricted to a more caudal sector of the notochord, whose rostral border is posterior to the caudal boundary of the HyPTh neural domain (Figs 2K, 2L, 3F and 3L inset). Previous studies [37] and other observations described below suggest that the *Gbx*-expressing domain of the notochord and overlying neural tissue begins at the rostral end of the major region we term Rhombencephalo-Spinal primordium (RhSp; Fig 2L). In summary, we observed that the amphioxus axial mesoderm is subdivided molecularly into various regions, which have direct correspondence with major subdivisions in the overlaying neural plate.

The incipient neural tube of amphioxus possesses distinct floor, basal, and alar plates

Previous gene expression studies provided evidence for the presence of longitudinal zones positioned parallel to the floor plate, implying DV patterning in the amphioxus CNS [69,82]. We thus investigated the extent of DV regionalization and its related boundaries by systematically searching for gene expression patterns with specific DV domains. We found that most of the examined patterns could be classified into three groups (Figs 3–9): (i) peripheral genes, with expression restricted to the periphery of the neural plate (future topologically dorsal or alar zone; *Six3/6*, *Lhx2/9b*, *Zic*, *Msx*, *Pax2/5/8*, *Pax3/7*, *Nova*); (ii) internal genes, with expression domains respecting the former peripheral longitudinal zone (*Pou3f*, *Sim*, *FoxD*, *Meis*, *Lef*, *Lhx1/5*, *Hox3*, *Hox6*, *FoxB*); and (iii) pan-DV genes, expressed across both aforementioned domains (*Otx*, *Gbx*, *Fezf*, *Irx*, *Pax4/6*, *Six3/6*, *Nkx2.2*, *Meis*, *Rx*, *Hox1*, *Wnt3*, *Wnt7*, *Nova*, *Ebf*). A few markers were ascribed to two of these categories since they have DV expression subdomains that differ depending on the AP partition in which they are expressed (see below and Fig 9). Altogether, these patterns suggest the existence of continuous basal and alar plate zones that extend longitudinally throughout the amphioxus neural tube primordium. As in vertebrates, the right and left moieties meet frontally around the rostral end of the floor plate (Fig 10A), as clearly exemplified by the alar expression of *Lhx2/9b* (Fig 6C′ and 6C″).

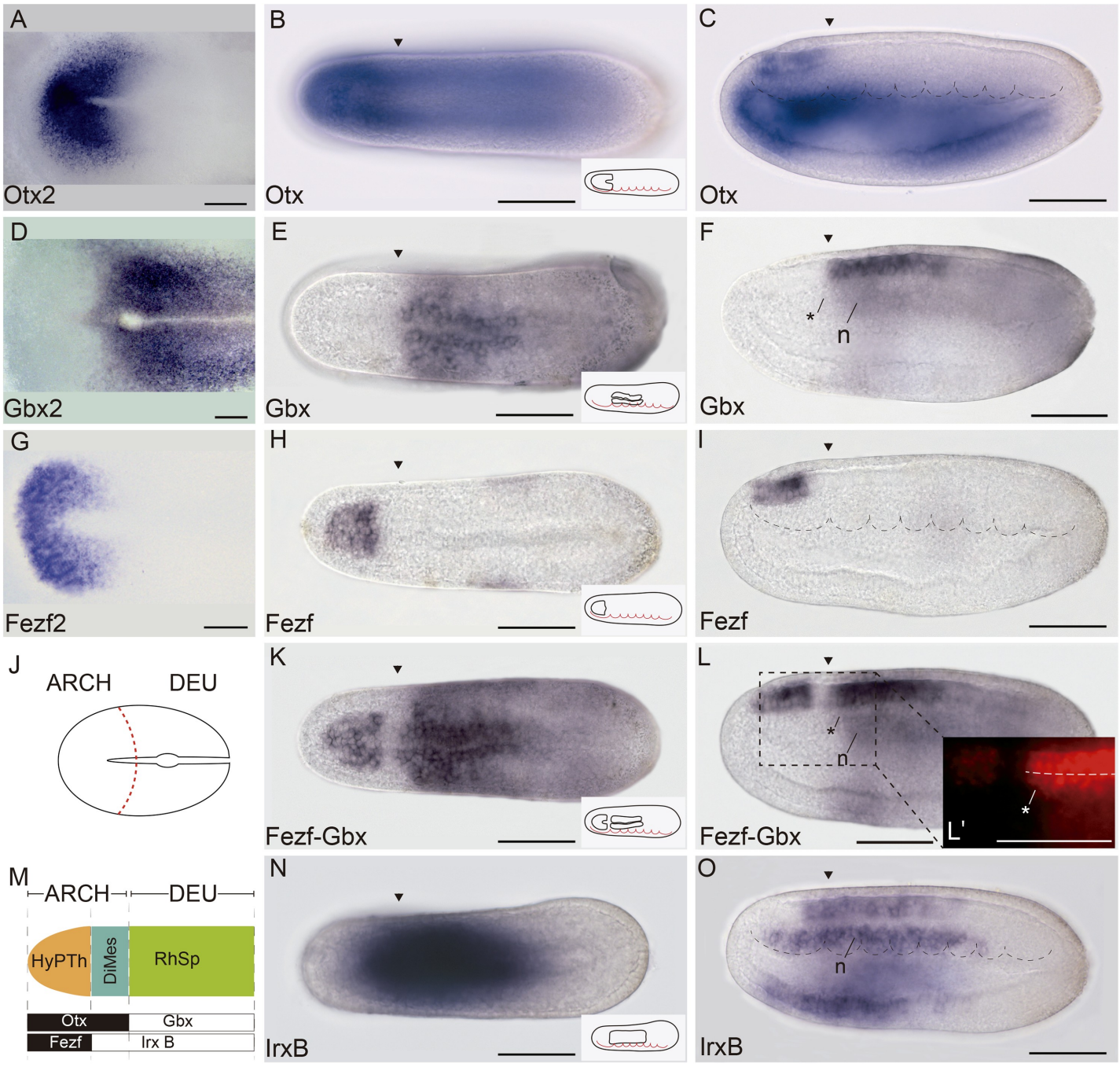

Fig 3. Three major molecular anteroposterior (AP) regions are observed in the incipient amphioxus neural tube. (A) Whole-mount in situ hybridization of chicken *Otx2* at Hamburger–Hamilton 5 (HH5) stage. (**B,C**) Expression of amphioxus *Otx* at 21 h post fertilization (hpf) in dorsal **(B)** and lateral **(C)** views. (**D**) Whole-mount in situ hybridization of chicken *Gbx2* at HH5 stage. (**E,F**) Expression of amphioxus *Gbx* at 21 hpf in dorsal **(E)** and lateral **(F)** views. **G)** Whole-mount in situ hybridization of chicken *Fezf2* at HH5 stage. (**H,I**) Expression of amphioxus *Otx* at 21 hpf in dorsal **(H)** and lateral **(I)** views. **(J)** Schematic representation of HH5 chicken neural plate with the archencephalic prototagma (ARCH) and deuteroencephalic prototagma (DEU) domains depicted. The boundary between ARCH and DEU correspond to the border between *Otx2* and *Gbx2* expression patterns **(A,D)**. (**K,L**) Double chromogenic in situ hybridization combining amphioxus *Fezf* and *Gbx* probes in dorsal **(K)** and lateral **(L)** views, showing two subdivisions in the amphioxus ARCH territory: a rostral hypothalamo-prethalamic primordium (HyPTh) domain (*Fezf* and *Otx* positive) and a caudal Di-Mesencephalic primordium (DiMes) domain (*Fezf negative* and *Otx* positive) **(L′)**. (**M**) Schematic representation of the three major AP subdivisions in the amphioxus central nervous system (CNS) at the 21 hpf stage and the relative expression of their key markers. (**N,O**) Single chromogenic in situ hybridization with an amphioxus *IrxB* probe in dorsal **(N)** an lateral **(O)** views. Insets in B, E, H, K, and N depict the neural components of the corresponding gene expression patterns. Arrowheads mark the ARCH–DEU boundary, and asterisks mark the corresponding limit at the notochord level, based on *Gbx* expression. Abbreviations: n, notochord. Scale bar: 50 μm.

https://doi.org/10.1371/journal.pbio.2001573.g003

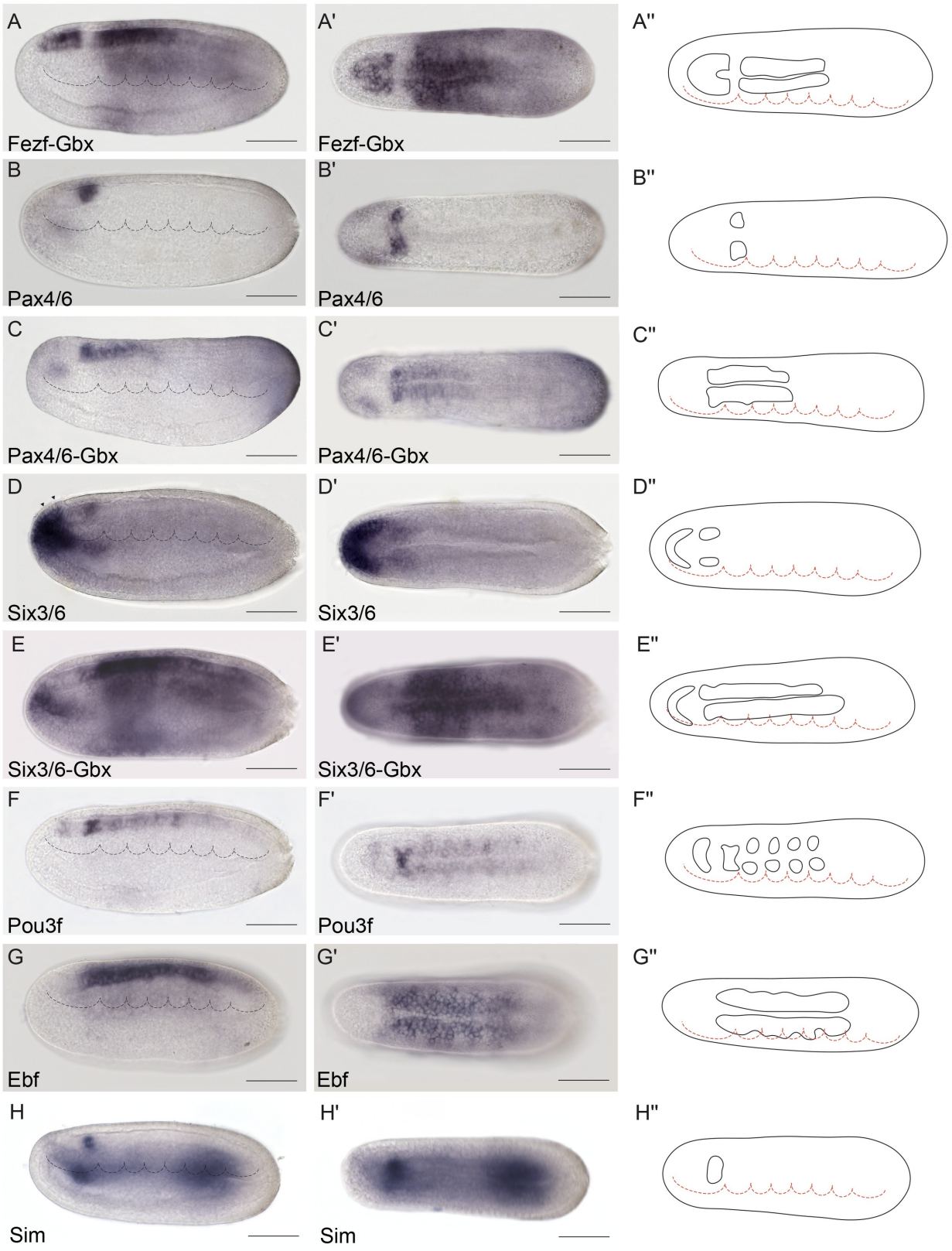

Fig 4. Genoarchitectonic signature of the Di-Mesencephalic primordium (DiMes). (A-A″) Combined *Fezf-Gbx* expression defines a gap of expression in the caudal archencephalic prototagma (ARCH), identified as the DiMes (as per Fig 3K and 3L, for

reference). **(B-E″)** Whole-mount chromogenic in situ hybridization of *Pax4/6* **(B-B″)** or *Six3/6* **(D-D″)** alone or each one combined with *Gbx* in a double in situ hybridization **(C-C″** and **E′-E″**, respectively) reveal that both genes are expressed in the DiMes domain. The two arrowheads in **(D)** indicate the expression of *Six3/6* in Rostral-hypothalamo–prethalamic primordium (Rostral-HyPTh). **(F-F″)** *Pou3f* is highly expressed in DiMes but with a decreased signal in the Rostral-HyPTh and Intermediate-HyPTh primordia and in some areas of the deuteroencephalic prototagma (DEU). **(G-G″)** *Ebf* mRNA was detected in the DiMes and DEU domains. **(H-H″)** *Sim* neural expression was observed exclusively in the DiMes domain at the analyzed stage. Expression patterns correspond to lateral **(A-H)** or dorsal views **(A′-H′)** at the 21 h post fertilization (hpf) embryonic stage and are represented in schematics dorsal views **(A″-H″)**. Somites (dotted lines) were used as main landmarks to localize the position of the patterns analyzed in the late neural plate. Scale bar: 50 μm.

https://doi.org/10.1371/journal.pbio.2001573.g004

Conserved *Otx* and *Gbx* expression patterns define a primary AP partition

In all vertebrates, dynamic antagonistic expression of *Otx* (rostral) and *Gbx* (caudal) in the neural plate eventually reaches an equilibrium at the caudal end of the midbrain, defining the MHB (Fig 3A and 3D; [5,83–88]). Clonal labeling studies performed in frogs at the 64 blastomere stage showed that this is the earliest detectable brain transverse boundary [89]. A comparable boundary is also present in amphioxus, aligned between the first and second somites [37], which we further corroborated at the 7-somite neurula stage in *B. lanceolatum* (Fig 3B–3F). Accordingly, it was suggested that the first intersomitic limit of amphioxus roughly marks the genetic homolog of the MHB of vertebrates [37,52,53,58,90]. Thus, it can be postulated that these early expression domains in both lineages define the boundary between a rostral *Otx*-positive "archencephalic prototagma" (ARCH; Fig 3J and 3M) and a caudal *Gbx*-positive "deuteroencephalic prototagma" (DEU; Fig 3J and 3M). In addition to *Gbx*, several other amphioxus genes show specific expression within DEU at this stage, abutting rostrally the ARCH–DEU boundary (*Wnt3*, *Wnt7*, *FoxB*, *Pax2/5/8*, and *Msx*; Figs 6G–6H″ and 7E–7G″).

The archencephalon is regionalized anteroposteriorly into the HyPTh and DiMes regions

We previously showed that the ARCH domain can be subdivided anteroposteriorly based on *Fezf* and *Irx* expression [36]. In both vertebrates and amphioxus, *Fezf* genes are expressed in the rostral-most part of the CNS at early neural tube stages, creating an anterior subdomain within the *Otx*-positive territory (Fig 3G–3I) and thus leaving a gap between the caudal end of their expression and the start of that of *Gbx* in DEU (Fig 3K and 3L). On the other hand, *Irx* genes are expressed within this gap, abutting rostrally with *Fezf* and extending posteriorly into the *Gbx*-positive DEU tagma (Fig 3K–3O). Studies in *Xenopus*, zebrafish, and mice, comparing *Fezf* and *Irx* expression patterns with fate mapping data, have shown that the transverse *Fezf-Irx* interface marks the prethalamo–thalamic boundary where the ZLI will develop [21,91–94]. Based on the expression patterns observed in the 7-somite amphioxus neurula, we accordingly defined a rostral *Fezf*-positive HyPTh and a caudal *Irx*-positive DiMes intercalated between the *Fezf*-positive and *Gbx*-positive domains (Fig 3K–3O). Remarkably, several genes, including *Pax4/6*, *Six3/6*, *Pou3f*, and *Sim*, are expressed specifically or most strongly within the DiMes (Fig 4, see also Fig 8A–8C″), supporting the distinct identity of this region. Moreover, other genes in addition to *Fezf* appear restricted to HyPTh (e.g., *Rx* throughout it, Fig 5B and 5B″, and *FoxD* in its basal plate subdomain, Fig 5C and 5C″; see also Figs 8D–8E″ and 9) or have distinct expression subdomains within HyPTh (e.g., *Nova*, S2C and S2″ Fig). On the other hand, other markers, such as *Ebf*, are expressed caudally to the *Fezf/Irx* limit, similarly to the three *Irx* genes (*IrxA-C*)(Figs 3N, 3O, 4G, 4G′, 6A and 6B″).

Triple fluorescent in situ hybridization and confocal 3-D reconstruction show that the *Fezf*-positive HyPTh, the *Pax4/6*-positive DiMes and the *Gbx*-positive RhSp domains abut sharply

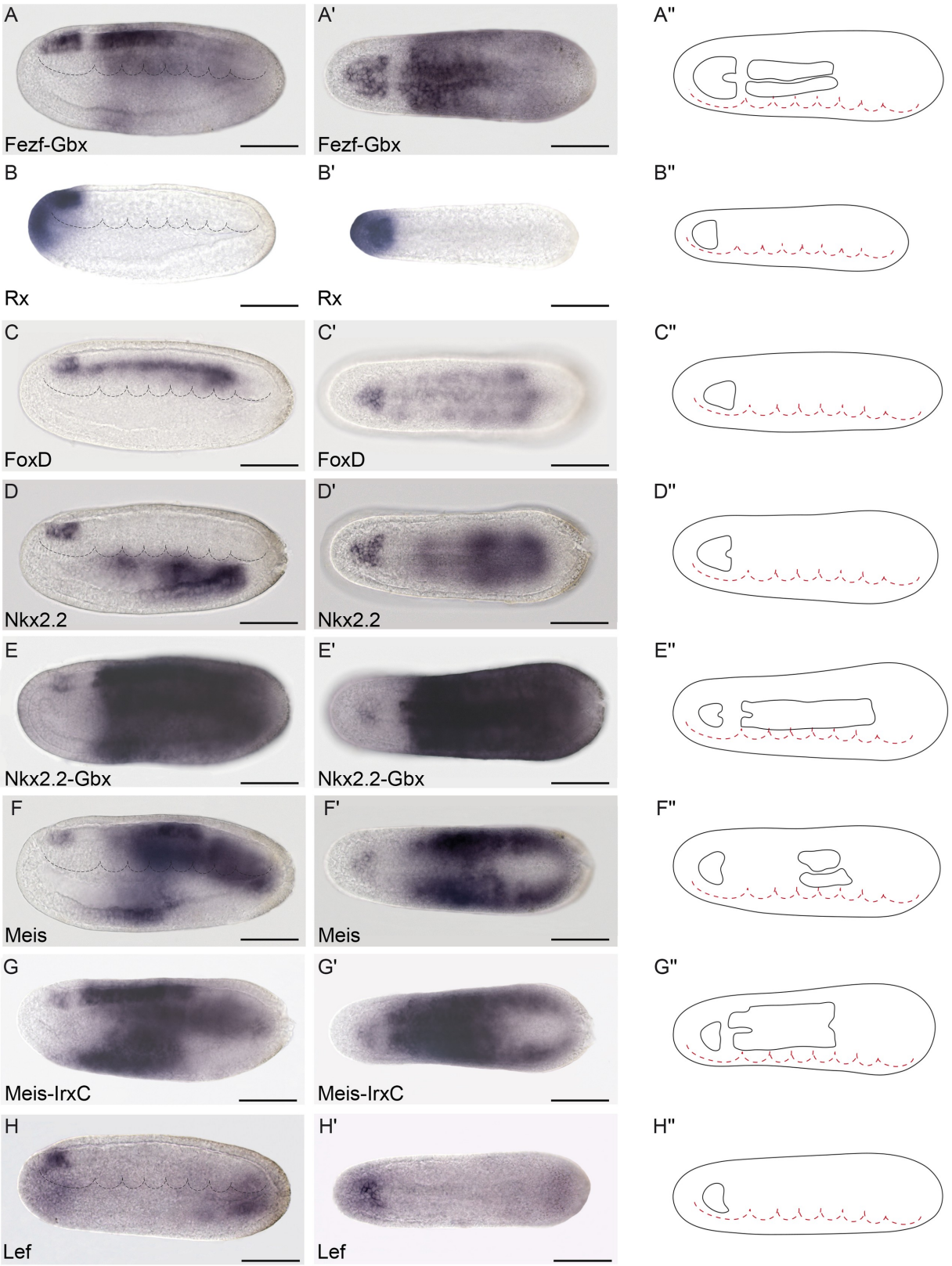

Fig 5. Genoarchitectonic signatures of the hypothalamo-prethalamic primordium (HyPTh) (I). (A-A″) Combined *Fezf-Gbx* expression defines a *Fezf*-positive rostral archencephalic prototagma (ARCH) territory identified as HyPTh (as per Fig 3K and 3L, for

reference). (**B-B″**) *Rx* is specifically expressed throughout the entire HyPTh primordium. (**C-C″**) Neural expression of *FoxD* was detected only in the basal and floor plates of HyPTh. (**D-E″**) *Nkx2.2* is expressed in the Rostral-HyPTh and Interm-HyPTh domains but not in Caudal-HyPTh (D-D″), as observed by a large gap in a double in situ hybridization for *Nkx2.2* and *Gbx* **(E-E″). (F-G″)** Similarly, *Meis* mRNA is only detected in the basal plate of the Rostral and Intermediate domains of HyPTh **(F-F″)**, leaving a gap of expression when combined with *IrxC* **(G-G″).** Further expression of *Meis* is also detected in specific deuteroencephalic prototagma (DEU) areas **(F-F″)**. **(H-H″)** *Lef* is expressed in the basal plate of Rostral-HyPTh and Interm-HyPTh. Expression patterns correspond to lateral **(A-H)** or dorsal views **(A′-H′)** at the 21 h post fertilization (hpf) embryonic stage and are represented in schematics dorsal views **(A″-H″)**. Somites (dotted lines) were used as main landmarks to localize the position of the patterns analyzed in the late neural plate. Scale bar: 50 μm.

https://doi.org/10.1371/journal.pbio.2001573.g005

one another. Interestingly, the intermediate domain, DiMes, is very small, consisting only of two rows of cells along the AP dimension (Fig 8A–8B″). Analogous fluorescent in situ hybridization comparison of *Fezf*, *Six3/6*, and *Gbx* patterns shows that *Six3/6* is also strongly expressed in the DiMes compartment (Fig 8C–8C″). The *Fezf* and *Gbx* markers are expressed with similar mutual relationships also at the 4/5-somite (early neurula) stage (S3A–S3B′ Fig), leaving an expression gap where weak *Six3/6* signal can already be detected (S3E–S3F′ Fig). Therefore, both the ARCH/DEU limit and the HyPTh and DiMes subdivisions within ARCH are established very early in amphioxus CNS development.

The HyPTh is divided into three AP domains

We next sought to identify further AP molecular partitions within the HyPTh and DiMes forebrain domains of the 7-somite neurula. Unlike the DiMes, for which we could not identify any molecular subdivision, eight examined markers showed restricted expression domains within HyPTh, sometimes limited to either alar or basal regions. Their combined pattern is consistent with the existence of three AP subdivisions within the HyPTh, which we termed Rostral HyPTh, Intermediate HyPTh and Caudal HyPTh (Rostral-HyPTh, Interm-HyPTh, Caudal-HyPTh; Fig 10A; see Discussion for possible homology relationships with partitions in the vertebrate forebrain). For instance, the expression of six rostral markers (*Nkx2.2*, *Nova*, *Meis*, *Pou3f*, *Lef*, *Lhx2/9b*) appears across Rostral-HyPTh and Interm-HyPTh, but seems to respect a transverse double row of cells that lie anterior to the *Irx*-expressing DiMes; topologically, this caudal negative domain of HyPTh (Caudal-HyPTh) would correspond in vertebrates to the primordium of the prethalamic region (Fig 10A). This partition can be visualized as a gap of negative labeling, e.g., by double in situ hybridization for *Meis* and *IrxC* or for *Nkx2.2* and *IrxB* (Figs 5G–5G′ and 8F–8F″, respectively).

While *Nkx2.2* and *Nova* signals are present at both alar and basal levels of Rostral-HyPTh and Interm-HyPTh (but not in the corresponding part of the floor plate; Fig 5D–5D″ and S3C–S3C″ Fig; see schematic details of expression in Fig 9), *Pou3f*, *Meis*, and *Lef* expression is restricted to the local basal region (also respecting the floor plate; Figs 4F–4F″, 5F–5F″ and 5H–5H″, respectively), and *Lhx2/9b* expression appears selectively in the peripheral alar region (Fig 6C–6C″). *Six3/6* is the only studied marker restricted to the Rostral-HyPTh, specifically in the alar plate (Figs 2J, 4D–4D″ and 8C–8C″; similar expression of *Six3/6* in the anterior-most part of the neural plate was also reported in *B. floridae* [81]). On the other hand, *Zic*, which is a well-known marker of the alar and roof plates in the CNS of vertebrates [95], is expressed throughout the presumptive alar plate of the HyPTh, but its expression is significantly stronger at the Caudal-HyPTh, showing decreasing signal towards the rostral alar parts of the HyPTh complex (S2G–S2G″ Fig). In contrast to the major HyPTh and DiMes partitions, the three HyPTh molecular subdivisions are not fully established at the 4/5-somite stage (S3 Fig).

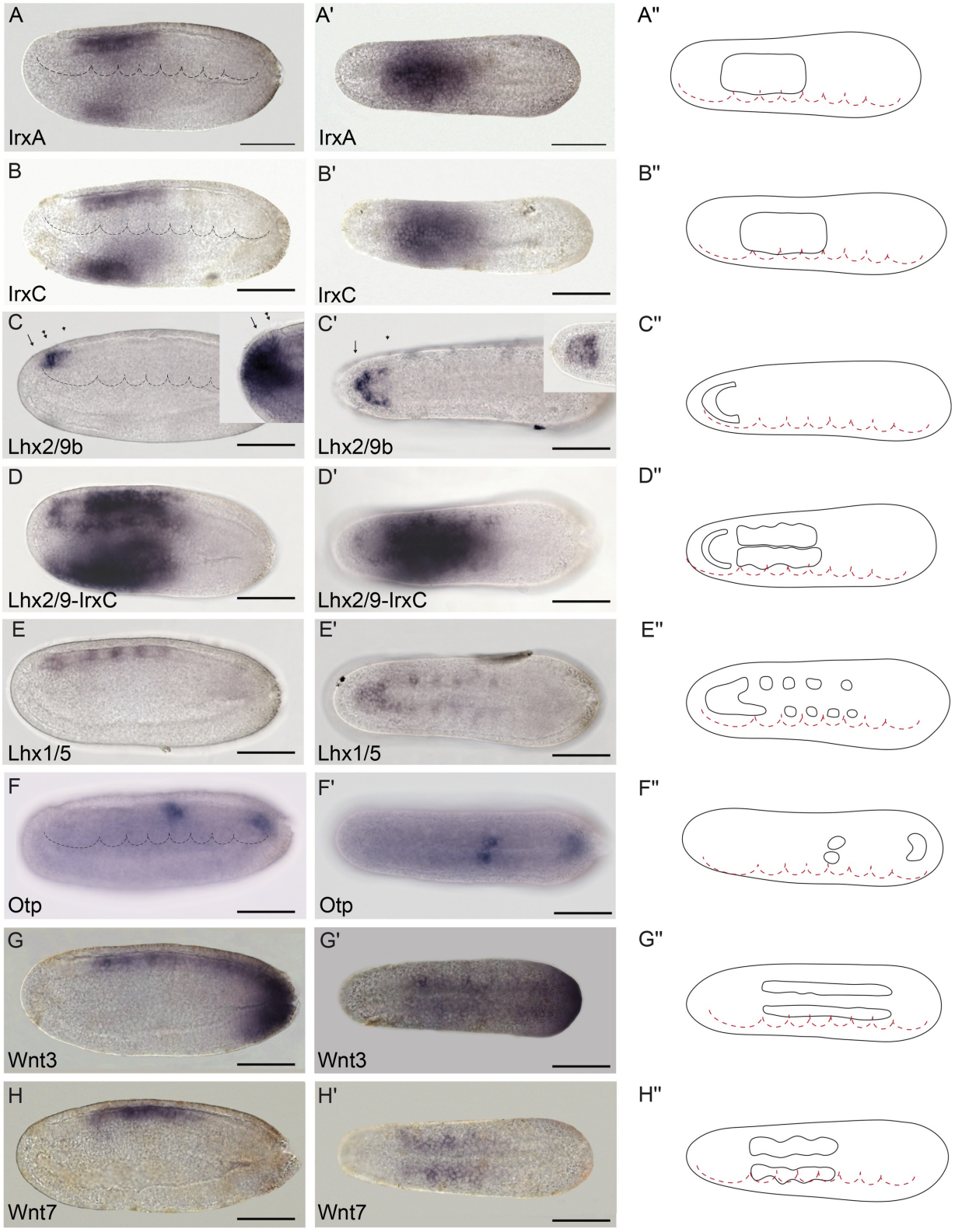

Fig 6. Genoarchitectonic signatures of the hypothalamo-prethalamic primordium (HyPTh) (II). (A-A″) *IrxA* mRNA expression is observed from the HyPTh/Di-Mesencephalic primordium (DiMes) boundary extending caudally to the rostral portion of the Rhombencephalo-Spinal primordium (RhSp) domain. **(B-B″)** *IrxC* mRNA expression is observed from the HyPTh/DiMes boundary, extending

caudally to the rostral portion of the RhSp domain. **(C-D″)** *Lhx2/9b* marks the alar plate in the Rostral-HyPTh and Intermediate-HyPTh domains **(C-C″)**, as shown by a gap of expression in a double in situ hybridization between *Lhx2/9b* and *IrxC* **(D-D″)**. The lateral view of *Six3/6* expression (inset in C) is provided for comparison with *Lhx2/9b* and highlights the restricted expression of *Six3/6* to the Rostral-HyPTh (compare the region between the arrow and the single arrowhead, which corresponds to the Rostral-HyPTh and Intermediate-HyPTh domains, with the region between the arrow and double arrowhead, which includes only the Rostral-HyPTh domain **(C,C′)**). On the other hand, a dorsal view of *Fezf* (inset in C′) shows expression across both the alar and basal plates of the HyPTh. **(E,E″)** *Lhx1/5* mRNA expression is observed only in the basal plate of the HyPTh and DiMes primordia and in some RhSp subdivisions (see inset in C′ for comparison). **(F-F″)** *Otp* is a key hypothalamic marker in vertebrates but was only found in amphioxus in one domain at the RhSp region. **(G-H″)** *Wnt3* and *Wnt7* mRNAs were detected from the DiMes/RhSp border, extending caudally in the entire RhSp region. Expression patterns correspond to lateral **(A-G)** or dorsal views **(A′-G′)** at the 21 h post fertilization (hpf) embryonic stage and are represented in schematics dorsal views **(A″-G″)**. Somites (dotted lines) were used as main landmarks to localize the position of the patterns analyzed in the late neural plate. Scale bar: 50 μm.

https://doi.org/10.1371/journal.pbio.2001573.g006

Anteroposterior regionalization of the amphioxus DEU domain

Numerous amphioxus genes have been previously reported to show iterative expression domains within the DEU, suggesting the existence of characteristic subdivisions within this partition ([96–99], and see S1 Table). Consistent with these studies, we identified several molecular AP partitions within the rostral-most subdomain of DEU, referred to here as the RhSp, which roughly ends caudal to the fifth somite at the 7-somite neurula stage (Figs 9C and 10A). *Gbx*, *Wnt3*, *Wnt7*, and *FoxB* appear selectively expressed throughout the RhSp; all of them abut rostrally the DiMes/RhSp boundary, and their expression domains end at different caudal levels, either coinciding with the end of somite five or extending further caudalwards (Figs 3E, 3F, 6G–6G″, 6H–6H″ and 7E–7E″). *Gbx*, *Wnt3*, and *Wnt7* occupy both alar and basal regions (but not the floor plate), as previously described [37,100,101], while *FoxB* is restricted to basal areas (Fig 7E; see also [102]). *Hox1*, *Hox3*, and *Hox6* genes are also expressed along alar and basal parts of the RhSp, with rostral expression borders that correspond with the intersomitic limits S3/S4, S4/S5, and S5/S6, respectively (Fig 7A–7C″; see also [53–57]). As mentioned above, these molecular partitions are complemented by patterns of iterated spots with negative intervals, which can be aligned with the center (*Lhx1/5* and *Pou3f*, Figs 6E–6E″ and 4F–4F″) or posterior half of the somites (*Nova*, S2C–S2C″ Fig) or the inter-somitic boundaries (*Pax3/7*, S2E–S2E″ Fig). In the case of *Pax2/5/8*, patches are less well defined, particularly caudally, where they become nearly continuous (Fig 7F–7F″). Finally, some genes show isolated spots of expression located at different positions within the RhSp AP subdivisions: *Msx* (Fig 7G–7G″), *Meis* (Fig 5F–5F″), *Zic* (S2G–S2G″ Fig), *Nkx6* (Fig 7D–7D″), and *Otp* (Fig 6F–6F″), sometimes correlating with the prospective position of the future pigmented photoreceptor spot.

Experimental suppression of the ZLI and IsO organizers in vertebrates alters di-mesencephalic patterning and generates a remnant that resembles the amphioxus DiMes

A major implication of our comparison of the overall CNS genoarchitecture between amphioxus and vertebrates is that the small amphioxus *Pax4/6*-positive DiMes corresponds topologically to the large vertebrate region comprising the thalamus, pretectum, and midbrain (Fig 10A–10B″, see Discussion). Patterning of this territory in vertebrates occurs under the dual control of the secondary brain organizers (ZLI and IsO, see Introduction), which induce the molecular subdivision and differential growth of an initially *Pax6*-positive primordium. Among other effects, these organizers inhibit the expression of *Pax6* at the two ends of the territory so that *Pax6* signal becomes restricted to the caudal pretectum (p1) and the epithalamus (dorsal-most part of p2)(Fig 11C′). Accordingly, we hypothesized that the small size and the

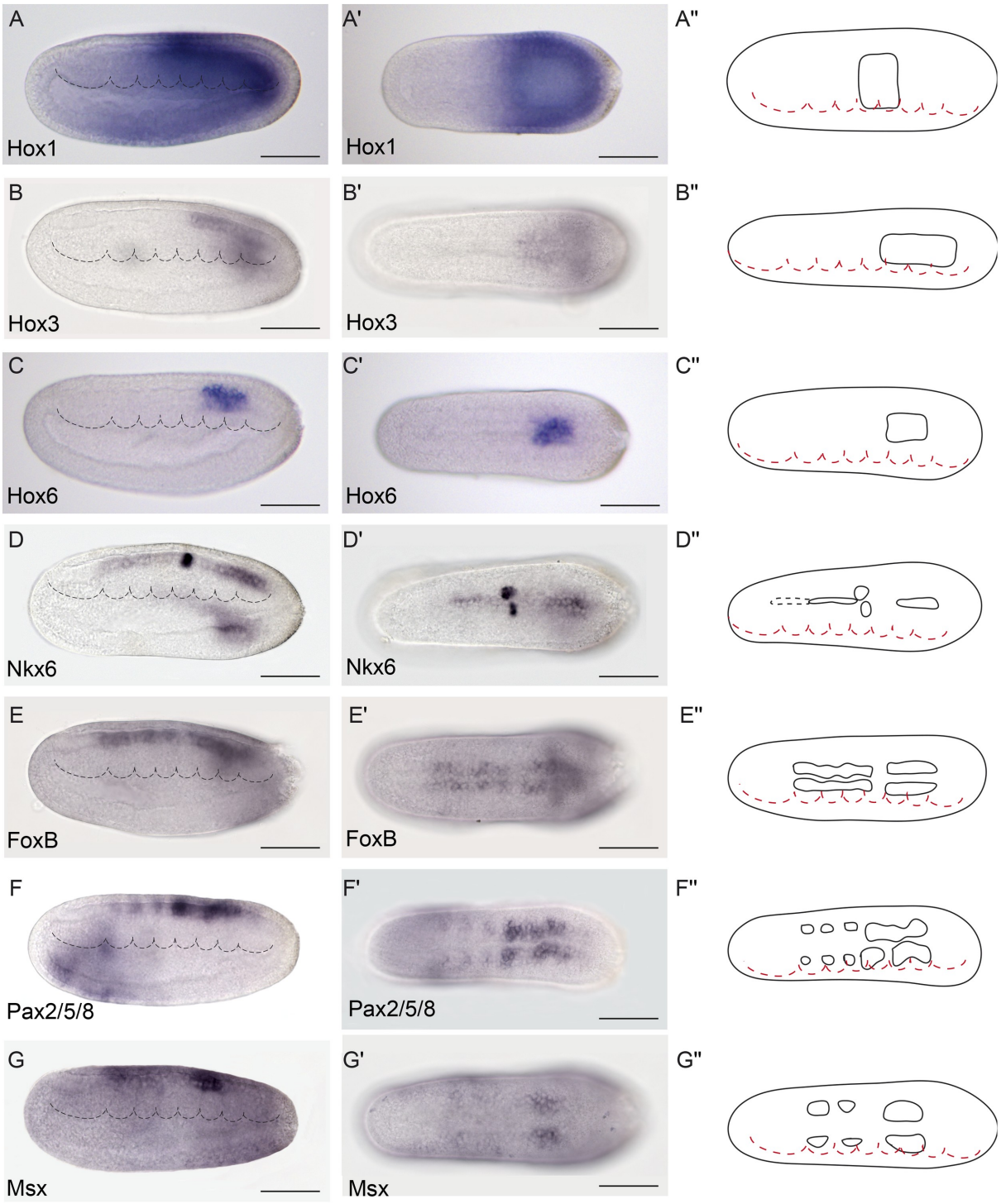

Fig 7. Genoarchitectonic signatures of the Rhombencephalo-Spinal primordium (RhSp). (A-C′′). *Hox1*, *Hox3*, and *Hox6* were expressed in the alar and basal plates of some caudal domains of the RhSp region in a sequential rostro-caudal order. **(D-D′′)** *Nkx6* was detected at different degrees of expression mainly at the floor plate of the Di-Mesencephalic primordium (DiMes) and RhSp domains and a localized bilateral spot at the equivalent position of the fifth somite. **(E-E´´)** *FoxB* mRNA was observed extending caudally from the DiMes/RhSp border into the basal plate of the entire RhSp region. **(F-G´´)** *Pax2/5/8* and *Msx* mRNAs were detected in some patches in the alar plate of the RhSp region. Expression patterns correspond to lateral **(A-G)** or dorsal views **(A′-G′)** at the 21 h post fertilization (hpf) embryonic stage, and are represented in schematics dorsal views **(A′′-G′′)**. Somites (dotted lines) were used as main landmarks to localize the position of the patterns analyzed in the late neural plate. Scale bar: 50 μm.

https://doi.org/10.1371/journal.pbio.2001573.g007

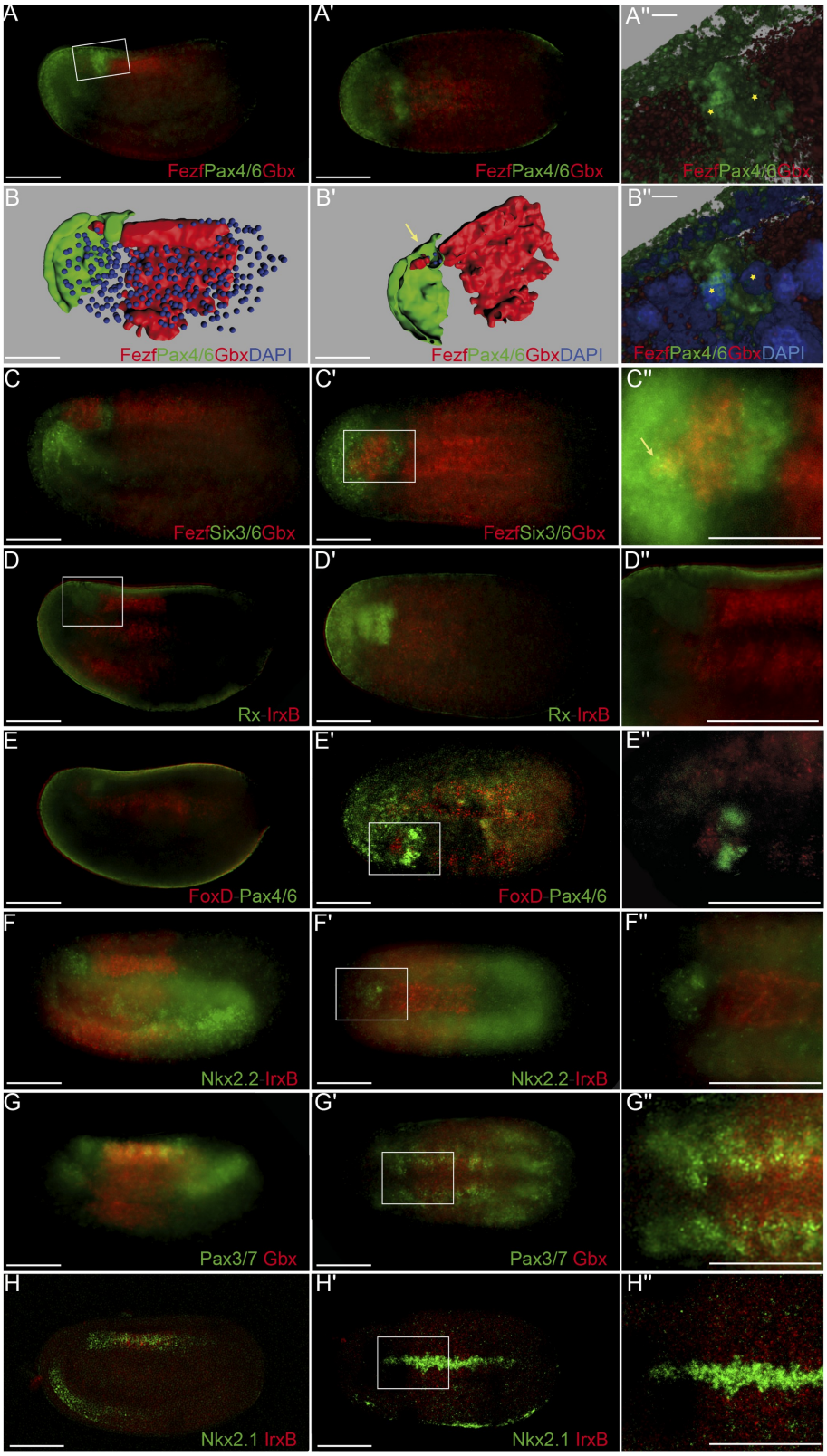

Fig 8. Precise genetic boundaries define three major anteroposterior (AP) partitions. (A-B″) Triple fluorescent in situ hybridization combining *Fezf-Pax4/6-Gbx* in lateral **(A)** and dorsal views **(A′)** reveals clear-cut boundaries between the hypothalamo–prethalamic primordium (HyPTh) *Fezf*+, the Di-Mesencephalic

primordium (DiMes) *Pax4/6*+, and the Rhombencephalo-Spinal primordium (RhSp) *Gbx*+ regions; details are summarized in a 3-D reconstruction **(B,B′)**. A magnified view of *Pax4/6* expression combined with DAPI showed that the DiMes domain consists of two rows of cells along the AP axis (asterisks)**(A″,B″). (C-C″)** Triple fluorescent in situ hybridization combining *Fezf-Six3/6-Gbx* probes in lateral **(C)** and dorsal views **(C′)** confirms a rostral *Fezf* + domain (HyPTh), a caudal *Gbx*+ domain (RhSp), and a double-negative domain in between characterized by *Six3/6* expression (DiMes). A magnified view **(C″)** helps to visualize a rostral domain with *Six3/6* and *Fezf* coexpression (yellow staining, arrow) that we identified as the Rostral-HyPTh domain. **(D-D″)** Double fluorescent in situ hybridization combining *Rx* and *IrxB* probes in lateral **(D)** and dorsal views **(D′)** show that *Rx* is expressed in the entire HyPTh territory, stopping caudally at the HyPTh/DiMes boundary; details can be observed in the magnified view **(D″)**. **(E-E″)** Double fluorescent in situ hybridization combining *FoxD* and *Pax4/6* probes in lateral **(E)**, dorsal **(E′),** and magnified dorsal **(E″)** views shows that the small territory expressing *FoxD* corresponds to the basal plate of the entire HyPTh primordium, stopping caudally at the DiMes border. **(F-F″)** Double fluorescent in situ hybridization combining *Nk2.2* and *IrxB* probes in lateral **(F),** dorsal **(F′),** and magnified dorsal **(F″)** views determines that *Nk2.2* is expressed only in the alar and basal plate of the Rostral-HyPTh and Intermediate-HyPTh domains, leaving a negative gap corresponding to the Caudal-HyPTh domain. **(G-G′)** Double fluorescent in situ hybridization combining *Pax3/7* and *Gbx* probes identifies patches of *Pax3/7* expression in the Caudal-HyPTh domain. **(H,H′)** Double fluorescent in situ hybridization combining *Nkx2.1* and *IrxB* probes shows that *Nk2.1* expression in the floor plate extends rostrally beyond the HyPTh/DiMes boundary. Scale bar in A-H′: 50 μm except A″ and B″, scale bar: 5 μm.

https://doi.org/10.1371/journal.pbio.2001573.g008

lack of internal regionalization of the DiMes, particularly with respect to *Pax4/6* expression, may be, at least in part, related to the absence of ZLI-like and IsO-like effects in amphioxus.

To gather support for this hypothesis, we turned first to loss-of-function transgenic mouse lines in which either the ZLI or the IsO are absent. Double *Fezf1*$^{-/-}$*Fezf2*$^{-/-}$ mutants [103] lack the ZLI organizer and largely lose the molecular identity of the alar thalamic field, displaying expanded expression of the pretectal markers *Pax6*$^{+}$ and *Ebf1*$^{+}$ (Fig 11B and 11B′–11B′′′′); the midbrain was not altered in these mice. We also studied *En1*$^{cre/+}$*; Fgf8*$^{flox/flox}$ mice (see Materials and Methods) in which the IsO is deleted across the MHB [104]. The resulting phenotype showed a reduction of the AP dimension of the pretecto-mesencephalic region down to one-third of its normal size and an abnormal caudal expansion of PAX6 immunoreaction (as well as of the posterior commissure), suggesting a lack of differential specification of the midbrain versus the pretectum (Fig 11C and 11C′–11C′′′′); in this case, the thalamus seemed normal.

Next, we tried to eliminate both the ZLI and the IsO together in zebrafish, using quadruple morpholino (4MO) treatment against *otx1a*, *otx2*, *eng2a*, and *eng2b*. Although effects in neural progenitors of other areas cannot be ruled out, double morpholinos against *otx1a* and *otx2* were successfully used previously to specifically abolish the ZLI [105], while double morpholino treatment against *eng2a* and *eng2b* caused the loss of the IsO [106], and expression of *pax6a* throughout the midbrain remnant [107]. Strikingly, the normal *pax6a*-negative gaps corresponding to the alar plate of the midbrain and diencephalic thalamus were abolished or severely reduced in nearly all (84%) 4MO specimens tested (Fig 11F; $n = 75$, $p = 3.84 \times 10^{-31}$, one-sided Fisher Exact test), often resulting in a continuous expression of *pax6a* between the rostral conserved part of the forebrain and the hindbrain (Fig 11G, 11H, 11K and 11L and sagittal sections in insets in Fig 11H and 11L). Supporting the effective suppression of the two organizers in this experiment, we observed disappearance of the dorsal ZLI spike expression of *shha* and of the MHB-related transverse band of *wnt1* expression (Fig 11D, 11E, 11H, 11I, 11L and 11M). In addition, all 4MO embryos showed a significant reduction of the zebrafish DiMes-like remnant at 28 h post fertilization (hpf) compared to the controls (Fig 11G′ and 11K′).

Discussion

Previous studies using gene markers have shown that the developing amphioxus CNS displays marked spatial molecular heterogeneity at different developmental stages ([61,97,102,108–112] and see S1 Table). However, most of these studies focused on individual genes across

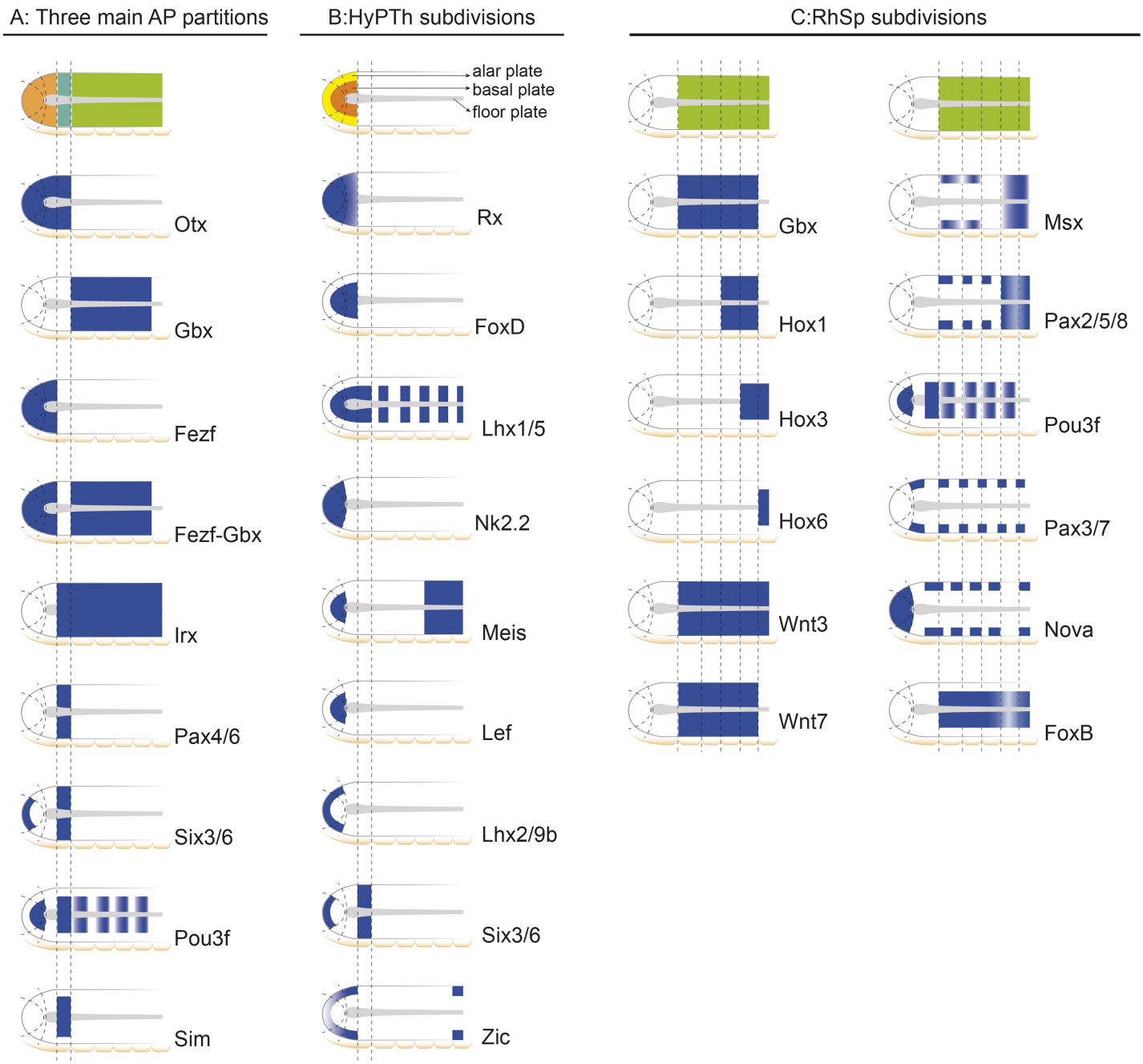

Fig 9. Schematic representation of informative markers used in this study. (A) Main tagmata and Hypothalamo-Prethalamic (HyPTh), Di-Mesencephalic (DiMes), and Rhombencephalo-Spinal (RhSp) primordia. **(B)** HyPTh internal subdivisions. **(C)** RhSp internal subdivisions.

https://doi.org/10.1371/journal.pbio.2001573.g009

diverse developmental time points, making it difficult to precisely compare the relative positions of their expression patterns and to elaborate a unified map. In this study, we built a comprehensive genoarchitectonic model of the amphioxus developing CNS by mapping many gene markers at a single developmental stage, allowing homochronic comparisons of gene expression patterns. We used 48 gene markers whose orthologs have known expression patterns in the developing vertebrate CNS and a well-established morphological interpretation within an explicit Bauplan (the updated prosomeric model [2,4]). We focused primarily on the

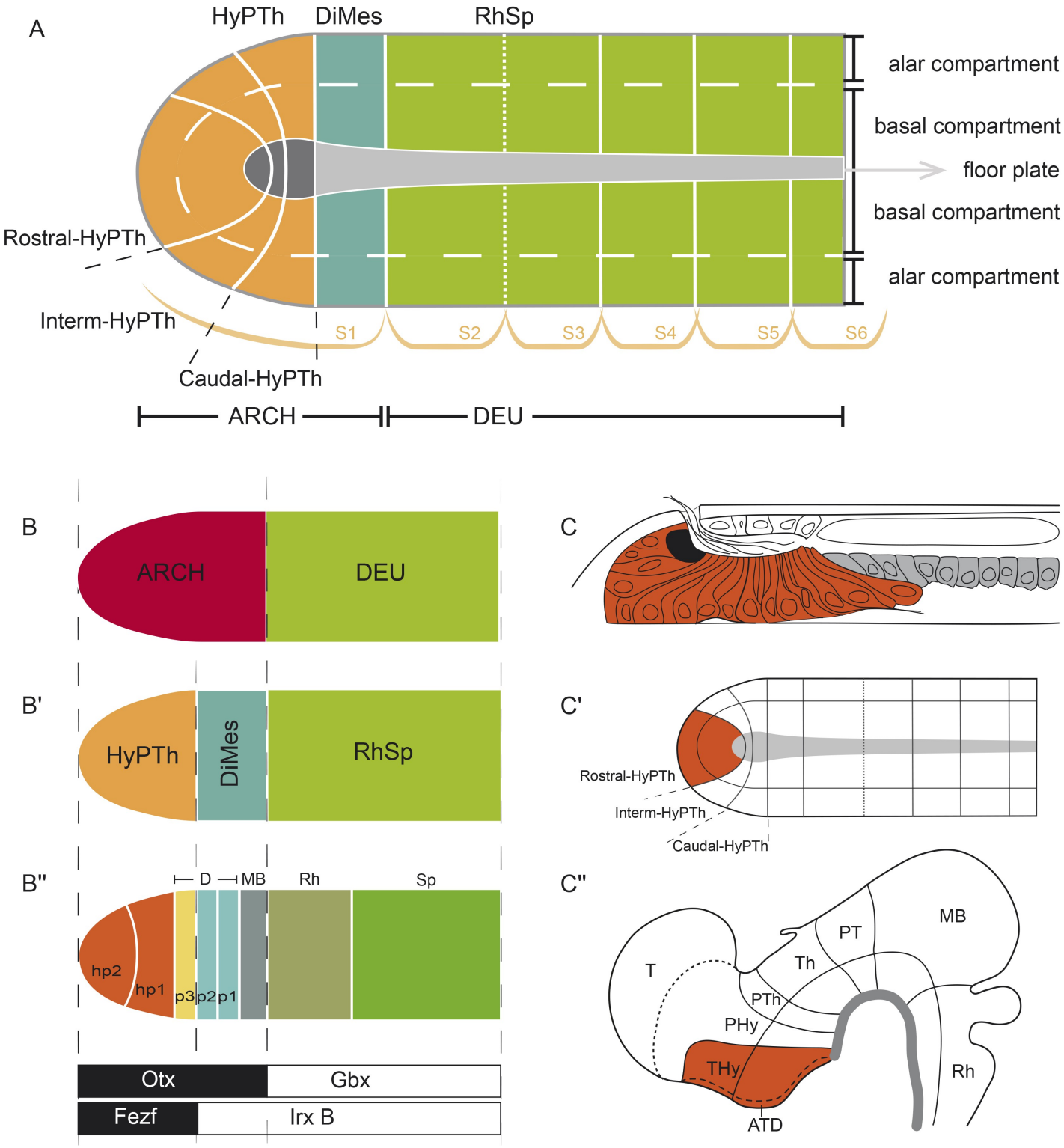

Fig 10. Genoarchitectonic model of the developing central nervous system (CNS) at the amphioxus 7-somite neurula stage. (A) Summary of all identified anteroposterior (AP) and dorsoventral (DV) partitions of the neural plate of amphioxus. (**B-B″**) Topological comparison of major molecular subdivisions between cephalochordates and vertebrates. (**C,C′**) Neural plate model highlighting the basal and alar plates of Rostral-hypothalamo–prethalamic primordium (Rostral-HyPTh) (orange) and the whole floor plate domain (gray) and its correspondence in a late larval stage (adapted from [90]). (**C″**) Vertebrate neural tube highlighting the Terminal-Hypothalamic prosomere (orange) and the whole floor plate (grey).

https://doi.org/10.1371/journal.pbio.2001573.g010

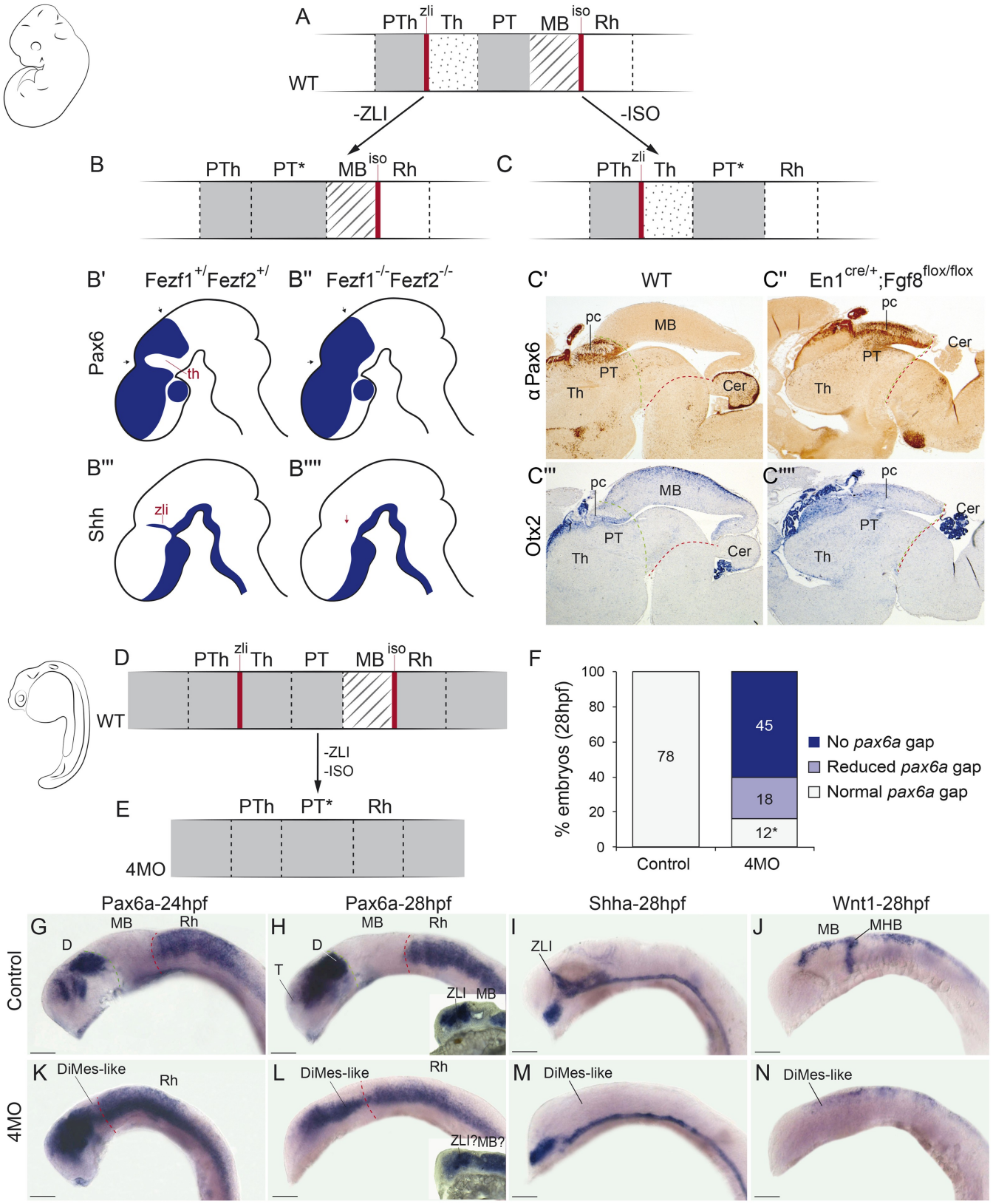

Fig 11. Experimental disruption of secondary organizers in vertebrates results in a Di-Mesencephalic primordium (DiMes)-like remnant. **(A-C)** A schematic representation of mouse *Pax6* neural expression pattern (solid grey) in wild-type condition (WT) **(A)** and abolishing the function

of the zona limitans intrathalamica (ZLI) **(B)** or isthmic organizers (IsO) **(C)**. (**B′-B′′′′**) Drawings adapted from the results of Hirata et al. 2006 upon ZLI abrogation during mouse development. (**C′-C′′**) Immunohistochemical detection of αPax6. (**C′′′-C′′′′**) In situ hybridizations for *Otx*. **(C′)** and **(C′′′)** are WT expression domains of *Pax6* and *Otx*, whereas **(C′′)** and **(C′′′′)** are conditional *En2-Fgf8* knockout (KO) mice. (**D,E**) Schematic representation of *pax6a* gene expression (solid grey) in zebrafish embryos in WT **(D)** or quadruple morpholino knockdown (4MO) of *otx1a*, *otx2*, *eng2a*, and *eng2b* **(E)** conditions. (**F**) Quantification of the phenotypes observed upon 4MO treatment. All treated embryos showed a reduction in the size of the gap, even those scored as normal (indicated by an asterisk). Embryos with "reduced *pax6a* gap" showed only a very small expression gap, often with weak *pax6a* expression in it. Embryos with "no *pax6a* gap" had a continuous expression of the gene. (**G-N**) Expression patterns of key genes in WT **(G-J)** or 4MO **(K-N)** embryos. Insets in H and L showed sagittal sections of a different representative embryo. Sections of the indicated embryos. Abbreviations: Cer, cerebellum; D, diencephalon; Rh, rhombencephalon; pc, posterior commissure; pTh, prethalamus; Th, thalamus; PT, pretectum; MB, midbrain; MHB, midbrain–hindbrain boundary; T, telencephalon. Anterior is to the left. Scale bar = 100 μm.

https://doi.org/10.1371/journal.pbio.2001573.g011

7-somite neurula stage, in which the majority (43/48, 89.6%) of the examined gene markers were expressed in the incipient neural tube. By the combination of these gene markers, we propose a genoarchitectonic model that, although simpler than that of vertebrates, reveals an unexpected complexity of molecularly defined regions in the developing amphioxus CNS, comprising at least nine AP and three distinct DV partitions (Fig 10). This model provides a base for future exploration of the development of the amphioxus CNS at earlier and later developmental stages and should help in elucidating the ontogenetic origins of larval and adult brain structures. Furthermore, it allows direct topological comparisons with equivalent genoarchitectonic models in vertebrates, since both lineages develop their CNS through homologous neural plates, providing more solid evidence for homology assignments between topologically equivalent regions than mere similarities of relative gene expression patterns.

Integrative genoarchitectonic model of the amphioxus incipient neural tube

Consistent with previous results [37,59,64], our data show that the incipient amphioxus neural tube is molecularly divided anteroposteriorly into a rostral archencephalic (ARCH) and a caudal deuterencephalic (DEU) portions from very early stages, similarly to vertebrates (Fig 10A and 10B). Traditionally, three main AP divisions are defined in the vertebrate ARCH (Fig 1): the secondary prosencephalon (encompassing hypothalamus plus telencephalon), the diencephalon, and the midbrain. On the contrary, the ARCH of amphioxus shows only two main divisions, which we termed DiMes and HyPTh (Fig 10B). DiMes is a small caudal region consisting of two rows of cells that occupies the topological position corresponding in vertebrates to the midbrain and the two diencephalic segments that lie caudal to the ZLI organizer; no internal subdivisions were detected within DiMes. In contrast, the HyPTh encompasses three molecularly distinct segments: a relatively large, bipartite, putative hypothalamus-homolog region (where neither telencephalic nor optic vesicles are present [113]) plus a caudal region that occupies the topological position corresponding to the vertebrate prethalamus. In the case of the DEU, its rostral portion, referred to here as RhSp primordium, may represent a field-homolog of the vertebrate hindbrain, and shows a number of gene expression patterns that configure periodic segment-like territories (Fig 9C).

Notably, these major AP partitions of the developing CNS are mirrored by molecularly defined subdivisions in the underlying axial mesoderm. Indeed, we provide evidence that the distinct molecular entity at the rostral tip of the amphioxus notochord may be homologous to the vertebrate prechordal plate, being thus essentially different from the notochord proper that underlies the brain floor plate (Fig 2). This potentially prechordal region lies topologically rostral to the HyPTh (not **under** it), as occurs with the prechordal plate in vertebrates [2,4], and is characterized by the absence of *Hh* and *Nkx6* and the specific expression of *Six3/6*, which is also characteristic of the vertebrate prechordal plate [24]. Therefore, it is possible that this

special notochord-looking region—which also shows unusual proliferation and rostralward growth [70,114]—may correspond to a variant prechordal plate homolog and/or plays partly equivalent signaling functions to this structure in amphioxus, despite the absence of some key vertebrate prechordal markers (*Gsc*, noggin, and chordin [79,115]).

Finally, regarding DV patterning, multiple markers provide extensive evidence for continuous molecularly distinct floor, basal, and alar zones throughout the length of the incipient neural tube (Figs 9 and 10). Although we did not find selective markers for the roof plate, it is possible that these may exist at later stages, upon neural tube closure. Consistent with the idea that the alar plate and roof plate are not differentially specified in amphioxus at these stages, orthologs of several vertebrate neural plate border makers (e.g., *Pax3/7*, *Msx*, and *Zic*) were found to be expressed broadly in the alar plate (Fig 9; observed also in *B. floridae* [116]).

Possible homology relationships between HyPTh partitions and vertebrate forebrain neuromeres

According to the updated prosomeric model [4], the nontelencephalic part of the vertebrate secondary prosencephalon can be subdivided into two main neuromeres: terminal (THy, hp2) and peduncular (PHy, hp1) hypothalamic prosomeres. In addition, THy includes a specialized rostral-most median part extending dorsoventrally, the acroterminal area [2,4,117](Fig 10C″). This molecularly distinct domain produces a number of specialized formations along the DV axis, including the alar preoptic lamina terminalis, the optic chiasma, the eye vesicles, the basal median eminence, and the neurohypophysis.

In amphioxus, HyPTh represents a relatively large, molecularly distinct forebrain region lying rostral to the DiMes. This domain has specific expression of *Fezf* throughout (Fig 9), which is also absent caudal to the ZLI limit in vertebrates [93,103,118]. Our analysis suggests that there are three molecularly distinct AP subdivisions within the amphioxus HyPTh, which we termed Rostral-HyPTh, Interm-HyPTh, and Caudal-HyPTh. By direct topological ascription, these might correspond, respectively, to the transverse THy (including a rostromedian acroterminal region) and PHy hypothalamic segments and a prethalamus-like segment next to the DiMes.

Six3/6 was the only studied marker that selectively labeled Rostral-HyPTh. Remarkably, in mice, *Six3* is expressed extensively dorsoventrally across the alar and basal zones of THy (including the acroterminal area), whereas *Six6* signal is restricted to a ventral suprachiasmatic part of the THy acroterminal alar plate, but none of them are expressed at PHy [2,117]. These data support a genetic equivalence between the Rostral-HyPTh and THy, in addition to their topological correspondence. Moreover, amphioxus develops in its acroterminal region (orange domain in Fig 10C and 10C′) a median primordial eye patch and, ventral to it, a median group of "infundibular cells" [90], which are located above the most anterior floor plate cells (gray cells in Fig 10C) and might represent a homologue of the vertebrate neurohypophysis. As mentioned above, in vertebrates, both the eyes and the neurohypophysis develop from the acroterminal area [2], further supporting the homology of vertebrate and amphioxus acroterminal domains and thus of Rostral-HyPTh and THy (Fig 10C–10C″).

In the case of the Caudal-HyPTh primordium, its topological position, lying directly rostral to the *Fezf-Irx* boundary, provides grounds to suggest field homology with the vertebrate prethalamus. Importantly, previous studies indicate that *Fezf* genes are essential to specify the prethalamic domain in vertebrates; however, unlike regions within the vertebrate DiMes counterpart (see below), this specification is independent of the ZLI organizing activity and occurs prior to its formation [93,103] and is thus compatible with the amphioxus scenario at the examined stage. Nonetheless, it should be noted that, although more weakly expressed, the

presence of *Rx* expression in Caudal-HyPTh (absent in the prethalamus of vertebrates [118]), suggests the alternative possibility that this partition may represent a primordium homolog to both the peduncular hypothalamus and prethalamic region.

Close developmental and evolutionary relationship of thalamus, pretectum, and midbrain

One of the most striking implications of our results is that the small, *Pax4/6*-positive DiMes of amphioxus corresponds topologically to the region comprising the vertebrate thalamus, pretectum, and midbrain (Fig 10). While this area is not subdivided in amphioxus and consists only of two cell rows at the neurula stage, the equivalent vertebrate region shows three major partitions and extensive cell proliferation. These partitions in vertebrates originate during development as a consequence of the action of the secondary brain organizers on a *Pax6*-positive primordium. In particular, *Shh* signaling from the ZLI is crucial for the specification of the thalamus [6–8,119], and *Fgf8* and *Wnt1* expression from the IsO are necessary for proper midbrain specification and differential caudal growth [5,10,12,13,120–123]. Moreover, due to the action of these organizers, the expression of *Pax6* in this primordium is mainly restricted to the pretectum and the epithalamus and becomes absent in the ventricular zone of the thalamus and midbrain (Fig 11) [124,125].

Therefore, altogether, these data suggest that the vertebrate thalamus, pretectum, and midbrain share a common origin, both ontogenetically (from an early and transient *Pax6*-positive area found between the prospective ZLI and IsO levels) and phylogenetically (homologous to the amphioxus DiMes region). This hypothesis has two major implications for our understanding of the vertebrate brain Bauplan and its evolutionary origins. First, it implies that two of the diencephalic prosomeres—pretectum (p1) and thalamus (p2)—are more evolutionarily related to the midbrain than they are to the third diencephalic prosomere—the prethalamus (p3)—which would, in turn, be more related with the secondary prosencephalon (see previous section). That is, the diencephalon proper would be neither an evolutionarily nor an ontogenetically primordial subdivision of the vertebrate brain. This striking implication is further supported by the differential responses of these regions to experimental manipulation of the organizers and their associated signaling molecules. Chicken-quail heterotopic grafts of the ZLI, as well as focalized ectopic expression of *SHH* using beads in chicken embryos, show that only pretectum and midbrain, but not the prethalamus, are competent to be re-patterned to a thalamic fate [6,7,119]. Similarly, quail-chick, rat-chick, or mouse-chick heterotopic grafts of the IsO generate an ectopic midbrain in pretectal and thalamic regions, but never in the prethalamus and secondary prosencephalon [126–129]. That is, thalamus, pretectum, and midbrain have similar developmental potentials that are not shared by the prethalamus. In fact, our hypothesis provides a plausible ontogenetic explanation that has long been missing for these intriguing observations, underscoring its explanatory power.

A second major related implication of our hypothesis is that the vertebrate thalamus, pretectum, and midbrain jointly share altogether a common ancestor with the amphioxus DiMes. Since neither *Hh* nor *Fgf8* and *Wnt1*, the key morphogens involved in ZLI and IsO activity, respectively, are expressed at the corresponding topological positions in amphioxus [40,69,130–132], it is plausible to speculate that vertebrate thalamus, pretectum, and midbrain partitions may have emerged evolutionarily from an ancestral *Pax4/6*-positive DiMes-like region concomitantly to the evolution of the ZLI and IsO brain organizers as orthogonal signaling centers. Alternatively, the undivided, small amphioxus DiMes may represent an evolutionary simplification upon the loss of the organizers [47,48], if they were already patterning the neural plate-derived CNS of the last common ancestor of chordates. Irrespectively, a major

prediction of both evolutionary hypotheses is that suppression of the organizers during vertebrate development should result in a (relatively) homogeneous, smaller, undivided, and fully *Pax6*-positive region lying between recognizable prethalamus and hindbrain, as we observed in mouse and zebrafish embryos with suppressed ZLI and/or IsO (Fig 11, and see also [103,107,133–136]). Although the converse experiment—the induction of ectopic organizers in amphioxus—is still not technically possible, future methodological developments could allow assessing if and how the DiMes may respond to these morphogens.

Finally, an independent line of evidence supporting the functional homology between the amphioxus DiMes and the corresponding vertebrate regions comes from the retinal projections in the two lineages. In vertebrates, primary eye projections target mainly the midbrain (optic tectum/superior colliculus), while secondary eye projections target mainly the pretectum and thalamus and, to a lesser extent, prethalamus and hypothalamus [137]. In amphioxus, projections from the single frontal eye have recently been mapped to a *Pax4/6*-positive region in the four gill slit larval stage [138], which likely corresponds to a DiMes derivative based on its topological position and *Pax4/6* expression.

Concluding remarks

Our comprehensive genoarchitectonic model of the developing amphioxus CNS at mid-neurula stage sheds new light onto the origins of the vertebrate brain. First, it shows that the basic blueprint of the vertebrate brain Bauplan was already present in the last common ancestor of chordates. The major AP and DV partitions identified in amphioxus have direct topological correspondence with vertebrate counterparts, even though these may be further elaborated in vertebrates. Such is the case of the eye vesicles and the telencephalon developing as alar expansions of a HyPTh-like region or the growth and regionalization of a DiMes-like region into thalamus, pretectum, and mesencephalon. Secondly, it highlights the importance of the evolution of secondary organizers in the gain or loss of brain partitions. Thirdly, it allowed us to propose novel homologies between amphioxus and vertebrate structures, such as the acroterminal hypothalamic area and the prechordal plate. Finally, it casts doubts on the relevance of the classic separation between forebrain and midbrain in vertebrates from an evolutionary and developmental perspective, suggesting that a redefinition of the main AP regions into which the vertebrate brain is classically divided (forebrain, midbrain, and hindbrain) could provide a better conceptual framework to understand the origins of the vertebrate brain.

Materials and methods

Ethics statement

All animal work in this study has been conducted following the Spanish and European legislation. Adult fish were only used to obtain eggs through natural mating (ethical committee approval number: 635/2014). All mouse experiments were performed according to protocols approved by the Universidad Miguel Hernandez OEP committee (UMH.IN.EP.01.13) and Conselleria Generalitat Valenciana (2014/VSC/PEA/00055). Chicken experiments were performed according to protocols approved by the ethical committee from the University of Murcia (137/2015).

Gene annotation and cloning

For all the previously annotated genes in the *B. floridae* genome, primer pairs were designed to span the full-length coding sequence when possible. A liquid cDNA library from different developmental stages of the European amphioxus (*B. lanceolatum*) was screened by PCR using

B. floridae specific primers. For previously unannotated genes, we performed tBLASTN searches in the *B. floridae* JGI v1.0 genome, using the aminoacidic sequences of the vertebrate orthologs. The corresponding genomic sequences were retrieved and a gene model was predicted by GeneWise2 and GeneScan, as previously described [139]. Cloned *B. lanceolatum* mRNAs used for in situ hybridization are available in S2 Table.

Amphioxus embryo collection, whole-mount in situ hybridization, and histology

Ripe adult amphioxus specimens were collected in Argelès-sur-mer, France. Spawning was induced as previously described [140] in a dry laboratory in Barcelona, Spain. After in vitro fertilization, embryos were cultured at 18 ºC for 15 h or 21 h (4/5 somite and 7 somite stages, respectively) and fixed with 4% PFA in MOPS buffer overnight at 4˚C.

Chromogenic whole-mount in situ hybridization was performed as previously described [36] using Nitrobluetetrazolium/bromochloroindolyl phosphate (NBT/BCIP) or BMP purple (Roche) as chromogenic substrate for the final alkaline phosphatase. Following whole-mount in situ hybridization, selected embryos were embedded in a 0.1 M PBS solution with 15% gelatine and 20% sucrose, frozen in isopentane, and sectioned with a cryostat at 12–14 μm-thick. Double-fluorescent in situ hybridizations were performed essentially as nonfluorescent in situ hybridizations, as described in [141] with two extra steps of incubation in 5% NAC and (50 mM DTT, 1% NP40, 0.5% SDS) in PBS1X before the hybridization step.

Dinitrophenol (DNP)-labeled antisense riboprobes were synthesized using DNP-11-UTP labeling reagent (PerkinElmer), and DIG-labeled antisense riboprobes were synthesized using DIG RNA labeling mix (Roche). Labeled riboprobes were detected using anti-DNP-POD (Perkin Elmer) and anti-DIG-POD (Roche) antibodies, and green and red fluorescent signals amplified with TSA -Plus -Fluorescein and Tetrarhodamine systems (Perkin Elmer), respectively.

Images were acquired using a Leica TCS-SPII confocal microscope or a Zeiss Axiophot. Confocal datasets were deconvolved with Huygens Professional version 16.05 (Scientific Volume Imaging, The Netherlands, http://svi.nl), analyzed, and assembled with ImageJ; for panels B and B′ in Fig 8, images were further processed with Imaris (7.2.3, Bitplane AG, software available at http://bitplane.com).

Fish husbandry, morpholino treatments, and in situ hybridization in zebrafish embryos

Breeding zebrafish (*Danio rerio*) were maintained at 28˚C on a 14 h light/10 h dark cycle as described in [142]. To disrupt the ZLI and IsO secondary organizers together, we performed a quadruple transient knockdown using four morpholino-antisense oligomers (MOs) that had been previously described to abolish each of the organizers individually: *otx1a* and *otx2* MO's for the ZLI [105], and *eng2a* and *eng2b* for the IsO [106]. As injection controls, we used a combination of the two nontargeting MOs that were used in the original articles (a morpholino-sense oligomer against *twhh* (Cont1) [105] and a standard control MO (Cont2) [106]). The combination of experiment or control MOs was injected at the one-cell stage into the yolk at the following concentrations (based on the original sources): *otx1a* (0.25 mM), *otx2* (0.25 mM), *eng2a* (0.5 mM), *eng2b* (0.5 mM), Cont1 (0.5 mM), Cont2 (1 mM). Each embryo was injected with 1.5 nl of the MO mix (injection of 1.0 nl produced similar, yet milder, phenotypes, whereas injection of 2.0 nl resulted in full mortality). Four independent experiments were performed (in different days), injecting approximately 100 eggs per condition and experiment.

Injected embryos were fixed in 4% PFA overnight at 4 ºC and used for whole-mount in situ hybridization as previously described [143]. A subset of stained embryos was cryosectioned, and both sections and whole embryos were mounted in 80% glycerol-PBS and photographed in a Zeiss Axiophot microscope. The full list of probe sequences is available in S3 Table.

Analysis of gene knockouts in mice

The *Fgf8* conditional mutant was generated by the Gail R. Martin laboratory [120], and the transgenic mouse line expressing *cre* under the *En1* promoter was generated in the Dr. Wolfgang Wurst laboratory [144]. Mutant embryos were generated by crossing double heterozygous males ($En1^{cre/+}$; $Fgf8^{flox/+}$) with homozygous $Fgf8^{flox/flox}$ conditional females. Immunohistochemistry (PAX-6) and in situ hybridization (*Otx2*) in paraffin sections were performed as previously described [145]. The primary PAX-6 rabbit polyclonal IgG antibody was diluted in PBTG (1:500; PRB-278P/Covance). The *Otx2* probe was synthesized as in [86].

In situ hybridization in chicken embryos

All the procedures involving extraction of brain samples and further tissue processing were done as previously described [146]. Fertilized chicken (*Gallus gallus domesticus*) eggs were bought from a national farm (Granja Santa Isabel; Córdoba, Spain) and incubated at 38 ºC and 65% controlled humidity in a forced draft incubator until the Hamburger–Hamilton stage five (HH5) [147]. Embryos were fixed by immersion in 4% paraformaldehyde in 0.1M phosphate buffered saline (PBS, pH 7.4) during 16 h at 4 ºC. Whole-mount in situ hybridization was done as previously described [146] using probes for *Otx2* and *Gbx2* reported in [24]. *Fezf2* probe was cloned using the following primers: F, GCTACAAACCCTTCGTCTGC and R, GCTCAGGGTCACTTGCTACC.

Supporting information

S1 Fig. Temporal expression of Nk2.1 during amphioxus development. Lateral views (A-F, F'), dorsal views (A'-E'), and schematic drawings (A"-F") of the neural component of Nk2.1 gene expression pattern from 15 to 36 hours post-fertilization. Anterior is to the left except in F. Somites are indicated using red dotted lines. Scale bar = 50μm.
(TIF)

S2 Fig. Additional gene markers used in this study. Other markers with neural expression used in this study in lateral (A-G) or dorsal views (A'-G'), and drawings of the neural component of each gene expression pattern with the relative position of somites (A"-G'). Markers with no expression in the amphioxus developing CNS at this stage are showed in lateral (H-N) and dorsal views (H'-N'). Anterior is to the left. Scale bar = 50μm.
(TIF)

S3 Fig. Expression of key gene markers at early neural stage.
(TIF)

S1 Table. Information on the neural expression of genes used in this study.
(XLSX)

S2 Table. Probes of amphioxus used for in situ hybridization.
(XLSX)

S3 Table. Probes of zebrafish used for in situ hybridization.
(XLSX)

Acknowledgments

We thank Hector Escrivà and Stéphanie Bertrand for providing access to amphioxus embryos, Nicholas Holland, Linda Holland; and Sky Yu for helpful comments on the manuscript, and Manel Bosch (CCiT-UB) for microscope imaging assistance.

Author Contributions

Conceptualization: Beatriz Albuixech-Crespo, Ignacio Maeso, Eduardo Puelles, Luis Puelles, Manuel Irimia, José Luis Ferran.

Data curation: Beatriz Albuixech-Crespo, Ignacio Maeso, Manuel Irimia, José Luis Ferran.

Funding acquisition: Jordi Garcia-Fernàndez, Luis Puelles, Manuel Irimia, José Luis Ferran.

Investigation: Beatriz Albuixech-Crespo, Laura López-Blanch, Demian Burguera, Luisa Sánchez-Arrones, Juan Antonio Moreno-Bravo, Ildiko Somorjai, Juan Pascual-Anaya, Manuel Irimia, José Luis Ferran.

Methodology: Beatriz Albuixech-Crespo, Laura López-Blanch, Demian Burguera, Luisa Sánchez-Arrones, Juan Antonio Moreno-Bravo, Ildiko Somorjai, Juan Pascual-Anaya, Manuel Irimia, José Luis Ferran.

Project administration: Jordi Garcia-Fernàndez, Manuel Irimia.

Resources: Eduardo Puelles, Jordi Garcia-Fernàndez, Manuel Irimia, José Luis Ferran.

Supervision: Eduardo Puelles, Paola Bovolenta, Jordi Garcia-Fernàndez, Luis Puelles, Manuel Irimia, José Luis Ferran.

Visualization: Beatriz Albuixech-Crespo, Luis Puelles, Manuel Irimia, José Luis Ferran.

Writing – original draft: Luis Puelles, Manuel Irimia, José Luis Ferran.

Writing – review & editing: Beatriz Albuixech-Crespo, Ignacio Maeso, Ildiko Somorjai, Juan Pascual-Anaya, Paola Bovolenta, Luis Puelles, Manuel Irimia, José Luis Ferran.

References

1. Nieuwenhuys R, Puelles L. Towards a New Neuromorphology. Cham: Springer International Publishing; 2016.
2. Puelles L, Martinez-de-la-Torre M, Bardet SM, Rubenstein JLR. Hypothalamus. In: Watson C, Paxinos G, Puelles L, editors. The mouse neurvous system, London, San Diego, CA: Academic Press/ Elsevier; 2012, p. 221–312.
3. Puelles L. Plan of the Developing Vertebrate Nervous System. In: Rubenstein JLR, Rakic P, editors. Pattering and Cell Type Specification in the Developing CNS and PNS, vol. 1, Amsterdam: Academic Press; 2013, p. 187–209.
4. Puelles L, Rubenstein JLR. A new scenario of hypothalamic organization: rationale of new hypotheses introduced in the updated prosomeric model. Front Neuroanat 2015; 9:27. https://doi.org/10.3389/fnana.2015.00027 PMID: 25852489
5. Hidalgo-Sánchez M, Millet S, Bloch-Gallego E, Alvarado-Mallart RM. Specification of the meso-isthmo-cerebellar region: The Otx2/Gbx2 boundary. Brain Res Rev 2005; 49:134–49. https://doi.org/10.1016/j.brainresrev.2005.01.010 PMID: 16111544
6. Kiecker C, Lumsden A. Hedgehog signaling from the ZLI regulates diencephalic regional identity. Nat Neurosci 2004; 7:1242–9. https://doi.org/10.1038/nn1338 PMID: 15494730
7. Vieira C, Garda AL, Shimamura K, Martinez S. Thalamic development induced by Shh in the chick embryo. Dev Biol 2005; 284:351–63. https://doi.org/10.1016/j.ydbio.2005.05.031 PMID: 16026780
8. Vue TY, Bluske K, Alishahi A, Yang LL, Koyano-Nakagawa N, Novitch B, et al. Sonic hedgehog signaling controls thalamic progenitor identity and nuclei specification in mice. JNeurosci 2009; 29:4484–97.

9. Crossley PH, Martinez S, Martin GR. Midbrain development induced by FGF8 in the chick embryo. Nature 1996; 380:66–8. https://doi.org/10.1038/380066a0 PMID: 8598907
10. Lee SM, Danielian PS, Fritzsch B, McMahon AP. Evidence that FGF8 signalling from the midbrain-hindbrain junction regulates growth and polarity in the developing midbrain. Development 1997; 124:959–69. PMID: 9056772
11. Martinez S, Crossley PH, Cobos I, Rubenstein JL, Martin GR. FGF8 induces formation of an ectopic isthmic organizer and isthmocerebellar development via a repressive effect on Otx2 expression. Development 1999; 126:1189–200. PMID: 10021338
12. Reifers F, Böhli H, Walsh EC, Crossley PH, Stainier DY, Brand M. Fgf8 is mutated in zebrafish acerebellar (ace) mutants and is required for maintenance of midbrain-hindbrain boundary development and somitogenesis. Development 1998; 125:2381–95. PMID: 9609821
13. Vieira C, Pombero A, García-Lopez R, Gimeno L, Echevarria D, Martínez S. Molecular mechanisms controlling brain development: An overview of neuroepithelial secondary organizers. Int J Dev Biol 2010; 54:7–20. https://doi.org/10.1387/ijdb.092853cv PMID: 19876817
14. Puelles L, Ferran JL. Concept of neural genoarchitecture and its genomic fundament. Front Neuroanat 2012; 6:47. https://doi.org/10.3389/fnana.2012.00047 PMID: 23181010
15. Shimamura K, Hartigan DJ, Martinez S, Puelles L, Rubenstein JL. Longitudinal organization of the anterior neural plate and neural tube. Development 1995; 121:3923–33. PMID: 8575293
16. Nieuwenhuys R, Nicholson C. Lampreys, Petromyzontidae. In: Donkelar HJ, Nicholson, editors. The Central Nervous System of Vertebrates, Berlin: Springer; 1998, p. 397–496.
17. Nieuwenhuys R. Deuterostome brains: synopsis and commentary. Brain ResBull 2002; 57:257–70.
18. Nieuwenhuys R. The forebrain of actinopterygians revisited. Brain BehavEvol 2009; 73:229–52.
19. Murakami Y, Uchida K, Rijli FM, Kuratani S. Evolution of the brain developmental plan: Insights from agnathans. Dev Biol 2005; 280:249–59. https://doi.org/10.1016/j.ydbio.2005.02.008 PMID: 15882571
20. Osorio J, Mazan S, Retaux S. Organisation of the lamprey (Lampetra fluviatilis) embryonic brain: insights from LIM-homeodomain, Pax and hedgehog genes. DevBiol 2005; 288:100–12.
21. Staudt N, Houart C. The prethalamus is established during gastrulation and influences diencephalic regionalization. PLoS Biol 2007; 5:878–88.
22. Ferran JL, Sánchez-Arrones L, Bardet SM, Sandoval JE, Martínez-de-la-Torre M, Puelles L. Early pretectal gene expression pattern shows a conserved anteroposterior tripartition in mouse and chicken. Brain Res Bull 2008; 75:295–8. https://doi.org/10.1016/j.brainresbull.2007.10.039 PMID: 18331887
23. Ferran JL, de Oliveira ED, Merchán P, Sandoval JE, Sánchez-Arrones L, Martínez-de-la-Torre M, et al. Genoarchitectonic profile of developing nuclear groups in the chicken pretectum. J Comp Neurol 2009; 517:405–51. https://doi.org/10.1002/cne.22115 PMID: 19790262
24. Sánchez-Arrones L, Ferrán JL, Rodríguez-Gallardo L, Puelles L. Incipient forebrain boundaries traced by differential gene expression and fate mapping in the chick neural plate. Dev Biol 2009; 335:43–65. https://doi.org/10.1016/j.ydbio.2009.08.012 PMID: 19699194
25. Morona R, Ferran JL, Puelles L, González A. Embryonic genoarchitecture of the pretectum in Xenopus laevis: A conserved pattern in tetrapods. J Comp Neurol 2011; 519:1024–50. https://doi.org/10.1002/cne.22548 PMID: 21344401
26. Pose-Méndez S, Candal E, Mazan S, Rodríguez-Moldes I. Genoarchitecture of the rostral hindbrain of a shark: basis for understanding the emergence of the cerebellum at the agnathan-gnathostome transition. Brain Struct Funct 2016; 221:1321–35. https://doi.org/10.1007/s00429-014-0973-8 PMID: 25552316
27. Mueller T, Wullimann MF. An evolutionary interpretation of teleostean forebrain anatomy. Brain BehavEvol 2009; 74:30–42.
28. Hauptmann G, Soll I, Gerster T. The early embryonic zebrafish forebrain is subdivided into molecularly distinct transverse and longitudinal domains. Brain ResBull 2002; 57:371–5.
29. Lauter G, Soll I, Hauptmann G. Molecular characterization of prosomeric and intraprosomeric subdivisions of the embryonic zebrafish diencephalon. JComp Neurol 2013; 521:1093–118.
30. Pombal MA, Megías M, Bardet SM, Puelles L. New and old thoughts on the segmental organization of the forebrain in lampreys. Brain Behav Evol 2009; 74:7–19. https://doi.org/10.1159/000229009 PMID: 19729892
31. Martínez-de-la-Torre M, Pombal MA, Puelles L. Distal-less-like protein distribution in the larval lamprey forebrain. Neuroscience 2011; 178:270–84. https://doi.org/10.1016/j.neuroscience.2010.12.030 PMID: 21185911
32. Morona R, Ferran JL, Puelles L, Gonzalez A. Gene expression analysis of developing cell groups in the pretectal region of Xenopus laevis. JComp Neurol 2016; 0:1–38.

33. Santos-Duran GN, Menuet A, Lagadec R, Mayeur H, Ferreiro-Galve S, Mazan S, et al. Prosomeric organization of the hypothalamus in an elasmobranch, the catshark Scyliorhinus canicula. Front Neuroanat 2015; 9:37. https://doi.org/10.3389/fnana.2015.00037 PMID: 25904850

34. Sugahara F, Pascual-Anaya J, Oisi Y, Kuraku S, Aota S, Adachi N, et al. Evidence from cyclostomes for complex regionalization of the ancestral vertebrate brain. Nature 2016; 531:97–100. https://doi.org/10.1038/nature16518 PMID: 26878236

35. Hirth F, Kammermeier L, Frei E, Walldorf U, Noll M, Reichert H. An urbilaterian origin of the tripartite brain: developmental genetic insights from Drosophila. Development 2003; 130:2365–73. PMID: 12702651

36. Irimia M, Piñeiro C, Maeso I, Gómez-Skarmeta JL, Casares F, Garcia-Fernàndez J, et al. Conserved developmental expression of Fezf in chordates and Drosophila and the origin of the Zona Limitans Intrathalamica (ZLI) brain organizer. Evodevo 2010; 1:7. https://doi.org/10.1186/2041-9139-1-7 PMID: 20849572

37. Castro LFC, Rasmussen SLK, Holland PWH, Holland ND, Holland LZ. A Gbx homeobox gene in amphioxus: Insights into ancestry of the ANTP class and evolution of the midbrain/hindbrain boundary. Dev Biol 2006; 295:40–51. https://doi.org/10.1016/j.ydbio.2006.03.003 PMID: 16687133

38. Kozmik Z, Holland ND, Kalousova A, Paces J, Schubert M, Holland LZ. Characterization of an amphioxus paired box gene, AmphiPax2/5/8: developmental expression patterns in optic support cells, nephridium, thyroid-like structures and pharyngeal gill slits, but not in the midbrain-hindbrain boundary region. Development 1999; 126:1295–304. PMID: 10021347

39. Takahashi T, Holland PWH. Amphioxus and ascidian Dmbx homeobox genes give clues to the vertebrate origins of midbrain development. Development 2004; 131:3285–94. https://doi.org/10.1242/dev.01201 PMID: 15201221

40. Holland LZ, Kene M, Williams N a, Holland ND. Sequence and embryonic expression of the amphioxus engrailed gene (AmphiEn): the metameric pattern of transcription resembles that of its segment-polarity homolog in Drosophila. Development 1997; 124:1723–32. PMID: 9165120

41. Shimeld SM, Holland ND. Amphioxus molecular biology: insights into vertebrate evolution and developmental mechanisms. Can J Zool 2005; 83:90–100.

42. Arendt D, Denes AS, Jékely G, Tessmar-Raible K. The evolution of nervous system centralization. Anim Evol Genomes, Foss Trees 2009; 363:1523–8.

43. Denes AS, Jékely G, Steinmetz PRH, Raible F, Snyman H, Prud'homme B, et al. Molecular Architecture of Annelid Nerve Cord Supports Common Origin of Nervous System Centralization in Bilateria. Cell 2007; 129:277–88. https://doi.org/10.1016/j.cell.2007.02.040 PMID: 17448990

44. Steinmetz PRH, Kostyuchenko RP, Fischer A, Arendt D. The segmental pattern of otx, gbx, and Hox genes in the annelid Platynereis dumerilii. Evol Dev 2011; 13:72–9. https://doi.org/10.1111/j.1525-142X.2010.00457.x PMID: 21210944

45. Lowe CJ, Terasaki M, Wu M, Freeman RM Jr., Runft L, Kwan K, et al. Dorsoventral patterning in hemichordates: Insights into early chordate evolution. PLoS Biol 2006; 4:1603–19.

46. Lowe CJ, Wu M, Salic A, Evans L, Lander E, Stange-Thomann N, et al. Anteroposterior patterning in hemichordates and the origins of the chordate nervous system. Cell 2003; 113:853–65. PMID: 12837244

47. Pani AM, Mullarkey EE, Aronowicz J, Assimacopoulos S, Grove EA, Lowe CJ. Ancient deuterostome origins of vertebrate brain signalling centres. Nature 2012; 483:289–94. https://doi.org/10.1038/nature10838 PMID: 22422262

48. Yao Y, Minor PJ, Zhao Y-T, Jeong Y, Pani AM, King AN, et al. Cis-regulatory architecture of a brain signaling center predates the origin of chordates. Nat Genet 2016;48.

49. Wagner G. Homology, Genes, and Evolutionary Innovation. vol. XXXIII. princeton university press; 2014.

50. Dehal P, Satou Y, Campbell RK, Chapman J, Degnan B, De Tomaso A, et al. The Draft Genome of Ciona intestinalis: Insights into Chordate and Vertebrate Origins. Science (80-) 2002;298.

51. Putnam NH, Butts T, Ferrier DEK, Furlong RF, Hellsten U, Kawashima T, et al. The amphioxus genome and the evolution of the chordate karyotype. Nature 2008; 453:1064–71. https://doi.org/10.1038/nature06967 PMID: 18563158

52. Williams N a Holland PW. Gene and domain duplication in the chordate Otx gene family: insights from amphioxus Otx. Mol Biol Evol 1998; 15:600–7. PMID: 9580990

53. Wada H, Garcia-Fernandez J, Holland PW, Garcia-Fernàndez J, Holland PW. Colinear and segmental expression of amphioxus Hox genes. Dev Biol 1999; 213:131–41. https://doi.org/10.1006/dbio.1999.9369 PMID: 10452851

54. Holland PW, Holland LZ, Williams N a, Holland ND. An amphioxus homeobox gene: sequence conservation, spatial expression during development and insights into vertebrate evolution. Development 1992; 116:653–61. PMID: 1363226

55. Garcia-Fernandez J, Holland PW, Garcia-Fernández J, Holland PW. Archetypal organization of the amphioxus Hox gene cluster. Nature 1994; 370:563–6. https://doi.org/10.1038/370563a0 PMID: 7914353

56. Pascual-Anaya J, Adachi N, Alvarez S, Kuratani S, D'Aniello S, Garcia-Fernandez J, et al. Broken colinearity of the amphioxus Hox cluster. Evodevo 2012; 3:28. https://doi.org/10.1186/2041-9139-3-28 PMID: 23198682

57. Schubert M, Holland ND, Laudet V, Holland LZ. A retinoic acid-Hox hierarchy controls both anterior/posterior patterning and neuronal specification in the developing central nervous system of the cephalochordate amphioxus. Dev Biol 2006; 296:190–202. https://doi.org/10.1016/j.ydbio.2006.04.457 PMID: 16750825

58. Holland LZ, Holland ND. Chordate origins of the vertebrate central nervous system. Curr Opin Neurobiol 1999; 9:596–602. https://doi.org/10.1016/S0959-4388(99)00003-3 PMID: 10508734

59. Holland LZ, Carvalho JE, Escriva H, Laudet V, Schubert M, Shimeld SM, et al. Evolution of bilaterian central nervous systems: a single origin? Evodevo 2013; 4:27. https://doi.org/10.1186/2041-9139-4-27 PMID: 24098981

60. Bertrand S, Escriva H, Escrivà H. Evolutionary crossroads in developmental biology: amphioxus. Development 2011; 138:2639–48.

61. Holland ND, Holland LZ, Holland PW. Scenarios for the making of vertebrates. Nature 2015; 520:450–5. https://doi.org/10.1038/nature14433 PMID: 25903626

62. Northcutt RG. Origin of the Isthmus? A Comparison of the Brains of Lancelets and Vertebrates. J Comp Neurol 2003; 466:316–8. https://doi.org/10.1002/cne.10892 PMID: 14556289

63. Northcutt RG. Evolution of centralized nervous systems: two schools of evolutionary thought. Proc Natl Acad Sci U S A 2012; 109 Suppl:10626–33.

64. Holland LZ. Chordate roots of the vertebrate nervous system: expanding the molecular toolkit. Nat Rev Neurosci 2009; 10:736–46. https://doi.org/10.1038/nrn2703 PMID: 19738625

65. Annona G, Holland ND, D 'aniello S. Evolution of the notochord. Evodevo 2015; 6.

66. Lacalli TC. Cell morphology in amphioxus nerve cord may reflect the time course of cell differentiation. Int J Dev Biol 2000; 44:903–6. PMID: 11206331

67. Lacalli TC. Sensory systems in amphioxus: A window on the ancestral chordate condition. Brain Behav Evol 2004; 64:148–62. https://doi.org/10.1159/000079744 PMID: 15353907

68. Holland LZ, Holland ND. A revised fate map for amphioxus and the evolution of axial patterning in chordates. Integr Comp Biol 2007; 47:360–72. https://doi.org/10.1093/icb/icm064 PMID: 21672845

69. Shimeld SM. The evolution of the hedgehog gene family in chordates: insights from amphioxus hedgehog. Dev Genes Evol 1999; 209:40–7. PMID: 9914417

70. Holland PW, Koschorz B, Holland LZ, Herrmann BG. Conservation of Brachyury (T) genes in amphioxus and vertebrates: developmental and evolutionary implications. Development 1995; 121:4283–91. PMID: 8575328

71. Terazawa K, Satoh N. Formation of the chordamesoderm in the amphioxus embryo: Analysis with Brachyury and fork head/HNF-3 genes. Dev Genes Evol 1997; 207:1–11. https://doi.org/10.1007/s004270050086 PMID: 20607475

72. Venkatesh T V., Holland ND, Holland LZ, Su MT, Bodmer R. Sequence and developmental expression of amphioxus AmphiNk2-1: Insights into the evolutionary origin of the vertebrate thyroid gland and forebrain. Dev Genes Evol 1999; 209:254–9. PMID: 10079369

73. Pera EM, Kessel M. Demarcation of ventral territories by the homeobox gene NKX2.1 during early chick development. DevGenes Evol 1998; 208:168–71.

74. Echelard Y, Epstein DJ, St-Jacques B, Shen L, Mohler J, McMahon JA, et al. Sonic hedgehog, a member of a family of putative signaling molecules, is implicated in the regulation of CNS polarity. Cell 1993; 75:1417–30. PMID: 7916661

75. Roelink H, Augsburger A, Heemskerk J, Korzh V, Norlin S, Altaba A, et al. Floor plate and motor neuron induction by vhh-1, a vertebrate homolog of hedgehog expressed by the notochord. Cell 1994; 76:761–75. PMID: 8124714

76. Muller F, Albert S, Blader P, Fischer N, Hallonet M, Strahle U. Direct action of the nodal-related signal cyclops in induction of sonic hedgehog in the ventral midline of the CNS. Development 2000; 127:3889–97. PMID: 10952887

77. Marti E, Takada R, Bumcrot DA, Sasaki H, McMahon AP. Distribution of Sonic hedgehog peptides in the developing chick and mouse embryo. Development 1995; 121:2537–47. PMID: 7671817

78. Ekker SC, Ungar AR, Greenstein P, von Kessler DP, Porter JA, Moon RT, et al. Patterning activities of vertebrate hedgehog proteins in the developing eye and brain. CurrBiol 1995; 5:944–55.

79. Neidert AH, Panopoulou G, Langeland JA. Amphioxus goosecoid and the evolution of the head organizer and prechordal plate. Evol Dev 2000; 2:303–10. PMID: 11256375

80. Kaltenbach SL, Holland LZ, Holland ND, Koop D. Developmental expression of the three iroquois genes of amphioxus (BfIrxA, BfIrxB, and BfIrxC) with special attention to the gastrula organizer and anteroposterior boundaries in the central nervous system. Gene Expr Patterns 2009; 9:329–34. https://doi.org/10.1016/j.gep.2009.02.003 PMID: 19233318

81. Kozmik Z, Holland ND, Kreslova J, Oliveri D, Schubert M, Jonasova K, et al. Pax-Six-Eya-Dach network during amphioxus development: Conservation in vitro but context specificity in vivo. Dev Biol 2007; 306:143–59. https://doi.org/10.1016/j.ydbio.2007.03.009 PMID: 17477914

82. Mazet F, Masood S, Luke GN, Holland ND, Shimeld SM. Expression of AmphiCoe, an Amphioxus COE/EBF Gene, in the Developing Central Nervous System and Epidermal Sensory Neurons. Genesis 2004; 38:58–65. https://doi.org/10.1002/gene.20006 PMID: 14994268

83. Simeone A, Acampora D, Mallamaci A, Stornaiuolo A, D'Apice MR, Nigro V, et al. A vertebrate gene related to orthodenticle contains a homeodomain of the bicoid class and demarcates anterior neuroectoderm in the gastrulating mouse embryo. EMBO J 1993; 12:2735–47. PMID: 8101484

84. Shamim H, Mason I. Expression of Gbx-2 during early development of the chick embryo. MechDev 1998; 76:157–9.

85. Simeone A, Acampora D. The role of Otx2 in organizing the anterior patterning in mouse. IntJDevBiol 2001; 45:337–45.

86. Garda AL, Echevarría D, Martínez S. Neuroepithelial co-expression of Gbx2 and Otx2 precedes Fgf8 expression in the isthmic organizer. Mech Dev 2001; 101:111–8. PMID: 11231064

87. Rhinn M, Lun K, Amores A, Yan YL, Postlethwait JH, Brand M. Cloning, expression and relationship of zebrafish gbx1 and gbx2 genes to Fgf signaling. MechDev 2003; 120:919–36.

88. Von Bubnoff A, Schmidt JE, Kimelman D. The Xenopus laevis homeobox gene Xgbx-2 is an early marker of anteroposterior patterning in the ectoderm. MechDev 1996; 54:149–60.

89. Jacobson M, Hirose G. Clonal organization of the central nervous system of the frog. II. Clones stemming from individual blastomeres of the 32- and 64-cell stages. JNeurosci 1981; 1:271–84.

90. Lacalli TC, Holland ND, West JE. Landmarks in the Anterior Central Nervous System of Amphioxus Larvae. Philos Trans R Soc B Biol Sci 1994; 344:165–85.

91. Hashimoto H, Yabe T, Hirata T, Shimizu T, Bae Y, Yamanaka Y, et al. Expression of the zinc finger gene fez-like in zebrafish forebrain. MechDev 2000; 97:191–5.

92. Matsuo-Takasaki M, Lim JH, Beanan MJ, Sato SM, Sargent TD. Cloning and expression of a novel zinc finger gene, Fez, transcribed in the forebrain of Xenopus and mouse embryos. MechDev 2000; 93:201–4.

93. Jeong JY, Einhorn Z, Mathur P, Chen L, Lee S, Kawakami K, et al. Patterning the zebrafish diencephalon by the conserved zinc-finger protein Fezl. Development 2007; 134:127–36. https://doi.org/10.1242/dev.02705 PMID: 17164418

94. Rodríguez-Seguel E, Alarcón P, Gómez-Skarmeta JL. The Xenopus Irx genes are essential for neural patterning and define the border between prethalamus and thalamus through mutual antagonism with the anterior repressors Fezf and Arx. Dev Biol 2009; 329:258–68. https://doi.org/10.1016/j.ydbio.2009.02.028 PMID: 19268445

95. Nagai T, Aruga J, Takada S, Gunther T, Sporle R, Schughart K, et al. The expression of the mouse Zic1, Zic2, and Zic3 gene suggests an essential role for Zic genes in body pattern formation. DevBiol 1997; 182:299–313.

96. Langeland JA, Holland LZ, Chastain RA, Holland ND. An amphioxus LIM-homeobox gene, AmphiLim1/5, expressed early in the invaginating organizer region and later in differentiating cells of the kidney and central nervous system 2006; 2:110–6. PMID: 16763670

97. Candiani S, Castagnola P, Oliveri D, Pestarino M. Cloning and developmental expression of AmphiBrn1/2/4, a POU III gene in amphioxus. Mech Dev 2002; 116:231–4. PMID: 12128231

98. Sharman AC, Shimeld SM, Holland PW. An amphioxus Msx gene expressed predominantly in the dorsal neural tube. Dev Genes Evol 1999; 209:260–3. PMID: 10079370

99. Holland LZ, Schubert M, Kozmik Z, Holland ND. AmphiPax3/7, an amphioxus paired box gene: insights into chordate myogenesis, neurogenesis, and the possible evolutionary precursor of definitive vertebrate neural crest. Evol Dev 1999; 1:153–65. PMID: 11324100

100. Schubert M, Holland LZ, Stokes MD, Holland ND. Three amphioxus Wnt genes (AmphiWnt3, AmphiWnt5, and AmphiWnt6) associated with the tail bud: the evolution of somitogenesis in chordates. Dev Biol 2001; 240:262–73. https://doi.org/10.1006/dbio.2001.0460 PMID: 11784062

101. Somorjai I, Bertrand S, Camasses A, Haguenauer A, Escriva H. Evidence for stasis and not genetic piracy in developmental expression patterns of Branchiostoma lanceolatum and Branchiostoma floridae, two amphioxus species that have evolved independently over the course of 200 Myr. Dev Genes Evol 2008; 218:703–13. https://doi.org/10.1007/s00427-008-0256-6 PMID: 18843503

102. Mazet F, Shimeld SM. The evolution of chordate neural segmentation. Dev Biol 2002; 251:258–70. PMID: 12435356

103. Hirata T. Zinc-finger genes Fez and Fez-like function in the establishment of diencephalon subdivisions. Development 2006; 133:3993–4004. https://doi.org/10.1242/dev.02585 PMID: 16971467

104. Chi CL, Martinez S, Wurst W, Martin GR. The isthmic organizer signal FGF8 is required for cell survival in the prospective midbrain and cerebellum. Development 2003; 130:2633–44. PMID: 12736208

105. Scholpp S, Foucher I, Staudt N, Peukert D, Lumsden A, Houart C. Otx1l, Otx2 and Irx1b establish and position the ZLI in the diencephalon. Development 2007; 134:3167–76. https://doi.org/10.1242/dev.001461 PMID: 17670791

106. Scholpp S, Brand M. Morpholino-Induced Knockdown of Zebrafish Engrailed Genes eng2 and eng3 Reveals Redundant and Unique Functions in Midbrain–Hindbrain Boundary Development 2001; 133:129–33.

107. Scholpp S, Brand M. Integrity of the Midbrain Region Is Required to Maintain the Diencephalic-Mesencephalic Boundary in Zebrafish no isthmus/pax2.1 Mutants. Dev Dyn 2003; 228:313–22. https://doi.org/10.1002/dvdy.10384 PMID: 14579372

108. Holland LZ. Evolution of basal deuterostome nervous systems. J Exp Biol 2015; 218:637–45. https://doi.org/10.1242/jeb.109108 PMID: 25696827

109. Holland LZ, Schubert M, Holland ND, Neuman T. Evolutionary conservation of the presumptive neural plate markers AmphiSox1/2/3 and AmphiNeurogenin in the invertebrate chordate amphioxus. Dev Biol 2000; 226:18–33. https://doi.org/10.1006/dbio.2000.9810 PMID: 10993671

110. Schubert M, Holland LZ, Panopoulou GD, Lehrach H, Holland ND. Characterization of amphioxus AmphiWnt8: insights into the evolution of patterning of the embryonic dorsoventral axis. Evol Dev 2000; 2:85–92. PMID: 11258394

111. Shimeld SM, van den Heuvel M, Dawber R, Briscoe J. An amphioxus Gli gene reveals conservation of midline patterning and the evolution of hedgehog signalling diversity in chordates. PLoS ONE 2007; 2: e864. https://doi.org/10.1371/journal.pone.0000864 PMID: 17848995

112. Gostling NJ, Shimeld SM. Protochordate Zic genes define primitive somite compartments and highlight molecular changes underlying neural crest evolution. Evol Dev 2003; 5:136–44. PMID: 12622730

113. Lacalli TC. Frontal Eye Circuitry, Rostral Sensory Pathways and Brain Organization in Amphioxus Larvae: Evidence from 3D Reconstructions. Philos Trans R Soc B Biol Sci 1996; 351:243–63.

114. Holland ND, Holland LZ. Stage- and tissue-specific patterns of cell division in embryonic and larval tissues of amphioxus during normal development. Evol Dev 2006; 8:142–9. https://doi.org/10.1111/j.1525-142X.2006.00085.x PMID: 16509893

115. Yu J-KK, Satou Y, Holland ND, Shin-I T, Kohara Y, Satoh N, et al. Axial patterning in cephalochordates and the evolution of the organizer. Nature 2007; 445:613–7. https://doi.org/10.1038/nature05472 PMID: 17237766

116. Yu J, Meulemans D, Mckeown SJ, Bronner-fraser M. Insights from the amphioxus genome on the origin of vertebrate neural crest 2008:1127–32. https://doi.org/10.1101/gr.076208.108 PMID: 18562679

117. Ferran JL, Puelles L, Rubenstein JLR. Molecular codes defining rostrocaudal domains in the embryonic mouse hypothalamus. Front Neuroanat 2015; 9:46. https://doi.org/10.3389/fnana.2015.00046 PMID: 25941476

118. Lu F, Kar D, Gruenig N, Zhang ZW, Cousins N, Rodgers HM, et al. Rax Is a Selector Gene for Mediobasal Hypothalamic Cell Types. J Neurosci 2013; 33:259–72. https://doi.org/10.1523/JNEUROSCI.0913-12.2013 PMID: 23283339

119. Vieira C, Martinez S. Sonic hedgehog from the basal plate and the zona limitans intrathalamica exhibits differential activity on diencephalic molecular regionalization and nuclear structure. Neuroscience 2006; 143:129–40. https://doi.org/10.1016/j.neuroscience.2006.08.032 PMID: 17045408

120. Meyers EN, Lewandoski M, Martin GR. An Fgf8 mutant allelic series generated by Cre- and Flp-mediated recombination. NatGenet 1998; 18:136–41.

121. McMahon AP, Bradley A. The Wnt-1 (int-1) proto-oncogene is required for development of a large region of the mouse brain. Cell 1990; 62:1073–85. PMID: 2205396

122. Thomas KR, Capecchi MR. Targeted disruption of the murine int-1 proto-oncogene resulting in severe abnormalities in midbrain and cerebellar development. Nature 1990; 346:847–50. https://doi.org/10.1038/346847a0 PMID: 2202907

123. McMahon AP, Joyner AL, Bradley A, McMahon JA. The midbrain-hindbrain phenotype of Wnt-1-/Wnt-1- mice results from stepwise deletion of engrailed-expressing cells by 9.5 days postcoitum. Cell 1992; 69:581–95. PMID: 1534034

124. Mastick GS, Davis NM, Andrew GL, Easter SS, Acampora D, Mazan S, et al. Pax-6 functions in boundary formation and axon guidance in the embryonic mouse forebrain. Development 1997; 124:1985–97. PMID: 9169845

125. Ferran JL, Sánchez-Arrones L, Sandoval JE, Puelles L. A model of early molecular regionalization in the chicken embryonic pretectum. J Comp Neurol 2007; 505:379–403. https://doi.org/10.1002/cne.21493 PMID: 17912743

126. Gardner CA, Barald KF. The cellular environment controls the expression of engrailed-like protein in the cranial neuroepithelium of quail-chick chimeric embryos. Development 1991; 113:1037–48. PMID: 1687983

127. Martinez S, Wassef M, Alvarado-Mallart RM. Induction of a mesencephalic phenotype in the 2-day-old chick prosencephalon is preceded by the early expression of the homeobox gene en. Neuron 1991; 6:971–81. PMID: 1675863

128. Bally-Cuif L, Alvarado-Mallart RM, Darnell DK, Wassef M. Relationship between Wnt-1 and En-2 expression domains during early development of normal and ectopic met-mesencephalon. Development 1992; 115:999–1009. PMID: 1360404

129. Bloch-Gallego E, Millet S, Alvarado-Mallart RM. Further observations on the susceptibility of diencephalic prosomeres to En-2 induction and on the resulting histogenetic capabilities. Mech Dev 1996; 58:51–63. PMID: 8887316

130. Holland LZ, Holland NN, Schubert M. Developmental expression of AmphiWnt1, an amphioxus gene in the Wnt1/wingless subfamily. DevGenes Evol 2000; 210:522–4.

131. Bertrand S, Camasses A, Somorjai I, Belgacem MR, Chabrol O, Escande M-LL, et al. Amphioxus FGF signaling predicts the acquisition of vertebrate morphological traits. Proc Natl Acad Sci U S A 2011; 108:9160–5. https://doi.org/10.1073/pnas.1014235108 PMID: 21571634

132. Shimeld SM. C2H2 zinc finger genes of the Gli, Zic, KLF, SP, Wilms' tumour, Huckebein, Snail, Ovo, Spalt, Odd, Blimp-1, Fez and related gene families from Branchiostoma floridae. Dev Genes Evol 2008; 218:639–49. https://doi.org/10.1007/s00427-008-0248-6 PMID: 18795322

133. Lavado A, Lagutin O V, Oliver G. Six3 inactivation causes progressive caudalization and aberrant patterning of the mammalian diencephalon. Development 2008; 135:441–50. https://doi.org/10.1242/dev.010082 PMID: 18094027

134. Schwarz M, Alvarez-Bolado G, Urbanek P, Busslinger M, Gruss P. Conserved biological function between Pax-2 and Pax-5 in midbrain and cerebellum development: evidence from targeted mutations. ProcNatlAcadSciUSA 1997; 94:14518–23.

135. Schwarz M, Alvarez-Bolado G, Dressler G, Urbánek Pavel, Busslinger M, Gruss P. Pax2/5 and Pax6 subdivide the early neural tube into three domains. Mech Dev 1999; 82:29–39. PMID: 10354469

136. Urbanek P, Fetka I, Meisler MH, Busslinger M, Urbánek P, Fetka I, et al. Cooperation of Pax2 and Pax5 in midbrain and cerebellum development. Proc Natl Acad Sci U S A 1997; 94:5703–8. PMID: 9159136

137. Hardie R. Visual System. In: Watson C, Paxinos G, Puelles L, editors. The mouse nervous system, Amsterdam: Academic Press/Elsevier; 2007, p. 1–26.

138. Suzuki DG, Murakami Y, Escriva H, Wada H. A comparative examination of neural circuit and brain patterning between the lamprey and amphioxus reveals the evolutionary origin of the vertebrate visual center. J Comp Neurol 2014; 0:1–11.

139. D'Aniello S, Irimia M, Maeso I, Pascual-Anaya J, Jiménez-Delgado S, Bertrand S, et al. Gene expansion and retention leads to a diverse tyrosine kinase superfamily in amphioxus. Mol Biol Evol 2008; 25:1841–54. https://doi.org/10.1093/molbev/msn132 PMID: 18550616

140. Fuentes M, Benito E, Bertrand S, Paris M, Mignardor A, Godoy L, et al. Insights Into Spawning Behavior and Development of the European Amphioxus (Branchiostoma lanceolatum). J Exp Zool B Mol Dev Evol 2007; 308:484–93. https://doi.org/10.1002/jez.b.21179 PMID: 17520703

141. Yu JKS, Holland LZ. Amphioxus whole-mount in situ hybridization. Cold Spring Harb Protoc 2009; 4:1–7.

142. Westerfield M. The zebrafish book. A guide for the laboratory use of zebrafish (Danio rerio). 4th ed. Univ. of Oregon Press; 2000.

143. Thisse C, Thisse B. High-resolution in situ hybridization to whole-mount zebrafish embryos. Nat Protoc 2008; 3:59–69. https://doi.org/10.1038/nprot.2007.514 PMID: 18193022

144. Kimmel RA, Turnbull DH, Blanquet V, Wurst W, Loomis CA, Joyner AL. Two lineage boundaries coordinate vertebrate apical ectodermal ridge formation. Genes Dev 2000; 14:1377–89. PMID: 10837030

145. Ferran JL, Ayad A, Merchán P, Morales-Delgado N, Sánchez-Arrones L, Alonso A, et al. Exploring Brain Genoarchitecture by Single and Double Chromogenic In Situ Hybridization (ISH) and Immunohistochemistry (IHC) in Whole-Mount Embryos. In: Hauptmann G, editor. In Situ Hybridization Methods, vol. 99, Neuromethods; 2015, p. 61–82.

146. Ferran JL, Ayad A, Merchán P, Morales-Delgado N, Sánchez-Arrones L, Alonso A, et al. Exploring Brain Genoarchitecture by Single and Double Chromogenic In Situ Hybridization (ISH) and Immunohistochemistry (IHC) on Cryostat, Paraffi n, or Floating Sections. In: Hauptmann G, editor. In Situ Hybridization Methods, vol. 99, Neuromethods; 2015, p. 83–107.

147. Hamburger V, Hamilton HL. A series of normal stages in the development of the chick embryo. JMorphol 1951; 88:49–92.

Artículo anexo 3

Stepwise assembly of the *Nova*-regulated alternative splicing network in the vertebrate brain

Manuel Irimia[a,1,2], Amanda Denuc[a], Demián Burguera[a], Ildiko Somorjai[a], Jose M. Martín-Durán[a], Grigory Genikhovich[b], Senda Jimenez-Delgado[a,3], Ulrich Technau[b], Scott W. Roy[c,1], Gemma Marfany[a,d,1], and Jordi Garcia-Fernàndez[a,d,1]

[a]Departament de Genètica, Facultat de Biologia, Universitat de Barcelona, Barcelona E08028, Spain; [b]Department for Molecular Evolution and Development, Center for Organismal Systems Biology, Faculty of Life Sciences, University of Vienna, 1090 Vienna, Austria; [c]Department of Biology, Stanford University, Stanford, CA 94305; and [d]Institut de Biomedicina (IBUB), Universitat de Barcelona, 08007 Barcelona, Spain

Edited* by Christine Guthrie, University of California, San Francisco, CA, and approved February 4, 2011 (received for review August 21, 2010)

Novel organismal structures in metazoans are often undergirded by complex gene regulatory networks; as such, understanding the emergence of new structures through evolution requires reconstructing the series of evolutionary steps leading to these underlying networks. Here, we reconstruct the step-by-step assembly of the vertebrate splicing network regulated by *Nova*, a splicing factor that modulates alternative splicing in the vertebrate central nervous system by binding to clusters of YCAY motifs on pre-RNA transcripts. Transfection of human HEK293T cells with *Nova* orthologs indicated vertebrate-like splicing regulatory activity in bilaterian invertebrates, thus *Nova* acquired the ability to bind YCAY clusters and perform vertebrate-like splicing modulation at least before the last common ancestor of bilaterians. In situ hybridization studies in several species showed that *Nova* expression became restricted to CNS later on, during chordate evolution. Finally, comparative genomics studies revealed a diverse history for *Nova*-regulated exons, with target exons arising through both de novo exon creation and acquisition of YCAY motifs by preexisting exons throughout chordate and vertebrate history. In addition, we find that tissue-specific *Nova* expression patterns emerged independently in other lineages, suggesting independent assembly of tissue-specific regulatory networks.

evo-devo | *pasilla* | amphioxus

Metazoans exhibit tremendous diversity in body plan patterning but widespread conservation of regulatory genes. This is consistent with new organismal structures arising largely by modification and reuse of preexisting molecular products. Novel metazoan body plan structures are often accomplished by gene regulatory networks, thus understanding the emergence of novel structures requires reconstructing the step-by-step assembly of the underlying networks.

The vertebrate brain is a particularly striking example. In addition to expressing a large fraction of tissue-specific genes, CNS genes show the highest level of alternative splicing (AS) (1). This transcript complexity is regulated by several CNS-specific AS factors, which regulate networks of CNS genes (2–5). We used a multidisciplinary approach to reconstruct the step-by-step origin of one of these networks, the *Nova*-regulated splicing network (6, 7). The two *Nova* genes in mammals are expressed exclusively in the CNS (8–10), enabling tissue-specific regulation of ≈700 AS events (11). *Nova* regulates specific exons by binding to clusters of tetranucleotide [CU]CA[CU] (YCAY) motifs in exons or near splice sites in pre-mRNAs; depending on the position of *Nova*-binding sites relative to splice sites, *Nova* can either enhance or inhibit the inclusion of a particular exon in transcripts (12, 13). Computational and HITS-CLIP studies have allowed genome-wide identification of functional *Nova*-binding motifs and a predictive RNA map of AS regulation based on the specific location of YCAY clusters (Fig. 1*A*) (12, 13). These studies have shown that genes with functional YCAY clusters are coregulated in the presence of *Nova* in neurons; notably, most of these genes are involved in axon guidance and synaptic function (4). This regulatory system is very well conserved across vertebrates: *Nova* expression is also restricted to brain in chicken and zebrafish, and conserved YCAY clusters in orthologous positions accurately predict tissue-specific regulation of exon inclusion levels between brain and liver (14). In total, nearly half of *Nova*-regulated alternatively spliced exons and most of their associated YCAY clusters are conserved from mouse to fish (14).

As with any regulatory network, the *Nova* vertebrate network minimally requires (*i*) ability of regulatory molecules to affect expression of target genes (in this case, *Nova* affecting target splicing by binding YCAY clusters); (*ii*) specific temporal and spatial expression of regulatory molecules (CNS-restricted *Nova* expression); (*iii*) presence of regulatory targets (the genes and exons regulated by *Nova*); and (*iv*) sensitivity of targets to regulatory molecules (YCAY clusters associated with target exons). Because all four elements are minimally required for a network to function, their evolutionary order of emergence—that is, the series of steps leading to assembly of the network—is obscure. For instance, CNS expression of *Nova* could have predated or postdated its binding function or its regulation of specific exons, regulated exons could be ancient and have been recruited for the network, or could be recently created, and so forth. To reconstruct the assembly of the vertebrate *Nova* network, we studied *Nova* protein expression and function, as well as the presence/absence of *Nova* target exons, across a variety of invertebrates.

Results

Vertebrate-like *Nova* Regulatory Activity Evolved Before the Last Common Ancestor of Chordates. We first asked whether invertebrate *Nova* proteins are capable of regulating AS in a similar manner to their vertebrate counterparts. We identified putative orthologs of *Nova* in the genome sequences of 23 metazoans and confirmed their orthology by phylogenetic analysis (Fig. S1 and Dataset S1). To study *Nova* protein function, we transfected human embryonic kidney cells (HEK293T), which do not naturally express *Nova*, with constructs expressing the *Nova* orthologs from either the cnidarian *Nematostella vectensis* (*NvNova*), isoform F of *Drosophila melanogaster* [*DmNova*, previously described as *pasilla* (*ps*) (15); isoforms are following FlyBase terminology: Flybase.org], the basal chordate amphioxus (*Branchiostoma floridae*; *BfNova*), or the mouse *Nova1* (*MmNova1*, as a positive control).

Author contributions: M.I., G.M., and J.G.-F. designed research; M.I., A.D., D.B., I.S., J.M.M.-D., G.G., and S.J.-D. performed research; M.I., U.T., and S.W.R. analyzed data; and M.I., G.G., U.T., S.W.R., G.M., and J.G.-F. wrote the paper.

The authors declare no conflict of interest.

*This Direct Submission article had a prearranged editor.

Data deposition: The sequences reported in this paper have been deposited in the GenBank database (accession nos. JF314355–JF314403).

[1]To whom correspondence may be addressed. E-mail: mirimia@gmail.com, scottwroy@gmail.com, gmarfany@ub.edu, or jordigarcia@ub.edu.

[2]Present address: Department of Biology, Stanford University, Stanford, CA 94305.

[3]Present address: Institute for Bioengineering of Catalonia, E08028 Barcelona, Spain.

This article contains supporting information online at www.pnas.org/lookup/suppl/doi:10.1073/pnas.1012333108/-/DCSupplemental.

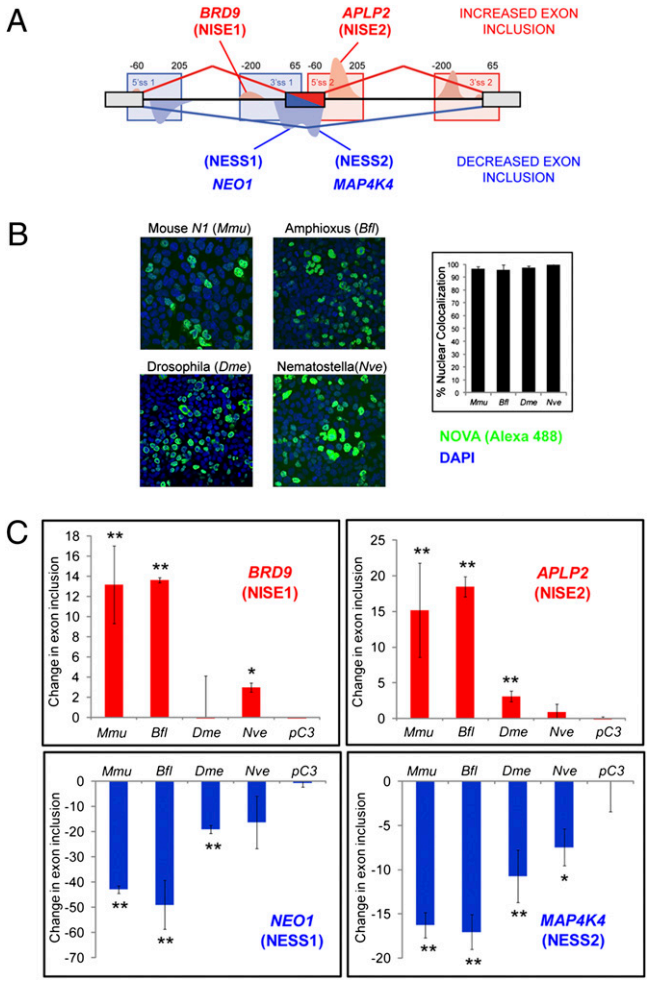

Fig. 1. Transfection of *Novas* from different species into human HEK293T cells. (*A*) Schematic representation of "internal" splicing reporter constructs and predicted *Nova* RNA-binding sites (modified from ref. 13). We studied previously described *Nova*-regulated alternatively spliced exons from genes endogenously expressed in HEK293T cells (BRD9, APLP2, NEO1, and MAP4K4). The effect of *Nova* regulation depends on the locations of *Nova* binding site within the exon or flanking intron, either enhancing (red) or silencing/inhibiting (blue) inclusion of the neighboring exon in mRNA transcripts. (*B*) Confocal images showing general colocalization between DAPI (blue, staining nuclei) and Alexa 488 (green, labeling *Nova*) for human HEK293T cells transfected with *Novas* from mouse (*Nova1*), amphioxus, *Drosophila* (isoform F), or *Nematostella*. *Right:* Percentages of nuclear localization of the *Nova* protein. (*C*) Level of exon inclusion within transcripts for internal reporters for cells transfected with the control (empty pcDNA3.1-HA vector) and for *Nova* constructs from each species. In all cases, mouse *Nova1* and amphioxus *Nova* produced highly significant changes in exon inclusion levels in the predicted direction, compared with the control. Positive/negative values in the *y*-axes denote increase/decrease in exon inclusion. */**Statistical significance at the $P < 0.05/0.01$ level as assessed by ANOVA.

Transfected *Nova* proteins were detected using antibodies against an N-terminal tag. As expected for a functional splicing factor, *Nova* proteins were found in the nucleus (Fig. 1*B*). In addition, we tested isoforms C and D from *DmNova*, which contain a different N terminus. These isoforms were found predominantly in the cytosol of transfected cells (Fig. S2). This is likely in part due to nuclear exportation, because treatment with leptomycin B significantly increased nuclear location for both isoforms ($P = 0.004$ and $P = 0.02$, respectively; Fig. S2).

To assess the ability of invertebrate *Novas* to interpret vertebrate-like splicing signals, we studied splicing of four genes whose splicing is regulated by *Nova* ("target genes"), used as internal (or endogenous) reporters. We used two criteria to select the four target genes. First, all four are endogenously expressed in non-transformed HEK293T cells and show a *Nova*-negative AS pattern due to the lack of *Nova* expression in these cells. Second, together, the four targets represent the major types of *Nova cis*-regulatory elements: splicing enhancers (*Nova* promotes exon inclusion: NISE1, *Brd9*; NISE2, *Aplp2*) and silencers (*Nova* inhibits exon inclusion: NESS1, *Neo1*; NESS2, *Map4k4*) (Fig. 1*A*).

For each *Nova* target exon, we used semiquantitative RT-PCR to compare levels of exon inclusion in transcripts from transfected and control cells. The effects on splicing patterns varied considerably among species. Both mouse and amphioxus *Novas* produced significant changes in splicing for all four exons (Fig. 1*C*; $P <$ 0.01 for each exon). For all four exons, the changes in inclusion levels were similar for the two species and in the direction predicted by the position of their YCAY cluster (Fig. 1*A*) (14), suggesting conserved *Nova* binding function across chordates/deuterostomes (16). The results observed for *D. melanogaster* and the cnidarian *N. vectensis* were less clear. Although changes in exon inclusion levels were observed in the expected direction, the effects were smaller and often not statistically significant, especially in the case of *NvNova* (Fig. 1*C*). Given the evolutionary divergence, these results could reflect differences in target binding or differences in *Nova* recruitment and protein interaction between the invertebrate and mammalian spliceosomes. Consistent with the latter, a recent study (17) has shown that the *DmNova* regulatory map is conserved to that of mammals, suggesting that the biochemical properties of *Nova* protein are conserved at least across bilaterians.

Restriction of *Nova* Expression to CNS Is Specific to Vertebrates and Tunicates. We next studied *Nova* gene expression. We compared in situ hybridization (ISH) of *Nova* genes during development in eight species, spanning all major Eumetazoan groups (Deuterostomes, Ecdysozoans, Lophotrochozoans, and nonbilaterians). We found great variation in expression patterns. Within chordates, similarity of expression to mammalian patterns reflected degree of relatedness. As expected, expression patterns were well conserved within vertebrates: both members of the zebrafish *Nova* family (two "*Nova2*" genes; Fig. S1) were expressed only in CNS (at stages 36 and 48 hpf; Fig. 2 *A–D*). CNS-specific expression extended to the closest living relatives of vertebrates, tunicates, represented by *Ciona intestinalis*: *CiNova* expression was found only in the developing CNS, from neurulation to larval stages (Fig. 2 *E–H*). However, the basal chordate amphioxus showed a substantially different expression pattern, albeit with some similarities to vertebrates. In contrast to vertebrates, expression was most pronounced in mesoderm at early stages: *BfNova* was first detected in the presumptive endomesoderm of gastrulae and later in presomitic mesoderm of early neurulae (Fig. 2 *I–K*), with strong mesodermal staining extending through the mid-late neural stage (Fig. 2 *L* and *M*). However, discrete expression was detected in repetitive neural precursors in the neural plate during mid-late neural stages (Fig. 2 *L* and *M*), reminiscent of motoneuron markers (18, 19) and consistent with vertebrate expression patterns (8). Larval expression is also much broader than in vertebrates: we detected *Nova* in derivatives of all germ layers, including the cerebral vesicle but also others such as mouth–pharynx-associated structures and hindgut (Fig. 2 *N* and *O*). Finally, real-time quantitative PCR analysis of adult amphioxus tissues (see below) underscored the clear but partial similarity between amphioxus and vertebrate expression: *Nova* expression was highest in the neural tube but was also observed in muscle and gill tissues (Fig. S3).

Perhaps surprisingly, beyond chordates, expression patterns were very different from vertebrates. Even the hemichordate *Saccoglossus kowalevskii*, representing the closest living relatives of chordates (Ambulacraria), showed very different expression.

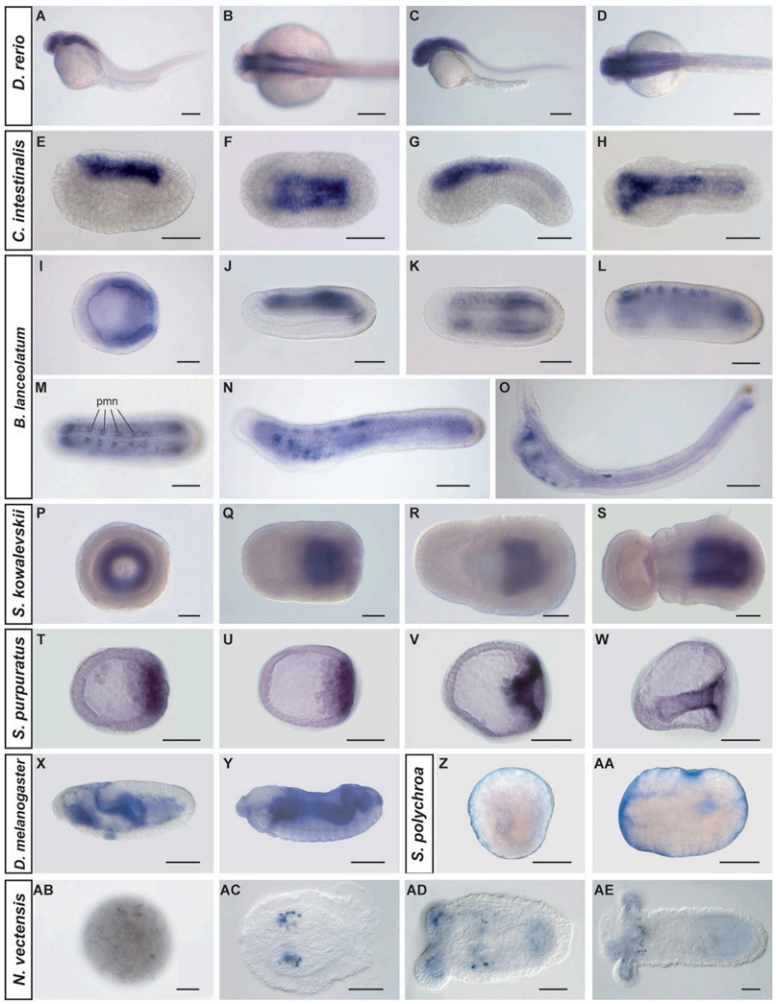

Fig. 2. Developmental expression of *Nova* genes in Eumetazoans. (*A–D*) The zebrafish *Danio rerio*. The *Nova2a* (*A* and *B*) and *Nova2b* (*C* and *D*) genes are widely expressed in the developing CNS. Forty-eight-hour embryos are shown in lateral (*A* and *C*) and dorsal (*B* and *D*) views. Expression is similar for other developmental stages. (*E–H*) The urochordate *C. intestinalis*. *CiNova* is expressed uniquely in developing neural plate in late neurula (*E*, lateral view; *F*, dorsal) and in tadpole larvae (*G*, lateral view; *H*, dorsal). (*I–O*) The cephalochordate amphioxus (*B. lanceolatum*). *BlNova* shows complex expression during development. *BlNova* is expressed early in the gastrula endomesoderm (*I*) and later in the posterior mesoderm of early- and midneurula (*J*, lateral view; *K*, dorsal). At late-neurula stages the expression continues in the mesoderm but starts also in the CNS, in some discrete cells, likely motoneuron precursors (pmn) (*L*, lateral view; *M*, dorsal). In later stages, expression continues in CNS and mesoderm and begins strongly in ectodermal and endodermal structures in the mouth and pharynx regions (*N* and *O*). (*P–S*) The hemichordate *S. kowalevskii*. Expression of *SkNova* is restricted to postpharyngeal endoderm during development: early gastrula (*P*), late gastrula (*Q*), early neurula embryo (*R*), and late neurula (*S*). (*T–W*) The sea urchin *S. purpuratus*. As in the hemichordates, *SpNova* expression is restricted to posterior endomesoderm at 16- to 30-h blastula (*T*), 30- to 38-h gastrulae (*U* and *V*), and 38- to 50-h gastrula (*W*) [pictures obtained from the Whole mount In Situ Hybridization (WISH) database; expression pattern is similiar to that of *P. lividus* (20)]. (*X* and *Y*) The fruitfly *D. melanogaster*. Developmental expression of the *Nova* ortholog *Dmps* is more complex. Expression is detected in salivary glands and digestive tube [pictures obtained from BDGP (38) and described by ref. 15]. (*Z–AA*) The planarian *S. polychroa*. Developmental expression of *SpolNova1* is observed in scattered cells in the germ band at stage 5 (*Z*) and is subsequently restricted to cerebral ganglia and mesenchyme at stage 7 (*AA*); signal in the pharynx is due to probe trapping. (*AB–AE*) The cnidarian *N. vectensis*. *NvNova* is ubiquitously expressed at a very low level, with some cells showing a slight upregulation of the expression in gastrula (26 h after fertilization) (*AB*). In 4-d planula (*AC*) the expression is in the prepharyngeal endoderm, and in 6d primary polyps (*AD* and *AE*) the expression also extends to some single cells in the ectoderm of the tentacles. Anterior/oral is to the left in all cases, except P, which is a view from the blastopore. (Scale bars, 50 μm in *T–W* and *AB–AE*; 100 μm in *E–S*, *X*, and *Y*; 250 μm in *A–D*, *Z*, and *AA*.)

The single *Nova* gene showed sharply restricted expression to postpharyngeal endoderm throughout development (Fig. 2 *P–S*); this is consistent with the expression for two other Ambulacraria species, the sea urchins *Strongylocentrotus purpuratus* and *Paracentrotus lividus* (Fig. 2 *T–W* and ref. 20, respectively). Expression in even more distantly related animals was also very different from vertebrates. As previously described, the fly ortholog *pasilla* is expressed in salivary glands (ectodermal derivative), gut (endoderm) and, posteriorly, the fat bodies (mesodermal) (Fig. 2 *X* and *Y*) (15); however, no expression was detected in CNS at any developmental stage (15). In the Lophotrochozoan planarian *Schmidtea polychroa*, *SpolNova1* is first detected in scattered cells at St5 and, later, in cerebral ganglia and mesenchyme at St7 (Fig. 2 *Z* and *AA*). Finally, expression of *NvNova* in the nonbilaterian *N. vectensis* was detected in scattered cells around the pharynx from 4 d after fertilization (most likely endodermal cells from the pharynx, although neuronal expression cannot be ruled out) and in single ectodermal cells, possibly neurons, of the tentacles after 6 d after fertilization (Fig. 2 *AB–AE*).

These results suggest that CNS-specific expression of *Nova* arose relatively recently within chordates (Fig. S4), most likely within the common ancestor of urochordates and vertebrates and after the divergence from cephalochordates. From a broader perspective, the diversity of expression patterns across metazoans indicates great flexibility of *Nova* expression and organismic function and strongly suggests that *Nova* has independently acquired distinct tissue-specific expression in different metazoan lineages.

***Nova*-Regulated AS Network Was Primarily Assembled Within Vertebrates.** Finally, we studied evolutionary conservation of known mouse *Nova*-regulated exons that are conserved from mammals to fish [34 exons in 28 genes (14); *Materials and Methods*]. For each invertebrate chordate, we studied each exon at four levels of conservation (21) (Fig. 3A): (*i*) presence of an orthologous gene in the genome (G), (*ii*) presence of an orthologous exon in the orthologous gene (E), (*iii*) AS of the exon (A), and (*iv*) putative regulatory conservation (i.e., presence of YCAY clusters in similar/equivalent positions) (R).

We found that all studied genes had putative orthologs in amphioxus (G-level), thus vertebrate/tunicate CNS *Nova*-regulated targets arose within preexisting genes. By contrast, most of the specific *Nova*-regulated exons (66.7%, E-level) were not found in amphioxus (either *in silico* or by RT-PCR; *Materials and Methods*). Lack of conservation is particularly striking for single exons (that is, "simple" exons: those that are not part of mutually exclusive exon sets or more complex AS patterns) for which inclusion is increased by *Nova*. Among these exons, 17 of 19 (89.5%) are absent in amphioxus [vs. 5 of 10 (50%) of *Nova*-silenced exons; $P = 0.030$ by a Fisher exact test] (Fig. 3*B*, *Inset*). Similarly, simple minor and major exons [defined as being supported by less and more than 50% of ESTs, respectively (14)] show significant differences, with half (7 of 14) of major exons being conserved compared with no (0 of 15) minor ones ($P = 0.002$ by Fisher's exact test). This minor–major difference echoes general patterns of evolutionary conservation of alternatively spliced exons in metazoans (22, 23).

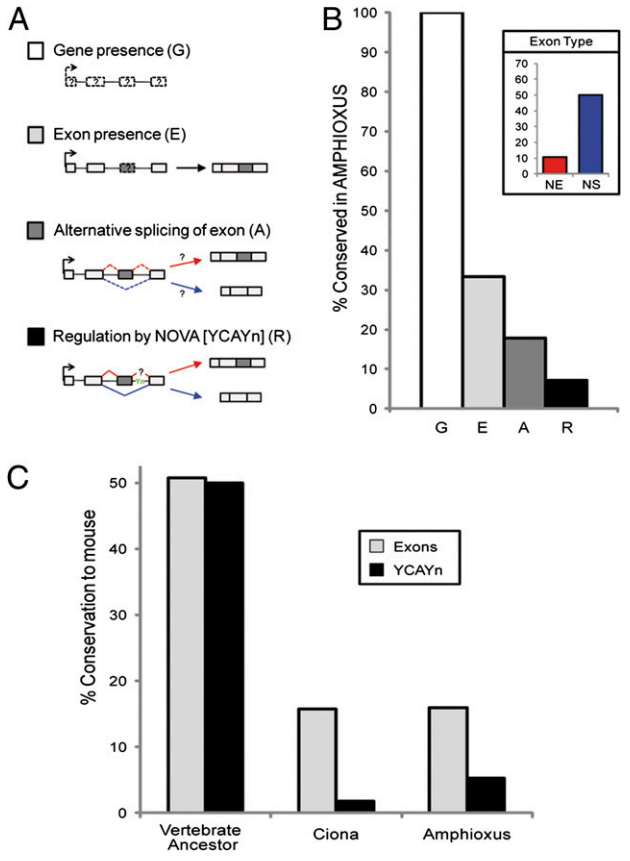

Fig. 3. Conservation of the *Nova*-regulated AS network in chordates. (*A*) Illustrations of four different levels of evolutionary conservation of AS events between vertebrates and studied invertebrates (21): presence of a putatively orthologous gene in the genome (G, white); presence of a putatively orthologous exon in the genome (E, light gray); whether the exon is also alternatively spliced (A, dark gray); and whether specific regulation of AS is conserved, in this case assessed by the presence of equivalent YCAY clusters (R, black). (*B*) Percentage of exons with each of four levels of conservation in amphioxus. All *Nova*-regulated genes are conserved in amphioxus, but less than 40% of specific *Nova*-regulated exons are, and only 2 of 29 events (6.9%) show mouse-like *Nova* regulation. (*C*) Evolutionary conservation of *Nova*-regulated exons (E level, gray) and presence of equivalent YCAY clusters (R level, black) between mouse and the inferred vertebrate ancestor and the two invertebrate chordates. Vertebrate data from ref. 14. For amphioxus and *Ciona*, tetrapod- or mammalian-specific exons are assumed to be not conserved.

We next studied splicing and regulation of conserved exons. Of the 11 conserved exons, 7 are alternatively spliced in amphioxus (A-level), of which only two genes showed YCAY clusters (R-level) in positions corresponding to mouse YCAY clusters (*TPM* and *JNK*) and another (*ITGA*) showed a putatively functionally equivalent cluster. To further analyze these three amphioxus AS events, we generated minigenes for each case and tested *Nova* regulation of their splicing by cotransfection with mouse *Nova1* in HEK293T cells (*Materials and Methods*). In each case, presence of *Nova1* resulted in significantly altered exon inclusion levels in the direction predicted by the positions of putative *Nova* binding motifs (relative to the negative control, the empty pcDNA3 vector; Fig. 4). For *JNK* and *ITGA*, the direction of the effect of *Nova* was conserved between mouse and amphioxus orthologs, consistent with conservation of regulatory pattern and structure.

The case of the *TPM* gene is more complex, however. For the mutually exclusive exons 6A/6B, amphioxus has a single YCAY signal (NISE2) near exon 6A, which is conserved with mouse. Consistent with the prediction, inclusion of amphioxus exon 6A is enhanced by *Nova* (Fig. 4*C*). The mouse case is more complicated: in addition to NISE, the mouse *TPM3* gene contains a second YCAY signal (NISS2), with an opposite predicted effect (inclusion of exon 6B). Although the predicted net result of these two opposed signals is not immediately obvious, consistent with previous results (4), we found that the net effect of *Nova* is an increase in exon 6B inclusion (i.e., NISS2 seems to dominate), opposite the finding in amphioxus.

Next, to assess the tissue-specific role of *Nova* in the regulation of the conserved exons in amphioxus in vivo, we dissected gut, neural tube, gills, and muscle tissues from an adult individual (Fig. S3). Quantification of *Nova* expression by quantitative PCR showed that expression varied across tissues, with the highest expression in neural tube and moderate and weak expression observed in muscle and gills, respectively. No expression was detected in the gut. These results were consistent when either of two different control housekeeping genes were used for normalization (*GAPDH* and cytosolic actin) and across three independent replicates (Table S1). We then compared isoform levels of the three conserved amphioxus AS events (*TPM*, *ITGA*, and *JNK*) across tissues. Consistent with in vivo regulation, *Nova*-enhanced isoforms for each gene were higher in neural tube than in gut alternative (splicing in gills and muscle were generally intermediate) (Fig. S3).

We also studied conservation of *Nova*-regulated exons in *C. intestinalis*. We found a similar picture to amphioxus (Fig. 3C and Fig. S5): most vertebrate *Nova*-regulated exons were not found in *C. intestinalis*, and only one conserved exon had a putatively conserved YCAY cluster, suggesting significant exon creation and YCAY recruitment after the vertebrate–urochordate divergence (Fig. 3*C*). Among exons whose inclusion is increased by *Nova*, 15 of 17 of the exons absent in amphioxus were also absent in *C. intestinalis* (Dataset S2), suggesting little exon creation within vertebrate–urochordate ancestors. Overall, levels of conservation of both exons and YCAY clusters drops dramatically in invertebrates (Fig. 3*C*).

Discussion

The case of *Nova* yields insights into the ordered sequence of evolutionary events leading to the construction of regulatory networks. In this case, the regulator first acquired the regulatory function: *Nova* evolved the ability to bind YCAY clusters and perform vertebrate-like splicing modulation at least by the last common ancestor of chordates, and, likely, of bilaterians (17). Second, the regulator acquired the requisite expression patterns: *Nova* expression became restricted to CNS in chordates, likely in vertebrate–tunicate ancestors. Finally, the regulatory targets arose: in the case of *Nova*, a combination of de novo emergence of new *Nova*-targeted exons and acquisition of *Nova* regulation by preexisting exons led to the modern wealth of *Nova* targets.

Evolution of *Nova* Targets. Our results attest to a variety of different evolutionary histories of *Nova*-regulated vertebrate exons. First, some exons are ancestral (shared with amphioxus) and thus predate the assembly of the CNS-specific *Nova* regulatory network. Most ancestral exons lack *Nova* binding motifs and/or evidence for AS in amphioxus, suggesting that they were ancestrally constitutive exons that were coopted for *Nova* regulation well after their origin. Other exons seem to have arisen within urochordate–vertebrate or vertebrate ancestors or during vertebrate evolution and thus postdate the evolution of CNS-specific *Nova* expression. As with the ancestral exons, some of these lack evidence for *Nova* binding motifs and/or AS in urochordates and/or vertebrates distantly related to mammals, again suggesting that the exon first arose and only later was coopted by the *Nova* network (14). Finally, some seem to be *Nova*-created exons: exon presence is closely associated with *Nova* binding motifs. As previously suggested (14), creation of these exons could be directly

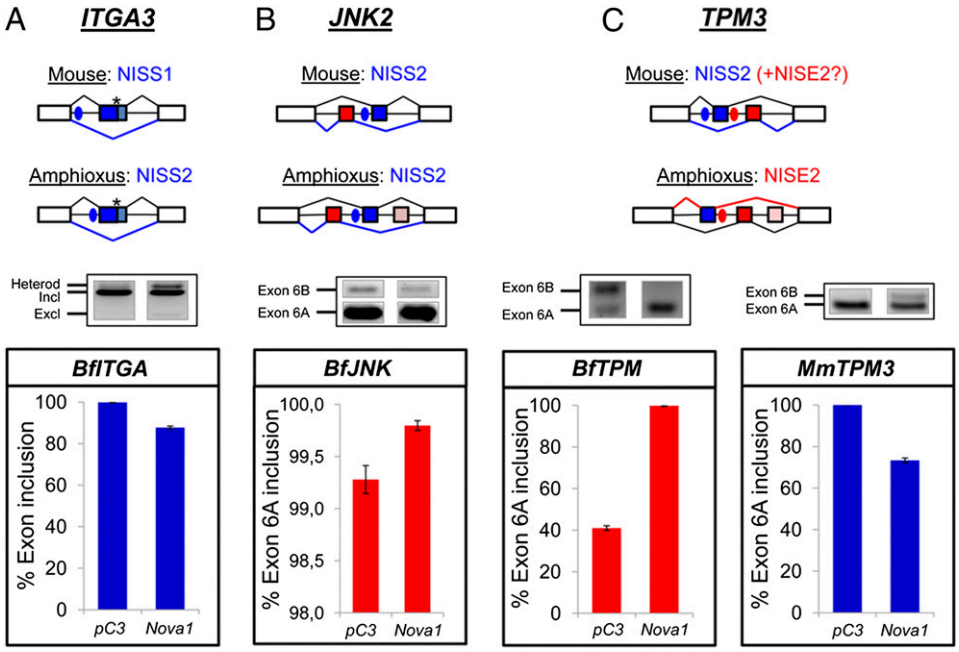

Fig. 4. Experimental validation of predicted *Nova*-regulated events in amphioxus. For each exon [from *ITGA3* (*A*), *JNK2* (*B*), and *TPM3* (*C*)], schematic representations of the local gene structures for amphioxus and vertebrate are shown at the top, with representative RT-PCR results and estimated percentage of exon inclusion for each studied minigene. Blue/red dots indicate YCAY clusters predicted to function as *Nova* enhancer/silencers. Blue/red bars indicate *Nova* silenced/enhanced exon inclusion. NISS, *Nova* intronic splicing silencer; NISE, *Nova* intronic splicing enhancer. Asterisks indicate in-frame STOP codons.

attributable to new *Nova*-binding motifs: the emergence of YCAY enhancer motifs could have led to the use of nearby cryptic splice sites, leading to creation of a new exon.

Evolution of *Nova* Expression. In addition, our gene expression results indicate a complex history for the biological role of *Nova* through metazoan history. First, we find that CNS-restricted expression is a relatively recent occurrence within the chordate lineage, with more complex or more promiscuous expression patterns in various invertebrates. This raises the question of the function of *Nova* in these species as well as in early metazoans. The reconstruction of *Nova*-regulated networks in other phyla may provide insights into this question. Equally intriguing, we find that *Nova* has independently acquired tissue-specific expression patterns in very different tissues in different metazoans lineages. The expression pattern is especially striking in Ambulacraria, in which *Nova* is largely restricted to the gut. This raises the exciting possibility of lineage-specific assembly of tissue-specific *Nova*-regulated AS networks in other lineages. *Nova* may have served as a powerful and multipurpose tool for the construction of complex regulatory networks, having been put to use for very different functions in different lineages. Regulators with such flexible potential functions could be centrally important in the emergence of complex but different structures in related lineages.

Materials and Methods

***In Silico* Identification of *Nova* Orthologs and Phylogenetic Analysis.** Using mouse *Nova* genes as queries, we performed tBLASTN searches against 17 genomes (*SI Materials and Methods*). We then downloaded each corresponding genomic region and built gene models using existing automatic gene model predictions, ESTs, ClustalW alignments of individual exons, and/or GeneWise2 software if necessary. For phylogenetic analysis, described sequences for ingroups and outgroups were downloaded from GenBank. Full-length amino acid sequences were aligned using ClustalW (24). Phylogenetic trees were then generated by the Bayesian method with MrBayes 3.1.2 (25, 26), with the Dayhoff+Gamma model, as recommended by ProtTest 1.4 (27–29) as previously described (30) (further details in *SI Materials and Methods*).

***Nova* Constructs, Internal Reporters, and Minigenes.** Full-length *Nova* cDNA sequences from mouse (*Nova1*), *B. floridae*, *D. melanogaster* (*ps,* isoforms C, D, and F), and *N. vectensis* were obtained by high-fidelity PCR. Each *Nova* cDNA sequence was cloned into a pcDNA.3.1 expression vector that contained an in-frame HA epitope at the 5′end to facilitate protein immunodetection. For *Drosophila* isoforms, subcellular location was also investigated after 2, 4, and 6 h of inhibition of nuclear exportation with 40 nM of leptomycin B (Fig. S2).

Candidate endogenous reporters for AS, namely APLP2, BRD9, MAP4K4, and NEO1, were selected from previously described *Nova*-regulated events (14) so as to include all major types of Nova *cis* regulators. Primers in the upstream and downstream constitutive exons were designed for each event to test the inclusion level of each alternatively spliced exon.

Minigenes for the AS events from mouse *TPM3* and amphioxus *ITGA* and *JNK* were generated using primers to amplify the upstream and downstream constitutive exons from genomic DNA and cloned into the expression vector pcDNA.3.1. For *BfTPM*, only the region containing exons 6A and 6B was cloned, using several primer sets for sequential cloning. To check the AS pattern of each minigene, specific primers in the upstream and downstream exons were designed. For *BfJNK* exons A and B were quantified separately using different specific primer sets.

Cell Culture, Transfection, RNA Isolation, and RT-PCR. HEK293T cells were transiently cotransfected with either pcDNA.3.1-HA empty vector (negative control) or one of the pcDNA.3.1-HA-*Nova* constructs. Forty-eight hours after transfection, cells were immunodetected according to standard protocols with anti-HA and AlexaFluor 488-conjugated anti-mouse IgG antibodies. Nuclei were counterstained with DAPI. To test the minigenes, each construct was cotransfected with either pcDNA.3.1-HA empty vector or pcDNA.3.1-HA-*MmNova1*. Total RNA was isolated from cells 40 h after transfection, and cDNA was prepared. AS patterns were quantified by measuring RT-PCR products performed under specific conditions to avoid PCR bias toward small fragments (31) (details in *SI Materials and Methods*). At least three biological replicates were analyzed for each set of experiments.

Cloning of Different *Nova* Orthologs and in Situ Hybridization. Primers were designed to span nearly the full length of the *Nova* transcript for zebrafish (*Nova2a* and *Nova2b*), *Branchiostoma lanceolatum*, *C. intestinalis*, *S. kowalevskii*, *S. polychroa*, and *N. vectensis*. For key species, 3′ UTR (*B. lanceolatum* and *S. kowalevskii*) and/or KH-free probes (*B. lanceolatum* and *S. polychroa*) were also used (Fig. S6). Standard ISH protocols (32–37) were used for each species at higher hybridization temperatures (5–10 °C higher) to avoid po-

tential cross-hybridization (details in *SI Materials and Methods*). Pictures of *D. melanogaster* and *S. purpuratus* ISHs were obtained with permission from the Berkeley *Drosophila* Genome Project (BDGP) gene expression project (http://insitu.fruitfly.org) (38) and the WISH database (http://goblet.molgen.mpg.de/eugene/cgi/eugene.pl) (39), respectively.

Analysis of the Vertebrate *Nova*-Regulated Network in *B. floridae* and *C. intestinalis*. Presence of *Nova*-regulated exons conserved from mammals to fish (14) (Dataset S2) were individually assessed *in silico* and by RT-PCR in amphioxus and *C. intestinalis* (details in *SI Materials and Methods*). All sequences were uploaded to GenBank (accession nos. JF314355–JF314403). All primer sequences are available upon request. *TACC2* could not be studied in amphioxus and *Ciona*; *TPM* data were obtained from ref. 40.

For studied exons that were present in any invertebrate genome, we assessed AS by RT-PCR using cDNAs from mixed stages. For exons that showed AS, we searched in the genome for *Nova*-binding motifs (YCAY clusters) corresponding to binding motifs described in mouse: either in orthologous positions or in other positions with generally equivalent effects (14). We used a permissive definition for YCAY clusters, based on ref. 14: at least three YCAY motifs within 50 bp, with a maximum inter-YCAY distance of 24 bp. Predicted amphioxus motifs were then validated using minigenes.

RT-PCRs of conserved *Nova* exons in amphioxus (Fig. S3) were performed on tissues from an adult amphioxus individual. Gut, neural tube, gills, and muscle were carefully dissected and RNA extracted and cDNA prepared using standard protocols. For real-time PCR quantification of *Nova* expression, *GAPDH* and cytosolic actin were used as controls for normalization, both yielding similar results.

ACKNOWLEDGMENTS. We thank Salvatore D'Aniello and Chris Lowe for *C. intestinalis* and *S. kowalevskii* samples, respectively. This work has been funded by Grants BMC2008-03776 (Ministerio de Ciencia e Innovación) and Institució Catalana de Recerca i Estudis Avançats Academia Prize (Generalitat de Catalunya) (to J.G.F.); and BFU2007-60823 and BFU2010-15656 (Ministerio de Ciencia e Innovación) (to G.M.). Research of U.T. is funded by the Norwegian Research Council, the Austrian Science Foundation, and the Marie Curie Initial Training Network-EVONET. M.I. held a Fellowship Program Initiative fellowship, A.D. held a BRD fellowship from the University of Barcelona, I.S. holds a postdoctoral Intra-European Fellowship funded by the Marie Curie FP7 People programme, J.M.M.-D. holds a FPU fellowship, and G.G. holds a Marie Curie Incoming International Fellowship.

1. Yeo G, Holste D, Kreiman G, Burge CB (2004) Variation in alternative splicing across human tissues. *Genome Biol* 5:R74.
2. Boutz PL, et al. (2007) A post-transcriptional regulatory switch in polypyrimidine tract-binding proteins reprograms alternative splicing in developing neurons. *Genes Dev* 21:1636–1652.
3. Calarco JA, et al. (2009) Regulation of vertebrate nervous system alternative splicing and development by an SR-related protein. *Cell* 138:898–910.
4. Ule J, et al. (2005) Nova regulates brain-specific splicing to shape the synapse. *Nat Genet* 37:844–852.
5. Zhang C, et al. (2008) Defining the regulatory network of the tissue-specific splicing factors Fox-1 and Fox-2. *Genes Dev* 22:2550–2563.
6. Warzecha CC, Sato TK, Nabet B, Hogenesch JB, Carstens RP (2009) ESRP1 and ESRP2 are epithelial cell-type-specific regulators of FGFR2 splicing. *Mol Cell* 33:591–601.
7. Matlin AJ, Clark F, Smith CW (2005) Understanding alternative splicing: Towards a cellular code. *Nat Rev Mol Cell Biol* 6:386–398.
8. Buckanovich RJ, Posner JB, Darnell RB (1993) Nova, the paraneoplastic Ri antigen, is homologous to an RNA-binding protein and is specifically expressed in the developing motor system. *Neuron* 11:657–672.
9. Buckanovich RJ, Yang YY, Darnell RB (1996) The onconeural antigen Nova-1 is a neuron-specific RNA-binding protein, the activity of which is inhibited by paraneoplastic antibodies. *J Neurosci* 16:1114–1122.
10. Yang YY, Yin GL, Darnell RB (1998) The neuronal RNA-binding protein Nova-2 is implicated as the autoantigen targeted in POMA patients with dementia. *Proc Natl Acad Sci USA* 95:13254–13259.
11. Zhang C, et al. (2010) Integrative modeling defines the Nova splicing-regulatory network and its combinatorial controls. *Science* 329:439–443.
12. Licatalosi DD, et al. (2008) HITS-CLIP yields genome-wide insights into brain alternative RNA processing. *Nature* 456:464–469.
13. Ule J, et al. (2006) An RNA map predicting Nova-dependent splicing regulation. *Nature* 444:580–586.
14. Jelen N, Ule J, Zivin M, Darnell RB (2007) Evolution of Nova-dependent splicing regulation in the brain. *PLoS Genet* 3:1838–1847.
15. Seshaiah P, Miller B, Myat MM, Andrew DJ (2001) pasilla, the *Drosophila* homologue of the human Nova-1 and Nova-2 proteins, is required for normal secretion in the salivary gland. *Dev Biol* 239:309–322.
16. Delsuc F, Brinkmann H, Chourrout D, Philippe H (2006) Tunicates and not cephalochordates are the closest living relatives of vertebrates. *Nature* 439:965–968.
17. Brooks AN, et al. (2010) Conservation of an RNA regulatory map between *Drosophila* and mammals. *Genome Res,* in press.
18. Jackman WR, Langeland JA, Kimmel CB (2000) islet reveals segmentation in the Amphioxus hindbrain homolog. *Dev Biol* 220:16–26.
19. Candiani S, Lacalli TC, Parodi M, Oliveri D, Pestarino M (2008) The cholinergic gene locus in amphioxus: Molecular characterization and developmental expression patterns. *Dev Dyn* 237:1399–1411.
20. Röttinger E, Besnardeau L, Lepage T (2006) Expression pattern of three putative RNA-binding proteins during early development of the sea urchin *Paracentrotus lividus*. *Gene Expr Patterns* 6:864–872.
21. Irimia M, Rukov JL, Roy SW, Vinther JL, Garcia-Fernandez J (2009) Quantitative regulation of alternative splicing in evolution and development. *Bioessays* 31:40–50.
22. Modrek B, Lee CJ (2003) Alternative splicing in the human, mouse and rat genomes is associated with an increased frequency of exon creation and/or loss. *Nat Genet* 34: 177–180.
23. Irimia M, et al. (2008) Widespread evolutionary conservation of alternatively spliced exons in *Caenorhabditis*. *Mol Biol Evol* 25:375–382.
24. Higgins DG, Thompson JD, Gibson TJ (1996) Using CLUSTAL for multiple sequence alignments. *Methods Enzymol* 266:383–402.
25. Huelsenbeck JP, Ronquist F (2001) MRBAYES: Bayesian inference of phylogenetic trees. *Bioinformatics* 17:754–755.
26. Ronquist F, Huelsenbeck JP (2003) MrBayes 3: Bayesian phylogenetic inference under mixed models. *Bioinformatics* 19:1572–1574.
27. Drummond A, Strimmer K (2001) PAL: An object-oriented programming library for molecular evolution and phylogenetics. *Bioinformatics* 17:662–663.
28. Abascal F, Zardoya R, Posada D (2005) ProtTest: Selection of best-fit models of protein evolution. *Bioinformatics* 21:2104–2105.
29. Guindon S, Gascuel O (2003) A simple, fast, and accurate algorithm to estimate large phylogenies by maximum likelihood. *Syst Biol* 52:696–704.
30. D'Aniello S, et al. (2008) Gene expansion and retention leads to a diverse tyrosine kinase superfamily in amphioxus. *Mol Biol Evol* 25:1841–1854.
31. Rukov JL, et al. (2007) High qualitative and quantitative conservation of alternative splicing in *Caenorhabditis elegans* and *Caenorhabditis briggsae*. *Mol Biol Evol* 24: 909–917.
32. Tena JJ, et al. (2007) Odd-skipped genes encode repressors that control kidney development. *Dev Biol* 301:518–531.
33. Irimia M, et al. (2010) Conserved developmental expression of Fezf in chordates and *Drosophila* and the origin of the Zona Limitans Intrathalamica (ZLI) brain organizer. *Evodevo* 1:7.
34. Yu JK, Holland LZ (2009) Amphioxus whole-mount in situ hybridization. *Cold Spring Harb Protoc* 2009:pdb.prot5286.
35. Lowe CJ, Tagawa K, Humphreys T, Kirschner M, Gerhart J (2004) Hemichordate embryos: Procurement, culture, and basic methods. *Methods Cell Biol* 74:171–194.
36. Martín-Durán JM, Amaya E, Romero R (2010) Germ layer specification and axial patterning in the embryonic development of the freshwater planarian *Schmidtea polychroa*. *Dev Biol* 340:145–158.
37. Genikhovich G, Technau U (2009) In situ hybridization of starlet sea anemone (*Nematostella vectensis*) embryos, larvae, and polyps. *Cold Spring Harb Protoc* 2009: pdb.prot5282.
38. Tomancak P, et al. (2007) Global analysis of patterns of gene expression during Drosophila embryogenesis. *Genome Biol* 8:R145.
39. Poustka AJ, et al. (2007) A global view of gene expression in lithium and zinc treated sea urchin embryos: New components of gene regulatory networks. *Genome Biol* 8: R85.
40. Irimia M, Maeso I, Gunning PW, Garcia-Fernàndez J, Roy SW (2010) Internal and external paralogy in the evolution of tropomyosin genes in metazoans. *Mol Biol Evol* 27:1504–1517.

Supporting Information

Irimia et al. 10.1073/pnas.1012333108

SI Materials and Methods

***In Silico* Identification of *Nova* Orthologs and Phylogenetic Analysis.** Using mouse *Nova1* and *Nova2* genes as queries, we performed tBLASTN searches against 17 genomes: *Xenopus tropicalis* JGI v4.1 (1), *Takifugu rubripes* JGI v4.0, *Branchiostoma floridae* JGI v1.0 (2), *Trichoplax adhaerens* Grell-BS-1999 v1.0 (3), *Nematostella vectensis* JGI v1.0 (4), *Ciona intestinalis* JGI v2.0 (5), *Daphnia pulex* JGI v1.0, *Lottia gigantea* JGI v1.0, and *Capitella teleta* JGI v1.0 at the Joint Genome Institute (JGI) Web page (http://genome.jgi-psf.org/euk_home.html); *Strongylocentrotus purpuratus* Build 2.1 (6), *Danio rerio* Build Zv8, *Tribolium castaneum* Build 2.1 (7), and *Anopheles gambiae* str. PEST (8) at the National Center for Biotechnology Information Web page (http://www.ncbi.nlm.nih.gov/blast/Blast.cgi); *Anolis carolinensis* AnoCar1.0 at the Ensembl Web page (http://www.ensembl.org); *Hydra magnipapillata* (9) at the Metazome Web page (http://hydrazome.metazome.net/cgi-bin/gbrowse/hydra/); *Schmidtea mediterranea* at SmedGD (10); and *Saccoglossus kowalevskii* 2008-Dec-09 linear scaffolds at the Human Genome Sequencing Center Baylor College of Medicine Blast Web page (http://blast.hgsc.bcm.tmc.edu/blast.hgsc?organism=20). We then downloaded each corresponding genomic region and built gene models using existing automatic gene model predictions, ESTs, ClustalW alignments of individual exons, and/or GeneWise2 software (11) if necessary. Annotation and comparison of intron positions and phases to improve the alignments were performed as previously described (12). For phylogenetic analysis, sequences for ingroups (*Nova1* and *Nova2* from *Mus musculus* and *Gallus gallus* and *ps_K* from *Drosophila melanogaster*) and outgroups (*Trichoplax adhaerens PCBP*, and the paralogs *M. musculus PCBP1* and *PCBP2* and *D. melanogaster mub*) were downloaded from GenBank. Full-length amino acid sequences were aligned using ClustalW (13). Phylogenetic trees were then generated by the Bayesian method with MrBayes 3.1.2 (14, 15), with the Dayhoff+Gamma model, as recommended by ProtTest 1.4 (16–18) under the Akaike information and the Bayesian information criteria. Two independent runs were performed, each with four chains. By convention, convergence was reached when the value for the SD of split frequencies stayed below 0.01. Burn-in was determined by plotting parameters across all runs for a given analysis: all trees before stationarity and convergence were discarded, and consensus trees were calculated for the remaining trees (2,500,000 generations).

***Nova* Constructs, Internal Reporters, and Minigenes.** Full-length *Nova* cDNA sequences from mouse (*Nova1*), *B. floridae*, *Drosophila psD*, and *Nematostella* were obtained by PCR from purified RNA, using iProof High-Fidelity DNA Polymerase (BioRad). Each *Nova* cDNA sequence was cloned into a pcDNA.3.1 expression vector that contained an in-frame HA epitope at the 5′ end to facilitate protein immunodetection. All final constructs were verified by sequencing.

Candidate endogenous reporters for alternative splicing, namely APLP2, BRD9, MAP4K4, and NEO1, were selected from previously described *Nova*-regulated events (19) as to include all major types of Nova *cis* regulators. Primers in the upstream and downstream constitutive exons were designed for each event to test the inclusion level of each alternatively spliced exon.

Minigenes for the alternative splicing (AS) events from mouse *TPM3* and amphioxus *ITGA* and *JNK* were generated using primers to amplify the upstream and downstream constitutive exons from genomic DNA and cloned into the expression vector pcDNA.3.1. For *BfTPM*, only the region containing exons 6A and 6B was cloned, using several primer sets for sequential cloning. To check the AS pattern of each minigene, specific primers in the upstream and downstream exons were designed. For *BfJNK* exons A and B were quantified separately using different specific primer sets. For *BfTPM* one primer spanning each alternatively spliced exon and yielding different final sizes were used in the same PCR. Although the AS pattern of this minigene was complex, the expected bands for each exon could be easily quantified. Primer sequences are available upon request.

Cell Culture, Transfection, RNA Isolation, and RT-PCR. HEK293T cells were transiently cotransfected with either pcDNA.3.1-HA empty vector or each of the pcDNA.3.1-HA-*Nova* constructs using Lipofectamine 2000 (Invitrogen). Forty-eight hours after transfection, cells were immunodetected according to standard protocols with anti-HA (Santa Cruz Biotechnology, 1:300) and AlexaFluor 488-conjugated anti-mouse IgG (Molecular Probes, 1:250) antibodies. Nuclei were counterstained with DAPI (Roche, 1:5,000). When testing the minigenes, each construct was cotransfected with either pcDNA.3.1-HA empty vector (negative control) or pcDNA.3.1-HA-*MmNova1*.

Total RNA was isolated from cells 40 h after transfection using the High Pure RNA Isolation Kit (Roche). RT-PCRs were performed using the Transcriptor High Fidelity cDNA Synthesis Kit (Roche). *GAPDH* was used as a control. The RT-PCRs to test the AS patterns were performed at 32 cycles for internal reporters and 27 cycles for minigenes, using long elongation times (4 min) to avoid PCR bias toward small fragments (20). The RT-PCR reactions were quantified by Multi Gauge v3.0 software (Fujifilm) after capturing the electrophoresis image with LAS-4000 MINI (Fujifilm). At least three biological replicates were analyzed for each set of experiments. The statistical significance was assessed by ANOVA.

Nuclear Location and Transport of *Drosophila Nova* Isoforms. Experiments regarding the inhibition of the nuclear transport were carried out starting with the transient transfection of the different constructs in pcDNA3.1-HA bearing the *D. melanogaster Nova* isoforms C, D, and F. Briefly, HEK293T cells were seeded on 24-well plates (2.5×10^5 cells/mL). After 12 h, cells were transiently transfected using Lipofectamine 2000 (Invitrogen), according to the manufacturer's instructions. After 48 h of expression, cells were treated with 40 nM leptomycin B (Alomone Labs) for 0 h, 2 h, 4 h, or 6 h and immediately proceeding with two washes in PBS and immunolocalization assays, performed as described above with anti-HA (Santa Cruz Biotechnology, 1:300) and AlexaFluor 488-conjugated anti-mouse IgG (Molecular Probes, 1:250) antibodies. Nuclei were counterstained with DAPI (Roche, 1:5,000).

Cloning of Different *Nova* Orthologs and in Situ Hybridization. Primers were designed to span nearly the full length of the *Nova* transcript for zebrafish (*Nova2a* and *Nova2b*), *Branchiostoma lanceolatum*, *C. intestinalis*, *S. kowalevskii*, *Schmidtea polychroa*, and *N. vectensis*. For key species, 3′ UTR (*B. lanceolatum* and *S. kowalevskii*) and/or KH-free probes (*B. lanceolatum* and *S. polychroa*) were also used (Fig. S6). PCR fragments were cloned into pCRII/TOPO (Invitrogen), and RNA probes were generated using T7 or SP6 RNA polymerases (Roche) using standard procedures.

Zebrafish embryos were raised at 28 °C in standard E3 medium and fixed at 48-h stages in 4% paraformaldehyde overnight at 4 °C. In situ hybridizations (ISH) were carried out as previously described (21). *B. lanceolatum* and *C. intestinalis* embryos were fixed and hybridized as previously described (22, 23); for *C. intestinalis*,

we used 15' of PK treatment. *S. kowalevskii* embryos were kindly provided by Chris Lowe, and ISH was performed as previously described (24). *S. polychroa* embryos were dissected, fixed, and hybridized as previously described (25), using 64 °C as hybridization temperature. ISH for Nematostella was carried out according to ref. 26. Highly stringent conditions were used for all studied species to avoid cross-hybridization with related mRNAs. In addition, for amphioxus an alternative probe was designed spanning the nonconserved sequence between the second and third KH domains, to minimize potential cross-hybridization; the same pattern was observed. Pictures of *D. melanogaster* and *S. purpuratus* ISHs were obtained with permission from the Berkeley *Drosophila* Genome Project gene expression project (http://insitu.fruitfly.org) (27) and WISH database (http://goblet.molgen.mpg.de/eugene/cgi/eugene.pl) (28), respectively.

Analysis of the Vertebrate *Nova*-Regulated Network of Alternatively Spliced Exons in *B. floridae* and *C. intestinalis*. Conservation of *Nova*-regulated exons conserved from mammals to fish, as previously reported (19) (Dataset S2), were assessed *in silico* and by RT-PCR in the amphioxus *B. floridae* and the ascidian *C. intestinalis*. For each studied gene, tBLASTN were performed on each invertebrate genome at the JGI Web page. Each genomic region was then downloaded, and the constitutive upstream and downstream exons were identified and annotated using available ESTs, sequence similarity comparisons using CLUSTALW, and/or intron position alignments. If the upstream and/or downstream exons could not be confidently detected, we searched for the next upstream/downstream exons until we could confidently identify a constitutive exon on each side of the expected alternatively spliced regions. Then we followed two strategies: first the alternatively spliced exons were searched for within the intronic sequence by sequence similarity or EST mapping (if the region could be properly annotated). Second, if the alternatively spliced exon could not be confidently identified, we designed primers in the constitutive adjoining exons for each species and performed RT-PCRs (39 cycles) using a cDNA library from mixed developmental stages. We cloned and sequenced the PCR products. If the directly upstream and/or downstream exons had not been identified in the first screening but were after PCR sequencing, new primers spanning only those exons were designed, and a new PCR was performed to assess the presence of different isoforms. All sequences were uploaded to GeneBank (accession nos. JF314355–JF314403). All primer sequences are available upon request. *TACC2* could not be studied in amphioxus and *Ciona*; *TPM* data were obtained from ref. 29.

For the alternatively spliced exons that were present at any invertebrate genome, we assessed AS by RT-PCR using cDNAs from mixed stages. For the positive cases at the AS level, we searched in the genome for *Nova*-binding motifs (YCAY clusters) at orthologous positions or in other locations with generally equivalent effects to the *Nova*-binding sites described in mouse (19). We used a permissive definition for YCAY clusters, based on ref. 19: at least three YCAY clusters within 50 bp, with a maximum inter-YCAY distance of 24 bp, which were then validated using minigenes for the case of amphioxus.

Putative *Nova*-regulated AS events in the vertebrate ancestor (Fig. 3C, main text) were inferred from the exons conserved from mammals to fish (19), using YCAY cluster scores from ref. 19, if available, or studying conservation of each mouse YCAY cluster in the orthologs and ohnologs (paralogs resulting from the two rounds of whole-genome duplication) from available fish genomes (*T. rubripes*, *Tetraodon nigroviridis*, *Oryzas latipes*, *D. rerio*, and *Gasterosteus aculeatus*).

RT-PCRs of conserved *Nova* exons in amphioxus (Fig. S3) were performed on tissues from an adult amphioxus individual. Gut, neural tube, gills, and muscle were carefully dissected and RNA extracted and cDNA prepared using standard protocols. For real-time PCR quantification of *Nova* expression, *GAPDH* and cytosolic actin were used as controls for normalization, both yielding similar results. Real-time PCRs were performed using SYBR GREEN PCR Master Mix (Applied Biosystems) with standard conditions and 7 ng of cDNA for each sample. Three replicated were performed for each sample and set of primers.

1. Hellsten U, et al. (2010) The genome of the Western clawed frog *Xenopus tropicalis*. *Science* 328:633–636.
2. Putnam NH, et al. (2008) The amphioxus genome and the evolution of the chordate karyotype. *Nature* 453:1064–1071.
3. Srivastava M, et al. (2008) The Trichoplax genome and the nature of placozoans. *Nature* 454:955–960.
4. Putnam NH, et al. (2007) Sea anemone genome reveals ancestral eumetazoan gene repertoire and genomic organization. *Science* 317:86–94.
5. Dehal P, et al. (2002) The draft genome of *Ciona intestinalis*: Insights into chordate and vertebrate origins. *Science* 298:2157–2167.
6. Sodergren E, et al. (2006) Sea Urchin Genome Sequencing Consortium (2006) The genome of the sea urchin *Strongylocentrotus purpuratus*. *Science* 314:941–952.
7. Richards S, et al. (2008) Tribolium Genome Sequencing Consortium (2008) The genome of the model beetle and pest *Tribolium castaneum*. *Nature* 452:949–955.
8. Holt RA, et al. (2002) The genome sequence of the malaria mosquito *Anopheles gambiae*. *Science* 298:129–149.
9. Chapman JA, et al. (2010) The dynamic genome of Hydra. *Nature* 464:592–596.
10. Robb SM, Ross E, Sánchez Alvarado A (2008) SmedGD: The *Schmidtea mediterranea* genome database. *Nucleic Acids Res* 36(Database issue):D599–D606.
11. Birney E, Durbin R (2000) Using GeneWise in the *Drosophila* annotation experiment. *Genome Res* 10:547–548.
12. D'Aniello S, et al. (2008) Gene expansion and retention leads to a diverse tyrosine kinase superfamily in amphioxus. *Mol Biol Evol* 25:1841–1854.
13. Higgins DG, Thompson JD, Gibson TJ (1996) Using CLUSTAL for multiple sequence alignments. *Methods Enzymol* 266:383–402.
14. Huelsenbeck JP, Ronquist F (2001) MRBAYES: Bayesian inference of phylogenetic trees. *Bioinformatics* 17:754–755.
15. Ronquist F, Huelsenbeck JP (2003) MrBayes 3: Bayesian phylogenetic inference under mixed models. *Bioinformatics* 19:1572–1574.
16. Drummond A, Strimmer K (2001) PAL: An object-oriented programming library for molecular evolution and phylogenetics. *Bioinformatics* 17:662–663.
17. Abascal F, Zardoya R, Posada D (2005) ProtTest: Selection of best-fit models of protein evolution. *Bioinformatics* 21:2104–2105.
18. Guindon S, Gascuel O (2003) A simple, fast, and accurate algorithm to estimate large phylogenies by maximum likelihood. *Syst Biol* 52:696–704.
19. Jelen N, Ule J, Zivin M, Darnell RB (2007) Evolution of Nova-dependent splicing regulation in the brain. *PLoS Genet* 3:1838–1847.
20. Rukov JL, et al. (2007) High qualitative and quantitative conservation of alternative splicing in *Caenorhabditis elegans* and *Caenorhabditis briggsae*. *Mol Biol Evol* 24:909–917.
21. Tena JJ, et al. (2007) Odd-skipped genes encode repressors that control kidney development. *Dev Biol* 301:518–531.
22. Irimia M, et al. (2010) Conserved developmental expression of Fezf in chordates and *Drosophila* and the origin of the Zona Limitans Intrathalamica (ZLI) brain organizer. *Evodevo* 1:7.
23. Yu JK, Holland LZ (2009) Amphioxus whole-mount in situ hybridization. *Cold Spring Harb Protoc* 2009:pdb.prot5286.
24. Lowe CJ, Tagawa K, Humphreys T, Kirschner M, Gerhart J (2004) Hemichordate embryos: Procurement, culture, and basic methods. *Methods Cell Biol* 74:171–194.
25. Martín-Durán JM, Amaya E, Romero R (2010) Germ layer specification and axial patterning in the embryonic development of the freshwater planarian *Schmidtea polychroa*. *Dev Biol* 340:145–158.
26. Genikhovich G, Technau U (2009) In situ hybridization of starlet sea anemone (*Nematostella vectensis*) embryos, larvae, and polyps. *Cold Spring Harb Protoc* 2009:pdb.prot5282.
27. Tomancak P, et al. (2007) Global analysis of patterns of gene expression during *Drosophila* embryogenesis. *Genome Biol* 8:R145.
28. Poustka AJ, et al. (2007) A global view of gene expression in lithium and zinc treated sea urchin embryos: New components of gene regulatory networks. *Genome Biol* 8:R85.
29. Irimia M, Maeso I, Gunning PW, Garcia-Fernàndez J, Roy SW (2010) Internal and external paralogy in the evolution of tropomyosin genes in metazoans. *Mol Biol Evol* 27:1504–1517.

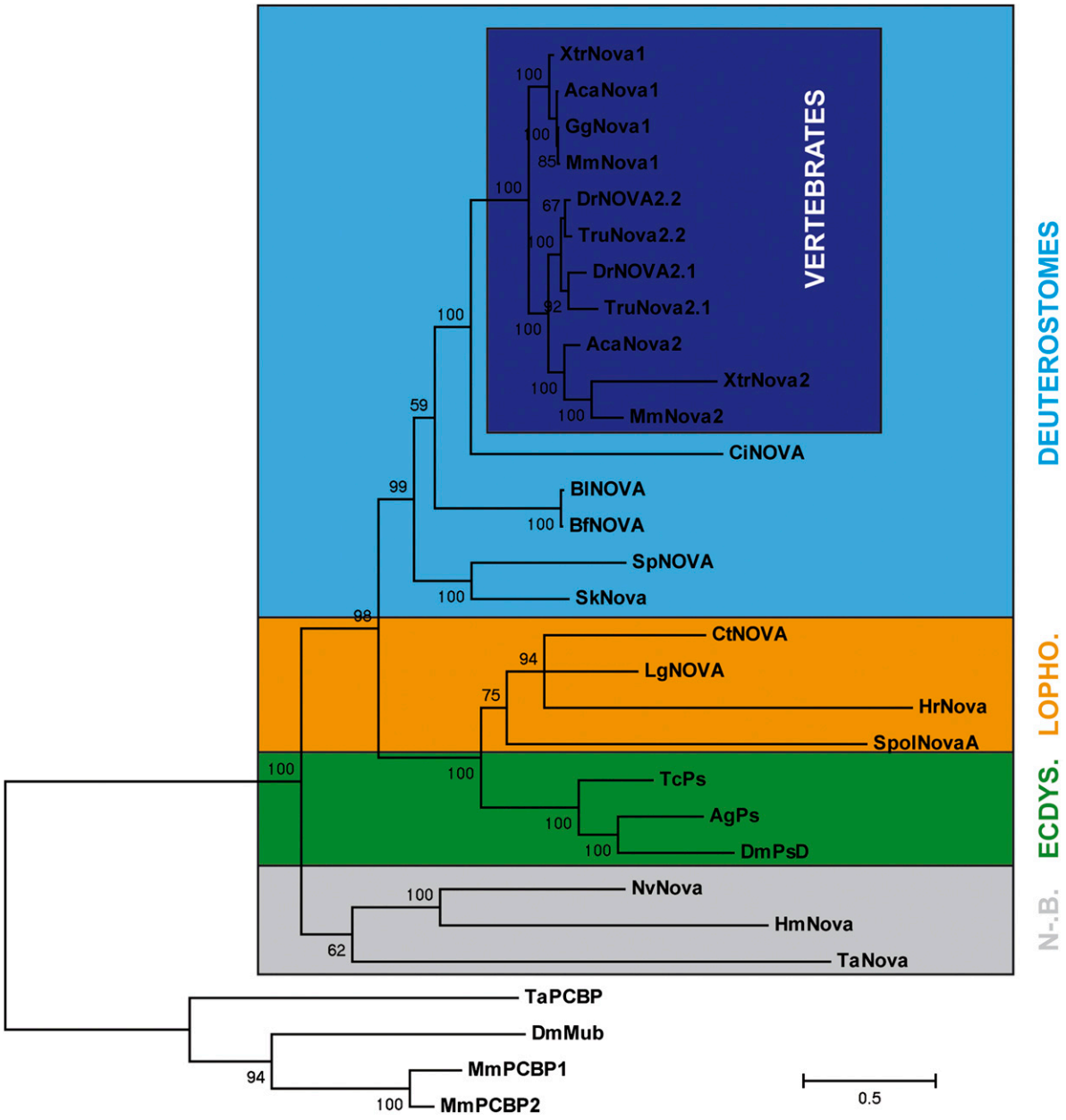

Fig. S1. Bayesian phylogenetic reconstruction of the *Nova* orthologs identified in different metazoan genomes. Phylogenetic trees were by the Bayesian method with MrBayes 3.1.2, with the Dayhoff+Gamma model, as recommended by ProtTest 1.4 under the Akaike information and the Bayesian information criteria. Two independent runs were performed, each with four chains. By convention, convergence was reached when the value for the SD of split frequencies stayed below 0.01. Burn-in was determined by plotting parameters across all runs for a given analysis: all trees before stationarity and convergence were discarded, and consensus trees were calculated for the remaining trees (2,500,000 generations). Lopho., Lophotrochozoans; Ecdys., Ecdysozoans; N.B., Non Bilaterians; Xtr, *Xenopus tropicalis*; Aca, *Anolis carolinensis*; Gg, *Gallus gallus*; Mm, *Mus musculus*; Tru, *Takifugu rubripes*; Dr, *Danio rerio*; Ci, *Ciona intestinalis*; Bf, *Branchiostoma floridae*; Bl, *Branchiostoma lanceolatum*; Sp, *Strongylocentrotus purpuratus*; Sk, *Saccoglossus kowalevskii*; Ct, *Capitella teleta*; Lg, *Lottia gigantea*; Hr, *Helobdella robusta*; Spol, *Schmidtea polychroa*; Tc, *Tribolium castaneum*; Dm, *Drosophila melanogaster*; Ag, *Anopheles gambiae*; Nv, *Nematostella vectensis*; Hm, *Hydra magnipapillata*; Ta, Trichoplax adhaerens.

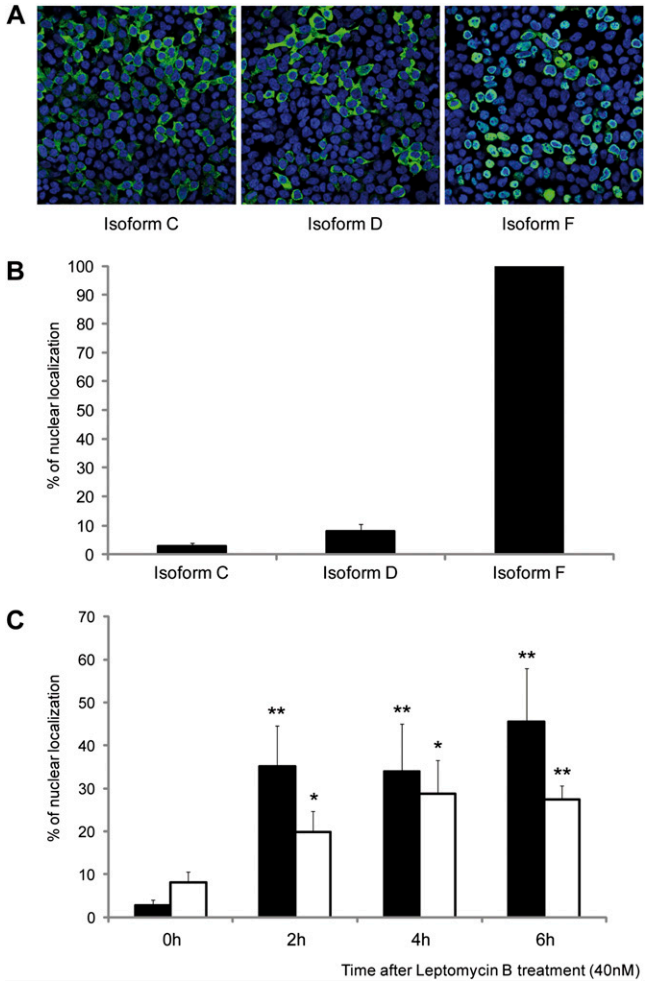

Fig. S2. Nuclear location of *Drosophila Nova* (pasilla) isoforms. (*A*) Confocal images of transfected cells (green) with DAPI staining (blue) showing nuclear and/or cytosolic location for each isoform. (*B*) Percentage of nuclear location of *Drosophila Nova* isoforms C, D, and F. (*C*) Percentage of nuclear location of *Drosophila Nova* isoforms C (black) and D (white) after 0, 2, 4, and 6 h of 40 nM leptomycin B.

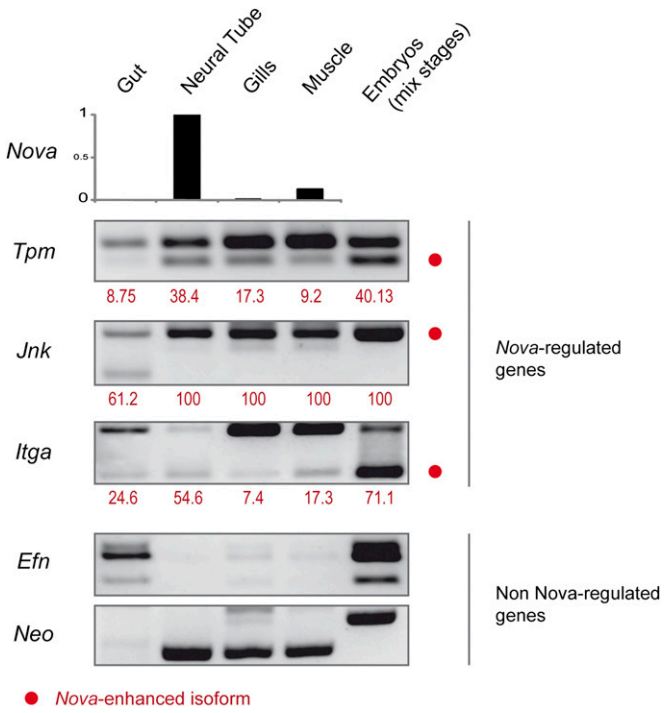

Fig. S3. RT-PCR of *Nova*-regulated exons in amphioxus tissues. Real-time PCR quantification of *Nova* in four amphioxus adult tissues: gut, neural tube, gills, and muscle. Values are relative to the tissue with the highest expression (neural tube, value = 1) and are averaged for the two housekeeping genes used as controls (*GAPDH* and cytosolic actin; raw data are shown in Table S1). RT-PCRs showing exon inclusion levels for each of the five alternative splicing events conserved between vertebrates and amphioxus are shown below. Each event is known *Nova*-regulated in vertebrates; three events (*Itga*, *JNK*, and *TPM*) have YCAY clusters in amphioxus ("*Nova*-regulated genes"), and two events do not (*EfnA* and *Neo*). RT-PCRs are shown for adult amphioxus gut, neural tube, gills, muscle, and mixed embryonic tissue. Red dots indicate gel position of *Nova*-enhanced isoforms. Red-font values correspond to the percentage of the *Nova*-enhanced isoform estimated by gel quantification.

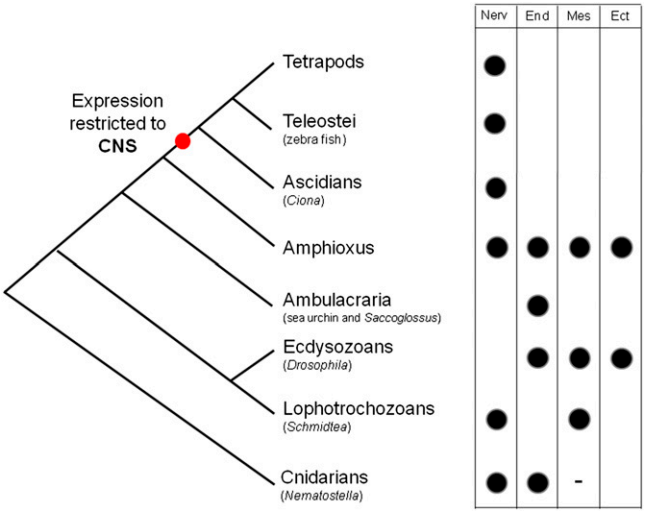

Fig. S4. *Nova* expression across metazoans. Summary of *Nova* expression in the studied species. Dots indicate expression of *Nova* in the nervous system (Nerv), endoderm (End), mesoderm (Mes), or ectoderm (Ect). The inferred time of restriction of *Nova* expression to the central nervous system is indicated by a red dot in the schematic phylogenetic tree.

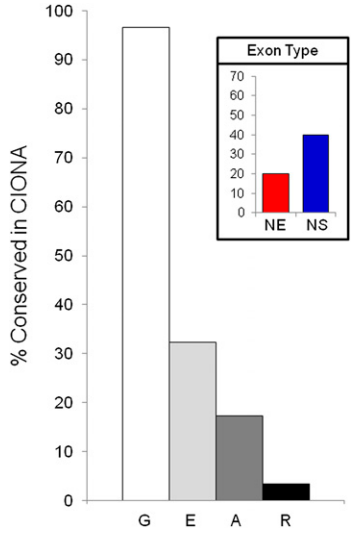

Fig. S5. Percentage of conservation for each of four levels in *Ciona*. G, ortholog gene presence; E, ortholog exon presence; A, alternative splicing of the orthologous exon; R, presence of equivalent YCAY clusters. *Inset:* E level for *Nova* enhanced/silenced exons (red, NE; blue, NS).

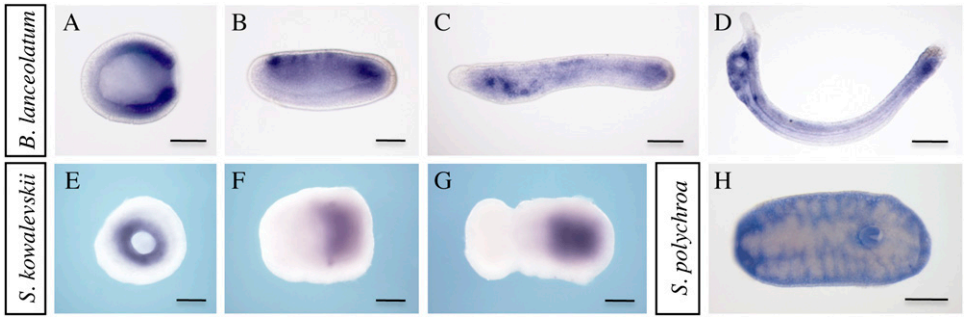

Fig. S6. Developmental expression using alternative *Nova* probes. *BlNova* is expressed early in the gastrula endomesoderm (*A*) and later in the posterior mesoderm of early- and midneurula (*B*, lateral view). At late-neurula and premouth stages (*C*, lateral view), expression continues in CNS and mesoderm and begins strongly in ectodermal and endodermal structures in the mouth and pharynx regions of larvae (*D*, lateral view). (*E*–*G*) The hemichordate *S. kowalevskii*. Expression of 3′ UTR probes for *SkNova* is restricted to postpharyngeal endoderm during development: early gastrula (*E*), late gastrula (*F*), and late neurula (*G*). (*H*) The planarian *S. polychroa*. The developmental expression of KH-free probe of *SpolNova1* is restricted to cerebral ganglia and mesenchyme at stage 7; signal in the pharynx is due to probe trapping. Anterior/oral is to the left in all cases except E, which is a view from the blastopore. (Scale bars, 100 μm in *A*–*G*; 250 μm in *H*.)

Table S1. Raw data for each individual replicate of the real-time PCR quantification of *Nova* expression across four amphioxus tissues

Tissue	Replicate 1	Replicate 2	Replicate 3	Average	By GAPDH		By actin	
Gut								
Nova	Undet	Undet	Undet	—	—	0.0000	—	0.0000
GAPDH	30.8163	29.8814	31.1233	30.6070	0.0000	1.0000	7.5544	0.0053
Actin	23.0574	23.0084	23.0921	23.0526	−7.5544	187.9708	0.0000	1.0000
Neural tube								
Nova	24.2645	23.4707	23.4811	23.7388	−0.6020	1.5178	0.1023	0.9315
GAPDH	24.9280	23.9706	24.1238	24.3408	0.0000	1.0000	0.7043	0.6137
Actin	23.7510	23.7537	23.4047	23.6365	−0.7043	1.6294	0.0000	1.0000
Gill								
Nova	39.3817	38.2141	37.1005	38.2321	9.9866	0.0010	18.3794	0.0000
GAPDH	28.6784	27.9685	28.0896	28.2455	0.0000	1.0000	8.3928	0.0030
Actin	19.8390	19.7713	19.9479	19.8527	−8.3928	336.1103	0.0000	1.0000
Muscle								
Nova	23.1215	22.5727	22.9292	22.8745	2.4169	0.1873	3.1156	0.1154
GAPDH	20.5341	20.5182	20.3202	20.4575	0.0000	1.0000	0.6987	0.6161
Actin	19.8985	19.4357	19.9422	19.7588	−0.6987	1.6231	0.0000	1.0000
	Relative to GAPDH	Fraction of NT expr	Relative to actin	Fraction of NT expr	Average			
Gut	0.0000	0.0000	0.0000	0.0000	0.0000			
Neural tube	1.5178	1.0000	0.9315	1.0000	1.0000			
Gill	0.0010	0.0006	0.0000	0.0000	0.0003			
Muscle	0.1873	0.1234	0.1154	0.1239	0.1236			

expr, expression; Undet, undetermined.

Dataset S1. Amino acid sequence, protein length, and chromosome/scaffold location for each of the studied *Nova* proteins

Dataset S1 (XLS)

Dataset S2. Features of studied *Nova*-regulated exons

Dataset S2 (XLS)

Length (green heading) and sequence conservation (pink) for different vertebrates was obtained from Jelen et al. (1). Other data: %EST (major/minor, >50%/<50% of available ESTs), REG (exon enhanced (E) or silenced (S) by *Nova* or mutually exclusive exon skipping event (ME), FS/Stop (whether the exon inclusion/exclusion generates a frame shift and/or introduces a STOP codon). Summary results for amphioxus (yellow) and *Ciona* (orange) comparisons: length (in nucleotides), % cons (percentage of conservation in nucleotides), Ex [exon presence, Yes (Y)/No (N)], AS (exon is alternatively spliced in the species), Reg (YCAY presence)

1. Jelen N, Ule J, Zivin M, Darnell RB (2007) Evolution of Nova-dependent splicing regulation in the brain. *PLoS Genet* 3:1838–1847.

Artículo anexo 4

OPEN ACCESS Freely available online

PLOS ONE

CERKL Knockdown Causes Retinal Degeneration in Zebrafish

Marina Riera[1,2,3], Demian Burguera[1,2], Jordi Garcia-Fernàndez[1,2], Roser Gonzàlez-Duarte[1,2,3]*

1 Departament de Genètica, Facultat de Biologia, Universitat de Barcelona, Barcelona, Spain, **2** Institut de Biomedicina (IBUB), Universitat de Barcelona, Barcelona, Spain, **3** CIBERER, Instituto de Salud Carlos III, Barcelona, Spain

Abstract

The human *CERKL* gene is responsible for common and severe forms of retinal dystrophies. Despite intense *in vitro* studies at the molecular and cellular level and *in vivo* analyses of the retina of murine knockout models, CERKL function remains unknown. In this study, we aimed to approach the developmental and functional features of *cerkl* in *Danio rerio* within an Evo-Devo framework. We show that gene expression increases from early developmental stages until the formation of the retina in the optic cup. Unlike the high mRNA-*CERKL* isoform multiplicity shown in mammals, the moderate transcriptional complexity in fish facilitates phenotypic studies derived from gene silencing. Moreover, of relevance to pathogenicity, teleost CERKL shares the two main human protein isoforms. Morpholino injection has been used to generate a *cerkl* knockdown zebrafish model. The morphant phenotype results in abnormal eye development with lamination defects, failure to develop photoreceptor outer segments, increased apoptosis of retinal cells and small eyes. Our data support that zebrafish Cerkl does not interfere with proliferation and neural differentiation during early developmental stages but is relevant for survival and protection of the retinal tissue. Overall, we propose that this zebrafish model is a powerful tool to unveil CERKL contribution to human retinal degeneration.

Citation: Riera M, Burguera D, Garcia-Fernàndez J, Gonzàlez-Duarte R (2013) *CERKL* Knockdown Causes Retinal Degeneration in Zebrafish. PLoS ONE 8(5): e64048. doi:10.1371/journal.pone.0064048

Editor: Hector Escriva, Laboratoire Arago, France

Received December 24, 2012; **Accepted** April 8, 2013; **Published** May 9, 2013

Funding: This study was supported by grants SAF2009-08079 (Ministerio de Ciencia e Innovación), SGR2009-1427 (Generalitat de Catalunya), CIBERER (U718), Retina Asturias and ONCE to RGD, and BFU2011-23291 (Ministerio de Ciencia e Innovación) and ICREA Academia Prize (Generalitat de Catalunya) to JGF. The funders had no role in study design, data collection and analysis, decision to publish, or preparation of the manuscript.

Competing Interests: The authors have declared that no competing interests exist.

* E-mail: rgonzalez@ub.edu

Introduction

Retinal dystrophies (RD), the major cause of incurable familial blindness in the Western world, are monogenic disorders characterized by progressive dysfunction of photoreceptor and retinal pigment epithelium (RPE) cells [1]. RD is a group of extremely heterogeneous diseases that show substantial clinical and genetic overlap. Moreover, mutations in a single gene appear to be associated to distinct clinical entities [2], as is the case for *CERKL*, that was initially characterized as an autosomal recessive Retinitis Pigmentosa (RP) gene [3], [4], [5], [6], [7], [8], and later shown to promote Cone-Rod Dystrophy (CRD), a RD disorder associated to a more severe phenotype [9], [10].

Highthroughput technologies have greatly improved our knowledge of the genetic basis of RD. Indeed, more than 180 RD genes have already been reported and this number is constantly increasing (Retnet, https://sph.uth.tmc.edu/retnet/). However, although RD genes are known to be involved in a variety of cellular and molecular processes in the retina, we are still far from understanding the contribution of most of them to the disease. CERKL ranks in this class, as all previous attempts have failed to provide valuable clues to explain its involvement in photoreceptor degeneration.

Human *CERKL* was initially identified as a 13 exon-gene, which encoded a polypeptide of 532 amino acids. This protein shared an integral diacylglycerol kinase (DAGK) signature [3] with Ceramide Kinase (CERK), an ubiquitously expressed paralog with ceramide kinase activity involved in cell survival and proliferation [11]. In CERKL, all the *in vivo* and *in vitro* assays with reported CERK substrates and a variety of lipid mixtures have failed to show any kinase activity [12], [13], [14], [15], [16]. Concerning cell survival, overexpression of CERKL in cultured cells showed protection against apoptosis induced by oxidative stress [14]. Moreover, studies with transfected cell lines have shown a dynamic subcellular localization of CERKL, shifting from the cytoplasm, where the protein is mainly associated to the endoplasmic reticulum and Golgi membranes, to the nucleus [14]. CERKL intracellular traffic regulation seems to be directed by two nuclear localization signals (NLSs) and two nuclear export signals (NESs) [6], [12], [13]. Concerning CERKL localization in the retina, immunohistochemistry on mouse cryosections revealed strong localization in cones, faint in rods, and moderate at the ganglion cell (GCL) and inner nuclear layers (INL) [17], [18], [19].

CERKL performance in the retina has been also approached through an accurate assessment of its transcriptional products in several tissues. Interestingly, in the retina, human and mouse *CERKL* revealed an unexpected high repertoire of mRNA isoforms (>20 isoforms in human and >30 in mouse were validated), which emerged from alternative splicing and additional promoters, among them that of *NEUROD1* gene [17], [18]. The high heterogeneity presumed at the protein level, together with its dynamic subcellular localization probably accounts for the multifunctional character of CERKL.

Animal models, whether natural or transgenic, provide invaluable tools for studies of disease pathogenesis and the identification of therapeutic targets [20]. To date, two mouse models of CERKL have been constructed. The first was obtained by deletion of the alternatively spliced exon 5, where the most prevalent mutation (R257X) is found [21]. The second was generated in our group by the deletion of the proximal promoter and exon 1. Both mouse models were viable and fertile, and did not show gross morphological alterations in the retina. Our targeted *Cerkl* deletion resulted in a knockdown rather than a knockout model, as gene transcription was attained from two previously unreported alternative promoters [19]. Moderate dysfunction was observed in the ganglion and/or amacrine cells, supported by aberrant electroretinographic recordings and increased retinal apoptosis and gliosis, whereas photoreceptor cells showed WT features [19]. The failure to reproduce the human phenotype in the mouse, not unusual in other hereditary retinal disorders, prompted us to explore zebrafish as an alternative model. In this context, *Danio rerio* seems to be an excellent tool to understand the mechanisms of human visual disorders, because human and zebrafish share the main cell types and general structure of the eye. Moreover, zebrafish biology allows ready access to all developmental stages, and the optical transparency of embryos and larvae allow real-time imaging of developing pathologies [22]. The ontogeny of the zebrafish eye begins as an evagination from the developing forebrain around 12 hours postfertilization (hpf), and ocular development is largely completed by 72 hpf, at which time the first visual responses can be detected [23], [24], [25], [26]. In this study we have identified the zebrafish *cerkl* ortholog, studied its expression during development and in the adult tissues, and drawn comparisons with vertebrate species. Besides, we have generated *cerkl* zebrafish knockdowns by morpholino injection and characterized a range of developmental abnormalities in the morphant phenotype, including retinal degeneration and apoptosis-like cell death. Finally, our analyses highlight our model as a simple and amenable tool to analyse CERKL contribution to RD pathogenesis.

Materials and Methods

Ethics statement

All procedures were performed according to the ARVO Statement for the Use of Animals in Ophthalmic and Vision Research, as well as the regulations of the Animal Care facilities at the University of Barcelona. The study was approved by the Ethics Committee for Animal Experimentation (CEEA) of the University of Barcelona. When needed, animals were sacrificed with excess of anaesthetic MS222, following the approved protocols.

Animal handling, tissue dissection and preparation of the samples

Zebrafish (*Danio rerio*) were maintained at 28.5°C on a 14-hour light/10-hour dark cycle. The transgenic strain *ath5:GFP* was a kind gift from Carolina Minguillón. Fertilized eggs were obtained and grown in incubators, and embryos were staged as described [27], [28]. Specific tissues and organs were dissected from adult zebrafish and immediately frozen in liquid nitrogen.

Identification of CERKL orthologs

The human CERKL isoform 1 (NM_201548.4) amino acid sequence was used as a query for a BLASTp search (http://www.ncbi.nlm.nih.gov). Protein sequences from several species were compared running a CLUSTALW2 alignment (www.ebi.ac.uk). Conservation of CERKL across different species was evaluated with the Jalview program (version 2.7).

RNA-seq expression analysis

Available RNA-seq data on zebrafish developmental stages and adult tissues was used to quantify *cerkl* expression according to the previously defined cRPKM value [29]. The reported RNA-seq data used in this study are shown in Table S1.

RNA extraction and RT-PCR

RNAs from a pool of zebrafish, frog and chicken embryos at different stages of development or from different tissues of adult specimens were extracted using the RNeasy Mini or Micro Kit (Qiagen, Valencia, CA), following the manufacter's instructions. RT-PCR assays were carried out with the Transcriptor High Fidelity cDNA Synthesis Kit (Roche Diagnostics, Indianapolis, IN), using 200 ng of total RNA. For semi-quantitative analysis, the cDNA was amplified according to standard protocols using GoTaq polymerase (Promega, Madison, WI). The level of expression and characterization of different isoforms was performed using a forward primer located in the 5′UTR and a reverse primer in the 3′UTR (Table S2). β-*actin*, *ODC* and *Gapdh* were used for normalization in zebrafish, frog and gallus samples, respectively (see primer sequences in Table S2). All PCR products were resolved on agarose gel electrophoresis and sequenced.

Cloning and overexpression of zebrafish CERKL in cultured cells

The full-length zebrafish *cerkl* transcript was amplified from adult retina oligo-dT cDNA using specific primers carrying *Bam*HI and *Xho*I restriction enzyme sites (see primer sequences, Table S2). The cDNA was inserted into a modified version of the pcDNA3.1 vector (Clontech Laboratories, Inc., Mountain View, CA) that adds a C-terminal hemagglutinin (HA) tag.

For protein expression, COS-7 cells were seeded and transfected using Lipofectamine 2000 reagent (Invitrogen Life Technologies, Carlsbad, CA), according to the manufacturer's protocol. After 48 h, immunolocalization was performed as previously described [14] incubating the cells with 1:275 anti-HA mouse monoclonal antibody (Covance, Princeton, NJ) followed by 1:300 AlexaFluor 488-conjugated anti-mouse secondary antibody (Invitrogen Life Technologies). Slides were counter-stained with 1:5000 DAPI (Roche Diagnostics, Indianapolis, IN) nuclear blue dye in PBS for 15 min. All preparations were mounted in Flouprep medium (BioMérieux, Craponne, France) and analyzed by confocal microscopy (SP2, Leica Microsystems, Wetzlar, Germany).

Histology and in situ hybridization

Embryos and adult zebrafish eyecups were fixed in 4% paraformaldehyde (PFA). For cryosections, embryos and adult eyecups were rinsed in sucrose at 4°C (successive incubations at 20% for 30 min, 30% for 30 min and 40% sucrose for 12 h) and then were embedded in O.C.T (Tissue-Tek, Sakura Finetech, Torrance, CA) and sectioned at −17°C. *In situ* hybridization on whole-mounts and cryosections were performed as previously described [30], [31] using digoxigenin (DIG)-labelled RNA sense and antisense probes (see primer sequences in Table S2). The BM Purple AP Substrate (Roche Diagnostics, Indianapolis, IN) reagent was used. Sections were cover-slipped with Fluoprep (Biomérieux, Craponne, France) and photographed using a Leica DFC Camera connected to a Leica DM IL optic microscope (Leica Microsystems).

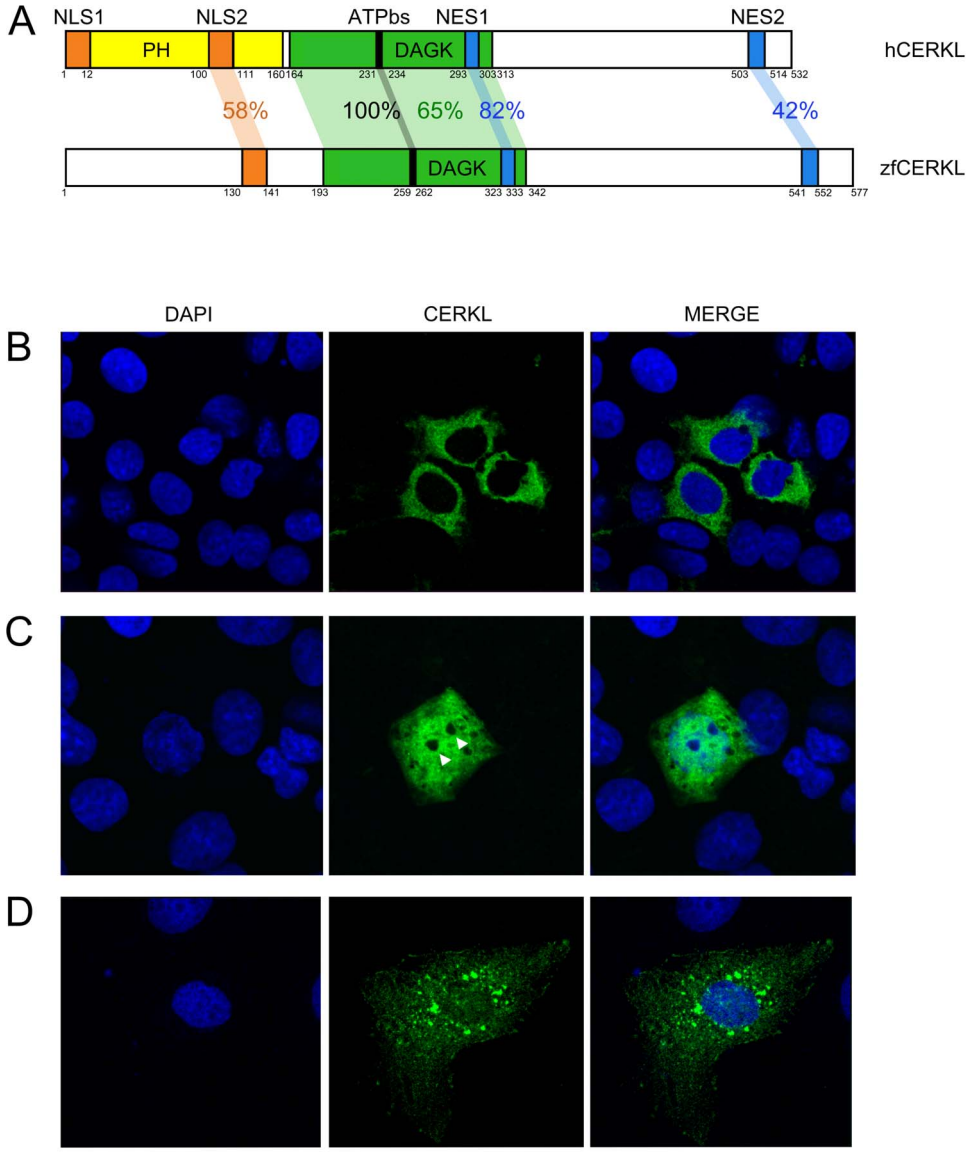

Figure 1. Human and zebrafish CERKL protein domains. (**A**) The reported hCERKL (NP_963842) protein domains described by either sequence homology (PH, pleckstrin homology; DAGK, diacylglycerol kinase and ATPbs, ATP binding site domains) or by functional analysis (NLS, nuclear localization signals; NES, nuclear export signals) and their conservation in zebrafish is shown in percentage of identity. (**B**–**D**) ZFCerkl-HA shares with human CERKL the dynamic subcellular localization in COS-7 transfected cells, shifting from the cytoplasm to the nucleus. Nuclei were stained with DAPI. Images correspond to individual optical sections. Photographs were at×63 magnification. (**B**) In most cells, ZFCerkl shows a uniform distribution in the cytosol and is absent from the nucleus. (**C**) Some cells per field showed localization of Cerkl in both, the cytosol and the nucleus, with clear exclusion from the nucleoli (white arrow). (**D**) Rarely, Cerkl contributes to cytosolic aggregates.
doi:10.1371/journal.pone.0064048.g001

Morpholino and mRNA injection

To knockdown ZF*cerkl*, we used two morpholino antisense oligonucleotides (MOs) targeting the acceptor splice site at the boundary of intron 3 and exon 4 (acMO, 5′-TCTCAGT-GACTGTGGAAAAGAAAGA-3′) and the donor splice site at the boundary of exon 9 and intron 9 (doMO, 5′-TAACCA-TACTCACAAATGTCTCCTC-3′). A standard control MO (coMO, 5′-CCTCTTACCTCAGTTACAATTTATA-3′) was also used. All the MOs were designed and synthesized by GeneTools (Philomath, OR). Eight nanograms of each MO were air pressured injected into 1 to 4-cell embryos. For the phenotypic rescue, human cDNA was cloned into the pCS2 vector. *In vitro* transcription of synthetic capped mRNA was performed using a capped RNA transcription kit (SP6 mMESSAGE mMACHINE; Ambion, Austin, TX) following the manufacturer's instruction. Two nanoliters of MO or mixed MO/mRNA was injected into each 1 to 4 cell-stage embryo. The final concentrations of MO and mRNA were 200 µM and 400 ng/ µl, respectively.

Haematoxylin and eosin staining and immunohistochemistry

Retina cryosections of 72 hpf embryos were haematoxylin and eosin stained under standard conditions. For immunohistochemistry, 14 µm sections were recovered on poly-lysine covered slides, dried for 1 h, washed in PBS (3× 10 min), and blocked in blocking solution (PBS containing 3% sheep serum, 1% BSA and 0.3%

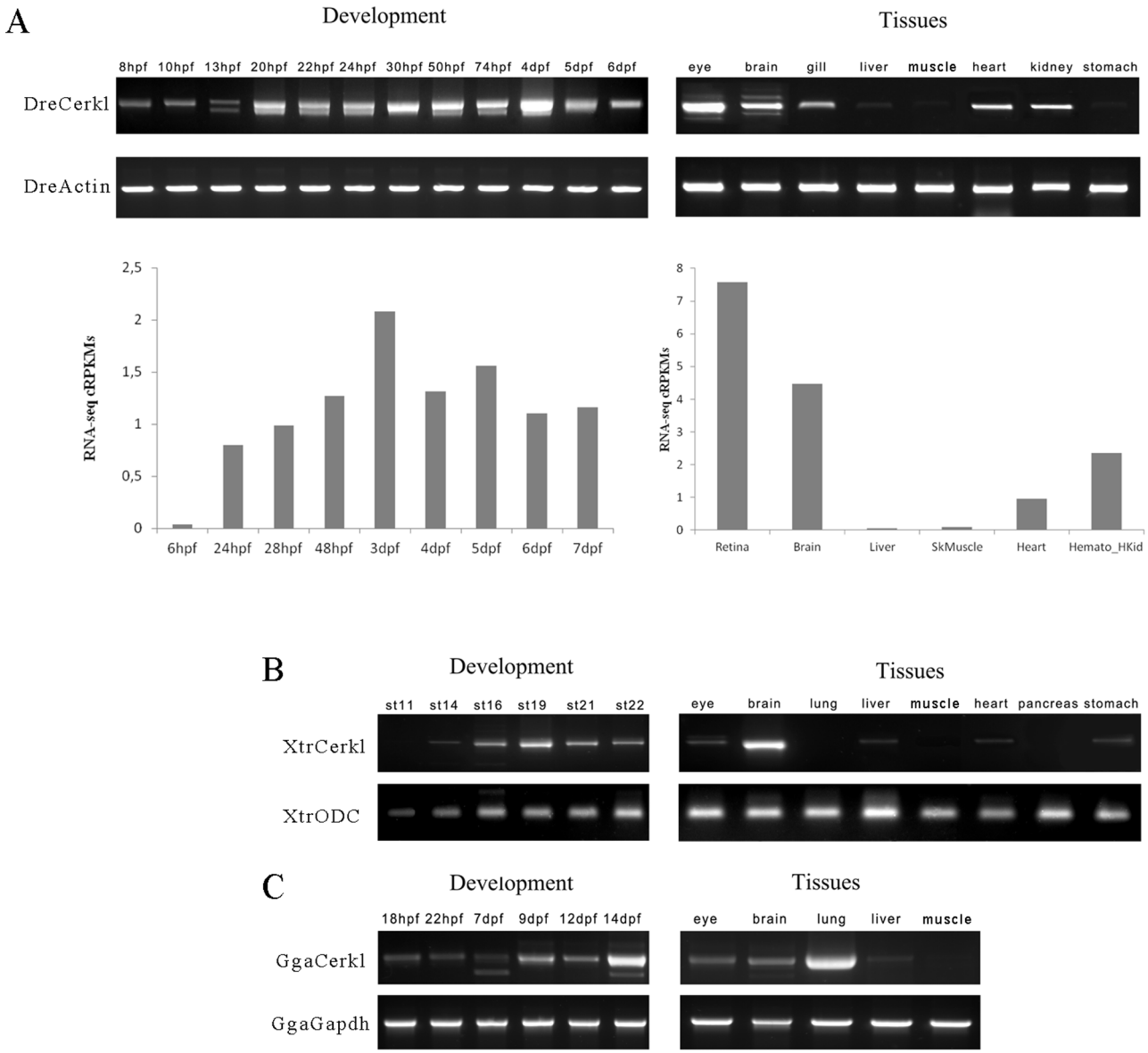

Figure 2. Expression of *cerkl* transcripts during embryonic development and adult tissues. (**A**) Temporal and spatial expression of zebrafish (Dre) *cerkl* assessed by RT-PCR (top) and RNA-seq data retrieved from databases (bottom) at different developmental stages and adult tissues. (**B and C**) Expression of *cerkl* in developmental stages and tissues of frog (Xtr) and chicken (Gga). hpf, hours post-fertilisation; dpf, days post-fertilization; st, stage.
doi:10.1371/journal.pone.0064048.g002

Triton X-100) for 60 min at room temperature (RT). Incubation with peanut agglutinin (PNA) conjugated to Alexa Fluor 647 (40 mg/ml; Invitrogen Life Technologies) and the primary antibody mouse anti-rhodopsin (1:500, Abcam, Cambridge, MA) was performed overnight at RT in blocking solution. Sections were rinsed three times in PBS again, followed by incubation with Alexa-Fluor568 goat anti-rabbit as secondary antibody (1:300, Invitrogen Life Technologies). Nuclei were stained with DAPI (Roche Diagnostics), sections were mounted in Fluoprep medium (Biomérieux) and analyzed by confocal microscope (SP5, Leica Microsystems). For eye measurements, 14 µm thick cryosections were examined under the microscope and imaged. Eye size was taken from the anterior to the posterior edge using the Fiji software. Significant differences between groups were analyzed by the Student's *t*-test.

Apoptotic cells in the retina cryosections of 72 hpf morphants were detected by immunofluorescence using anti-active Caspase-3 as primary antibody (1:200, BD Pharmingen, San Jose, CA) and Alexa-Fluor568 goat anti-rabbit as secondary antibody (1:300, Invitrogen Life Technologies) following the protocols already described. For apoptosis quantification, nuclei were counted using the Fiji software.

Results

Homology search and cloning of the zebrafish *cerkl*

To identify zebrafish *cerkl (ZFcerkl*), a BLAST search of the Ensembl zebrafish database was performed using the human CERKL protein isoform 1 sequence (NP_963842). A single copy of the zebrafish *cerkl* gene was detected, encompassing 195 kb on

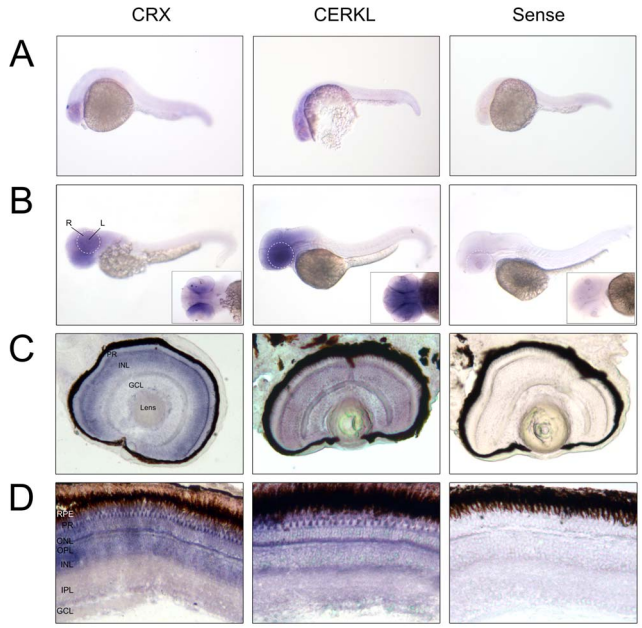

Figure 3. *Cerkl in situ* hybridization on embryo and adult zebrafish. (**A and B**) Whole-mount RNA *in situ* hybridization analysis showing *cerkl* expression in the retina and brain of embryos at 24 and 50 hpf. R, retina; L, lens. (**C and D**) *In situ* hybridization on zebrafish retina cryosections of 72 hpf embryos and adult tissue. *Cerkl* expression is detected in the three nuclear layers of the embryo retina, whereas adult expression appears in the inner segment of the photoreceptors and some cells located at the basal layer of the INL. Positive control (antisense *CRX*), strongly labels the inner photoreceptor segment and inner nuclear layer. The negative control was performed with sense *cerkl*. RPE, retinal pigment epithelium; PR, photoreceptor; ONL, outer nuclear layer; OPL, outer plexiform layer; INL, inner nuclear layer; IPL, inner plexiform layer; GCL, ganglion cell layer.
doi:10.1371/journal.pone.0064048.g003

chromosome 9. The genomic region of ZF*cerkl* shows conserved synteny over more than 1,8 Mb with the human *CERKL* locus on chromosome 2, and both largely share the same gene order and transcriptional orientation, with the only exception of a chromosomal inversion encompassing 4 genes (*dnajc*, *frzb*, *nckap1*, *dusp19*) located 5′ upstream of *cerkl* (Fig. S1).

The predicted zebrafish transcript encompasses 13 exons, spans approximately 2 kb and encodes a protein of 577 amino acids, the latter showing 59% identity and 82% similarity with the human counterpart. CERKL alignments between zebrafish and human revealed 65% identity between the DAGK domains (Fig. 1A). The ATP binding site (ATPbs) GGDG motif contained in this domain, already described in CERK, was fully conserved not only in zebrafish but also in 5 vertebrate species (Fig. S2). Concerning the nuclear localization and export signals (NLS and NES, respectively), the human NLS1 sequence (MPWRRRRNRVSA) was not conserved in zebrafish, neither in the rest of the species analysed, whereas NLS2 (SVKLKRRCSVKQ) showed 58% identity, with preservation of all but one (L) of the five key residues (underlined). The NES1 (LHIIMGHVQL) and NES2 (LMEVASEVHIRL) domains of human and zebrafish CERKL displayed 82% and 42% identities, respectively. The *in silico* predicted pleckstrin homology (PH) domain, essential for CERK localization, translocation, and enzymatic activity in human, encoded in exons 1 and 2 [32], showed very low conservation among vertebrate species. Remarkably, the multi-species comparison of CERKL protein sequences revealed two previously unidentified highly conserved regions, one in exon 7 (hCERKL, 318–352 aa), and the other encompassing exons 10 and 11 (hCERKL, 400–448 aa), with unassigned function so far (Fig. S2).

On the basis of these predictions, specific primers were designed (Table S2) to clone zebrafish *cerkl* cDNA by RT-PCR into a modified version of the pcDNA 3.1 vector that adds a C-terminal hemagglutinin (HA) tag. The construct was transfected into COS-7 cells, and an anti-HA immunodetection was performed. The ZFCerkl protein shared with hCERKL the dynamic subcellular localization, shifting from the cytoplasm (where is found with a uniform pattern or in aggregates) to the nucleus. Remarkably, in contrast with the human homolog, ZFCerkl showed clear exclusion from the nucleoli (Fig. 1B–D).

Regulated expression of vertebrate *cerkl* orthologs during embryogenesis and in adult tissues

The temporal and spatial expression pattern of ZF*cerkl* during embryogenesis was examined by semi-quantitative RT-PCR (Fig. 2A, see Table S2 for primer sequences). Expression was faint at early developmental stages, from 75%-epiboly (8 hpf) up to the 8-somite stage (13 hpf) embryos, followed by two marked increases in gene expression around the 22-somite (20 hpf) and 30 hpf stages, just when the optic cup starts forming the neural retina [33]. Moreover, the expression persisted during development up to 6 days post fecundation (dpf), reaching a maximum at 4 dpf. Adult tissue expression was examined in total RNA from eye, brain, gill, fin, heart, liver, muscle and stomach. Expression was highest in eye, moderate in brain, heart and kidney, and low in gills. Our RT-PCR semiquantitative analysis was supported by available zebrafish RNA-seq data (Fig. 2A) [34], [35], [36], [37], [38].

We then aimed to assess whether *cerkl* tissue-specific regulation and developmental expression was evolutionary conserved among other vertebrate species: *Gallus gallus* and *Xenopus tropicalis*. In agreement with mammals, *cerkl* expression in both species was mainly detected in eye and brain (Fig. 2B and C) [17], [18], which suggested a conserved role in the eye and the anterior central nervous system (CNS). Interestingly, high levels of transcription were also detected in the lung of *Gallus*. Further work should clarify if this is a case of *cerkl* co-option in the avian lineage.

Tissue specific expression in zebrafish was also assessed in whole embryos and in embryonic and adult retinas by *in situ* hybridization (ISH) (Fig. 3). *Crx* antisense and *cerkl* sense riboprobes were used as positive and negative controls, respectively. Faint *Cerkl* expression was already detected at 24 hpf by whole-mount ISH (Fig. 3A). Fifty hpf embryos showed *cerkl* expression restricted to the anterior region and, particularly, in the eye and brain (Fig. 3B). To further characterize the retinal expression pattern, ISH on cryosections was performed. Our data revealed strong hybridization signal at 72 hpf embryos in the three nuclear layers (Fig. 3C), whereas adult expression concentrated in the inner segment of photoreceptors and staining was not homogeneous along the inner nuclear and ganglion cell layers (Fig. 3D).

Alternative splicing and the NeuroD1 promoter among vertebrates

To assess and compare the diversity of *cerkl* mRNA isoforms in vertebrate, 45-cycle PCR reactions were performed using primers located in exons 1 and 13 of *cerkl* of *Danio rerio, Gallus gallus* and *Xenopus tropicalis* (Fig. 4A). Keeping in mind that some AS events and additional alternative promoters could have escaped our experimental approach, 3 *cerkl* mRNA variants were identified in zebrafish, 2 in *Xenopus tropicalis* and 3 in *Gallus gallus*. In zebrafish,

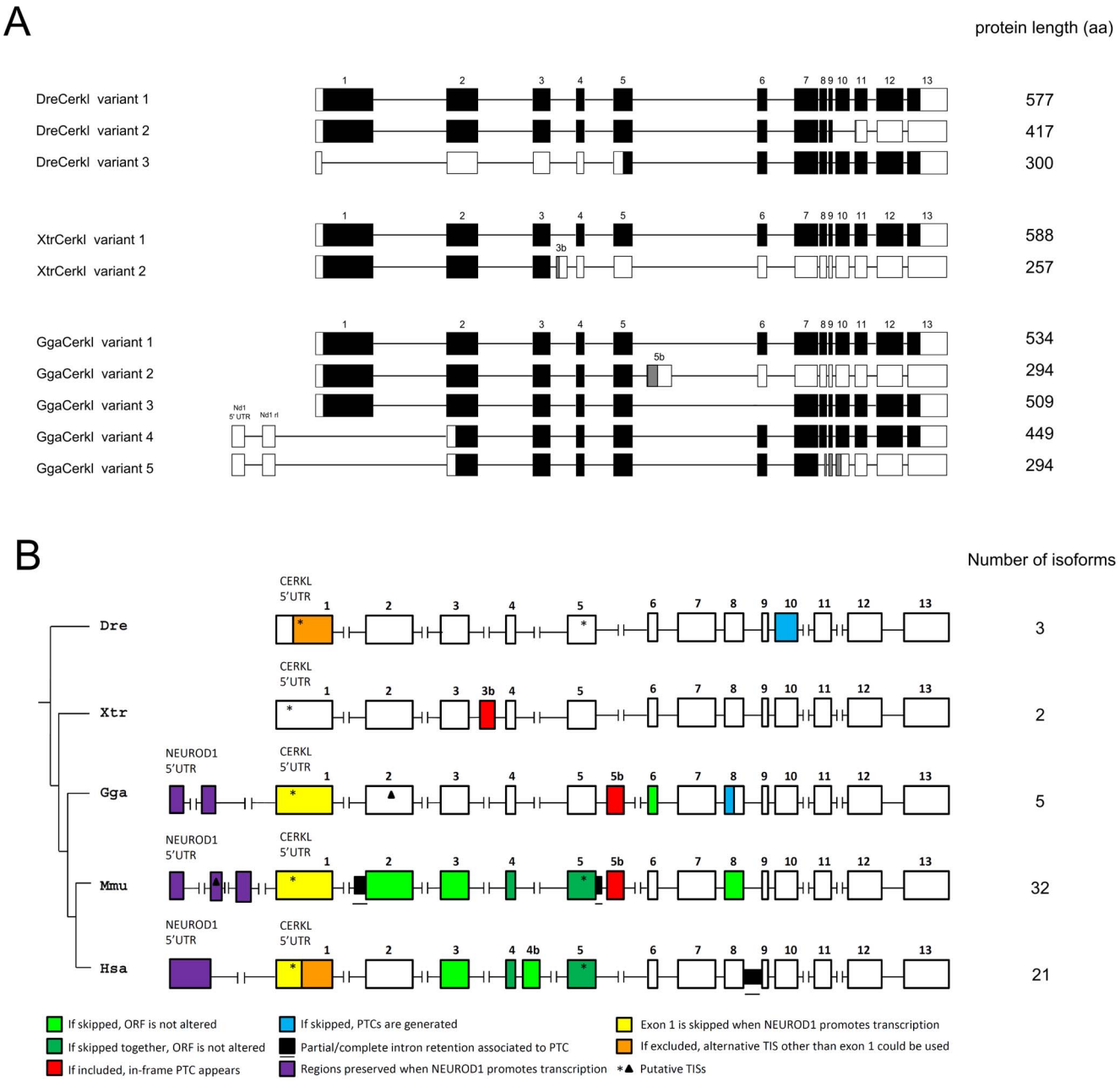

Figure 4. Alternatively spliced *cerkl* isoforms in vertebrates. (**A**) Scheme of the *cerkl* mRNA transcripts identified in zebrafish (Dre), frog (Xtr) and chicken (Gga). Exons are boxed and the coding sequence (CDS) for each isoform, considering the largest ORF, is shown in black. Grey boxes represent alternative ORFs. Protein length (in aa) is indicated (right column). (**B**) Schematic view of *CERKL* gene structure as well as the translational impact of all alternative exons (AEs) detected in *Danio rerio* (Dre), *Xenopus tropicalis* (Xtr), *Gallus gallus* (Gga), *Mus musculus* (Mmu) and *Homo sapiens* (Hsa). Exons preserved in all protein isoforms are shown by empty boxes. AEs are colored: light green, if when skipped, the ORF is not altered; dark green for those that maintain the ORF when skipped together; red, if they contain an in-frame stop codon and thus, when preserved, produce a truncated C-terminus protein. In blue, exonic sequences that, when skipped, the ORF generates a premature stop codon; black underlined flattened boxes indicate partial/complete intron retention associated to truncated peptides, purple depicts the regions preserved when *NEUROD1* promotes transcription. The latter isoforms lead to whole exon 1 depletion and subsequent loss of the conventional initiator methionine. In the canonical human and zebrafish *CERKL* first exon two donor splice sites are contained, one at the 3′end of the exon, and the other in the middle (the boundary shown in orange). When this second splice site is used, protein translation begins in exon 5. Asterisks show initiator methionines validated in human only but conserved among vertebrates. A methionine in exon 2 of *Gallus gallus* that could be used to initiate translation when exon 1 is skipped is depicted by a triangle. The number of *CERKL* isoforms in each species is indicated (right column). PTC: premature termination codon; TIS: translation initiation site.

doi:10.1371/journal.pone.0064048.g004

variant 1 was the major isoform and encompassed all the exons; variant 2 skipped exon 10 and encoded a C-terminus truncated protein without the NES2 domain; and variant 3, adult eye-specific, was generated from a novel splice donor site within exon 1. In the later form, protein synthesis would start at a conserved methionine in exon 5, as already described in human [18], and

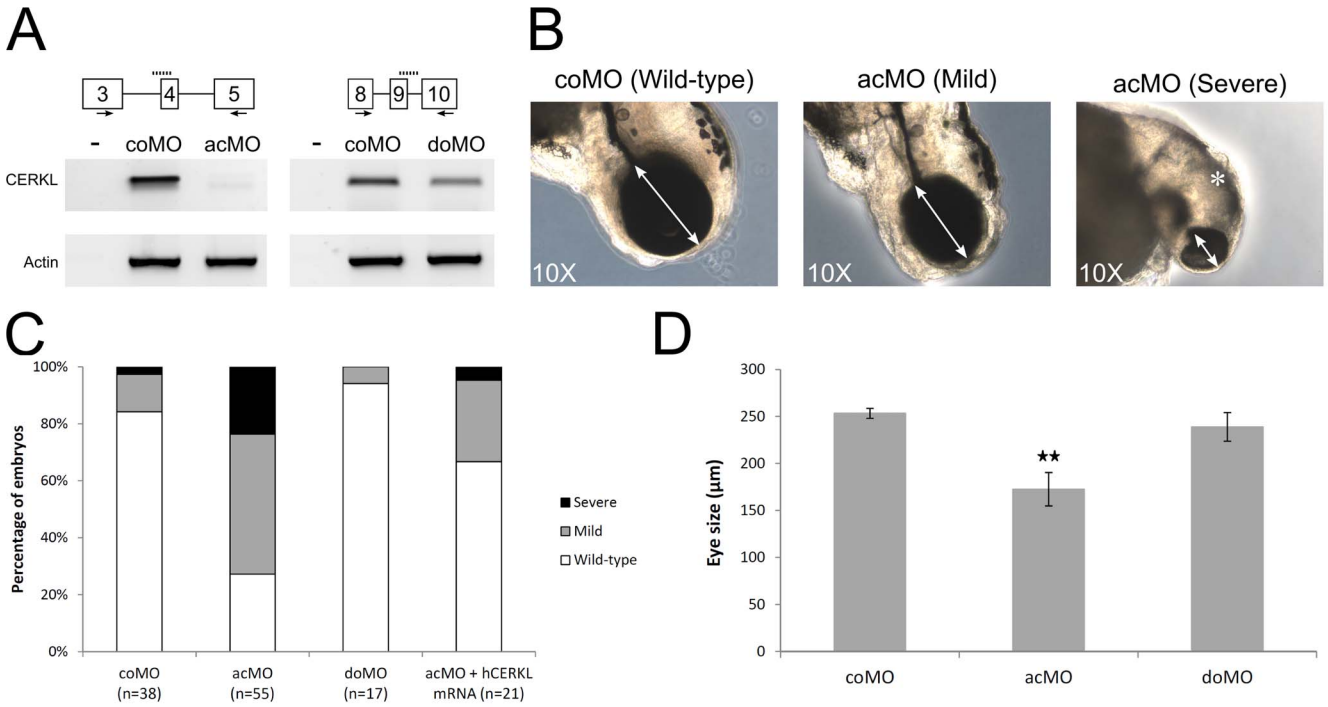

Figure 5. Effects of ZF*cerkl* silencing in eye development. (**A**) Two morpholinos targeting an acceptor (acMO) and donor splice site (doMO) of ZF*cerkl* were used. The morpholino targeting site is depicted by a discontinuous line. To assess the knockdown effect, a RT-PCR analysis of control and ZF*cerkl* morphants injected with 8 ng of MO was performed (primers used are depicted with arrows). Silencing with acMO was almost complete, when compared with *cerkl* expression in 72 hpf control MO-injected embryos (coMO), whereas in doMO animals the WT spliced isoform was decreased by 35%. β-*Actin* was used for normalization. (**B**) acMO-injected embryos displayed either small eye phenotype (named mild phenotype) or very small eye, small head, and body and curved tail (named severe phenotype). White double-head arrows denote diameter of the eyes. * denotes small and curved head in severe-phenotype morphants. (**C**) Phenotype frequency of morphants. The *cerkl*-knockdown phenotype was rescued when human *CERKL* mRNA was co-injected with acMO. n, number of individuals. (**D**) Eye size (in diameter) was measured in at least ten independent embryos from each group. Data were analyzed by *t*-test and are presented as mean ± SEM. ** $P<0.001$. Mean eye size was 253.4 µm for control, 172.7 µm for acMO and 239 µm for doMO morphants.
doi:10.1371/journal.pone.0064048.g005

truncation would affect the full NLS2 and ATP binding site signatures, and a fraction of the DAGK domain. In *Xenopus tropicalis*: variant 1 was the main isoform with all the canonical exons, and variant 2, eye-specific, incorporate an alternative exon (3b), between exons 3 and 4, containing an in-frame stop codon. In *Gallus gallus*: variant 1, the main isoform, comprised all the annotated exons; variant 2 included a stop-containing exon (5b, between exons 5 and 6) and encoded a C-terminal truncated protein; and variant 3, skipped exon 6 and generated an in-frame shortened peptide.

We also aimed to characterize *CERKL* expression in the three analysed species from the upstream transcriptional start site (TSS) of *NEUROD1* [18], [19], a transcriptional factor involved in photoreceptor development [39]. RT-PCR eye cDNA assays with specific primers spanning the *neuroD1* 5′UTR and exon 2 or 13 of *cerkl* showed that NeuroD1 promoted *cerkl* expression in chicken, but not in zebrafish or frog. The use of the alternative promoter generated a novel 5′UTR exon, between *neuroD1* and *cerkl Gallus* genes, and generated two new isoforms (named 4 and 5) (Fig. 4A). If translated, the peptides would show truncations at the N-terminus, as the canonical methionine in exon 1 was skipped and translation could be initiated from a species-specific methionine in exon 2. A general picture of the alternative exons and their impact on the predicted ORF in human, mouse, chicken, frog and zebrafish *CERKL* is shown in Fig. 4B.

Validation of *cerkl* morpholinos

To evaluate whether the knockdown of ZF*cerkl* caused a retinal defect, two antisense morpholinos (MOs) that targeted all mRNA isoforms were used, acMo and doMO (see the Material and Methods section), and a standard negative control (coMO). In order to assess splicing blockage by ZF*cerkl* MOs, we performed RT-PCR analyses from a pool of 10–12 embryos at different stages (24, 30, 52 and 72 hpf) using specific primers flanking the target region (Fig. 5A, black arrows). In the case of acMO, almost complete depletion (85%) of *cerkl* transcripts was attained, whereas doMO blockage was less intense, only reaching the 35%. The poor blocking ability of doMO was taken to mimic the heterozygous condition of human carriers.

To further investigate the putative *ZFcerkl* aberrant splice products produced by acMO and doMO blocking, semi-quantitative RT-PCR assays were devised. Nor exon skipping neither intron retention could be identified using specific primers located at the flanking exons or introns of each MO targets. Assuming that transcripts from the targeted alleles would have skipped exon 4 or exon 9, or retained intron 3 or intron 9, in acMO and doMo, respectively, a premature translation-termination codon (PTC) would appear in all cases. To verify if the PTC-containing mRNAs-ZFCerkl were degraded via the nonsense-mediated mRNA decay (NMD) surveillance mechanism, another RT-PCR assay was carried out with two pairs of primers located in exons far away from the original morpholino targets (see Table S2 for primer sequences). Expression levels were in accordance with

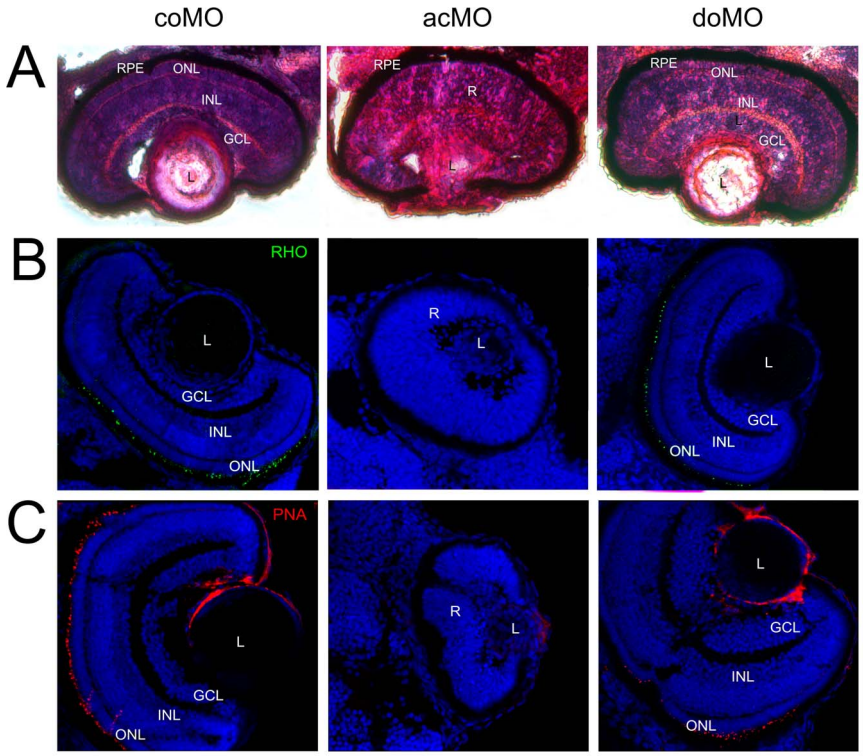

Figure 6. Eye histology in control and ZF*cerkl* morpholino-injected embryos at 72 hpf. (**A**) Zebrafish eye sections were stained with H&E. Control morphants (coMO) showed normal retinal lamination with three cell layers (GCL, INL, and ONL). In "mild" acMO-injected embryos, lamination did not occur and the three layers were not visible. The retinal pigment epithelium (RPE) developed normally in control and ZF*cerkl* morphants. (**B**) Immunostaining with anti-rhodopsin and (**C**) anti-PNA identified rod and cone outer segments, respectively, in control and doMO morphants. Outer segments were absent in acMO morphants. Nuclei were stained with DAPI. Some nonspecific staining was seen in the lens when stained with PNA. Photographs were at×40 magnification.
doi:10.1371/journal.pone.0064048.g006

those reported for the first pair of primers in each case, thus supporting NMD transcript depletion (Fig. S3). Indeed, this is in agreement with late reports showing that NMD effectors are deeply involved in zebrafish embryonic development and survival [40].

ZF*cerkl* suppression in retinopathy

In accordance with our previous observations showing greater blocking ability for the acMO, microinjection of 8 ng MO into 1 to 4 cell-stage embryos resulted in morphogenesis defects in 73% of the animals, whereas no mutant phenotypes were observed neither with doMO-, nor with coMO- injected embryos, from stage 24 hpf to 5 dpf. First evidences of distortions in the visual system were detected at 48 hpf. The main traits were eye size reduction with overall structure preservation and clear boundaries between the lens and the neural retina in acMO embryos. By 72 hpf, around 70% of the acMO morphants showed the small eye phenotype ("mild" form), and some (23%) also exhibited small heads, markedly curved body axes and short tails ("severe" form) (Fig. 5B). Phenotypic rescue was attained after co-injection of the acMO and the mRNA encoding human wild type *CERKL* (Fig. 5C). Analyses of the diameter length of the eye on histological sections indicated a 29% reduction of the acMO treated embryos compared with coMO animals (Fig. 5D).

To investigate the effect of *cerkl* knockdown on retinal development, histological and immunological analysis of 72 hpf retinas of ZF*cerkl*-deficient morphants and controls were carried out. By this stage, the outer segment of photoreceptors is normally formed. In our case, the acMO-injected morphants showed defective lamination as the three retina cell layers (GCL, INL and outer nuclear layer, ONL) were absent, whereas wild type lamination was observed in doMO and control embryos (Fig. 6A). Moreover, the outer segments of rod and cone photoreceptors (detected with anti-rhodopsin and anti-PNA, respectively) were absent in acMO embryos (Fig. 6B, C). The development of the retinal pigmented epithelium (RPE) was unaffected. Another relevant trait of the acMO morphants was the abnormal lens morphology, possibly related to the retardation of ocular development because of *cerkl* knockdown.

Knockdown of ZF*cerkl* leads to cell death

The aberrant eye phenotype could be due to increased cell death or reduced proliferation. Immunodetection of Caspase-3 (a marker of the first stages of apoptosis [41]) was used to assess cell death in single optical sections (Fig. 7A). Positive cells were scored in 4 independent embryos from each group. Our results revealed a 16-fold increase of cell death in acMO embryos (Fig. 7B) and supported increased apoptosis of retinal cells.

Cerkl does not contribute to retinal cell proliferation and early differentiation

To assess if the acMO phenotype in zebrafish was due to defective cell proliferation or differentiation during early retinal development or a secondary degeneration process, whole-mount ISH assays with early retinal markers *pax6a* and *otx2* were performed (Fig. 8A and B). *Pax6a* contributes to the control of cell

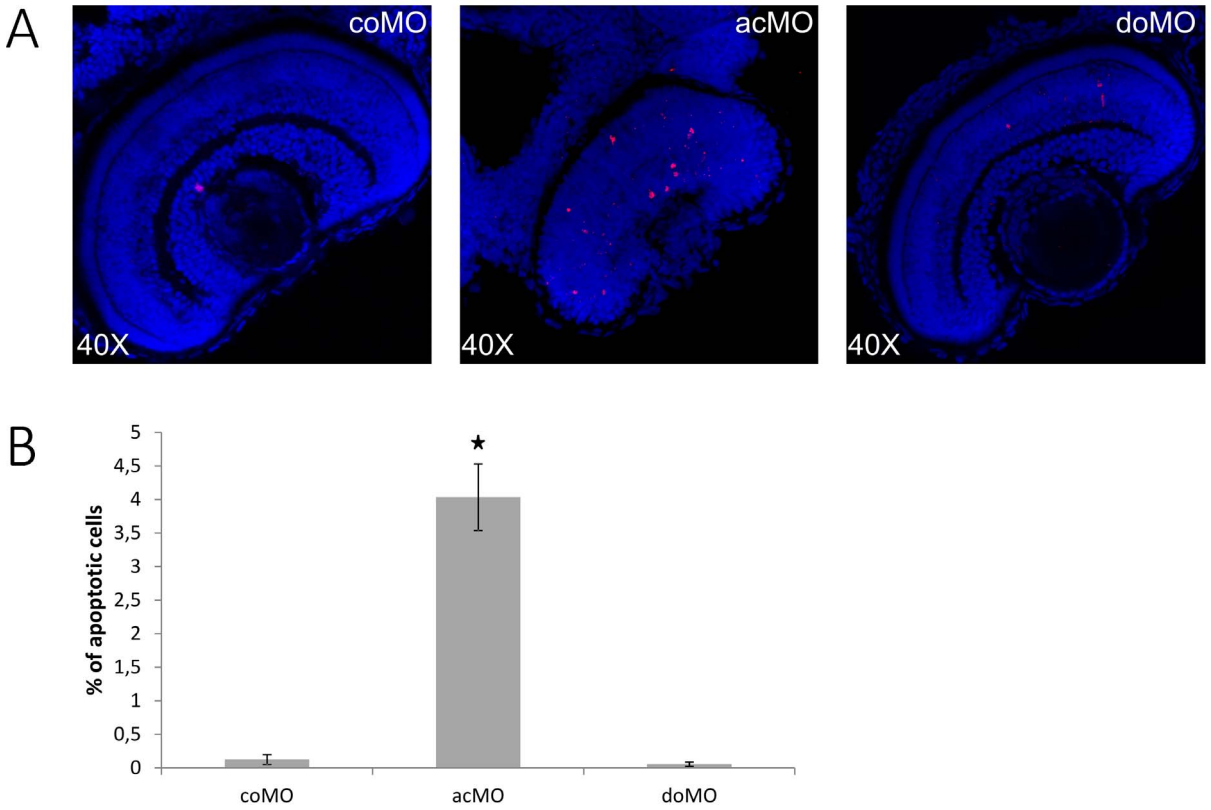

Figure 7. Increased cell death in ZF*cerkl* morpholino (acMO)-injected embryos. (**A**) Immunodetection of apoptosis by anti-active Caspase-3 in retina cryosections of 72 hpf control (coMO) and ZF*cerkl* morpholino-injected embryos (acMO and doMO). Caspase-3-positive cells (shown in red) increased in acMO morphants. Nuclei were stained with DAPI. (**B**) The percentage of apoptotic cells in each retina within a single cell layer was quantified in four independent embryos from each group, plotted and analysed by *t*-test. Data are presented as mean ± SEM. * P = 0.005.
doi:10.1371/journal.pone.0064048.g007

proliferation, maintenance of the retinogenic potential of the retina progenitor cells, and amacrine cell fate specification [42], whereas *otx2* is a key regulatory gene for retinal photoreceptor determination [43]. Our results indicated that at early stages, 22 and 24 hpf, when in the optic vesicle all cells are still proliferating, the expression pattern of both, *pax6a* and *otx2,* was unaffected in the acMO morphants. As expected, *pax6a* was detected in the developing forebrain, hindbrain, spinal cord, and eye, and *otx2* in the eye and midbrain. At 48 and even more evident at 72 hpf, when all cells are postmitotic, the acMO embryos exhibited a considerable decrease in hybridization intensity compared to the controls, treated and stained under the same conditions. The distribution of differentiation markers in the acMO morphants was further analyzed using the *ath5:GFP* transgenic strain. *Ath5* is a transcription factor expressed in a wave-like pattern that prefigures the wave of the retinal ganglion cell (RGC) genesis, the first cell type to differentiate in the vertebrate retina, which has been previously reported as affected in our mouse model *Cerkl*$^{-/-}$. The wave of *ath5* expression and RGC differentiation in zebrafish occurred during the second day post-fertilization, starting in the ventronasal patch and spreading from there to the rest of the nasal and central retina [28]. By 48 hpf, the RGC wave filled the central and peripheral retina in control embryos, whereas it was delayed in acMO morphants (Fig. 8C). Hence, our results suggested that *cerkl* was not essential for driving the RGC differentiation wave, as the ventronasal patch was formed and the wave started spreading. However, in agreement with the above results in cell death, the delay and disorganization in RGC neurogenesis supported Cerkl contribution to cell survival, and suggested that the small eye phenotype and the defective retina lamination were a consequence of a secondary degeneration process.

Discussion

After intense studies, the role in photoreceptor degeneration of *CERKL*, a gene causing autosomal recessive RP and CRD [3], has remained elusive up to now. We have gathered data showing that CERKL protects cells form oxidative stress [14] and, lately, in our *Cerkl*$^{-/-}$ murine model, in favor of a consistent and notable decrease of the retinal sphingolipid content particularly, the glucosyl/galactosylceramide species [16]. Although these results could be suggestive of CERKL and glucosylceramide involvement against oxidative stress, we still are far from understanding CERKL role in pathogenesis. In this work, we have aimed to gain new insights into CERKL retinal function generating a zebrafish knockdown model.

Transfection of ZFCerkl in cultured COS-7 cells supported the dynamic nuclear-cytoplasmic localization (Fig. 1) and the NLS2 major role in directing nuclear trafficking as previously described in human [13]. The role of CERKL in the nucleus is still unclear and does not seem to be related to the transcriptional regulation of sphingolipid-related genes [16]. However, the physiological relevance of NLS2 is stressed by its structural conservation across species and R106S, a mutation-causing RP, precisely located in this domain [6].

We have shown that high transcriptional complexity of CERKL in mammals (namely human and mouse) arise from the

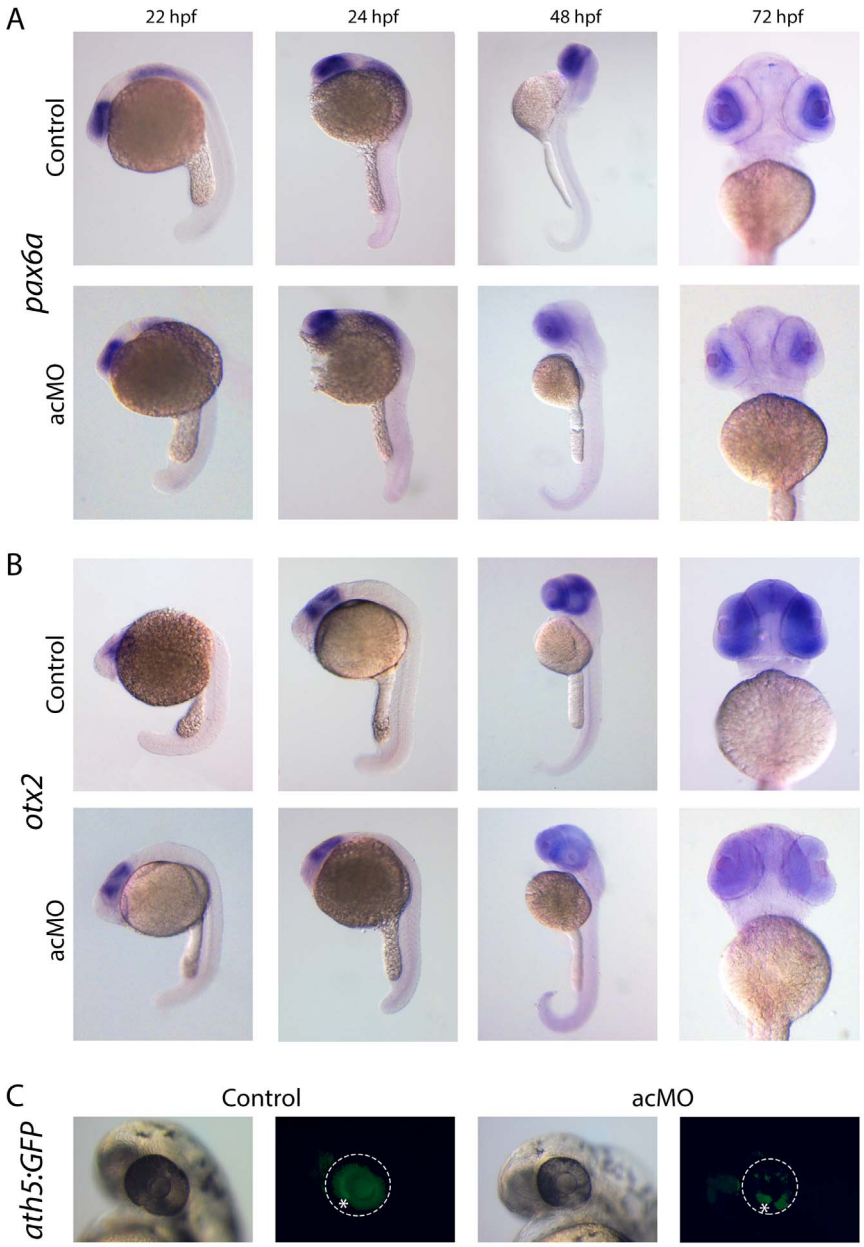

Figure 8. Expression of retina cell markers in acMO-injected embryos at early developmental stages. (**A and B**) At 22 and 24 hpf, the spatiotemporal pattern of *pax6a* (A) and *otx2* (B) in acMO-injected animals was similar to that of controls: *pax6a* was detected in the forebrain, hindbrain, spinal cord and eye, and *otx2* in the eye and midbrain. By 48 and becoming more evident at 72 hpf, acMO embryos exhibited a marked reduction in the expression of both markers. (**C**) The expression of the *ath5* transcription factor was assessed *in vivo* in acMO-injected embryos of the transgenic *ath5:GFP* strain. At 48 hpf, the wave of ath5 expression, which prefigures the wave of retinal ganglion cell genesis, filled the central and peripheral retina of control embryos, whereas the pattern appeared delayed and disorganized in the acMO morphants, although RGC genesis was not fully abolished. * denotes the ventronasal patch of RGC genesis.
doi:10.1371/journal.pone.0064048.g008

combination of tissue-specific promoters (among them *NEUROD1*) and alternative splicing [17], [18], [19]. Although the regulatory meaning of AS is largely unknown, even sometimes considered as background spliceosomal noise [44], [45], [46], it could also be related to the fine-tuning of key biological processes. Interestingly, recent work has revealed that adaptive novelties have arisen through changes in AS regulation, as ganglion-specific splicing of *TRPV1* underlies infrared sensation in vampire bats [47]. Thus, we aimed to assess *cerkl* transcript diversity in zebrafish, as well as in frog and gallus, and compare them with those reported for mouse and human. Our data showed that the full length (13 exons) coding region was the only isoform shared, and that AS events were seldom conserved in *CERKL*. In terms of exon cassettes, exons 3, 4 and 5 were alternatively spliced only in human and mouse, which supported an evolutionary novelty acquired at some point in the mammalian lineage. Concerning the identification in mouse and chicken of alternative exons between exon 5 and 6 (5b), both bearing a premature stop codon, the convergent inclusion of introns seems the most probably scenario, although an homologous origin could not be fully discarded. Our data are in

agreement with the low level of conservation of AS events between vertebrate groups, especially those involving reading frame disruption [48], [49]. Interestingly, the use of NEUROD1 as an alternative promoter for *CERKL* expression appears to be restricted to the amniote species analysed (Fig. 4). Concerning translation, the shorter N-terminal Cerkl protein isoform of zebrafish is the truncated species that mostly resembles the corresponding size variant of mammals.

Cerkl morpholino knockdown treatment in wild-type zebrafish embryos clearly affected eye size (Fig. 5) and retinal morphology. At 72 hpf, morphant retinas were defective in lamination and the photoreceptors lacked the outer segments, normally present at this stage (Fig. 6). The number of apoptotic retinal cells was significantly increased in Cerkl-deficient embryos. Cell death did not appear to affect other ocular structures, as cornea and RPE, which highlighted that *cerkl* knockdown effects were restricted to the retina. Similar defects have also been observed for genes encoding transcription factors (e.g., math5, NR2E3) [50], [51], cell cycle regulators (e.g., Cdkn1b/c, cdk5) [52], and photoreceptor ciliary proteins (e.g., RPGR, RP2, TOPORS, BBS9) [53], [54], [55], [56]. Whether the shared phenotype reveals functional overlaps or secondary effects of retinal neurodegeneration, remains to be elucidated. The analysis of different early retinal development markers in acMO morphants suggested that Cerkl might contribute to cell survival but not to cell proliferation or differentiation during early retina development (Fig. 8), in agreement with the reported anti-apoptotic effects reported in cell cultures and animal models [14], [19], [57].

CERKL mutations causing RP and CRD disorders are inherited as an autosomal recessive trait. Unlike the phenotype observed in zebrafish *cerkl*-knockdown embryos, patients do not exhibit developmental abnormalities, and neurodegeneration begins at the second-third decade of life. In addition to a dose-dependent effect, another plausible explanation for the lack of developmental defects in humans may be an increased level of complexity, redundancy or robustness in the retinal gene network of mammals that allows for compensation during embryonic development, but fails to maintain a proper function in adulthood.

In conclusion, we propose that although human, mouse and zebrafish *CERKL* phenotype features could be partially dose-dependent, further experiments are needed to identify the functional relevance of each isoform and their individual contribution to the pathogenic threshold. Moreover, the species-specific differences observed deserve further analysis at the temporal and cell-specific level. Interestingly, the availability of a zebrafish model is a powerful tool to elucidate how *cerkl* depletion results in the occurrence of apoptotic cell death after defective retinal lamination and photoreceptor outer segment formation, and provides new scenarios to understand human retinal degeneration.

Supporting Information

Figure S1 Syntenic organization of the *CERKL* genomic region. Schematic view of the structure and gene organization of the 1.8 Mb genomic locus encompassing *CERKL* in *Homo sapiens* (Hsa), *Xenopus tropicalis* (Xtr) and *Danio rerio* (Dre). The discontinuous lines in the *Xenopus* locus represent the end of the scaffold. Conserved genes are shown in color, while empty arrows depict the end of the syntenic region. Two chromosomal rearrangements are shown in the compared region: a tandem duplication of the TTN gene in zebrafish, located at the right border, and a chromosomal inversion encompassing 4 genes (at the left boundary, framed in red). Concerning the inverted segment, human and *Xenopus tropicalis* share gene order and orientation, suggesting that the chromosome rearrangement took place after the split of tetrapod and teleost lineages. Ancestral condition is unknown, as basal vertebrate genome assemblies are not available.
(TIF)

Figure S2 Conservation of CERKL across different species. Accession numbers for the amino acid sequence of each species are: NP_963842, human (*Homo sapiens*); XP_002799006, macaque (*Macaca mulatta*); XP_002712274, rabbit (*Oryctolagus cuniculus*); NP_001041641, mouse (*Mus musculus*); XP_002932061, frog (*Xenopus tropicalis*), XP_421973, chicken (*Gallus gallus*); NP_001082943, zebrafish (*Danio rerio*).
(TIF)

Figure S3 Validation of cerkl morpholinos. Transcriptional products obtained with the following sets of primers: (**A**) exons 3-5 and 11-13 for acMO samples, and (**B**) exons 8-10 and 11-13 for doMO samples. The comparable decrease in band intensity suggests transcript depletion in both cerkl morphants.
(TIF)

Table S1 Zebrafish RNA-seq data. The reported RNA-seq data showing tissue resource, accession number and name of the study are indicated.
(DOCX)

Table S2 Primer sequences used for gene expression, cloning and *in situ* hybridization. The sequences of all the primers used are shown.
(DOCX)

Acknowledgments

We would like to acknowledge the generous support and technical advice from Dr. Carolina Minguillón, Dr. Maria Marsal, Amayra Hernández-Vega and Xavier Esteban on *Danio rerio* manipulation and mating. The cDNAs from *Xenopus tropicalis* and *Gallus gallus* were a kind gift from Dr. José Luis Ferran. We also want to thank Manuel Irimia for his help with RNA-seq analysis and Enrique Navas for helping with the laboratory experiments.

Author Contributions

Conceived and designed the experiments: MR DB JGF RGD. Performed the experiments: MR DB. Analyzed the data: MR DB. Contributed reagents/materials/analysis tools: MR DB JGF RGD. Wrote the paper: MR DB JGF RGD.

References

1. den Hollander AI, Black A, Bennett J, Cremers FP (2010) Lighting a candle in the dark: advances in genetics and gene therapy of recessive retinal dystrophies. J Clin Invest 120(9): 3042-53.
2. Berger W, Kloeckener-Gruissem B, Neidhardt J (2010) The molecular basis of human retinal and vitreoretinal diseases. Prog Retin Eye Res 29(5): 335-75.
3. Tuson M, Marfany G, Gonzalez-Duarte R (2004) Mutation of CERKL, a novel human ceramide kinase gene, causes autosomal recessive retinitis pigmentosa (RP26). Am J Hum Genet 74(1): 128-38.
4. Auslender N, Sharon D, Abbasi AH, Garzozi HJ, Banin E, et al. (2007) A common founder mutation of CERKL underlies autosomal recessive retinal degeneration with early macular involvement among Yemenite Jews. Invest Ophthalmol Vis Sci 48(12): 5431-8.
5. Pomares E, Marfany G, Brion MJ, Carracedo A, Gonzalez-Duarte R (2007) Novel high-throughput SNP genotyping cosegregation analysis for genetic diagnosis of autosomal recessive retinitis pigmentosa and Leber congenital amaurosis. Hum Mutat 28(5): 511-6.

6. Ali M, Ramprasad VL, Soumittra N, Mohamed MD, Jafri H, et al. (2008) A missense mutation in the nuclear localization signal sequence of CERKL (p.R106S) causes autosomal recessive retinal degeneration. Mol Vis 14: 1960-4.
7. Avila-Fernandez A, Riveiro-Alvarez R, Vallespin E, Wilke R, Tapias I, et al. (2008) CERKL mutations and associated phenotypes in seven Spanish families with autosomal recessive retinitis pigmentosa. Invest Ophthalmol Vis Sci 49(6): 2709-13.
8. Tang Z, Wang Z, Wang Z, Ke T, Wang QK, et al. (2009) Novel compound heterozygous mutations in CERKL cause autosomal recessive retinitis pigmentosa in a nonconsanguineous Chinese family. Arch Ophthalmol 127(8): 1077-8.
9. Aleman TS, Soumittra N, Cideciyan AV, Sumaroka AM, Ramprasad VL, et al. (2009) CERKL mutations cause an autosomal recessive cone-rod dystrophy with inner retinopathy. Invest Ophthalmol Vis Sci 50(12): 5944-54.
10. Littink KW, Koenekoop RK, van den Born LI, Collin RW, Moruz L, et al. (2010) Homozygosity mapping in patients with cone-rod dystrophy: novel mutations and clinical characterizations. Invest Ophthalmol Vis Sci 51(11): 5943-51.
11. Sugiura M, Kono K, Liu H, Shimizugawa T, Minekura H, et al. (2002) Ceramide kinase, a novel lipid kinase. Molecular cloning and functional characterization. J Biol Chem 277(26): 23294-300.
12. Bornancin F, Mechtcheriakova D, Stora S, Graf C, Wlachos A, et al. (2005) Characterization of a ceramide kinase-like protein. Biochim Biophys Acta 1687(1-3): 31-43.
13. Inagaki Y, Mitsutake S, Igarashi Y (2006) Identification of a nuclear localization signal in the retinitis pigmentosa-mutated RP26 protein, ceramide kinase-like protein. Biochem Biophys Res Commun 343(3): 982-7.
14. Tuson M, Garanto A, Gonzalez-Duarte R, Marfany G (2009) Overexpression of CERKL, a gene responsible for retinitis pigmentosa in humans, protects cells from apoptosis induced by oxidative stress. Mol Vis 15: 168-80.
15. Nevet MJ, Vekslin S, Dizhoor AM, Olshevskaya EV, Tidhar R, et al. (2012) Ceramide Kinase-Like (CERKL) Interacts with Neuronal Calcium Sensor Proteins in the Retina in a Cation-Dependent Manner. Invest Ophthalmol Vis Sci 53(8): 4565-74.
16. Garanto A, Nawajes MM, Egido-Gabás M, Marfany G, Fabriàs G, et al. (2013) Specific sphingolipid content decrease in Cerkl knockdown mouse retinas. Experimental Eye Research In press.
17. Vekslin S, Ben-Yosef T (2010) Spatiotemporal expression pattern of ceramide kinase-like in the mouse retina. Mol Vis 16: 2539-49.
18. Garanto A, Riera M, Pomares E, Permanyer J, de Castro-Miro M, et al. (2011) High transcriptional complexity of the retinitis pigmentosa CERKL gene in human and mouse. Invest Ophthalmol Vis Sci 52(8): 5202-14.
19. Garanto A, Vicente-Tejedor J, Riera M, de la Villa P, Gonzalez-Duarte R, et al. (2012) Targeted knockdown of Cerkl, a retinal dystrophy gene, causes mild affectation of the retinal ganglion cell layer. Biochim Biophys Acta 1822(8): 1258-69.
20. Rivas MA, Vecino E (2009) Animal models and different therapies for treatment of retinitis pigmentosa. Histol Histopathol 24(10): 1295-322.
21. Graf C, Niwa S, Muller M, Kinzel B, Bornancin F (2008) Wild-type levels of ceramide and ceramide-1-phosphate in the retina of ceramide kinase-like-deficient mice. Biochem Biophys Res Commun 373(1): 159-63.
22. Lieschke GJ, Currie PD (2007) Animal models of human disease: zebrafish swim into view. Nat Rev Genet 8(5): 353-67.
23. Morris AC (2011) The genetics of ocular disorders: insights from the zebrafish. Birth Defects Res C Embryo Today 93(3): 215-28.
24. Gestri G, Link BA, Neuhauss SC (2011) The visual system of zebrafish and its use to model human ocular diseases. Dev Neurobiol 72(3): 302-27.
25. Maurer CM, Huang YY, Neuhauss SC (2011) Application of zebrafish oculomotor behavior to model human disorders. Rev Neurosci 22(1): 5-16.
26. Fadool JM, Dowling JE (2008) Zebrafish: a model system for the study of eye genetics. Prog Retin Eye Res 27(1): 89-110.
27. Dowling J (1987) The Retina: An Approachable Part of the Brain. Cambridge, MA: Harvard Universitry Press.
28. Kay JN, Link BA, Baier H (2005) Staggered cell-intrinsic timing of ath5 expression underlies the wave of ganglion cell neurogenesis in the zebrafish retina. Development 132(11): 2573-85.
29. Labbe RM, Irimia M, Currie KW, Lin A, Zhu SJ, et al. (2012) A comparative transcriptomic analysis reveals conserved features of stem cell pluripotency in planarians and mammals. Stem Cells 30(8): 1734-45.
30. Thisse C, Thisse B (2008) High-resolution in situ hybridization to whole-mount zebrafish embryos. Nat Protoc 3(1): 59-69.
31. Yan YL, Miller CT, Nissen RM, Singer A, Liu D, et al. (2002) A zebrafish sox9 gene required for cartilage morphogenesis. Development 129(21): 5065-79.
32. Carre A, Graf C, Stora S, Mechtcheriakova D, Csonga R, et al. (2004) Ceramide kinase targeting and activity determined by its N-terminal pleckstrin homology domain. Biochem Biophys Res Commun 324(4): 1215-9.
33. Li Z, Hu M, Ochocinska MJ, Joseph NM, Easter SS, Jr. (2000) Modulation of cell proliferation in the embryonic retina of zebrafish (Danio rerio). Dev Dyn 219(3): 391-401.
34. Luo J, Uribe RA, Hayton S, Calinescu AA, Gross JM, et al. (2012) Midkine-A functions upstream of Id2a to regulate cell cycle kinetics in the developing vertebrate retina. Neural Dev 7(1): 33.
35. Pauli A, Valen E, Lin MF, Garber M, Vastenhouw NL, et al. (2012) Systematic identification of long noncoding RNAs expressed during zebrafish embryogenesis. Genome Res 22(3): 577-91.
36. Scott GR, Johnston IA (2012) Temperature during embryonic development has persistent effects on thermal acclimation capacity in zebrafish. Proc Natl Acad Sci U S A 109(35): 14247-52.
37. Ulitsky I, Shkumatava A, Jan CH, Subtelny AO, Koppstein D, et al. (2012) Extensive alternative polyadenylation during zebrafish development. Genome Res 22(10): 2054-66.
38. Yang D, Liu Q, Yang M, Wu H, Wang Q, et al. (2012) RNA-seq liver transcriptome analysis reveals an activated MHC-I pathway and an inhibited MHC-II pathway at the early stage of vaccine immunization in zebrafish. BMC Genomics 13: 319.
39. Brockerhoff SE, Fadool JM (2011) Genetics of photoreceptor degeneration and regeneration in zebrafish. Cell Mol Life Sci 68(4): 651-9.
40. Wittkopp N, Huntzinger E, Weiler C, Sauliere J, Schmidt S, et al. (2009) Nonsense-mediated mRNA decay effectors are essential for zebrafish embryonic development and survival. Mol Cell Biol 29(13): 3517-28.
41. Rodriguez-Mari A, Canestro C, Bremiller RA, Nguyen-Johnson A, Asakawa K, et al. (2010) Sex reversal in zebrafish fancl mutants is caused by Tp53-mediated germ cell apoptosis. PLoS Genet 6(7): e1001034.
42. Lakowski J, Majumder A, Lauderdale JD (2007) Mechanisms controlling Pax6 isoform expression in the retina have been conserved between teleosts and mammals. Dev Biol 307(2): 498-520.
43. Nishida A, Furukawa A, Koike C, Tano Y, Aizawa S, et al. (2003) Otx2 homeobox gene controls retinal photoreceptor cell fate and pineal gland development. Nat Neurosci 6(12): 1255-63.
44. Melamud E, Moult J (2009) Stochastic noise in splicing machinery. Nucleic Acids Res 37(14): 4873-86.
45. Melamud E, Moult J (2009) Structural implication of splicing stochastics. Nucleic Acids Res 37(14): 4862-72.
46. Ellis JD, Barrios-Rodiles M, Colak R, Irimia M, Kim T, et al. (2012) Tissue-specific alternative splicing remodels protein-protein interaction networks. Mol Cell 46(6): 884-92.
47. Gracheva EO, Cordero-Morales JF, Gonzalez-Carcacia JA, Ingolia NT, Manno C, et al. (2011) Ganglion-specific splicing of TRPV1 underlies infrared sensation in vampire bats. Nature 476(7358): 88-91.
48. Barbosa-Morais NL, Irimia M, Pan Q, Xiong HY, Gueroussov S, et al. (2012) The evolutionary landscape of alternative splicing in vertebrate species. Science 338(6114): 1587-93.
49. Merkin J, Russell C, Chen P, Burge CB (2012) Evolutionary dynamics of gene and isoform regulation in Mammalian tissues. Science 338(6114): 1593-9.
50. Wang SW, Kim BS, Ding K, Wang H, Sun D, et al. (2001) Requirement for math5 in the development of retinal ganglion cells. Genes Dev 15(1): 24-9.
51. Haider NB, Naggert JK, Nishina PM (2001) Excess cone cell proliferation due to lack of a functional NR2E3 causes retinal dysplasia and degeneration in rd7/rd7 mice. Hum Mol Genet 10(16): 1619-26.
52. Dyer MA, Cepko CL (2001) p27Kip1 and p57Kip2 regulate proliferation in distinct retinal progenitor cell populations. J Neurosci 21(12): 4259-71.
53. Shu X, Zeng Z, Gautier P, Lennon A, Gakovic M, et al. (2010) Zebrafish Rpgr is required for normal retinal development and plays a role in dynein-based retrograde transport processes. Hum Mol Genet 19(4): 657-70.
54. Shu X, Zeng Z, Gautier P, Lennon A, Gakovic M, et al. (2011) Knockdown of the zebrafish ortholog of the retinitis pigmentosa 2 (RP2) gene results in retinal degeneration. Invest Ophthalmol Vis Sci 52(6): 2960-6.
55. Veleri S, Bishop K, Dalle Nogare DE, English MA, Foskett TJ, et al. (2012) Knockdown of Bardet-Biedl syndrome gene BBS9/PTHB1 leads to cilia defects. PLoS One 7(3): e34389.
56. Chakarova CF, Khanna H, Shah AZ, Patil SB, Sedmak T, et al. (2012) TOPORS, implicated in retinal degeneration, is a cilia-centrosomal protein. Hum Mol Genet 20(5): 975-87.
57. Mandal NA, Tran JT, Saadi A, Rahman AK, Huynh TP, et al. (2012) Expression and localization of CERKL in the mammalian retina, its response to light-stress, and relationship with NeuroD1 gene. Exp Eye Res 106: 24-33.

Agraïments

A Manu. Por el camino recorrido y por constituir mi mayor apoyo durante la tesis. Por el algoritmo macroevolutivo. Por llevarme a todos lados al principio. Por Toronto y los koreanos. Porque casi no hay mail que no respondas al instante. Por co-optarme en el CRG para acabar lo empezado. Por entender lo necesario que es el respeto mútuo. Porque esta tesis no se explica sin tus fraseos y tus solos.

Al Jordi, per pescar-me des del primer moment. Per totes les oportunitats brindades, per la confiança i per no negar-me mai res, especialment els plans més delirants. A Carlos, el tudelano más majo que conozco (y seguramente que existe). Freak is the new black ;) A la Bea, pels inicis i per si un dia les coses milloren. A l'Aina, per transmetre'm sempre bon rotllo. A la Roser, per les canyes a Banyuls, les sortides en vaixell i la camisa de franel·la. A l'Ari, l'Anna, la Rocío, el William i l'Steph, per recordar-me com és de necessari romandre motivat. Als qui han format part de les planàries humanes: Cisco, Chema, Sara, Susana, María, Loli, Miquels, Marta, Àlex, Jose, Eudald, Gus, Nídia... a les mosques i als nouvinguts que no he arribat a conèixer, molta sort!

A la anterior generación de anfioxos. A Nacho, por ser un referente en sentido crítico y alguien del que siempre es interesante conocer su opinión. Por las veces que hemos tenido tiempo suficiente para charlar tranquilamente, menos seguro de las que me hubiesen gustado. A Champi, por las risas que me echo cuando coincidimos y lo que me apetecería colaborar contigo alguna vez. Ojalá algun día me anime y te haga una visita a Japón. A Ildiko, por hacerme entender que la poyata es una cosa seria, y que los mejores experimentos requieren paciencia y dedicación. A Senda, no coincidimos en el ambiente cefalocordado, pero siempre me has ayudado cuando ha estado en tu mano.

Al meu "tron", el Kike. Per ser el millor descobriment d'aquesta tesi. Perquè sense tu, aquests anys no haurien estat ni una centèssima part d'enriquidors, divertits i interessants del que han sigut. Per tots els moments d'aprenentatge i fascinació per l'evolució que hem viscut junts, perquè l'única ciència que val la pena és la que es comparteix. Espero que mai deixem de veure'ns, explicar-nos la vida, xerrar de literatura, política, filosofía… i d'enviar-nos fistradas diodenarls, tikitikitii! I el més important, per la nostra amistat. Perquè tot això només hagi estat una molt bona introducció.

A Salvatore, por ser un colega jefazo con una ilusión y unas ganas de hacer ciencia que son contagiosas. Por las cuatro (!) estancias en Napoli y tu constante interés y preocupación por mis movidas. To Ina, my window to the sea urchin world. For everything you showed to me, the ~2500 embryo injections, and your honest interest to discuss all the results. To Mena and Nietta, always available to give me clues about the urochordate mysteries. To Claudia (Cuomo), for all the times you helped me with a thousand things, even getting sperm from the urchins. I wouldn't get half of my results if you were not there. To Ylenia, because you are an example of kindness, amazing talent and professionality. You deserve the best. To Margherita, for all the good vibrations I got from you. Hope to meet you from time to time in exotic international meetings ;) To Carmen, because of your brave character, good judgement, and being a reference in terms of following your own path. To Evgeniya, who demonstrated me that being both crazy and a great person is not incompatible. To Ivan and Alberto for being old-school biologists who know that the true beauty is under the sea. To Rosaria, we did not coincide many times, but you always seemed to me extremely enthusiastic and friendly. To Claudia (Racioppi), because I still do not know how I've been so lucky to collaborate with you. I wish you all lots of personal and scientific satisfaction.

To my beloved, tiny but mighty, CRG colleagues. Según voy entrando al lab: A Lucía, por ser una dinamizador laboral y social nata. A Antonio, por tu inapreciable ayuda y tu sanísimo escepticismo científico, estás hecho un gran investigador. A Andre, por disfrutar como nadie de mi receta de castañas al microondas. A Javi, por tu perenne buen talante y lo jachondo que eres siempre. Exon skipping. To Chris, for your sense of humor and your patience with me when I don't understand your pirate accent. Al Jon, per soportar millor o pitjor les meves punkarrades. Al Jordi, perquè tot i que va ser molt breu, hi ha persones amb les que connectes de seguida. To Beth, for being such an easy-going person who knows that life deserves to be experienced with passion and excitement. A la Laura, per la teva motivació zoo-neuro-freak i les teves ganes inacabables d'aprendre coses noves. To Thom, for your interesting reflections without prior notice that are unexpected. A Bárbara, por tu buen rollito, tus consejos y sabiduría poyatiles y tu compromiso de hacer siempre un trabajo excelente. A Vicky, por ser una luchadora increíble, tenemos mucho que aprender de ti, no tengo ninguna duda de que lo vas a petar. Y por supuesto, a Yamile, por los millones de mails a cualquier hora, reuniones, conversaciones, más mails e imitaciones de acento pésimas que has tenido que aguantar. No sé que hubiera hecho sin

tu ayuda. Te debo todas las cenas, cervezas, margaritas y tequilas del mundo. Gracias por ser tan simpática y efusiva, me lo he pasado genial contigo. Espero que todo te vaya bien chido, nomás!

A Ana, mi esponjóloga preferida, por tu actitud vital y lo natural que es para ti echar un cable siempre. Por ser un reflejo del tipo de científico que me gustaría ser. A Chelo, por el pretecho y porque si tú no me has librado de díscolo, ya nadie podrá. Por las semanas en Murcia y por tomarnos en serio cuando lo normal hubiera sido darnos por unos giles pelotudos. A Lucía, porque se nota a la legua lo buena gente y buena investigadora que eres. Mucho ánimo con tu tesis, ojalá pudiese ayudarte tanto como lo has hecho tu conmigo. A la Marina, per enfrontar-nos plegats al cruel món dels zebrafish que habiten peixeres diabòliques d'universitat. Pels moments divertits i emocionants que vam passar tot i les dificultats afegides ;)

A la troupe biòloga (i adoptats), especialment als qui s'han quedat pringant a la facultat uns anyets més post-carrera per fer això que en diuen tesi/curros/WTF. A l'Alba, per ser de les persones més amables, simpàtiques i altruistes que conec. Pel teu interès sincer envers els qui t'envolten. Al David, perquè és brutal com de ràpid pots arribar a apreciar i a sobre fer-te amic per sempre d'un infiltrat. Ja pots estar tranquil respecte les potencials escriptures funeràries. Al Mays, perquè poques persones em transmeten tant bon feeling com en mr. Mojo Working. N'hem de fer una de grossa quan acabem la tesi. A la Berta, per tots els dinars 13:45h i lo fàcil que és parlar amb tu. Al Marc, per ser tant autèntic i preparar una mistela que tombaria un senglar. A Nora, por Tarifa, las metanorfosis y por apuntaros a swing. Al meu brother Eudald, què t'he de dir mamonasso. Doncs que espero que seguim igual tota la vida, però amb més temps per veuren's i fer coses plegats. Ens ho hauriem de manegar per col·laborar amb algun tema i tenir l'excusa perfecte per fer-nos unes visites post-cock. A la familia Llorente Martínez, incloent-hi el membre més recent. En especial, al futur profe Edukator Melenas, perquè algun dia ens ho muntarem per anar a la Polinesia amb unes barbes gegants a gaudir de l'oceà i comentar les vicissituts del gran F.

A l'Anna, una pontsicana internacional, per tots els bons moments viscuts, els viatges per Quebec, Nepal, Sardenya, etc... Espero que tot et vagi genial per Vancouver, perquè t'ho mereixes. Als meus companys de pis durant aquests darrers anys. A l'Esmail, pels gin-

tonics, els limoncellos i la bogeria final de tesi... que per fi s'ha acabat! Et desitjo el millor a Noruega i que puguis surfejar sempre que el cos t'ho demani. A la Marta, per fer-me riure amb els teus comentaris asalvatjats que no passarien cap tipus de censura. A Aran, por todas las comidas, cafeses e interesantes conversaciones tete-a-tete. Por ser una gran compi, colega, y prácticamente familia ;). To Greta, my favourite anglo-italian person, whose natural sympathy and kindness made us become her instant friends. Al Pablo i a l'Uri, per mantenir l'amistat durant totes les nostres etapes vitals des dels 90. Si es que ja tenim una edat...

A mi familia, por haberme apoyado y animado siempre en todo. Por transmitirme unos valores que me han permitido comprender cuales son las cosas verdaderamente importantes. Así da gusto. Os quiero.

A tothom qui em deixo perquè he d'entregar la tesi d'una vegada...
Una abraçada,
Demi